
annual
report 2001
NEUTRONS
FOR SCIENCE

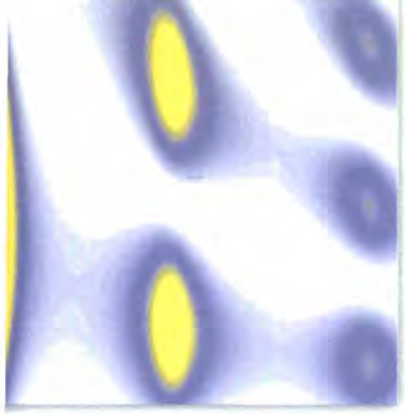

annual report 2001

The Institut Laue-Langevin

The Institut Laue-Langevin (ILL) is an international research centre using neutrons to probe the microscopic structure and dynamics of a broad range of materials from the molecular, atomic and nuclear point of view. The combination of the world's most powerful neutron source with dedicated instrumentation enables the study of a wide variety of scientific questions. Problems in solid-state physics, materials science, chemistry, the biosciences and the earth sciences as well as nuclear physics and engineering are investigated. For these diverse studies, the Institute offers its experimental facilities (some 30 instruments) to scientists from its partner nations via a peer-review system; confidential industrial experiments are also welcomed and a limited amount of beamtime is granted to scientists from non-partner countries.

We thank all the people who helped make this report.

Editors: Giovanna Cicognani, Christian Vettier
Design and Typesetting: Lignes droites communication (38 Echirolles)
Photography by Serge Claisse (ILL) and Artechnique – artechnique@wanadoo.fr
Printing: Imprimerie du Pont-de-Claix – April 2002

Further copies can be obtained from:
Institut Laue-Langevin
Scientific Coordination Office (SCO)
BP 156 - F-38042 Grenoble Cedex 9 (France)
Tel: +33 (0)4 76 20 72 40 - Fax: +33 (0)4 76 48 39 06
email: kjenkins@ill.fr or sco@ill.fr
Web: www.ill.fr

contents 2001

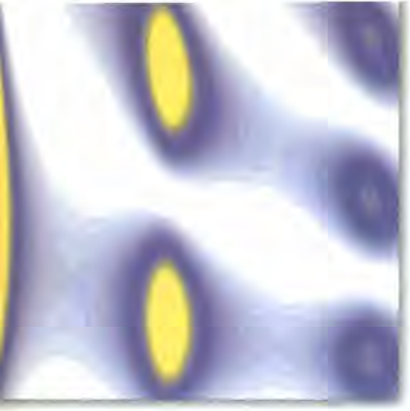

director's report 2001

The goal of the ILL is clear – to maintain and enhance our position as the world's most productive neutron scattering centre. To achieve this we cannot simply stand still. The world is changing and science is changing. The population at large – our ultimate source of funding – is, paradoxically, becoming increasingly suspicious of the direction in which science is taking us as a society and yet, at the same time, embracing with gusto the very products of technological advance which are the fruits of scientific research. Of course we have competitors in the neutron field, whose aim is to succeed to the position which the ILL occupies: ISIS in the UK; the SNS in the USA; the JHP in Japan; and, further in the future, the ESS in Europe. We wish them all well. Our field is sufficiently strong to allow friendly competition and collaboration to coexist to mutual advantage.

the ILL itself is changing and is responding to the challenge

But the ILL itself is changing and is responding to the challenge. Whilst the ambitious Millennium Programme is the visible expression of change, more fundamental changes are being addressed and adopted within the whole organisation. The ILL is becoming more outward looking. Our scientists are on more advisory panels than ever before – LLB, SNS, FRMII, FZ Jülich, ARRII, ESS... Our reactor engineers are collaborating with other centres worldwide – Taiwan, St. Petersburg, Australia, Munich, China... Our Directors are active in European groupings – the EIROforum, the ESS Council, ENSA and the EU Round Table. Nearer to home, the links with ESRF and with EMBL are becoming stronger and more productive, and our interactions with the town of Grenoble and the Rhône-Alpes Region are increasing. The ILL is becoming more responsive. Consultation with our user community has been enhanced – on a simple level by the introduction of user satisfaction forms and an electronic club for users, by the organisation of a series of User Forums, and by the hugely popular Millennium Symposium held in Spring 2001. The Scientific Council has been restructured to enhance its scientific mandate. The instrument sub-com-

mittee is playing a central role in the definition of the Millennium Programme. At the same time, the introduction of the 35 hour working week in France has resulted in the implementation of a formal system for out of hours support by the technical services supporting the users and for Sunday working for our scientists, previously illegal.

the implementation of a formal system for out of hours support by the technical services

The ILL is becoming very safety and security aware. Grenoble is a region of moderate seismic activity. This year has seen the completion of a series of calculations which simulate the reactor and the surrounding buildings. Equally well new instrumentation is being built following strict codes of earthquake resistance. A series of inspections, of a confidential nature, have been conducted by external authorities, all with a positive outcome. Safety training of staff and visitors has been augmented as have access arrangements to specific zones.

2001 has been a year of very positive achievements for the ILL. We have now secure supplies of fuel until beyond 2007. Operational procedures have been reviewed, confirmed and strengthened where necessary. The Millennium Programme with its second year completed is progressing at full steam ahead. The Millennium Symposium was highly successful. A comprehensive ILL Roadmap has been published. Earlier instrument upgrade programmes are now completed and delivering science. There are now nine instruments being rebuilt and two neutron guides. The underlying infrastructure is being systematically renewed and upgraded. Collaborative projects with ESRF for an engineering research support laboratory FaME and a Partnership for Structural Biology with EMBL as the third partner have been started. Scientific output has been excellent in quality, well ahead of the field in terms of quantity, and cost effective in terms of value for money. Most importantly, there is a renewed commitment to the Institut by our Associates – now three equal partners once again – and by our Scientific Partners with a clear recognition that modest investment will bring a high leverage in terms of scientific output.

Our staff have risen to the challenge admirably and I wish to thank them publicly for that.

On a personal note, I did not expect a year ago to be writing the 2001 Director's report. It is a role which I savour and, in spite of (or perhaps, because of) all the trials and tribulations and all the challenges, I am enjoying the job. I shall endeavour to do my best. We have, however, said *au revoir* to Dirk Dubbers during 2001 and I wish to express my gratitude to him for his unquestioned commitment to the ILL. It was he who had the vision to launch the Millennium Programme. As he wrote last year *"the ILL has the wind in its sails."* It most certainly has!

"the ILL has the wind in its sails"

Colin Carlile

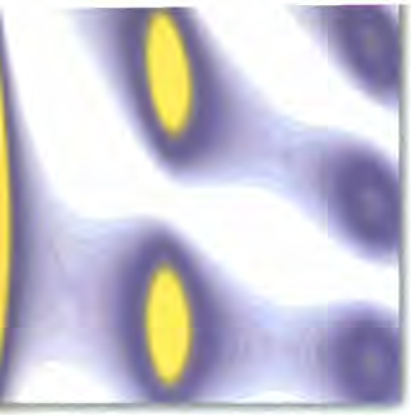

what is the ill ?

Formally, the ILL is a non profit-making French company under civil law, which is governed by an International Convention signed at Foreign Ministry level by three countries - France, Germany and the United Kingdom. Our Associates - the CNRS and the CEA representing France, the FZ Jülich representing Germany and the EPSRC representing the United Kingdom - own and administer the Institut. They are also responsible for all liabilities and eventual decommissioning costs. Currently the third Convention, which runs until 31st December 2003 is operational and the fourth Convention is presently being prepared for signature.

Although the ILL is an international organisation, its staff are not paid tax-free salaries, but instead they are enveloped within the French tax, employment and social security systems which has marked advantages but also marked disadvantages from whichever point of view you look at it. The Institut is answerable to French legal bodies and to French security authorities. We exist and operate within the French "loi de travail". Our staff representative bodies are those laid down by French law and are a significant presence in the ILL's daily life. We have strong links to the Mairie of Grenoble and surrounding communities, to the Préfecture of the Isère and to the Council of the Rhône-Alpes Region.

Whilst our Associates own the facility and contribute the largest amount to the almost 62 M€ annual operating costs, the ILL also benefits from the scientific partnerships of six other nations - Austria, the Czech Republic, Italy, Spain, Switzerland and Russia – who together contribute 14.2% of the operational costs of the Institut. All nine partner countries in addition can and do contribute to capital projects at the Institut, within the Institut's priorities but according to their own priorities also.

the ILL also benefits from the scientific partnerships of six other nations

Our governing body is the Steering Committee which meets twice-yearly and is made up of representatives of the Associates and the Partners together with Directors and Staff Representatives. Within the framework of the International Convention, the Steering Committee has the ultimate responsibility for determining operational and investment strategies for the Institut.

The Institut has a Director and two Associate Directors, one from each of the Associate countries, appointed on short-term contracts normally of 5 years. The Director's rôle is in general taken alternately by the German and British appointee. The two Associate Directors are also responsible respectively for the Science Division and the Projects and Techniques Division. The Head of the Administration Division is also appointed on a short-term contract, whereas the Head of the Reactor Division is a permanent ILL employee. These five people together constitute the Management Board of the Institut and are responsible for its day-to-day operation.

The scientific life of the Institut is guided by the Science Policy Board, with input from the ILL's nine scientific colleges. A Scientific Council, comprising 17 external scientists from the member states, advises the Directors on scientific directions for the Institut, on the evolution of the instrument suite to best meet the needs of the programme and assesses the scientific output of the Institut. It is helped in this process by the Instrument Sub-Committee and by the Chairmen of the 8 Scientific Sub-Committees who twice-yearly peer review the experiment proposals.

Our community of users is world wide although scientists from non-partner nations have access only by collabora-

our interactions wit have been enhance

tion with colleagues from partner nations. This use enriches the scientific life of the Institut but has been increasing of late thanks to the improved instrumentation, a trend which will require

some attention. Our interactions with our user community have been enhanced in the past two years in order to be better informed of their needs and to be more responsive to emerging demands. The Millennium Symposium in April 2001 was the major event of the year but our informal series of User Forums, at which researchers on site on a given day are invited to a meeting with Directors and ILL group leaders, have also been important. We are transforming our interactions to electronic means – proposals are now 100% electronic as are feedback forms. Much of our communication with users is now electronic although the Annual Report will remain in printed form for some time yet.

The ILL is composed of four Divisions, each with its distinct role and, it is true to say, its own culture. Efforts have been made to bring those cultures close together whilst recognising the need for differences. The Science Division staffs the instruments and delivers the science; the Projects and Techniques Division designs and builds new instruments, develops new concepts and maintains beamlines and instruments operational; the Reactor Division delivers the neutrons, operates and mans the reactor 24 hours per day every day of the year and has responsibility for all aspects of security; the Administration Division deals with personnel matters particularly being responsible for interactions with staff representative bodies, with purchasing and with finance – this year having seen the seamless transition to the Euro – and with site and building maintenance; and the Director's Services deal with radiological safety, with conventional safety and with health and working practices – 2001 has seen a significant strengthening of the safety culture of the Institut which will continue.

Why Neutrons ?

Neutron beams have the power, when directed at samples, to probe what is invisible using other radiations. They can appear to behave either as particles or as waves or as microscopic magnetic dipoles. Their specific properties enable them to reveal information which is often impossible to access using other techniques.

Electrically Neutral – they are non-destructive and can penetrate deep into matter making them an ideal probe for biological materials and samples under extreme conditions.

Microscopically Magnetic – they possess a magnetic dipole moment which makes them sensitive to both electronic and nuclear spins. Precise details of the magnetic behaviour at the atomic level can be investigated.

Wavelengths of Ångstroms – their wavelengths range from 0.1 Å to 1000 Å making them an ideal probe of atomic and molecular structures ranging from monatomic single crystals to complex biopolymers.

Energies of millielectronvolts – their energies are of the same magnitude as the energies of diffusive motions in solids and liquids, the coherent waves in single crystals (phonons and magnons) and the vibrational modes in molecules. An energy exchange between the incoming neutron and the sample of between 1μeV (even 1 neV with spin-echo) and 1 eV can readily be detected.

Randomly sensitive – the variation of scattering power from nucleus to nucleus varies in a quasi-random manner. This means that light atoms are visible in the presence of heavy atoms and neighbouring atoms may be distinguished. In addition isotopic substitution (for example D for H, or one nickel isotope for another) can allow contrast to be varied in certain samples. The neutron is particularly sensitive to hydrogen atoms.

The ILL's neutron source is the finest in the world, being based on a single element 58.3 MW nuclear reactor designed for high brightness. The main moderator is the ambient D_2O coolant surrounding the core which delivers intense beams of thermal neutrons to 11 beamlines and to four neutron guides. A graphite hot source operating at 2400K delivers hot neutrons – energies up to 1 eV and wavelengths down to 0.3 Å – to 3 beamlines. Two liquid deuterium cold sources at 25K deliver cold neutrons – energies down to 200 μev and wavelengths up to 20 Å – to 1 beamline and 9 neutron guides. An ultra-cold neutron source, fed from the top of one of the cold sources, delivers neutrons vertically through the reactor pool to 5 instruments on the operational floor of the reactor. In all there are more than 40 operational instruments, 25 of which have full public access.

The ILL monitors the papers published as a result of the use of our facilities. This indicates about 350 papers per year. Every third year a more rigorous search is done which uncovers a further 300 papers. The average number of papers published per year is therefore ~ 450. With an annual budget of ~ 62 M€, the cost per paper is around 130 k€. We pay particular attention to papers published in high impact journals. Data indicate ~ 80 such papers per year which, interestingly, is equivalent to the output of ESRF.

Beam days delivered for science equals 4663 for 2001. The cost per beam day of science therefore stands at a very cost effective 12,010 € per day.

Directors directing

From the left, M. Destot, Major of Grenoble, and Mme Berger, Director of the CNRS, with Christian Vettier (French Director, Head of Science Division) during their visit to the ILL on 4 September. The visitors were impressed with the ILL's facilities and good relations were cemented with our Institut. ◀

The "Millennium Programme" was presented to over 350 international neutron users and the scientific community at a special symposium on 6 and 7 April. From the left, Colin Carlile (ILL Director), Anton Heidemann (Deputy Head of the Projects and Techniques Division) and Reinhard Scherm (P.T.B., Braunschweig, ILL Director 1994-1997). ▼

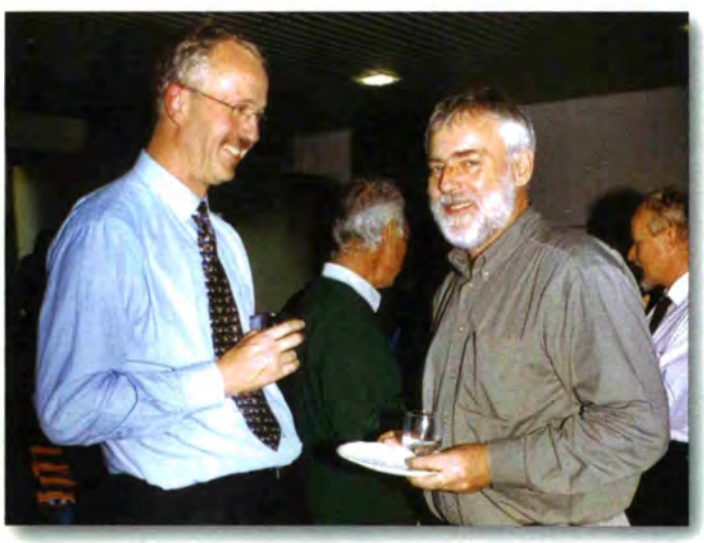

▲ In September the ILL welcomed Norbert König (left) as the new Head of the Administration Division and in January 2002 Werner Press (right) as the new Associate Director from Germany, who takes up the post of Head of the Projects and Techniques Division.

On 25 September at his farewell "pot", the ILL thanked Dirk Dubbers for his contribution over almost four years as ILL Director. Colin Carlile, nominated as Director of the Institut for a five-year period, hands over a parting gift, as the baton changes hand. ▶

scientific highlights 2001

Science at the Institut Laue Langevin combines the scientific programme achieved by the users of our facility and the research accomplished by the ILL staff. Visitors from all around the world and ILL scientists are making use of our advanced facilities to perform their top class science. Not only does the ILL provide neutron beams and instruments to users, but vigorous and ambitious in-house research programmes are also encouraged and carried out in all fields of research. In particular, strong pro-active moves have been made to facilitate access to neutron experiments in Life Sciences, which has led to the creation of the Deuteration Facility laboratory. In magnetism, the distinction of Jane Brown who was awarded the Walter Hälg prize from the European Neutron Scattering Association and the Guthrie Prize and Medal from the Institute of Physics (UK) demonstrates the world-class calibre of the in-house research activity at ILL.

strong pro-active moves have been made to facilitate access to neutron experiments in life science

The scientific programme carried out at the ILL focusses on the use of neutrons for a wide variety of scientific applications ranging from Particle Physics to Chemistry and Life Sciences, taking in Material Sciences and basic Condensed Matter Physics. Indeed, neutrons at ILL are exploited in many ways, both as a probe and as the subject of investigation. The unique characteristics of neutrons - to penetrate deeper into materials, to detect the different isotopes of the same element and to probe the dynamics of atoms and molecules over a wide energy range – allow the investigations of concrete problems such as: conformations of hydrogen bonds; lubrication, high temperature synthesis; and the structure of model membranes. The large variety of this programme is witnessed by the scientific summaries from Colleges and by the highlights proposed by scientists from our user community.

Experimental achievements depend fundamentally on the performances of our instruments and their continuous development. Quality of service and support are also required to generate world-leading science. A further aspect which has been observed is the growing need for simulations to explore the information contained in experimental data, either based on computer calculations and/or theoretical models.

The ILL relies on the many collaborators who submit their contributions to the highlights in order to illustrate the richness and the breadth of the research performed at the most powerful neutron scattering facility in the world. We are very grateful to those who have eagerly contributed to this year's version.

Magnetism

- **Ross Stewart**, College 4 Secretary
  http://www.ill.fr/Colleges/C4/index.htm
- **Clemens Ritter**, College 5B Secretary
  http://www.ill.fr/pages/science/iGroups/dif_1.html

The polarised hot neutron single crystal diffractometer D3, with Andrew Wills on keyboards.

The study of magnetism has been the realm of neutron scattering and continues to be. The determination of magnetic structures is still as important today as it was 50 years ago. The increased flux and resolution of neutron instruments nowadays permits the determination of temperature, field and pressure dependent changes in magnetic properties in parallel with accompanying subtle structural changes.

The success of neutrons in the profound study of GMR-manganites, double perovskites or magnetocaloric materials is overwhelming. Complicated magnetic structures having sine-wave, helical or spiral-type antiferromagnetic structures are routinely studied now; legion is the number of revisited magnetic structures. Frustrated magnetic systems, such as pyrochlores or jarosites may be studied progressively, first by powder diffraction and then by single-crystal diffraction and finally with polarised neutrons to pinpoint the crossover between short-range and long-range magnetic order as a function of magnetic dilution or minor deviations of the lattice from perfect - frustrated - symmetry.

Magnetic powder diffraction is the necessary first step in the study of magnetic shape memory alloys, where the martensitic transition prohibits single crystal diffraction studies due to the irreproducible formation of multi-domains. Magnetic multilayers of sub-micron thickness can be measured on single crystal diffractometers in 3-axis mode to minimise background. Vortex lattices of classical and unconventional superconductors are now not only merely detected, but their formation processes and dependence on temperature, applied field and electric current are being studied.

Elastic magnetic scattering studies with polarised neutrons have been used for a long time in the determination of spin-densities and complex magnetic structures. More demanding are the recent experiments determining the magnetisation density in molecular magnets or separating orbital and spin contributions in paramagnetic transition metals.

This year has seen several new developments in ILL instrumentation with relation to studies of magnetic phase transitions and excitations. Notably, in the field of neutron polarisation analysis (NPA) with the IN20 3-axis, D3 single crystal and D7 diffuse scattering spectrometers.

In the case of IN20 the new horizontally focusing Heusler monochromator has been installed, providing an order of magnitude increase in neutron flux at 1.3Å. No less than three out of seven contributions to this year's magnetism section of the ILL annual report are NPA studies on IN20, and it is clear that this upgrade will have a major impact in the study of magnetic excitations using polarised neutrons. Notable amongst these contributions is the study of Caciuffo and his team on the study of magnetic excitations in UO_2 using inelastic spherical neutron polarimetry with CRYOPAD II, in which there are shown to be no spin-fluctuations along the magnetic propagation vector in the low energy magnon branch. As the authors point out, this anomalous result, in a "well-characterised" magnet, highlights the exciting scientific insights which come about as a result of new and effective instrumentation.

The investigation of the nature of the interplay between magnetic fluctuations and superconductivity continues to develop. This year, reports on the p-wave superconductor $SrRuO_4$ and an investigation of the pseudogap in $YBa_2Cu_3O_{6+x}$ are included. Experiments scheduled for the coming year on $ZrZn_2$ and UGe_2 were highlighted by the Scientific Council in October 2001 and are likely to extend our understanding of these unconventional superconductors.

The characterisation of magnetic spin-fluctuations in unconventional metallic magnets exhibiting so-called Non-Fermi-Liquid (NFL) ω/T scaling in systems such as $CeNiGa_2$, UCu_4Pd and β-Mn, mostly on

the IN6 cold-TOF spectrometer, continues to prove both scientifically intriguing and experimentally challenging, requiring as it does, measurements as a function of the chosen quantum-critical-point parameter (either pressure or field). The recent provision of fields of up to 2.5 T on IN6 will greatly aid future studies of these fascinating materials.

Last, but not least, we would like to mention that Jane Brown has been rewarded for her outstanding, and ongoing, contribution to neutron scattering, in being awarded both the Walter Hälg prize of the European Neutron Scattering Association and the Guthrie Prize and Medal of the U.K. Institute of Physics.

Chemistry and Structure

GWENAELLE ROUSSE, COLLEGE 5A SECRETARY
HTTP://WWW.ILL.FR/PAGES/SCIENCE/IGROUPS/DIF_1.HTML

The first year of this Millennium has seen many successful studies of chemistry and structure at the ILL. Neutron diffraction, either from powder samples or single crystals is a fascinating microscope to locate atoms within a structure. Neutrons have remarkable properties which make neutron methods highly valuable in chemistry: neutrons penetrate bulky samples, allowing the identification of many components in multi-phase materials, and neutrons are sensitive to chemical elements independently of their atomic number. One obvious exploitation of the latter property is the neutron's ability to locate very light elements, such as hydrogen (or its isotope deuterium, ^{2}H). These unique properties are exploited by scientists who are interested in the compositions and structures of new chemical compounds. Very often, new specimens are available in polycrystalline form, which is why neutron powder diffraction is such a popular technique.

High resolution powder diffraction performed on D2B has revealed the structures of some clathrate hydrates, small water cages in which gas molecules (e.g. methane) are trapped. These clathrate hydrates, found on the ocean floor, exist only at high gas pressure and low temperature. Therefore neutron diffraction, in combination with numerical simulations, provides a unique tool with which to establish possible crystallographic models for these cages. Another example of the complementa- rity between neutron diffraction and numerical simulations is the absorption of gas molecules within carbon nanotubes. Using single crystal neutron diffraction (for example on the diffractometers D9 and D19), unexpectedly strong and very short N··H··O and C-H··O hydrogen bonds have been characterised in a variety of compounds, e.g. pyridine-3,5-dicarboxylic acid and $(H_7O_3)[AuCl_4]\cdot$15-crown-5.

Neutron diffraction has helped not only to locate atoms and molecules, but also to give details vital to understanding reaction mechanisms themselves. For

Sample positioning on the four-circle single-crystal and fibre diffractometer D19 by Ingrid Parrot.

instance, in-situ experiments on the high flux powder diffractometer D1B led to the determination of the reaction mechanism for the formation of the thallium superconductor, $Tl_2Ba_2Ca_2Cu_3O_z$. An even more striking example of the investigation of chemical mechanisms is the real-time self-propagating synthesis of the titanium carbide, Ti_3SiC_2. For this experiment, a time resolution of 0.9 s was used on the ultra-high flux diffractometer D20.

It is hoped that the results which are presented in this report will encourage new users to submit new research proposals and to take advantage of the new areas of research that are made accessible through the upgrades of instruments at the ILL (D2B, D19 and the new VIVALDI) carried out through the Millennium programme. We wish you great success with your experiments at the ILL!

Materials Science

CHARLES DEWHURST, COLLEGE 7 SECRETARY

Materials science is the study of the properties of materials and how those properties are determined by composition and structure. As an interdisciplinary science, materials science combines aspects of physics, chemistry, metallurgy and engineering to help understand real-world problems with real-world materials. Here at the ILL, the broad range of available neutron scattering, diffraction, reflection and spectroscopic techniques provide powerful tools to aid the investigation and understanding of materials in such a diverse subject area. Many of these experiments are performed at the ILL with a clear sight of industry, engineering or technological relevance.

Directly related to engineering materials is the article presented in this section by Bruno et al. who have used the D1A diffractometer as a high-resolution strain scanner to investigate the residual stress across a welded Ti_6Al_4V component, a lightweight alloy used in the aerospace industry for the construction of spacecraft liquid fuel tanks. Other metallurgy-based experiments performed at the ILL include, for example, investigating strain profiles in aero engine fan blades, using SANS to determine irradiation damage in reactor pressure vessel steels or the formation of precipitates and crystallisation processes of molten metals and alloys for structural applications.

The stress distribution in critical regions of this experimental crankshaft from Volkswagen was determined on the D1A diffractometer used in the strain scanner mode.

An unusual class of molecular materials are Buckyballs; hollow, close to spherical molecules consisting of an outer shell of 60 (or more) carbon atoms. Buckyballs have yet to find their niche application but a number of potential uses have already been outlined, for example advanced lubrication products, electrical properties or gas storage in the open C_{60} structure. Schober et al. using the inelastic neutron spectrometer IN6 report on investigations into the dynamic properties of the C_{60} Buckyball system, their ordering and the effects of interstitial guest molecules on the dynamics and lubrication of this nano-scale molecular ball system. Other workers use inelastic neutron spectroscopy to investigate the dynamics of guest molecules in similar nano-porous or open structures, for example in open-ended carbon nano-tubes, gas-hydrates (clathrates), hydrogen stored in metals, zeolites - used industrially as nano-filters and catalysts, or mesoporous materials prepared with regular structures using surfactant phases as templates. Molecular mixing and adsorption studies also constitute a significant scientific interest and experimental effort at the ILL.

An article by Gorria et al. describes D1B diffraction measurements on amorphous FeZr powders which reveal crystallisation processes and new metastable phases. Although concerned primarily with the metal physics surrounding the processing of these amorphous metallic materials, the underlying interest lies in the unusual magnetic states and extremely soft magnetic properties for applications such as transformer core materials and magnetic recording heads. Applied magnetism work by other groups has used SANS to investigate nuclear and magnetic grain size and magnetisa-

tion reversal properties in commercial thin film recording media and magnetic ordering and correlations in self-organised arrays of magnetic nano-particles. Understanding the magnetic granularity and coupling ultimately determines storage capacities of conventional magnetic recording media. The novel magnetic properties of thin film magnetic multilayers constitutes a wide research area naturally lending itself to investigation by spin-polarised neutron reflectometry. Lauter-Pasyuk et al. present EVA reflectometry studies of the coupling and domain structures in Cr / Fe multilayers and a separation of spin dependent off-specular reflectivity components from an initially unpolarised neutron beam. In other work, the interlayer magnetic coupling and phase transitions in an Fe/V thin film multilayer system can be tuned by the uptake of hydrogen, enough to modify the interlayer coupling from being ferromagnetic to antiferromagnetic. Ferro-fluids, while not conventional magnetic systems, exhibit novel ordering phases at interfaces with a solid substrate as demonstrated by EVA measurements reported by Vorobiev et al.

Finally, while not directly related to new or applied materials, Zucali et al. describe work on natural mineralogical samples of a particular Alpine material. Analysis of crystallographic orientation and texture elucidate the deformation mechanisms and mechanical properties of rocks during subduction and other geological processes.

Clearly, the scope of materials science based research at the ILL is broad using the suite of available ILL instruments to investigate the diverse structural, magnetic and dynamic properties of materials. The selection of articles presented below is just a small sample of the experiments that are being performed.

Liquids and Glasses

● **Miguel Gonzalez**, College 6 Secretary
http://www.ill.fr/Colleges/C6/C6_home.html

Liquids and glasses ranging from quantum liquids to glassy polymers have been studied with neutrons over the years from the point of view of their structures and their dynamics. Several methods are exploited (diffraction, quasi-elastic scattering and inelastic scattering) on different instruments to investigate short-range order and fluctuations.

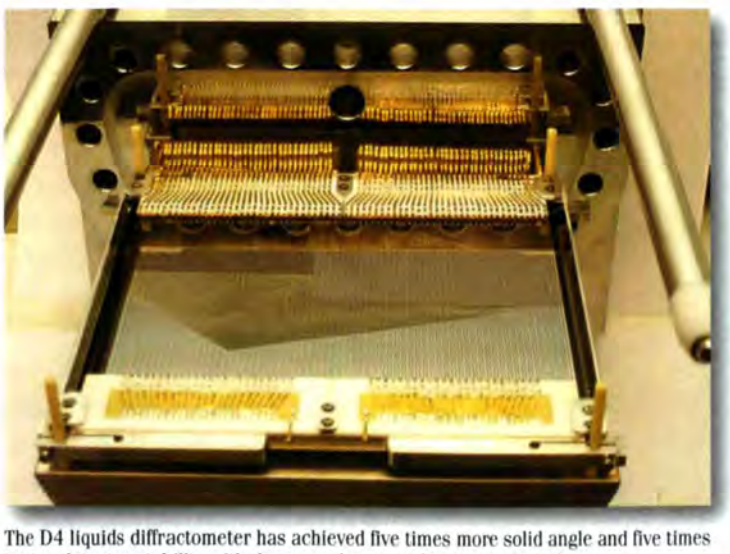

The D4 liquids diffractometer has achieved five times more solid angle and five times better detector stability with the new microstrip detector built in-house.

Canonical subjects which have been studied in the past are now evolving and incorporating new ideas. In particular, the study of excitations in quantum liquids have been rejuvenated by new experiments on ^{3}He films (Godfrin et al.) or in ^{4}He confined in porous materials (Stirling et al.) which focused on the additional two dimensional excitations which appear in these systems. Other examples are provided by the effort to better understand the nature of the vibrational modes on glass-forming systems, such as the study of acoustic modes in single crystals of α-quartz as a function of the disorder introduced by neutron irradiation (Rufle et al.) or the investigation of amorphous polymorphs, of Y_2O_3-Al_2O_3 (Koza et al.).

A major trend which has been observed recently is the increase in the number of studies combining neutrons and X-rays. This is specially the case on structural investigations aimed at obtaining partial structure factors of molecular liquids or liquid alloys, but the complementarity between both techniques extends also to inelastic measurements, as exemplified by the work of Sacchetti et al. on the collective dynamics in water (see ILL annual report 1999) per-

formed with hot neutrons on IN1. Inelastic X-ray scattering experiments provide extremely useful data on disordered systems because X-rays do not suffer from the kinematic conditions which neutrons do but they probe mainly the dynamics of the oxygen atom, while neutrons can sense the collective dynamics of both D and O in heavy water. An additional direction worth noting is the use of computer simulation techniques (Reverse Monte Carlo, classical or ab-initio Molecular Dynamics, etc.). This is due to the complexity of the problems investigated, so in many cases the lack of theories to interpret the experimental results makes unavoidable a recourse to simulation. Furthermore, in some cases the simulation is not just a tool to interpret the results, but it even precedes the experiment.

The three contributions selected to illustrate the use of neutrons for the study of liquids and glasses serve to outline this variety of the field and to show nicely some of the unique possibilities offered by neutrons to tackle the complex problems encountered. They also illustrate the technical challenges involved in many of the experiments performed and the increasing effort invested by many groups to relate their basic investigations to practical applications or with other scientific areas, such as geophysics or biology.

Thus, the first contribution exemplifies the use of isotopic labelling in neutron diffraction. The solutions investigated have fascinating electronic properties, but they also pose great technical difficulties to prepare and measure them. The second contribution deals with another technique (neutron reflectivity) and shows the utility of neutrons to investigate the adhesion properties of lubricants under shear. This study clearly has a lot of potential applications which required the development of a new cell to investigate *in situ* the effect of shear in a liquid. Finally, the last contribution has to do with dynamics and shows the results obtained by means of inelastic neutron measurements on silicate melts at high temperature, of relevance both for earth sciences and technology.

The study of amorphous matter is a multidisciplinary task. The combination of new ideas and approaches together with the use of complementary techniques guarantees exciting science. Furthermore, instrument upgrades (D4 has operated very successfully during 2001 and the new hot source will bring an additional increase in flux, and IN5 is being renewed incorporating a focusing guide and a new chopper system) will allow new experiments to be done.

Biology

Giovanna Fragneto, College 8 Secretary
http://www.ill.fr/Colleges/C8/C8_home.html

Neutron scattering experiments provide information on the structure and dynamics of biological macromolecules which helps in understanding biological function. The main advantage of neutron scattering in biological systems is the particular scattering behaviour of hydrogen. The fact that its scattering length is similar to that of other light atoms and that deuterium has a scattering length of opposite sign allow H/D labelling techniques to be used in a powerful way. At low resolution, contrast variation can be used to highlight particular parts of molecular complexes while at high resolution key protons can be observed. The very large incoherent cross section of hydrogen allows the observation of the internal dynamics of totally or partially labelled macromolecules. Furthermore, neutrons are such a gentle probe that samples under investigation do not suffer from radiation damage.

The ILL offers a broad suite of experimental techniques for static studies, such as small angle neutron scattering from proteins in solutions, protein crystallography or membrane diffraction, as well as dynamics studies of biological molecules with inelastic or quasi-elastic scattering methods. In fact, the range of time scales accessible to neutron scattering is that of interest for the internal dynamics of protein molecules and both amplitude and frequency information are available simultaneously. Instruments mainly concerned are IN5, IN6, IN13 and IN16.

Neutron crystallography is used to identify key protons in small proteins, nucleic acids and sugars. The Laue diffractometer LADI has allowed unique structural determinations and is to be upgraded to allow faster

data collection. In cell biology the functioning of very large molecular complexes, such as for example molecular motors, is of primary interest. Such large complexes cannot usually be solved by crystallography and only solution scattering can allow the observation of conformational changes induced for example by binding of ions, cofactors etc. in a solution environment which is very close to that of the living cell. D11 and D22 are used for SANS studies and among the recent interesting experiments are a time-resolved study of EDTA-induced swelling of tomato bushy stunt virus or the temperature dependence of the ATP-induced structural change of the thermosome.

Screening crystals for a protein crystallography experiment.

Since many biological processes occur at interfaces, the possibility of using neutron reflection to study structural and kinetic aspects of model as well as real biological systems is of considerable interest. D17, a high flux reflectometer, with time-of-flight and monochromatic options, has opened up the way at the ILL to a variety of experiments which have been carried out so far mainly on new models for biological membranes at the solid/liquid interface as well as on protein and peptide adsorption. Multilamellar lipid stacks, purple membrane, and peptide induced channels in membranes, have been extensively studied on the small momentum transfer diffractometer D16, where recently a pilot experiment has been carried out to study collagen packing in diseased bones which has shown that suitable diffraction patterns could be obtained from hydrated cancerous bones. This will enable future investigations of the effects of hydration, mineralisation and disease.

Finally, it should be mentioned that the Deuteration Laboratory at the ILL, a facility that will specialise in the deuteration of proteins and other biological molecules for neutron studies both by users and in-house scientists, has become operational. This facility will boost the use of neutrons by the life sciences community.

Soft Matter

● **Isabelle Grillo**, College 9 Secretary
http://www.ill.fr/Colleges/C9/

The expression "Soft Matter" embraces various fields of research, such as polymers, organic and inorganic colloids or assemblies of amphiphilic molecules. All these systems exhibit common features with organisation between objects and typical sizes and shapes from the scale of a few Angströms up to thousands of Angströms. Neutron scattering techniques such as small and wide angle scattering, grazing incidence and reflectivity are particularly well adapted to investigate the time averaged bulk or surface structure of colloidal samples. In parallel, inelastic scattering and spin-echo experiments are used to follow the motion of molecules and entities and to understand their dynamics.

Temperature, osmotic pressure, concentration, ionic strength are the main relevant parameters that control the thermodynamic stability of soft matter systems. The stability and organisation of the component particles (surfactant monomers, colloidal particles...) depend on the equilibrium between attractive and repulsive molecular forces and even a small change in the force balance may induce a reorganisation of the system. This explains the richness and diversity of phase diagrams as illustrated by the surfactant icosahedra or the collective giant oscillations in lamellar phases (Demé et al.) but also the difficulty to obtain stable stacked surfactant membranes for applications to biology (Fragneto et al.) or thin polymer films (Müller-Buschbaum et al.).

Isabelle Grillo, mounting the stop-flow apparatus on the small-angle scattering diffractometer D22.

If the steady state of many systems is now well characterised, data and models of kinetics, intermediate phases and structures are still under development. The knowledge of the phase evolution is crucial to understand and modify the characteristics of the final state and the study of non-equilibrium systems, for example under shear or during extrusion, is an emerging field. ILL's high flux SANS spectrometers open up the possibility of new experiments with real time measurements and rapid kinetics. Real time signifies a movie of the sample after a perturbation (pH or temperature jump, ionic strength variation, dilution, mixing, application of a magnetic field, light excitation...). Rapid means short acquisition times of the order of few hundred milliseconds in order to detect the early stages of formation of a sample. The article about vesicle growth (Gradzielski et al.) reveals different intermediate states leading to the steady state and thus demonstrates the importance of real time measurements combined with SANS to improve the understanding of phase formation mechanisms.

Soft matter is matter in motion, changing, evolving towards the lowest energetic states as a function of internal and external constraints. Neutron scattering experiments remain a unique tool for observing such changes.

Fundamental and Nuclear Physics

VALERY NESVIZHEVSKY, COLLEGE 3 SECRETARY
HTTP://WWW.ILL.FR/NFP/NPP/HOME.HTM

Nuclear and particle physics cover an extremely broad range of physical phenomena (nuclear and atomic physics, fundamental symmetries and new experimental techniques) with characteristic energies spanning at least from 10^{-19}eV to 10^{8}eV. All types of known forces are involved: weak and strong interactions, electromagnetic and gravitational forces. A distinctive feature of most experiments is that they require a completely new instrumental configuration to be set in place, which is essential to develop new instruments and methods.

In the field of nuclear physics, γ-ray spectroscopy of very neutron-rich nuclei is extremely active, confirming the need for a multi-detector array. As an example, the study of the double magic nucleus ^{78}Ni is possible today at Lohengrin due to the very low background level achieved. ^{78}Ni is the most neutron rich doubly magic nucleus, which supposedly can be reached in a nuclear reaction. Besides, the use and development of the new BID (β-induced Doppler broadening) technique, using the Gams spectrometers, is remarkable. This method follows from the well-known GRID method which was developed at the ILL, but it uses the β-decay in order to induce recoil and Doppler broadening. This method has allowed access to the structure and properties of a new set of nuclei, which would be extremely difficult to reach with other techniques. Moreover, it provides a more classical but very precise study of β-decay itself, which could shed light on the physics beyond the Standard Model of the weak interaction. Many other experiments are progressing, related to waste disposal and/or transmutation. Worth noting are also systematic studies of delayed neutron emission.

Fundamental neutron physics plays a particular role due to the great simplicity of theoretical interpretations. Neutrons are considered here simultaneously as a tool and as the object of investigations. Such studies include i) precise observations of the neutron β-decay in order to get the Standard Model constants and to search for new physics beyond it, ii) the search for CP-violating effects with free neutrons and during neutron-induced reactions, and

iii) the development of new methods and techniques such as UCN storage, neutron optics, neutron sources, etc.

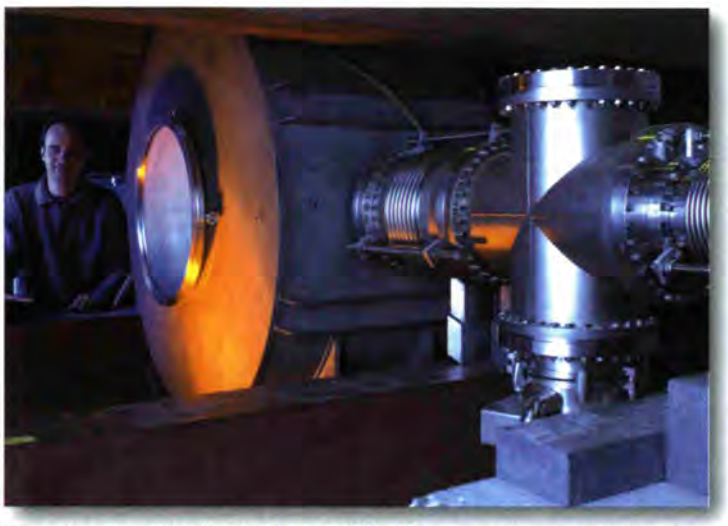

Valery Nesvizhevsky at the installation PERKEO from Heidelberg University is taking data at the new PF1B high-intensive cold neutron beam at the ILL.

It is worth noting the persistent efforts to measure more precisely specific β-decay parameters, particularly the so-called A-asymmetry, which correlates the spin of the decaying neutrons to the direction of emission of electrons. Such parameters give hints to the physics beyond the Standard Model. The storage and production of Ultra Cold Neutrons (UCN) are the focus of deep interest. Intense activity at both cold and UCN beams have improved the experimental techniques themselves: shaping and analysis of polarised and unpolarised cold neutron beams, neutron spectrometry, revealing the phenomenon of small energy changes of UCN in bottles. The first P-odd asymmetry measurement with a light nucleus (^{10}B) has been carried out at the new high-intensity ballistic super-mirror neutron guide for cold neutrons H113 (PF1B) which has allowed an unprecedented precision better than 10^{-7}. Recent and intensive studies of asymmetries in polarised cold neutron induced fission have already yielded big surprises and further exciting physical results are expected soon.

Modelling and Theory

- **Mark Johnson**, Leader of Computing for Science
  http://www.ill.fr/Computing/club.html
- **Efim Kats**, Leader of Theory Group
  http://www.ill.fr/Colleges/C2/TheoryCollegeHome.html

Interpreting and understanding scientific data requires numerical and theoretical models. In this "Modelling and Theory" section, modelling refers to systems of interacting atoms and molecules in the solid state, where atom-atom interactions allow the evolution of the system to be calculated and (meta-) stable structures to be determined. Force-field based methods are applied here in Monte Carlo search routines to probe binding sites for gas atoms/molecules in bundles of nanotubes, which are otherwise characterised by neutron diffraction and thermodynamic techniques. Solid state first principles calculations must be used when more accurate energies and forces are required. Here they are used to gain insight into the energies associated with disorder in molecular crystals and therefore the nature of disorder at elevated temperatures. Elsewhere in this Annual Report (Cowan et al.) these quantum chemistry methods are used to accurately calculate vibrational spectra of hydrogen bonded systems from known crystal structures without any refinement of force constants. Finally, modern Monte Carlo search routines have also been used to determine the structure of phase III of methane, a problem of more than 30 years standing. Consequently the complex tunnelling spectra of methane have been interpreted and shown to be consistent with the new structure.

Theoretical models are required when systems, or the length scale of phenomena being studied, become too big for direct atomistic simulations. This is the case for mesoscale charge transfer along DNA molecules which is modelled here by Bicout and Kats in terms of unistep superexchange and multistep hopping. The hypothesis that both charge transfer mechanisms depend on the interaction between electronic degrees of freedom and molecular vibrations will be tested directly when the vibrational modes can be modelled with solid state quantum chemistry methods. Furthermore, recent quasielastic measurements at the ILL of the dependence of DNA dynamics on the level of hydration and temperature (Annual Report 2000, page 56) suggest that these factors could also affect the charge transfer rate.

Field effect on the phase segregation in the electron doped mixed valence manganite $Sm_{0.15}Ca_{0.85}MnO_3$

C. RITTER (ILL)

P.A. ALGARABEL, J.M. DE TERESA, L. MORELLON AND M.R. IBARRA (UNIVERSITY OF ZARAGOZA)

Using high resolution neutron diffraction and small angle scattering the existence of nano- and microscopic phase segregation above and below T_N was studied in the electron doped manganite $Sm_{0.15}Ca_{0.85}MnO_3$. The different nature of the coexisting phases and their field and temperature dependence are explained considering the interplay of magnetic and structural correlations, which give rise to different structural and magnetic ground states (P-Pnma, G+F-Pnma, G-Pnma, C-$P2_1/m$).

Mixed valence perovskites of type $R_{1-x}A_xMnO_3$ (R=rare earth, A= earth alkaline) are famous for their large magnetoresistance effect called CMR ("Colossal magnetoresistance"). For compounds with x = 1/3, the intrinsic origin of the CMR effect was explained in terms of nanoscopic phase segregation in the paramagnetic phase (magnetic polarons, see ILL Annual Report 1997).

Although less common, the CMR effect exits also in the electron doped compounds with $0.8 < x < 0.9$. This report presents recent work on $Sm_{0.15}Ca_{0.85}MnO_3$[1]. Similar behaviour can be found in $Bi_{0.15}Ca_{0.85}MnO_3$ [2] and $Tb_{0.15}Ca_{0.85}MnO_3$ [3]. $Sm_{0.15}Ca_{0.85}MnO_3$ exists in a paramagnetic state with an orthorhombic Pnma crystallographic structure (P-Pnma); at 120 K a first order magnetic transition to a C-type antiferromagnetic state takes place. This transition is accompanied by a structural transformation into the monoclinic $P2_1/m$ phase. The structural transformation does not extend over the whole sample volume and even at low temperatures a small fraction of the volume sample remains in the Pnma crystallographic structure with a G-type antiferromagnetic structure (G-Pnma phase). The volume fraction of both phases as a function of temperature and applied magnetic field were determined using the high resolution diffractometer D2B. Figure 1 shows the thermal dependence of the volume phase fraction of the two magnetic and crystallographic phases (C-$P2_1/m$ and G-Pnma) in zero field and under an applied magnetic field of 6 T. At zero magnetic field, the majority phase is C-$P2_1/m$ with a phase fraction in volume of more than 90% in the temperature range studied (figure 2a). Under an applied magnetic field of 6 T the amount of Pnma phase growths (figure 2b), this increase being more important as we approach T_N from lower temperature. This behaviour clearly indicates that the magnetic and crystallographic structures can be reversed by applying a magnetic field.

It should be underlined that under the application of a magnetic field a ferromagnetic contribution to the Bragg reflections appears as the Pnma phase fraction increases (figure 2b). Therefore it is postulated that another metastable state exists in this compound: the ferromagnetic orthorhombic state (F-Pnma phase). This phase has not been detected at zero magnetic field, however, the existence of G-Pnma and F-Pnma at zero magnetic field was found in the case of $Sm_{0.1}Ca_{0.9}MnO_3$ [4].

The neutron diffraction measurements performed in the ordered region are able to explain the origin of the CMR-effect as resulting from a structural transition from a high-resistivity , high-volume, spontaneous C-$P2_1/m$ (monoclinic) phase to a low-resistivity, low-volume ferromagnetic Pnma (F-Pnma, orthorhombic) phase induced by the applied magnetic field.

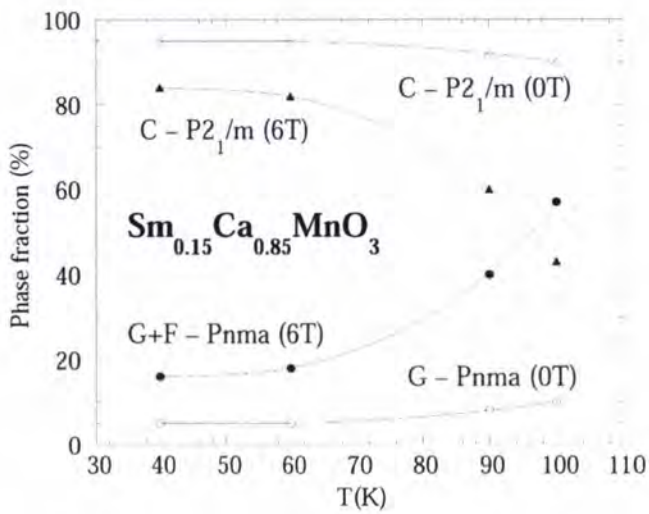

Figure 1: Thermal dependence of the two spontaneous low temperature magnetic and crystallographic phases in zero field and under an applied field of 6 T.

Having established the phase separation at T_N and its sensitivity to an applied field we decided to use small angle neutron

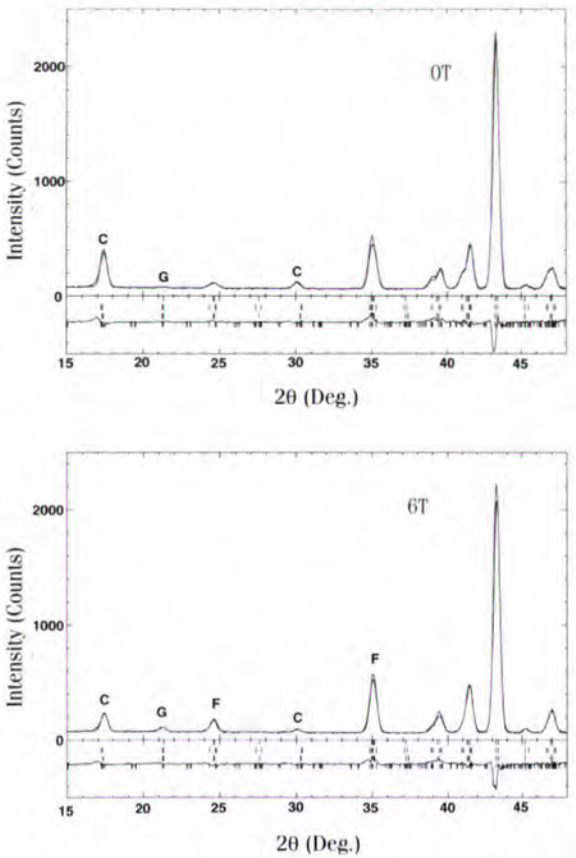

Figure 2: Low angle part of the high resolution neutron diffraction spectra of $Sm_{0.15}Ca_{0.85}MnO_3$ a) at 0 T, b) at 6 T.
C and G label magnetic peaks originating from antiferromagnetic C-type or G-type magnetic order while F labels ferromagnetic peaks.

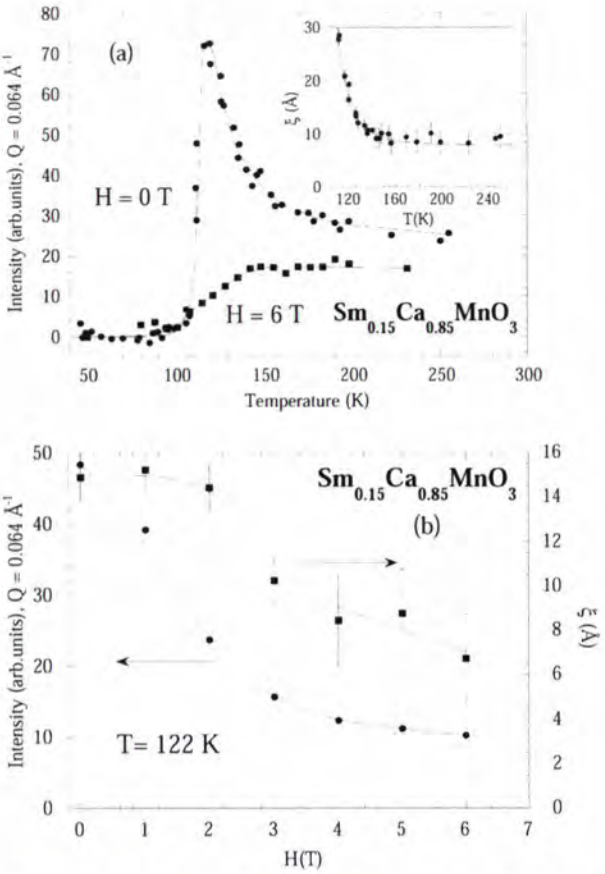

Figure 3: a) Thermal dependence of the SANS intensity at a fixed Q value (Q=0.064 Å^{-1}) in zero field and under a field of 6 T. The inset shows the temperature dependence of the correlation length of the monoclinic clusters. b) Field dependence of the SANS intensity and the correlation length at T = 122 K.

scattering (SANS) in order to get further information about the nanoscopic behavior of the sample. In figure 3a we show the thermal dependence of the SANS intensity at a fixed Q value (Q = 0.064 Å^{-1}) after subtraction of the incoherent nuclear contribution as measured on D16. We can observe a sharp increase below 150 K, which drastically disappears below $T_N \approx 112$ K. This is an indication of the existence of clusters above T_N. The size of these clusters can be associated with the correlation length ξ, which tends to diverge as we approach the structural transition (see the inset of figure 3a). Since the low temperature phase is the monoclinic $P2_1/m$, one can explain the spontaneous SANS results assuming a nucleation process below 150 K in which well-defined monoclinic nanodomains are formed. Under an applied magnetic field, this nucleation process is suppressed (figure 3a). This assumption is corroborated by the study of the SANS intensity and the correlation length under field at 122 K, e.g. just above T_N, as shown in figure 3b. The decrease of the SANS intensity under field as shown in figure 3b confirms the suppression of this nucleation process, i.e. the $P2_1/m$ nanodomains are unstable under field, and consequently the correlation length decreases. This magnetic field behavior discards the existence of Pnma ferromagnetic clusters, because the F-Pnma phase is stable under applied magnetic field according to the neutron scattering experiments.

Summarising, the CMR and magnetovolume effects observed in electron-doped $Sm_{0.15}Ca_{0.85}MnO_3$ have their origin in the induced magnetic and crystallographic transition. We propose that this structural and electronic instability occurs due to in the coexistence of different metastable ground states, G-Pnma, G+F-Pnma, P-Pnma, C-$P2_1/m$, very close in energy. This gives rise to nanoscopic phase segregation in the paramagnetic phase close to the transition temperature and microscopic phase segregation at low temperature. Under an applied magnetic field the G+F-Pnma state is the most stable phase at low temperatures. ■

References

[1] P.A. Algarabel et al., Phys. Rev. B (accepted)
[2] A. Llobet et al., Chem. Mater. 12 (2000) 3648
[3] J. Blasco et al., Phys. Rev. B 62 (2000) 5609
[4] M. Respaud et al., Phys. Rev. B 63 (2001) 144426-1.

Spherical neutron polarimetry and anisotropic magnetic excitations in UO_2

R. Caciuffo (INFM, University of Ancona)

P.J. Brown and M. Enderle (ILL)

G.H. Lander (Institute for Transuranium Elements, Karlsruhe)

J.A. Paixão (University of Coimbra)

Spherical neutron-polarimetry has been applied to study the nature of magnetic fluctuations in the ordered phase of uranium dioxide. The rotation of the neutron polarisation at magnetic Bragg peaks is consistent with a transverse 3k magnetic structure with [0 0 1] propagation vector. Unexpected, anomalous behaviour is exhibited by the lowest energy spin-wave branch for which no components of the transverse fluctuations are observed along the magnetic propagation vector.

Spherical neutron polarimetry (SNP) [1] has proved to be very useful in determining complex magnetic structures [2], but has not, as yet, often been associated with inelastic scattering studies. Although general expressions for the cross section and polarisation of the scattered neutrons were derived almost 40 years ago [3,4], only one recent paper can be found in the literature where the results of inelastic scattering experiments with three-dimensional polarisation analysis are reported [5]. Such experiments can in principle give a wealth of information on the interaction between electronic, spin and vibrational degrees of freedom in strongly correlated electron systems. For this reason, considerable efforts are being made at the ILL to develop a reliable and user-friendly implementation of SNP for inelastic scattering.

Here, we give a brief account of the results we have obtained on uranium dioxide using IN20 equipped with the CRYOPAD-II device, in place of the adiabatic coil arrangement normally employed for standard, uniaxial polarisation analysis. Although we did not observe the rotation of the neutron spin which could be given by interference between nuclear and magnetic scattering [5], we show that information not attainable with conventional techniques can easily be obtained in experiments with CRYOPAD on a triple-axis spectrometer. Uranium dioxide is one of the most studied actinide systems [6]. Above $T_N = 30.8$ K, UO_2 is a paramagnetic semiconductor with the face-centred cubic fluorite structure. Below T_N, a type-I triple k antiferromagnetic structure is established, with each Fourier component $\mathbf{m}_k$ perpendicular to its propagation vector $\mathbf{k}$. $\mu_{ord} = 1.74\ \mu_B$ at T = 4.2 K. The magnetic transition is accompanied by a small internal distortion of the oxygen sublattice.

Using CRYOPAD it is possible to drive the polarisation $\mathbf{P}_i$ of the incident neutron beam along any given direction, and to analyse both the longitudinal and the transverse components of $\mathbf{P}_f$, the polarisation of the scattered beam. In this way, all sixteen correlation functions defining the most general expression of magnetic neutron scattering [2,3] can be measured. The experiment was performed on a large (99 g) single crystal mounted with [1-10] vertical. CRYOPAD was installed on the triple-axis spectrometer IN20, which was operated in the fixed-$\mathbf{k}_f$ mode ($k_f = 2.662$ Å^{-1}), with the standard, Heusler-Heusler, monochromator-analyser configuration. The rotation of the neutron polarisation scattered with zero energy-transfer by magnetic Bragg reflections was checked and found to be consistent with the transverse 3-$\mathbf{k}$ magnetic structure, with <0 0 1> propagation vector.

Measurements were made at inelastic positions, spanning the whole magnetic Brillouin zone. An example of the results obtained for the excitations belonging to the lowest energy magnon branch propagating along the [0 0 ζ] direction [6] is shown in figure 1. The three panels on the left show neutron groups measured in a constant-Q, longitudinal scan at $\mathbf{Q} = (0\ 0\ 1.25)$, the three panels on the right show results at the same point of the dispersion curve but measured in a transverse scan at $\mathbf{Q} = (1\ 1\ 0.25)$. The red and blue symbols correspond, respectively, to intensities measured of neutrons scattered with spin up and down with respect to the chosen analysis direction. A difference between these two counts implies a component of polarisation of the scattered beam in this direction.

To understand the results from the CRYOPAD it must be recalled that only components of magnetic fluctuation amplitudes perpendicular to the scattering vector act on the neutron polarisation [1,2]. Of these, those parallel to the neutron polarisation leave it unchanged, whereas the components that are perpendicular lead to a precession of the neutron spin about that fluctuation component by 180°. As usual, the x direction is defined along

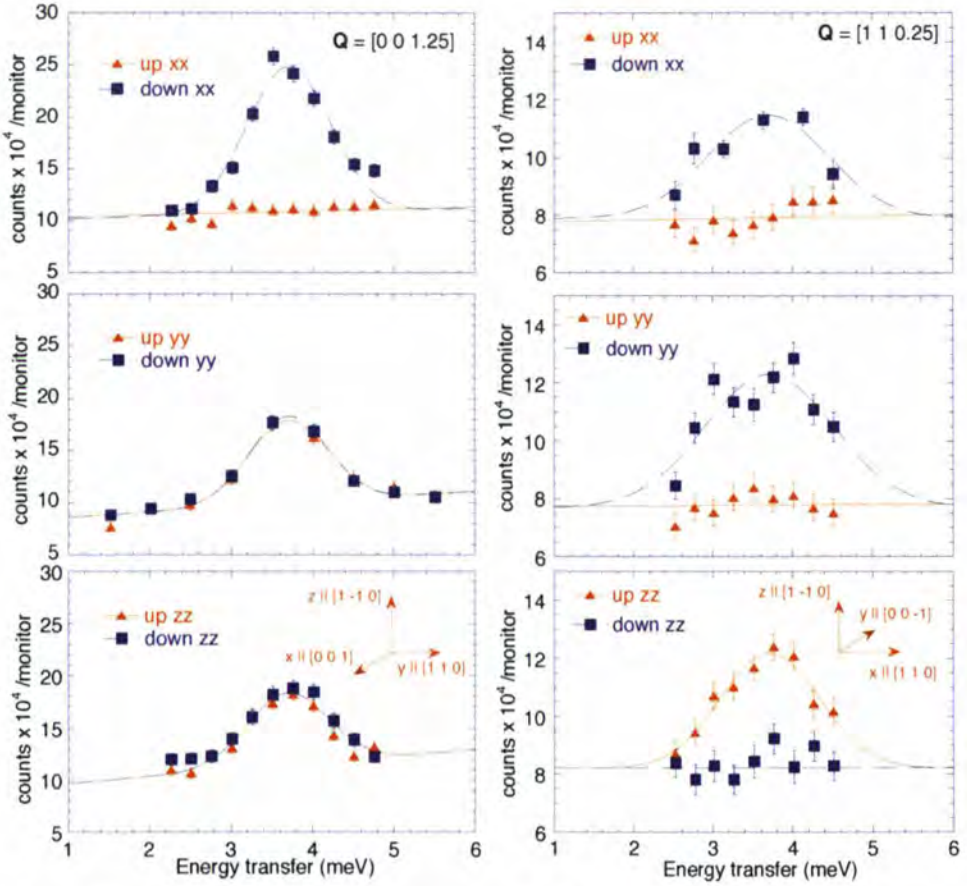

Figure 1: Constant-**Q** scans for four different polarisation channels. Data are collected at 5 K and correspond to a magnon excitation belonging to the lowest energy spin wave branch. The *x*-axis is parallel to the momentum transfer **Q**, so that it is along the [0 0 1] direction for the left of the figure, but along the [1 1 0] direction on the right. The *z*-axis is vertical, and always parallel to the [1 –1 0] direction. The *y*-axis completes a right-handed Cartesian frame (along [1 1 0] for the left panels and [0 0 -1] for the right panel). Labels such as *xy* refer to a situation in which the initial polarisation vector is parallel to *y* and the *x* component of the final polarisation is analysed.

the momentum transfer Q, y perpendicular to Q in the scattering plane and *z* perpendicular to the scattering plane. The results for Q parallel to [0 0 1] show that the polarisation along *x* is reversed if $\mathbf{P}_i$ is along *x*, but the beam is depolarised both along *y* and *z* if it is initially polarised along these directions. This shows we have two components for the transverse fluctuation, which is a normal situation with fluctuations both along *y* and *z*. On the other hand, if Q is parallel to [1 1 0], the components of the inelastic fluctuations should also be *y* and *z*. Surprisingly, the polarisation of a beam initially aligned along *z* is preserved along that same direction ($P_{fz} > 0$), but is *reversed* when the initial alignment is along *x* and *y* ($P_{fx} < 0$; $P_{fy} < 0$). This requires there to be no fluctuations along *y*, i.e. *no components of the fluctuations are present along the magnetic propagation vector*. All inelastic fluctuations must be confined to the (1 1 0) plane perpendicular to [0 0 1]. This is confirmed by the observation that $P_{fy} = 0$ when $\mathbf{P}_i$ is along *z*. The same behaviour is observed all along the lowest-energy magnon branch, which is one that has been assumed to be strongly hybridised with a transverse acoustic phonon.

A different behaviour is observed for the two highest-energy branches. The results obtained indicate isotropic fluctuations, not only at the magnetic and nuclear zone centres, but also within the whole Brillouin zone.

Despite the fact that we anticipated observing "mixed" magnon-phonon excitations in UO_2, and, as a result, cross terms of the form *xy*, *xz*, etc in the polarisation dependence, no such off-diagonal terms were observed in the polarisation matrix. However, the observation of an unexpected anisotropy in the lowest-energy magnon is a theoretical challenge. Is this a consequence of the magnon-phonon interaction, the 3-**k** magnetic configuration of UO_2, or of an anisotropy induced by the large orbital moment of the 5*f* electrons? More experiments and theory are needed, but our unexpected results show what a new instrumental technique can bring to an old and apparently well understood system. ■

References

[1] P.J. Brown et al., Proc. R. Soc. (London) A 442 (1993) 147 ; F. Tasset, Physica B, 297 (2001) 1 • [2] P.J. Brown et al., J. Phys.: Condens. Matter, 10 (1998) 663, and refs. therein. • [3] M. Blume, Phys. Rev. 130 (1963) 1670 • [4] S.V. Maleyev et al., Sov. Phys. Solid State 4 (1963) 2533 • [5] L.P. Regnault et al., Physica B 267-268 (1999) 227 • [6] R. Caciuffo et al., Phys. Rev. B 59 (1999) 13892.

Charge order in α-NaV_2O_5: complementarity of neutrons and synchrotron radiation

J.E. Lorenzo, S. Grenier and Y. Joly (Lab. Cristallographie, CNRS Grenoble)

B. Grenier and L.P. Regnault (DRFMC, CEA Grenoble)

O. Cepas, T. Chatterji, A. Hiess and T. Ziman (ILL)

J.P. Boucher (Lab. Spectrometrie Physique, UJF Grenoble)

The nature of the charge ordering in α'-NaV2O5 has fascinated the scientific community during the last years, and the determination of its 3D configuration have challenged both theory and experiments. A variety of experimental techniques have been used, each contributing to a partial but nevertheless incomplete picture of the charge ordering pattern. In view of this we have attempted a different approach, that is the use of rather unconventional crystallographic methods. As we shall explain below it is the combination of inelastic neutron scattering performed at the ILL triple axis spectrometers IN8 and CRG/CEA-IN22 with resonant X-ray diffraction experiments performed at the ID20 ESRF beamline that has led us to solve this problem.

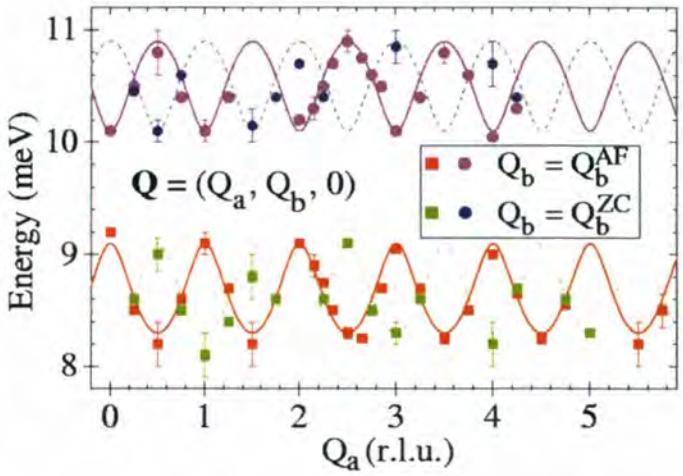

Figure 1: The excitation spectra of α'-NaV_2O_5 is composed of 2 different branches with an energy gap centred at 9.6 meV. Here the dispersion of the two excitations is shown along a*-direction at 2 different Q_b positions. The structure factor of the upper ones is labelled as $S_{b+}(Q_a)$ and that of the lower ones as $S_{b-}(Q_a)$. The curves are theoretical predictions fitted to the data.

The problem of charge ordering in α'-NaV_2O_5 has been widely discussed since the early stages of the work. Indeed the room temperature structure was believed to contain 2 different V-sites, with valence states V^{4+} (of electronic configuration $3d^1$ carrying a S=1/2) and V^{5+} ($3d^0$). Recent refinements [1] turn out to consistently converge towards a more symmetric space group with only one V-site assigned as $V^{4.5+}$. Interestingly, this compound undergoes a rather unusual antiferromagnetic order below T_C=34K, characterised by a S=0 non-magnetic ground state separated from the first S=1 excited state by an energy gap: only the excitations carry on the magnetic signature of this new state. In addition, a structural distortion develops below T_C resulting in the appearance of superlattice peaks of modulation wavevector q=(1/2, 1/2, 1/4) [2]. These two very peculiar features are present in the canonical Spin-Peierls compound $CuGeO_3$, and have led, in a first place, to consider α'-NaV_2O_5 as the second inorganic compound belonging to the Spin-Peierls family.

The analysis and understanding of the low temperature structure is the goal of this work. On the basis of physical considerations, several theoretical models of charge ordering have been proposed [3], as for instance an alternating order of V^{4+} and V^{5+} *in-line* chains or a *zig-zag* arrangement of both species in the rungs of the ladders. Previous X-ray and neutron structural refinements have been hindered by the large size of the unit cell (2a 2b 4c) and therefore by the large number of uncorrelated parameters present in the refinement. From conventional X-ray diffraction experiments (and refinement) different groups [4] have proposed the solution where only half of the ladders are distorted, which turns out to be in disagreement with, among others, the number of distinct sites found in ^{51}V and ^{23}Na NMR studies [5] and with the number of vibration modes observed in Raman scattering experiments [6].

Another way to access the complex electronic re-distribution occurring below the phase transition is by analysing the structure factor of the magnetic excitations [7]. The magnitude of the dispersion of these excitations reflects the low dimensionality of the magnetic interactions.

very dispersive along b* (J_b=60 meV) and nearly dispersionless perpendicular to b* ($\Delta J \sim 1$ meV) (figure 1). Magnetic excitations are supposed to be S=1 triplets, involving two spins in neighbouring rungs, and the spin density in the rung can be directly correlated to electronic density. For simplicity we have purposely misused the V^{4+} and V^{5+} chemical notation to distinguish between both sites in the rung, although each spin is associated with a two-sites electronic wavefunction that depends on the charge density of the rung.

The structure factor of magnetic excitations have been measured along two reciprocal space directions (Q_{a^*}, Q_{b^*}, 0) with $Q_{b^*}=Q^{ZC}_{b^*}=1/2$ and $Q_{b^*}=Q^{AF}_{b^*}=1$ (figure 2). Note that the choice $Q_{c^*}=0$ facilitates the calculation as the excitations are projected onto the (a^*-b^*)-plane, at the expense of a loss of information on the actual arrangement of the four layers stacked along the c-direction. From this figure one can immediately see that the in-line chain model can be disregarded as, contrary to what has been observed, it should give zero intensity along the $Q_{b^*}=1$ line. The experimental data agrees well with the picture where all ladders are modulated in *zig-zag*, with a *fitted* charge transfer parameter amounting to 0.3 e (solid lines).

Although the X-ray resonant scattering results [8], not covered here in any detail, are self-contained, the picture issued from inelastic neutron scattering data analysis is fundamental and has served to identify possible solutions and finally to determine the 3D charge order arrangement. The charge ordering pattern deduced from the X-ray results is rather complex, with several *degenerated* possibilities of stacking of layers along the c-direction (figure 3). Similarly to the neutron data, the deduced charge transferred is rather small (0.1 e) and both results are striking when compared to the bond-valence analysis of the V-O distances that yields a charge transfer of 0.5 e. Finally, and as conclusion, this compound illustrates well how complex the picture of the spin-singlet quantum ground state can be, as well as the manifold of interactions with the underlying lattice. ■

Figure 2: Structure factors (a) $S^{AF}(Q_a)$ and (b) $S^{ZC}(Q_a)$ for the two magnetic branches. Stars represent the sum of structure factors of both branches and the solid line is a fit to a *zig-zag* model where the correction due the V^{4+}, S=1/2, magnetic form factor has been included.

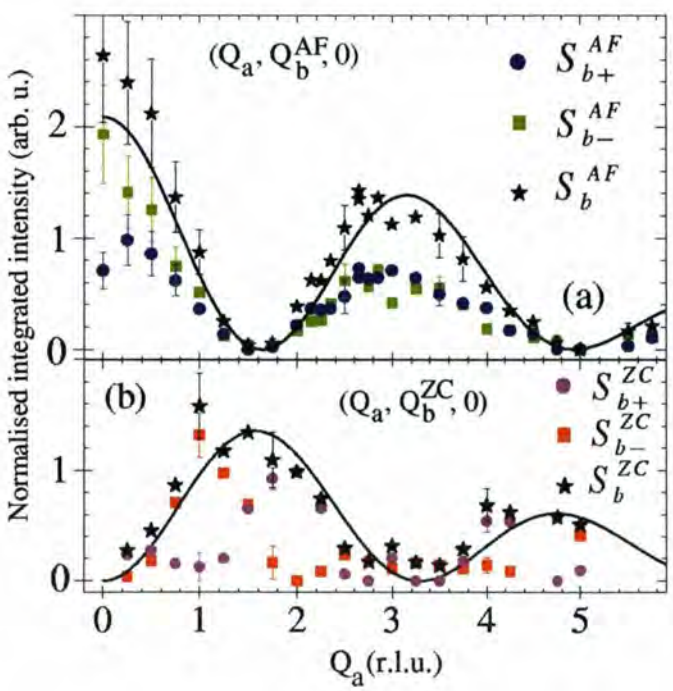

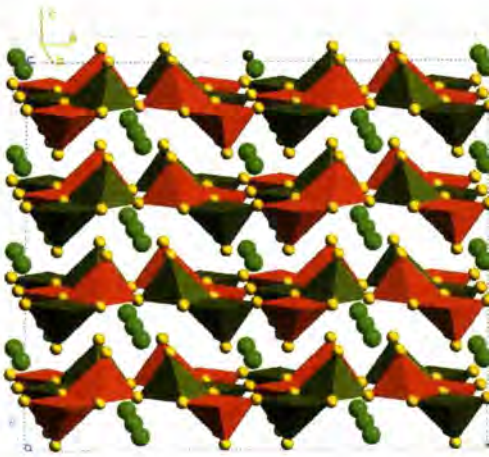

Figure 3: One of the four possible models of charge ordering of α'-NaV_2O_5 low temperature structure, as obtained from the X-ray resonant scattering experiments [8]. Ladders of pointing-upwards and downwards pyramids alternate along the a-axis and run along the b-direction. Inelastic neutron scattering data shown in figures 1 and 2 [7] have been obtained through a single layer model, corresponding to the first layer from the top. Green(red) pyramids represent large(small) charge densities, V^{4+}(V^{5+}) in the chemical notation. Vanadium atoms are located inside the pyramids, closer to their corresponding apical oxygen (in yellow).

References

[1] H.Smolinski, et al., Phys. Rev. Lett. 80, 5164 (1998); A. Meetsma, et al., Acta Cryst. C 54 (1998) 1558; H.G. von Schnering, et al., Z. Krystallogr. 213 (1998) 246 • [2] Y. Fujii, et al., J. Phys. Soc. Jpn. 66, 326 (1997); T. Chatterji, et al., Sol. State Commun. 108 (1998) 23 • [3] M. Mostovoy and D. Khomskii, cond-mat/9806215; H. Seo and K. Fukuyama, J. Phys. Soc. Jpn. 67 (1998) 2602; J. Riera, et al., Phys. Rev. B 59 (1999) 2667 • [4] J. Ludecke, et al., Phys. Rev. Lett. 82 (1999) 3633 • [5] Y. Fagot-Revurat, et al., Phys. Rev. Lett. 84 (2000) 4176 • [6] M.J. Konstantinovic, et al., Sol. State Commun.112 (1999) 397 • [7] B. Grenier, et al., Phys. Rev. Lett. 86 (2001) 5966 • [8] S. Grenier, et al., submitted to Phys. Rev. Lett. (August 2001) and cond-mat/0109091.

Switching off quantum mechanics

M.E. Enderle (ILL)

H.M. Rønnow (CEA, Grenoble)

A. Klöpperpieper
(University of Saarbrücken)

An array of little compass needles with well-defined directions is the classical picture of an ordered magnetic material. Magnetic excitations – spin waves – are small oscillations of the needles about their ordering direction. However, quantum mechanics dictates a minimum size S = 1/2 of the spin, which then can only fluctuate between up and down relative to a given direction. A linear array of such spins 1/2 coupled by antiferromagnetic interaction is perhaps the most fundamental macroscopic quantum system. Here, as a consequence of Heisenberg uncertainty principle for many coupled particles, quantum fluctuations destroy the classical order, so that the direction of an individual spin becomes undefined. Only the quantum mechanical states of the entire coupled "chain" of spins are well-defined. The magnetic excitation spectrum reflects that the excited states are multiparticle wave functions like the groundstate and not small oscillations of compass needles around a preference direction. However, it is possible to "switch off" the macroscopic quantum behaviour of the spin 1/2 chain: applying a large magnetic field restores the classical individual of compass needles. This is demonstrated on $CuSO_4.5D_2O$ which almost ideally realises isolated antiferromagnetic chains of spins 1/2 [1].

In insulators, the dominant interaction between spins is superexchange. The description of its symmetry – a scalar product of neighbour spins – is nevertheless difficult to treat theoretically for small spin values. Large spins can be regarded as vectors; this even works for spins 1/2 if the interaction is ferromagnetic and if the spins align parallel to each other. Néel introduced antiparallel compass needles as the corresponding groundstate for antiferromagnetic interactions. However, the antiferromagnetic spin 1/2 chain never orders into a Néel state. Instead the interaction binds the spins into a macroscopic wave function, a chain state. If this groundstate is depicted within a basis of individual compass needle states, one observes quantum fluctuations, which destroy the Néel state. If the quantum fluctuations occurred as a function of time (like thermal fluctuations), snapshots could be taken within the basis of individual compass needle states. Each snapshot would show typical arrangements of neighbouring needles. In such a snapshot of the groundstate (figure 1) large parts of the chain look like the Néel state – up to a domain wall where the order is reversed. The next snapshot would show that the domain wall has moved somewhere else. The average over these quantum fluctuations leads to an expectation value of zero for the individual spin states.

In this picture, the elementary excitation is represented by an additional domain wall introduced into the ground state, the so-called spinon. It should be seen as a delocalised mode, defined by a momentum k and the energy $\pi J |\sin kd|$ (d is the distance between the spins) [2]. As a single domain wall carries spin 1/2, neutrons can only excite pairs of domain walls. The domain walls are independent – a given momentum transfer k can excite all pair combinations with $k = k_1 + k_2$. The corresponding band of energy transfers $E(k) = E_1(k_1) + E_2(k_2)$ ranges from $E(k) = \pi J |\sin kd|$ to $2\pi J |\sin kd/2|$. Spin waves, in contrast, correspond to a spin flip of one compass needle [3]. When delocalised over the whole chain, they resemble small oscillations of the compass needles about some ordering direction. Such a spin flip is a domain wall pair, bound to a minimum dis-

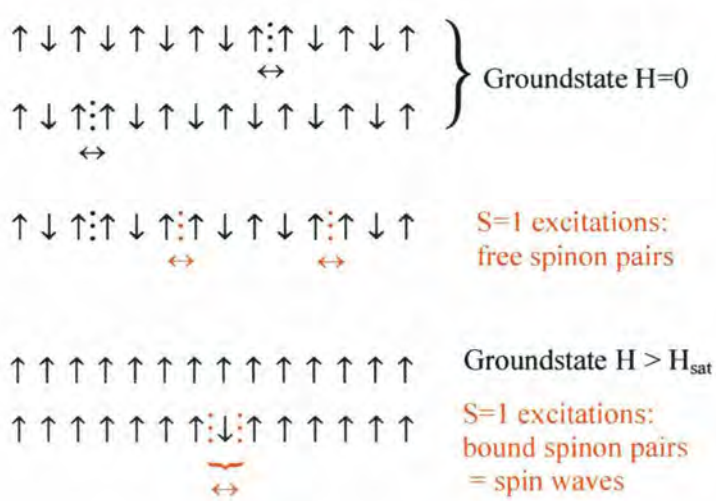

Figure 1: Above: "Snapshots" of the groundstate of the spin 1/2 antiferromagnetic Heisenberg chain, and of its magnetic excitations, pairs of free domain walls. Below: The ground state at saturation is static, its excitations discrete spin-waves – a domain wall pair bound to minimum distance.

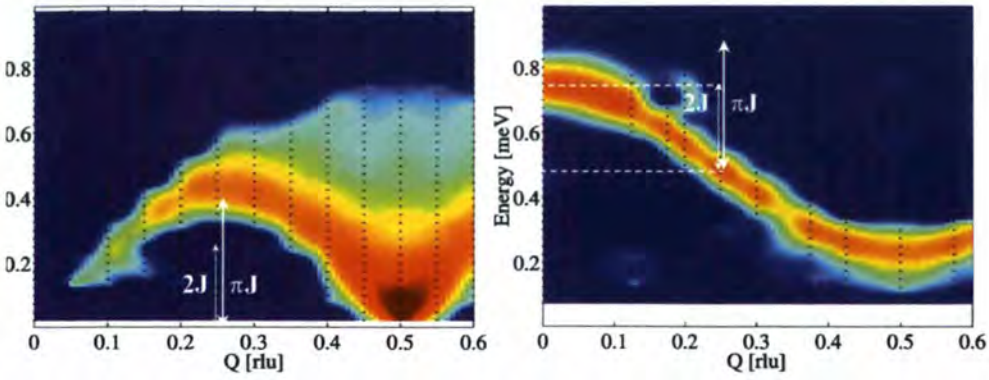

Figure 2: Excitation spectrum of the one-dimensional antiferromagnetic chains in $CuSO_4.5D_2O$ at B = 0 (left) and B = 5 T (right), with the intensity transformed into a colour scale. The continuum of excitations at B = 0 collapses into a single discrete spin-wave branch at 5 T, and the amplitude of the dispersion shrinks from πJ to 2J. The black dots indicate the measured points.

tance. It would carry spin 1 and appear as a discrete branch at $E(k) = 2J | \sin kd |$ in the excitation spectrum. The quantum character of the spinon pair excitations is reflected in the continuous intensity distribution and the renormalisation factor $\pi/2$.

Applying a magnetic field will polarise the system and hence reduce the quantum fluctuations. In the saturated phase, the direction of the individual spin is recovered – it is parallel to the magnetic field (figure 2). The elementary excitation can be imagined as the flipping of one spin 1/2 into the unfavourable direction – a domain wall pair bound to minimum distance – hence a spin wave. Therefore, the excitation spectrum in the saturated phase should be a discrete branch, described by the unrenormalised dispersion relation of a classical compass-needle assembly, $E(k) = 2J (\cos kd + 1) + g\mu_B(H-H_c)$ [4].

The antiferromagnetic interaction of the isolated spin chains in $CuSO_4.5D_2O$ is sufficiently small to be overcome by a standard neutron magnet. This has allowed the comparison between classical and quantum excitation spectra of a spin chain for the first time on the same material, simply by applying a magnetic field. The experiment was performed on IN14 with k_f = 1.15 Å^{-1} and 77 K-Be-filter in k_i, equipped with an orange cryostat or the vertical 5.5 T cryomagnet and a dilution insert. The temperature of the mixing chamber was kept at 100 mK.

The left panel of figure 3 displays the excitation spectrum with momentum transfer along the chain axis at B = 0. The continuum of excitations is clearly visible, and the band width of the elementary excitations can be read from the maximum of the lower continuum boundary, 0.413 meV. The right-hand panel displays the excitation spectrum of the spin chains at B = 5 T. The width of the excitations is now resolution-limited, the dispersion is cosine-shaped– and the amplitude of the cosine has shrunk to 0.258 meV. These amplitudes of sine (cosine) determine directly the quantum renormalisation factor of the spin 1/2 chain. The observed factor of 1.60 agrees with the theoretical prediction of $\pi/2$ within 2%.

Figure 3 shows three scans at the antiferromagnetic zone center, at B = 0, 3.6 T and 5 T. The continuum scattering, clearly visible at B = 0, is absent at 3.6 T (just above the saturation field) as well as at 5 T, and a discrete excitation is observed instead.

The entirely altered excitation spectrum at large magnetic fields reflects the different character of the ferromagnetic and the antiferromagnetic groundstate: the continuous excitation spectrum at zero field is due to free spinon pairs, the fingerprint of the macroscopic quantum ground state of the antiferromagnetic spin 1/2 chain. The resolution limited peaks above H_c are discrete spin waves (bound domain wall pairs) – small perturbations of the fully magnetised state which is indistinguishable from a classical ferromagnetic ground state.

With the present and subsequent experiment it will be possible for the first time to study in detail how this evolution takes place. Here we have emphasised the remarkable feature that the continuum – and hence the macroscopic quantum behaviour – has been "switched off" by the large magnetic field. ■

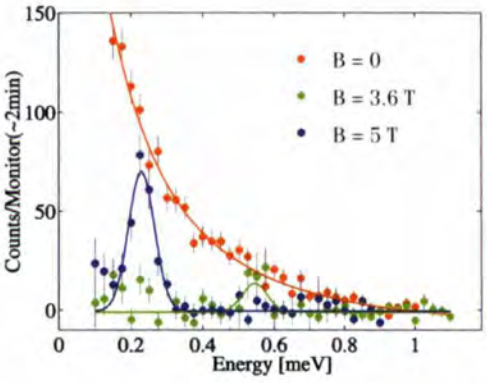

Figure 3: Scattered intensity of the antiferromagnetic chains in $CuSO_4.5D_2O$ (background subtracted): Scans at constant wave vector transfer corresponding to the antiferromagnetic zone center, at 100 mK. B = 0, 3.6 T and 5 T.

References

[1] L.J. de Jong and A.R. Miedema, Adv.Phys. 23 (1974) 1 • [2] G. Müller et al.; Phys.Rev.B 24 (1981) 1429; J.B. Bonner and J.C. Parkinson, Phys.Rev.B 32 (1985) 4703 • [3] E.G. H.-J. Mikeska and M. Steiner, Adv.Phys. 40 (1991) 191 • [4] E.G. K.H. Hellwege, Einführung in die Festkörperphysik, Springer-Verlag, 1981.

Unconventional superconductors:
how are the spins paired in ?

J.A. Duffy and S.M. Hayden (University of Bristol)

Y. Maeno and Z. Mao (Kyoto University and CREST, Japan Science and Technology Corporation)

J. Kulda and G.J. McIntyre (ILL)

We have studied the magnetisation density in the mixed state of the unconventional superconductor Sr_2RuO_4. On entering the superconducting state we have found no change in the magnitude or distribution of the induced moment for a magnetic field of 1 T applied within the RuO_2 planes. Our results are consistent with a spin-triplet Cooper pairing with spins lying in the basal plane. This is in contrast with similar experiments performed on conventional and high-Tc superconductors.

It is well known that superconductivity occurs when electrons pair up to form so-called Cooper pairs which condense into a macroscopic quantum state. The Cooper pairs are able to share the same quantum state because their quantum mechanical properties are different to those of the constituent electrons. The macroscopic nature of the quantum state gives the superconductor its unique properties. In the first superconductors to be discovered, such as mercury and lead, the Cooper pairs form with the spins of the constituent electrons aligned in an anti-parallel "singlet state", the total spin of the pair S = 0. In recent years many new forms of superconductivity have been discovered such as heavy fermions and high-temperature superconductors. Many of these materials have properties that are fundamentally different from the first superconductors to be discovered. In particular, the quantum state of the Cooper pair and attractive interaction that allows the Cooper pair to form are different. These materials are known as "unconventional" superconductors.

Sr_2RuO_4 is a recently discovered unconventional superconductor. Many of its physical properties, such as the electronic specific heat in superconducting state, are at variance with conventional behaviour. Soon after the discovery [1] of superconductivity in Sr_2RuO_4 it was proposed [2,3] that the superconductivity might be triplet (S = 1) in nature with a parallel alignment of the electron spins within the Cooper pairs. A signature of triplet superconductivity is the existence of finite spin susceptibility at low temperatures in the superconducting state. In a conventional singlet superconductor, the anti-parallel pairing of the spins causes the spin susceptibility to tend to zero at low temperatures. Clearly a measurement of the susceptibility in the normal state is trivial. However, the spin suscep-

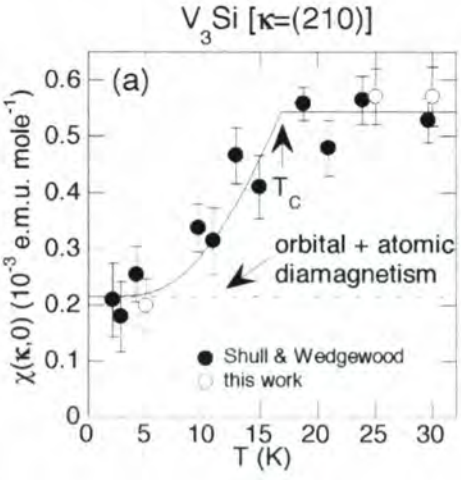

Figure 1: The susceptibility of the conventional s-wave singlet superconductor V_3Si measured by Shull and Wedgewood [4] using the present neutron scattering method. At low temperatures a residual orbital contribution to the susceptibility remains.

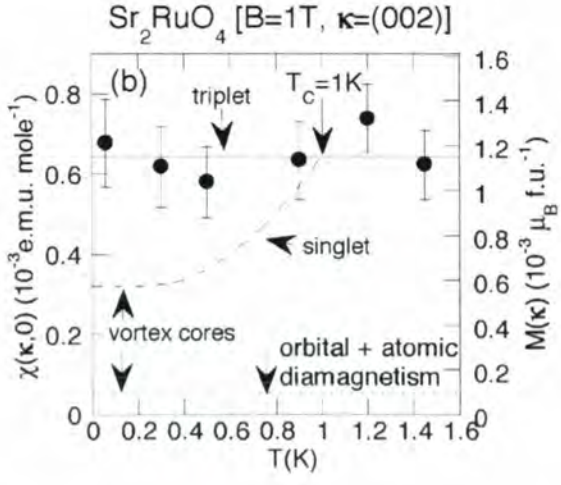

Figure 2: The temperature dependence of the susceptibility and induced moment of Sr_2RuO_4 measured using polarised neutron scattering. The dashed line is the Yosida [7] behaviour expected for a singlet-paired superconductor.

tibility in the superconducting state can only be measured by a microscopic probe such as neutron scattering. A direct measurement would only see the diamagnetism due to the Meissner effect.

The knowledge of the spin susceptibility in the superconducting state provides constraints on the pairing wavefunction of a superconductor. Such information can be obtained indirectly by nuclear-resonance techniques through the measurement of the polarisation of the *s*-electrons on a given site. Alternatively, neutron scattering can directly measure the magnetisation density induced by an applied magnetic field. A diffraction experiment allows the Fourier components of the magnetisation to be measured, even in the superconducting state. Experimentally we determine the flipping ratio R, defined as the ratio of cross sections for initial neutron-spin states that are parallel or antiparallel to the applied magnetic field and with arbitrary final spin state. This technique was first used by Shull and Wedgewood [4] to study V_3Si and more recently it has been applied to heavy-fermion [5] and high T_C [6] superconductors. In a conventional superconductor with spin-singlet pairing, the spin susceptibility is suppressed on entering the superconducting state because electrons with anti-parallel spins pair up. For $\boldsymbol{B}$ parallel to $\boldsymbol{B}_{c2}$ the temperature dependence is described by the Yosida function [7]. Wedgewood and Shull [4] observed a reduction of the susceptibility, due to the formation of spin singlets (S = 0). We have reproduced the Wedgewood-Shull result on V_3Si using the same experimental set-up as for our Sr_2RuO_4 measurements. Our results are consistent with Wedgewood and Shull and are shown as open circles in figure 1.

We have used the IN20 spectrometer to measure the induced magnetisation density in the mixed state of Sr_2RuO_4 [8] by polarised neutron diffraction. On entering the superconducting state we have found no change in the magnitude or distribution of the induced moment for a magnetic field of 1 T applied within the RuO_2 planes. Our results are consistent with a spin-triplet Cooper pairing with spins lying in the basal plane. This is in contrast with similar experiments performed on conventional and high-T_C superconductors, where the spin susceptibility is suppressed in the superconducting phase. Figure 2 shows the temperature dependence of the induced moment corresponding to the (002) Bragg peak in Sr_2RuO_4, for B = 1 T. This component was chosen for detailed study because its amplitude is proportional to the sum of the moments induced on the in-plane ruthenium and oxygen atoms ($\mu_{Ru}+2\mu_O$) above T_C =1 K. On entering the superconducting state ($T < T_C = 1$ K), we find that there is no change in this component of the induced moment within the experimental error. In contrast to the V_3Si measurement, we investigated Sr_2RuO_4 at relatively high fields, $B/B_{C2} = 0.68$, thus the presence of normal vortices leads to a significant density of quasiparticles and finite spin susceptibility in the mixed state. The dashed line in figure 2 is a Yosida function modified to include the finite susceptibility in a field: this prediction is still at variance with the data. Thus, the absence of a change in spin susceptibility is not compatible with spin-singlet or even-parity pairing.

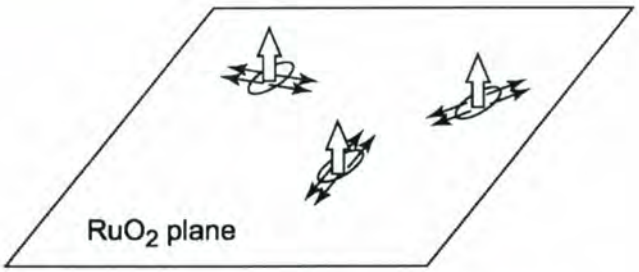

Figure 3: A schematic representation of triplet pairing in Sr_2RuO_4.

The absence of a change in the spin susceptibility can be explained if Cooper pairs form from electrons with parallel spins. Such "equal-spin pairing" (ESP) was first proposed in the context of ^{3}He by Anderson and Morel [9]. Within an ESP scenario the superconducting state is a superposition of the two possible (S = 1) parallel paired states. In an applied magnetic field, one state is favoured yielding a net spin moment and the same susceptibility as in the normal state [10]. An EPS-type pairing implies an odd-parity or spin-triplet state, thus the present experiment supports the notion that the superconducting wavefunction in Sr_2RuO_4 has an odd-parity representation and that this material can be identified as a "p-wave" triplet superconductor. ■

References

[1] Y. Maeno et al., Nature 372 (1994) 532 • [2] T.M. Rice and M. Sigrist, J. Phys.: Condens. Matter 7 (1995) 643 • [3] G. Baskaran, Physica B 223-224 (1996) 490 • [4] C.G. Shull and F.A. Wedgewood, Phys. Rev. Lett. 16 (1966) 513 • [5] C. Stassis et al., Phys. Rev. B 34 (1986) 4382 • [6] J.X. Boucherle et al., Physica B 192 (1993) 25 • [7] K. Yosida, Phys. Rev. 110 (1958) 769 • [8] J.A. Duffy, S.M. Hayden, Y. Maeno, Z. Mao, J. Kulda, and G.J. McIntyre, Phys. Rev. Lett 85 (2000) 5412 • [9] P.W. Anderson, Basic Notions of Condensed Matter Physics. • [10] A.J. Leggett, Rev. Mod. Phys. 47, 404 (1975); J. C. Wheatley, ibid 47, 423 (1975).

Type II superconductivity:
vortex lattice in Nb behaves just as Abrikosov predicted

S.J. Levett, C.D. Dewhurst and R. Cubitt (ILL)

E.M. Forgan, P.G. Kealey and D. Fort (University of Birmingham)

Type II superconductivity is characterised by the 'mixed' or 'vortex' state where quantized lines of magnetic field thread a Type II superconductor to form a vortex lattice. With the intensity and resolution now available from small-angle neutron scattering (SANS) instruments, and suitable samples, it is possible to observe neutron diffraction from the vortex lattice up to the temperature or field range where superconductivity is destroyed. Here we report SANS measurements on an extremely pure sample of niobium. We show, in a way never demonstrated before, a beautiful confirmation of the Abrikosov [1] picture of the vortex lattice to a temperature within 20mK of the upper critical field line.

The last fifteen years or more has seen an enormous increase in research activity in superconductivity, primarily due to the discovery of the so-called High-Temperature-Superconductors in 1986 [2]. These, and other subsequently discovered 'unconventional' superconductors typically boast one or more extreme physical properties including large anisotropy, strong thermal activation effects, unconventional pairing states, competition with magnetic order etc. The focus of topical research has lead to the discovery and publication of numerous significant articles that highlight the complex vortex behaviour in these systems where the vortex lattice has been observed to melt, de-couple between layers, disorder and entangle [3,4]. The focus of vortex lattice researchers has become finely tuned to, or at least come to expect, complex behaviour and possible thermodynamic transitions or crossovers in the magnetic field - temperature superconducting phase diagram.

Vortex physics has come a long way since the first theoretical prediction of Type II superconductivity and the vortex lattice by Abrikosov in 1957 [1]. The Abrikosov behaviour of vortices has mostly been relegated to a special case in the limelight of one or more vortex lattice phase transitions in the new materials. Here we demonstrate the intrinsic behaviour of vortices in pure niobium, one of the few elemental type II superconductors. A previous report [5] claims evidence for melting of the vortex lattice in Nb where a liquid-like ring of diffracted intensity had been observed at high temperatures. On the other hand, a coincident 'peak effect' in the magnetisation suggests that this data is more consistent with a static disordering (pinning) of the vortex lattice at high temperatures by crystal impurities or defects [4]. Our data confirms the Abrikosov picture of the vortex lattice to a temperature within 20 mK of the upper critical field line, $B_{c2}(T)$ in an extremely pure sample of Nb. In this article we show no melting, decoupling, disordering or entanglement phase transitions or crossovers. Rather, a clean demonstration of classic Type II superconductivity.

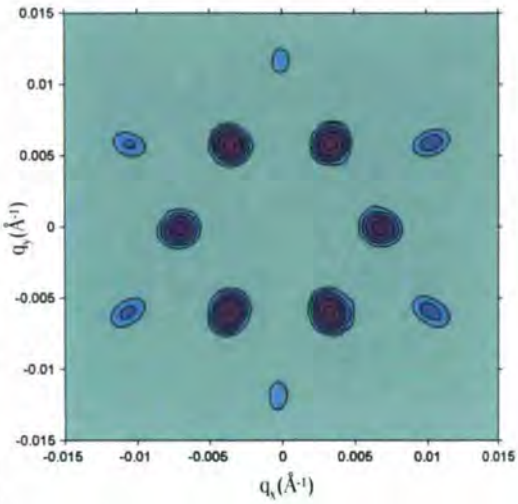

Figure 1: Diffraction pattern on the D22 SANS multidetector from the vortex lattice at 3.2 K and 0.2 T (background subtracted, logarithmic scale).

A high quality Niobium single crystal sample [6] was prepared and mounted in a sapphire-windowed cryostat between the pole pieces of an electromagnet on the D22 SANS diffractometer. A field of 0.2 T was applied parallel to the [111] direction and collinear with the incident neutron beam. D22 was used in a high-resolution mode using 10 Å neutrons with a 10% wavelength spread from a 30 mm aperture at a distance almost 20 m from the sample. The scattered neutrons were detected on a 128x128 pixel (each 7.5 mm^2) multidetector at a distance of 17 m from the sample.

The diffraction pattern from the vortex lattice obtained after cooling in a field of 0.2 T to 3.2 K is shown in figure 1. The image shown is the sum of counts obtained with the sample angle rocked vertically and horizontally to maximise each of the spots in turn at the appropriate Bragg angle. In a plot of intensity verses rocking angle, the

angular width of the peak gives the straightness of the vortex lines along the field direction. This, combined with the radial and azimuthal widths of the diffraction spots in the multidetector gives an indication of the perfection of the vortex lattice. Figure 2(a) shows the rocking curve width, determined by a Gaussian fit to the intensity verses rocking angle (inset) while figure 2(b) shows the radial and azimuthal widths of a two-dimensional Gaussian fit to the right-hand diffraction spot on the multidetector. It is clear from the temperature dependence of azimuthal spot width that at no temperature do the spots spread out into a ring as $B_{c2}(T)$ is approached (the $B_{c2}(T)$ boundary lies at a temperature ~ 5.4 K for an applied field of 0.2 T [6]). In fact, a steady decrease in the rocking curve width and small decrease in the radial width of the spot with increasing temperature indicates that in most respects the vortex lattice actually becomes more perfect as $B_{c2}(T)$ is approached. We note also that there is no hysteresis in figure 2 between increasing and decreasing temperature sweeps. All of these results are in complete accord with the absence of a first order transition or vortex lattice melting in this classic Type II superconductor.

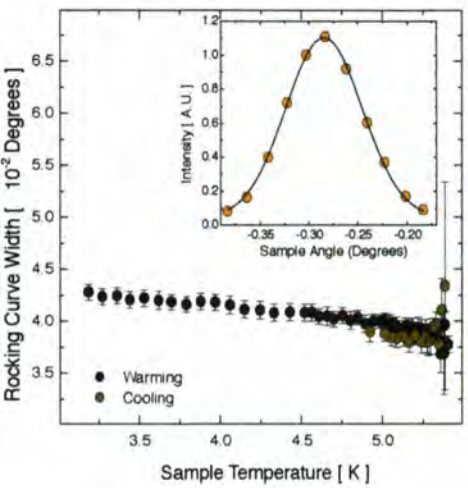

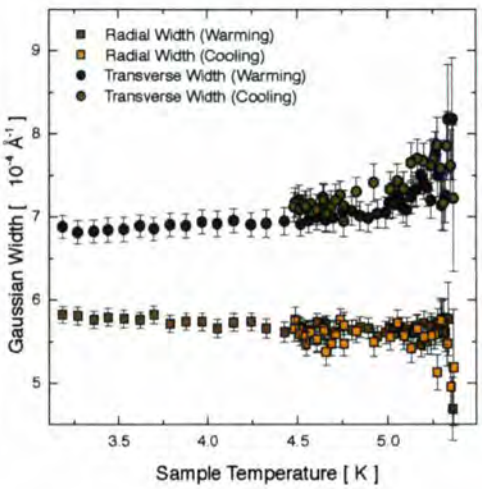

Figure 2: (a) Width of a Gaussian fit to the rocking curve (inset) for the [1,0] peak and (b) Radial and Transverse widths of a Gaussian fit to the [1,0] Bragg peak obtained at the peak of the rocking curve as a function of temperature.

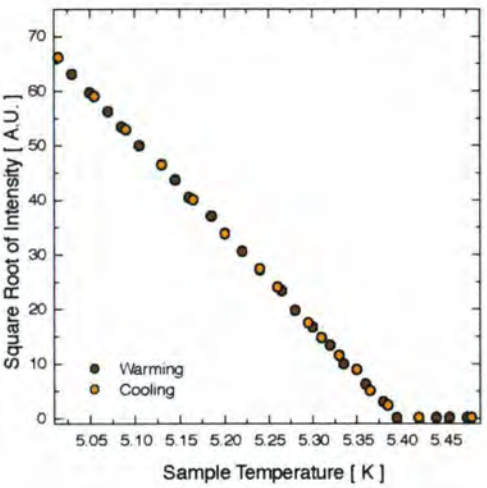

Figure 3: Square root of the rocking-rocking-curve-integrated intensity of the [1,0] Bragg peak in the vicinity of B_{c2}. The linear behaviour is expected from the Abrikosov solution to the Ginzburg-Landau equations.

The rocking-curve integrated intensity, I_{hk}, of an $(\underline{h,k})$ diffraction spot depends on the square of the form factor, F_{hk}, of the spatial variation of the magnetic field via:

$$I_{hk} = 2\pi V\phi \left(\frac{\gamma}{4}\right)^2 \frac{\lambda_n^2}{\Phi_0^2 Q_{hk}} |F_{hk}|^2 \qquad (1)$$

where ϕ is the neutron flux, γ is the neutron magnetic moment, V is the illuminated sample volume, Φ_0 is the flux quantum, λ_n is the neutron wavelength and Q_{hk} is the magnetic scattering vector. Figure 3 shows the square root of the rocking-curve integrated intensity, $\sqrt{I_{10}}$, as a function temperature close to $B_{c2}(T)$ and is directly proportional to F_{10}. The Abrikosov solution to the Ginzburg-Landau (GL) equations results in an expression for F_{hk} as:

$$F_{hk} \approx \frac{(-1)^v e^{-\pi v/\sqrt{3}} (T_{c2} - T)}{1 + 1.16(2\kappa^2 - 1)} \frac{dB_{c2}}{dT} \qquad (2)$$

at constant B. Where $v = (h^2 + hk + k^2)$, κ is the GL parameter and dB_{c2}/dT is the initial gradient of the upper critical field at $T_c(0)$. It is satisfying to see in figure 3 a linear variation of F_{hk} with temperature as expected from equations 1 and 2 and Abrikosov theory. We note also that the line goes linearly to zero with no breaks or discontinuities in intensity as would be expected at a flux line lattice melting transition. ■

References:

[1] A. A. Abrikosov, Sov. Phys. J.E.T.P. 5 (1957) 1174 •
[2] J. G. Bednorz and K. A. Muller, Z. Phys. B 64 (1986) 189 •
[3] R. Cubitt et al. Nature 365 (1993) 407 •
[4] G. Blatter et al., Rev. Mod. Phys. 66 (1994) 1125 •
[5] X. S. Ling et al., Phys. Rev. Letts. 86 (2001) 712 •
[6] E. M. Forgan et al, accepted to Phys. Rev. Letts. (2001).

Magnetic order in $YBa_2Cu_3O_{6+x}$ superconductors

H.A. Mook and P. Dai
(Oak Ridge National Laboratory, USA)

S.M. Hayden (University of Bristol)

A. Hiess (ILL)

S.H. Lee
(NIST Center of Neutron Research)

F. Dogan
(University of Washington, Seattle)

One of the most unusual features of the cuprate superconductors is that the gap normally associated with superconductivity appears far above the superconducting transition temperature for the underdoped materials. There is no consensus on the exact nature of this pseudogap, but it seems likely that magnetism in some form plays a major role. We have used the IN20 spectrometer to perform polarised neutron diffraction measurements on a very high quality crystal of $YBa_2Cu_3O_{6.6}$ to search for magnetic order related to the pseudogap transition. A complicated ordering process is observed with at least two different types of magnetic order. However, one of the transitions is found to occur at the pseudogap temperature. This order is unusual in that it is consistent with the moment pointing mostly along the c axis, while all known previously observed magnetism in the $YBa_2Cu_3O_{6+x}$ materials is in the a-b plane. This order may be related to recent theoretical descriptions of the pseudogap phase in which orbital currents are a competing order parameter with superconductivity.

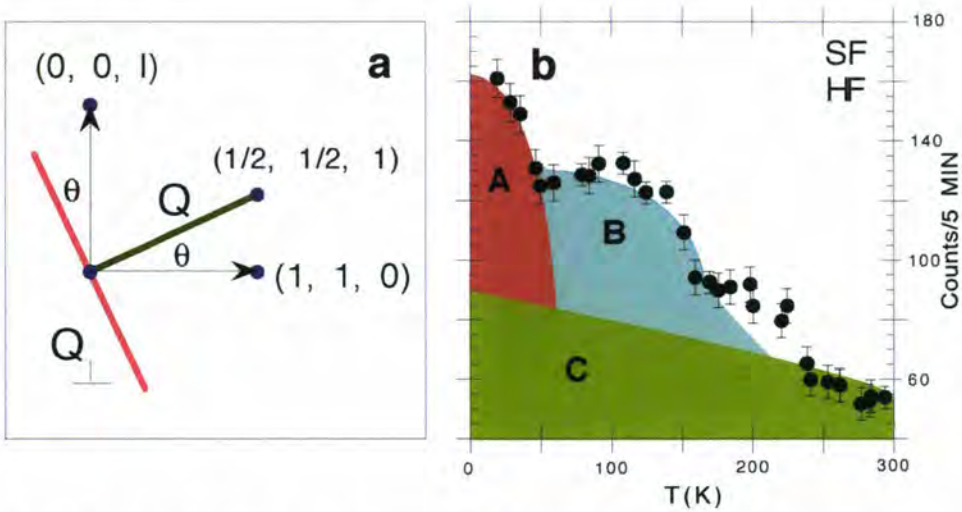

Figure 1: The scattering plane diagram for the (1/2, 1/2, 1) reflection is shown in **a**. **b** gives the temperature dependence of the magnetic SF HF scattering as determined from the height of the (1/2, 1/2, 2) reflection above background determined away from the peak. The scattering has three distinct regions with a rapid rise in the intensity below 200 K defining region B, and a another intensity rise at about 60 K (below T_c) defining region A.

It is well understood that superconductivity produces a gap in the quasiparticle spectra, and in conventional materials this gap disappears as the temperature is increased to T_c where the superconducting electron pairs are no longer bound together. The problem is that for the underdoped cuprate materials this gap appears to get bigger as T_c gets smaller. This so called pseudogap [1] has so far defied understanding, however, Chakravarty et al. [2] recently proposed that a novel state termed the d-density wave (DDW), is formed below the pseudogap temperature T*. In this state physical currents circulate around the Cu-O bonds breaking translational symmetry as well as time reversal and rotational symmetry. The moments from the bond currents result in peaks at the (h/2, k/2, l) superlattice positions of the reciprocal lattice that can be detected by a neutron scattering experiment of sufficient sensitivity. The expected moment is very small, on the order of $0.01\mu_B$.

An experiment to observe this state was made on the IN20 polarised beam spectrometer using a high quality single crystal of $YBa_2Cu_3O_{6.6}$, Tc = 63 K. The neutron polarisation direction was either vertical to the scattering plane (VF) or along the scattering vector **Q** (HF). For spin flip (SF) scattering in the HF case the observed signal stems from moments lying in the plane $\mathbf{Q}_\perp$ shown in the scattering plane diagram figure 1a. Moments both along the [0, 0, l] direction (**c***), and in the **a*-b*** plane are thus observed with a large contribution coming from the basal plane direction perpendicular to the scattering plane. For the VF case only moments both in $\mathbf{Q}_\perp$ and the scattering plane are observed so that the SF signal stems largely from **c*** directed moments. Figure 1b shows the temperature dependence of the HF, SF scattering for the (1/2, 1/2, 2) reflection. The scattering has three distinct regions which we have labeled A, B and C. The most interesting region from the viewpoint of this report is B, and the scattering is found to differ

considerably in this region from that in region C. The scattering for the (1/2, 1/2, 1) reflection in region C is shown in figure 2a. SF scattering is found to be very small for the VF case compared to the HF result showing a moment directed in the **a*-b*** plane. The scattering is also found to be resolution limited showing long-range magnetic order. The scattering along l for region C, shown in figure 3, displays only one clear peak at (1/2, 1/2, 1) and this may deviate slightly from l=1. The scattering for region C is characteristic of a magnetic moment that is positionally disordered off the $YBa_2Cu_3O_{6.6}$ lattice along **c***. This moment appears to derive from an impurity phase that has a high transition temperature.

The order parameter for B increases starting at about 200 K or near T* for a material with the T_c value of our sample. This is the first measurement that demonstrates that a phase transition may take place T*. Figure 2b shows measurements for the (1/2, 1/2, 1) reflection made at 70 K which is the region of highest intensity in region B, but still above T_c. Now the VF scattering is about 1/3 as large as the HF scattering showing an appreciable **c*** moment.

In fact this **c*** moment can essentially account for the increased intensity in region B. Figure 3 shows that the increase in intensity comes at positions associated with the $YBa_2Cu_3O_{6.6}$ lattice as can be particularly noted for the (1/2, 1/2, 2) reflection. The peaks are found to be about 50% wider in the B phase so that the correlation length is shorter. The correlation length in the **c*** direction is also shorter in region B based on the width of the (1/2, 1/2, 1) reflection. The shorter correlation length plus the increase in intensity identifies a new phase since a broadening by itself would decrease the intensity. Region A has not been investigated in detail. No extra peak broadening is observed or difference in the SF VF/HF ratio. It is interesting that the scattering increases below T_c and this region should be investigated at a later date.

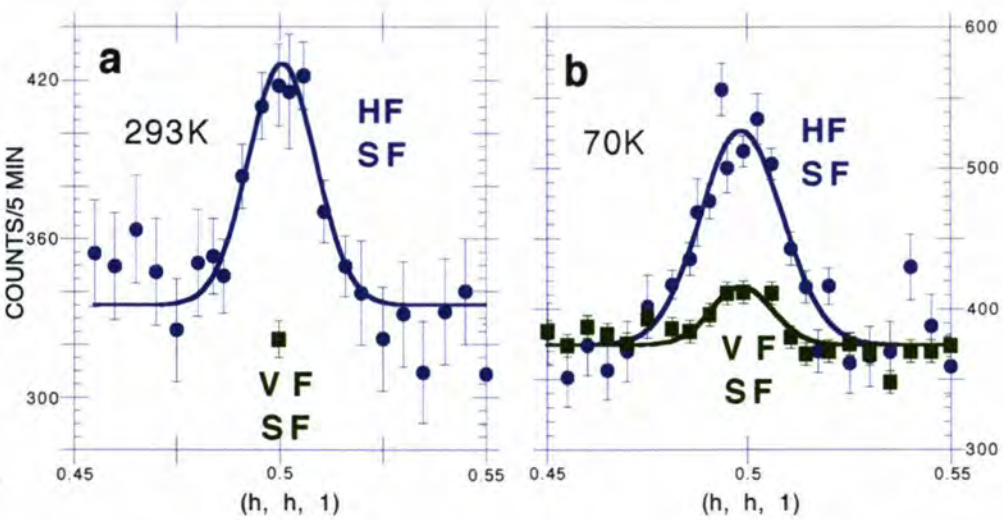

Figure 2: **a** and **b** show HF and VF SF data at 293 and 70 K. The VF result at (1/2, 1/2, 1) for 293K is very small, but there is an appreciable VF contribution at 70 K.

The scattering in the B phase corresponds to a moment of about 0.01 μ_B, appears at T*, and is at least partially directed along the c* axis. These characteristics are exactly what is expected for the DDW phase. The observation of this phase would explain the origin of the pseudogap, provide an understanding of the T_c vs hole doping behaviour, and greatly narrow the search for the superconducting mechanism for the cuprate materials. The present experiment does not confirm the presence of such a phase, but certainly provides evidence that such a phase should be seriously considered. In further experiments we will more thoroughly characterise the new phase, hopefully in samples that are free from background impurity scattering. ■

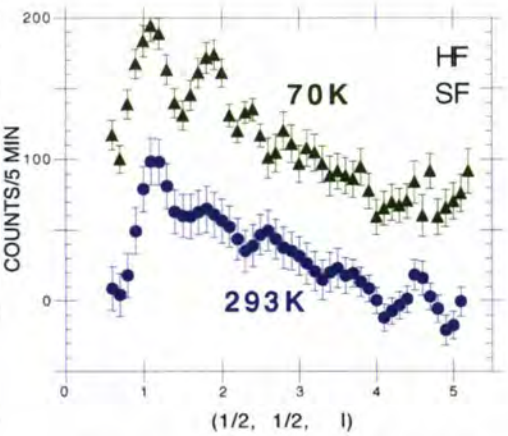

Figure 3: Data taken along the **c*** axis for region C and B. The data at 70 K is displaced upward by 50 counts. The pattern for C is characteristic of a disordered magnet while the increased intensity in B occurs at the lattice positions.

References

[1] M. Buchanan, Nature 409 (2001) 8 • [2] S. Chakravarty, R.B. Laughlin, D.K. Morr, C. Nayak, Phys. Rev. B 64 (2001) 094503.

Self-propagating synthesis of Ti_3SiC_2 at high temperature

D.P. Riley and E.H. Kisi
(University of Newcastle, Australia)

T.C. Hansen and A.W. Hewat
(ILL)

In-situ neutron diffraction on D20 at 0.9 s time resolution was used to capture the reaction mechanism during the self-propagating high-temperature synthesis (SHS) of Ti_3SiC_2 from Ti/SiC/C mixtures. The diffraction patterns indicate that the SHS proceeded in five stages: (i) pre-heating of the reactants, (ii) the $\alpha \rightarrow \beta$ phase transformation in Ti, (iii) pre-ignition reactions, (iv) the formation of a single solid intermediate phase in <0.9 s and (v) the rapid nucleation and growth of the product phase Ti_3SiC_2. The $\alpha \rightarrow \beta$ phase transformation in Ti is a necessary precursor to the reaction as is the subsequent reaction of Ti and free C just before SHS ignition. The intermediate phase is believed to be a solid solution of Si in TiC such that the overall stoichiometry is approximately 3Ti:1Si:2C. Lattice parameters and known thermal expansion data were used to estimate the ignition temperature at ~900°C (confirmed by the $\alpha \rightarrow \beta$ phase transformation in Ti) and the combustion temperature at ~2200°C.

Ti_3SiC_2 is a layered ternary carbide material, space group $P6_3/mmc$, with a=3.0675 Å and c=17.657 Å. The crystal structure, shown in figure 1, has double layers of TiC octahedra interleaved with single layers of Si. This laminated structure leads to an unusual combination of properties that is neither ceramic nor metallic. It has the refractory and high temperature properties normally associated with ceramics, combined with the electrical and thermal conductivity of a metal [1-3]. In addition, the material exhibits ductility due to shearing of the layered structure that enables it to be readily machined with ordinary machine tools [1-4]. Other mechanical properties include excellent thermal shock resistance, reasonable fracture toughness, a high Young's Modulus and good high temperature strength [1,2,5]. Unfortunately, the material is difficult to synthesise as a pure phase, being often accompanied by unacceptably large amounts of TiC and titanium silicides (Ti_xSi_y).

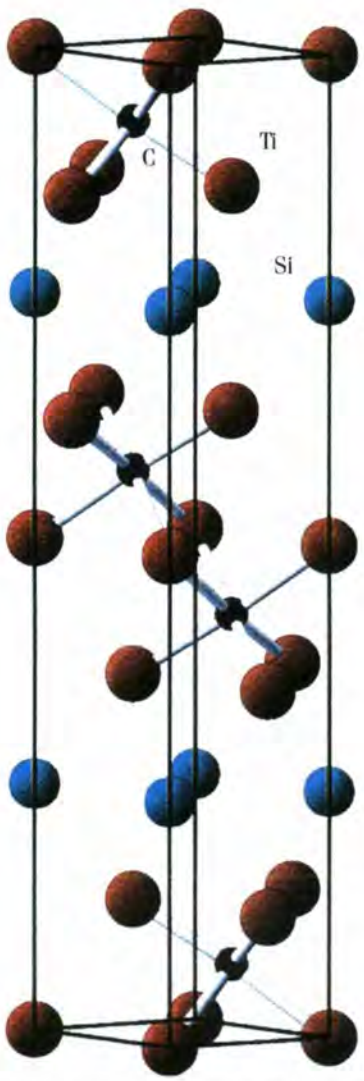

Figure 1: Structure of Ti_3SiC_2. Ti atoms are shown red, Si are blue and C is black.

The heat of formation for Ti_3SiC_2 is quite large making it an excellent candidate for Self-propagating High-temperature Synthesis (SHS). SHS aims to utilise the heat of reaction as the primary energy source in the production of a material. Once ignited by an ignition source (laser, electron beam, furnace or electric arc) the reaction becomes self-sustaining and converts reactants to products very rapidly (0.1-100s). We have been studying SHS reactions in the Ti-Si-C system, but the extreme speed of the reactions has prevented a clear understanding of the reaction mechanism emerging. Our most recent experiment, on D20 has allowed *in-situ* neutron powder diffraction data to be recorded at 0.9s time resolution (0.5s patterns + 0.4s data download) for the overall reaction $3Ti + SiC + C \rightarrow Ti_3SiC_2$.

Cold-pressed pellets of the reactants were heated in the D20 furnace at ~100°C/min through the critical range 800-1000°C to initiate the reaction whilst diffraction patterns were simultaneously recorded. An overview of part of the diffraction patterns for one SHS reaction is shown in figure 2 and a three dimensional rendering of a similar region

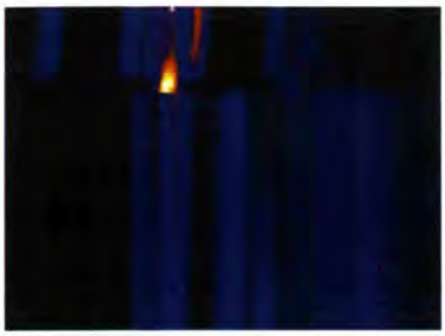

Figure 2: LAMP plot of diffraction patterns recorded during SHS of Ti_3SiC_2. The horizontal axis is 2θ (24 - 42°), the vertical axis is time and the diffracted intensity is indicated by brightness/colour changes.

is shown in figure 3. The SHS reaction proceeded in five stages. *Pre-heating of the reactants* assists in the ignition by reducing the overall heat requirement. The diffraction patterns show only the expected thermal expansion below 880°C. *The α → β phase transformation in Ti* forms the next stage. This phase transition is readily seen at the left-hand end of figure 3 and was found to be a necessary precursor to the SHS reaction in all cases studied. *The pre-ignition reaction* stage consists of local reaction of Ti with free C in the sample. As this reaction is exothermic, it provides local temperature increases that are the real ignition sources. The fourth stage is the formation of a *single solid intermediate phase* in <0.9s and is the true SHS or combustion reaction in this system. It produces a pronounced discontinuity in the diffraction data of figures 2 and 3. It can be seen in the figures that the intermediate phase has a simple NaCl structure (like TiC) and that it persists for six seconds as the only phase present. The combustion temperature was estimated at 2200°C from the lattice contraction of the product phases. We believe that the intermediate phase is a solid solution of Si in TiC that is relatively stable at the combustion temperature but becomes unstable as the temperature decreases. The final stage is the rapid nucleation and growth of the product phase Ti_3SiC_2 as shown by figures 2 and particularly 3. The work has been submitted for publication [6] and work on extracting the reaction kinetics is underway.

This experiment has demonstrated the power of in-situ neutron diffraction to reveal the reaction mechanisms, structural details and micro-structural evolution of complex multi-component systems. SHS in Ti/SiC/C occurs very rapidly, converting the entire sample into a cubic intermediate phase in 0.5s or less at a combustion temperature estimated at 2597K, and there were no signs of a substantial amount of a liquid phase in the reaction. We would like to test the generality of these observations with other starting mixtures (e.g. 3Ti+Si+2C), and extend in-situ SHS experiments to other systems. ■

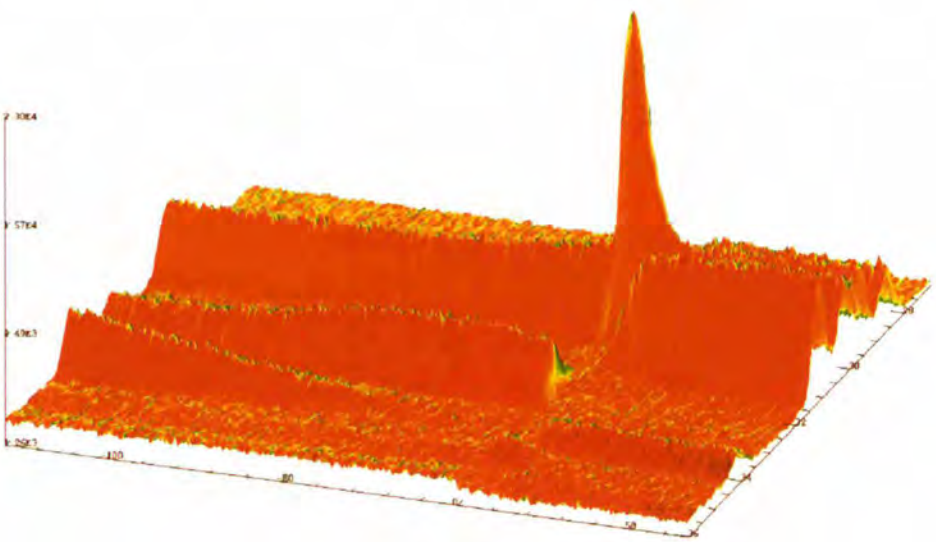

Figure 3: 3-D LAMP plot of a portion of the diffraction patterns during SHS of Ti_3SiC_2. The reaction progression is from left to right on the x-axis. The y-axis represents 2θ and the z-axis is the diffracted intensity.

References

[1] M.W. Barsoum, T. El-Raghy, "Synthesis and characterization of a remarkable ceramic: Ti_3SiC_2", J. Am. Ceram. Soc., 79 (1996) 1953-56 • [2] M.W. Barsoum, T. El-Raghy, "A Progress report on Ti_3SiC_2, Ti_3GeC_2, and the H-phases, M2BX", J. Mat. Synth. Process. 5, 3 (1997) 197-216 • [3] S. Myhra, J.W.B. Summers, E.H. Kisi, "Ti_3SiC_2 - A layered ceramic exhibiting ultra-low friction", Materials. Letters., 39 (1999) 6-11 • [4] T. El-Raghy, P. Blau and M.W. Barsoum, "Effect of grain size on friction and wear behaviour of Ti_3SiC_2", Wear, 238 (2000) 125-130 • [5] H.I. Yoo, M.W. Barsoum,T. El-Raghy, "Ti_3SiC_2 has negligible thermopower", Nature, 407, 6804 (2000) 581-2 • [6] "Ultra-high speed neutron diffraction study of self-propagating high-temperature synthesis of Ti_3SiC_2: I Reaction Mechanism", D.P. Riley, E.H. Kisi, T.C. Hansen and A.W. Hewat, J. Am. Ceram. (submitted).

Formation pathway of the superconductor Tl-2223 revealed by *in-situ* powder diffraction

● PH. GALEZ, TH. HOPFINGER, J.L. JORDA AND M. LOMELLO-TAFIN (UNIVERSITY OF SAVOIE, ANNECY)

● J.L. SOUBEYROUX (ILL AND CNRS, GRENOBLE)

● E. SUARD (ILL)

The reaction pathway for the formation of $Tl_2Ba_2Ca_2Cu_3O_z$ (Tl-2223) has been investigated by in-situ neutron powder diffraction. The experiment was carried out in an initially evacuated closed system on a sample with nominal composition $Tl_{1.7}Ba_2Ca_2Cu_3O_z$. We find that the formation path implies Tl_2BaO_4, $Tl_6Ba_4O_{13}$ and $Tl_2Ba_2CaCu_2O_8$ (Tl-2212) according to the sequence: Precursors ⇒ Tl_2BaO_4 ⇒ $Tl_6Ba_4O_{13}$ ⇒ Tl-2212 ⇒ Tl-2223.

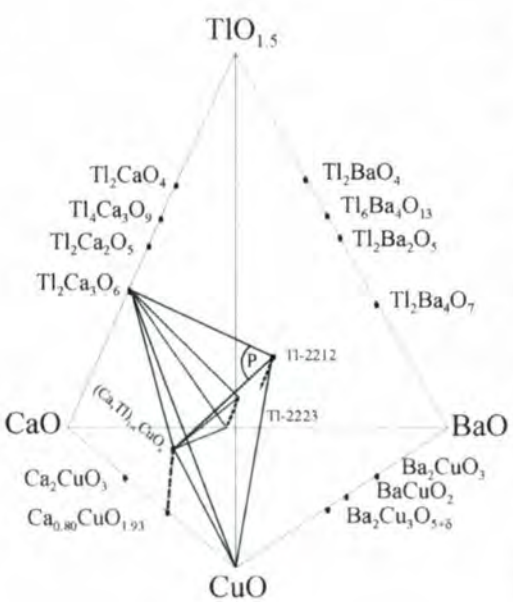

Figure 1: Schematic quaternary diagram with the equilibrium fields corresponding to the sample $Tl_{1.7}$ delimited by dotted lines.

The Tl-based high-Tc superconducting cuprates form a double TlO layer family with ideal composition $Tl_2Ba_2Ca_{n-1}Cu_nO_{2n+4}$ (n = 1 to 4) [1]. Among these phases, $Tl_2Ba_2Ca_2Cu_3O_{10}$ (Tl-2223) has the highest superconducting temperature 127 K [2]. These compounds are of interest for practical applications, in passive microwave superconducting devices. It has been suggested that high-quality Tl-2223 films could be formed through an entirely solid-state route [3]. Among the processing parameters, temperature and oxygen partial pressure play an important role, so the experiments have been conducted in an initially evacuated closed system. The reacted samples were also characterised by high-resolution neutron powder diffraction, ac susceptibility measurements, scanning electron microscopy and energy dispersive X-ray spectroscopy.

The appropriate amounts of Tl_2O_3, $BaCuO_2$ and Ca_2CuO_3 powders were thoroughly mixed, pressed into pellets, tightly wrapped in thin gold foil and sealed in an evacuated quartz tube. Variable temperature neutron data were collected on the high-flux powder diffractometer D1B at λ = 2.524 Å. The collection time for a single pattern was 5 minutes. The sample was rapidly heated (+10 K min^{-1}) from room temperature to 675 K, the heating was then reduced to +2 K min^{-1} until the maximum temperature, 1078 K, was reached. The sample was held at this temperature for 400 min and finally cooled at room temperature. Examination of the last diffraction pattern revealed that the sample contained Tl-2223 as the main phase, with $Tl_2Ca_3O_6$, $(Ca,Tl)_{1-x}CuO_2$, $BaCO_3$ and traces of CuO. This defines the equilibrium field delimited by dotted lines in figure 1.

The whole experiment can be displayed in a simple 2D graph (figure 2a) where each intensity value corresponds to a particular shade. Besides the three starting oxides and the five phases detected in the reacted sample, three intermediate compounds were observed during the formation process : Tl_2BaO_4, $Tl_6Ba_4O_{13}$ and an unidentified phase. The information is summarised in figure 2b which gives the time and temperature at which the different phases appeared and/or disappeared. The progressive decomposition of $BaCuO_2$ and Tl_2O_3 begins at about 680 K and is followed by the formation of an unknown phase, Tl_2BaO_4 and $Tl_6Ba_4O_{13}$. At the same time, CuO appears and its amount increases progressively. The Tl_2BaO_4 phase vanishes at 880 K while the amount of $Tl_6Ba_4O_{13}$ still increases up to a maximum at 905 K. Then $Tl_6Ba_4O_{13}$ starts to decompose and Tl-2212 is progressively formed. The latter phase appears at 860 K and its main intensity peak reaches its maximum value at 1070 K (figure 3). The conversion from Tl-2212 to Tl-2223 is accompanied by a significant decrease of the weight fractions of $Tl_2Ca_3O_6$, $(Ca,Tl)_{1-x}CuO_2$ and CuO which provide the necessary Ca and Cu.

The refinement of the structure of Tl-2223 so obtained has been performed on data recorded on D2B. Tl and O atom disorder within the TlO layer have been detected and indicate a tendency to a

tetrahedral coordination for Tl atoms. For more details about the structure see reference [4].

This in-situ neutron experiment has demonstrated that the synthesis of the Tl-2223 compound can be done from the Tl-2212 compound at 1075 K without the previous formation of a liquid phase. However this conversion does not occur when the nominal Tl content is greater than 2 because of the coexistence with the $Tl_2Ca_3O_6$ phase. ■

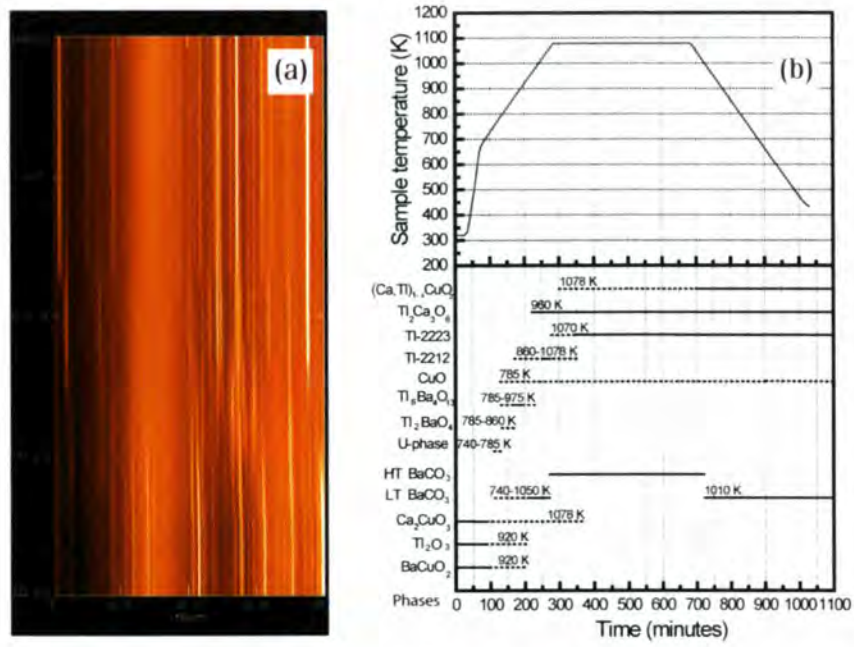

Figure 2: a) 2D representation of the in-situ diffraction experiment with the Bragg angle as the abscissa and temperature as the ordinate. b) Schematic representation of the *in-situ* diffraction experiment showing the time intervals during which the different phases were observed. The broken parts of the lines refer to periods during which the weight fractions increased or decreased significantly. The solid part of the line, the time during which the phase is present.

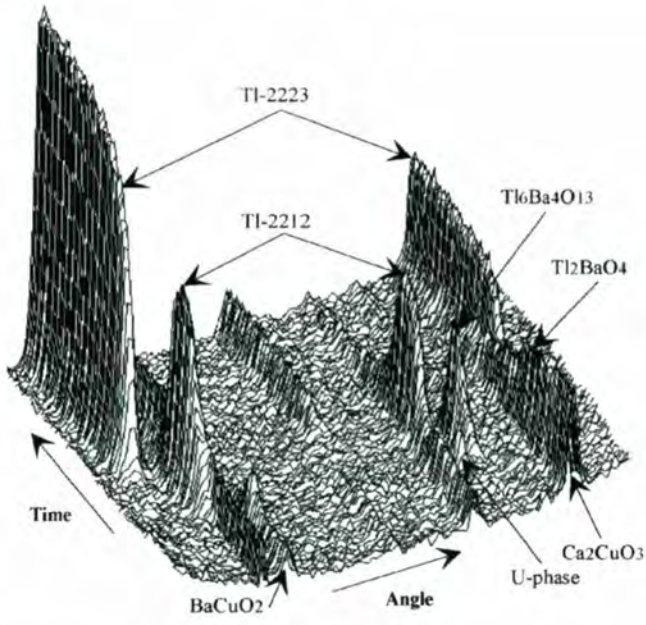

Figure 3: Low-angle part ($6° \leq 2\Theta \leq 26°$) of the first 120 diffraction patterns of $Tl_{1.7}$.

References

[1] S. Kondoh, Y. Ando, M. Onada, M. Sato and J. Akimitsu, Solid State Comm.,65 (1988) 1329 • [2] T. Kaneko, H. Yamauchi and S. Tanaka, Physica C 178 (1991) 377 • [3] W.L. Holstein and L.A. Parisi, J. Matter. Res. 11 (1996) 1349 • [4] Ph. Galez, J.L. Soubeyroux, T. Hopfinger, C. Opagiste, M. Lomello-Tafin, C. Bertrand and J.L. Jorda, Supercond. Sci. Technol., 14 (2001) 583.

Short N··H··O hydrogen bonds:
neutron diffraction, inelastic neutron scattering and computational results

- I.D. Williams and S.M.-F. Lo (Hong-Kong University of Science and Technology)
- J.A.K. Howard (University of Durham)
- J.A. Cowan (University of Durham and ILL)
- G.J. McIntyre, M. Johnson and A. Ivanov (ILL)

It has been proposed and disputed that short strong low-barrier hydrogen bonds play an essential role in stabilising the intermediate state of certain enzymatic reactions. Neutron scattering studies are essential to understand fully the properties of these short hydrogen bonds. While short O-H···O hydrogen bonds have been comprehensively characterised in many neutron diffraction studies, ours are among the first neutron diffraction studies of very short N··H··O hydrogen bonds. Investigations on one of these short bonds have led to the observation of some novel temperature dependent behaviour, namely transfer of the hydrogen from the nitrogen to the oxygen with increasing temperature.

In the process of enzymatic catalysis the enzyme and the substrate bind to form a metastable intermediate state during which the substrate is modified, finally the substrate is released and the enzyme relaxes to its stable state. It has been proposed [1] that the intermediate state can be stabilised by the transformation of a weak hydrogen bond into a short strong one, which is accomplished by a subtle modification of the local environment of the hydrogen bond.

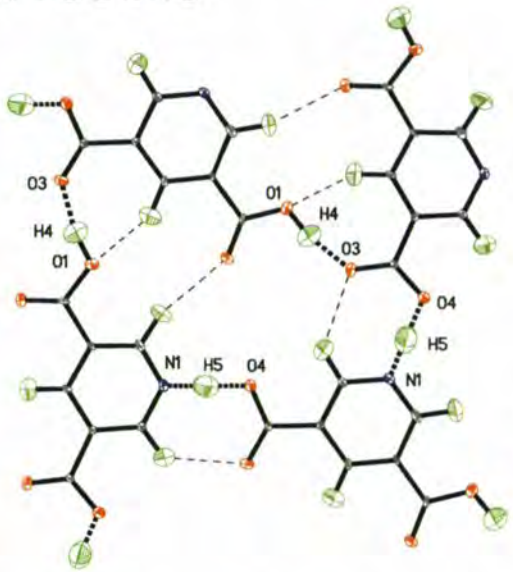

Figure 1: The co-operative hydrogen-bond network in pyridine-3,5-dicarboxylic acid enhances the N··H··O bond. Strong hydrogen bonds are indicated by heavy dashed lines and weak C-H···O hydrogen bonds by thin dashed lines. The important hydrogen bond is between N1 and O4.

Neutrons are the most effective probes for studying short hydrogen bonds. X-rays are sensitive to the electrons of atoms and in most cases the nucleus can be confidently placed at the centre of the electron density. However in these short hydrogen bonds the electron cloud of the hydrogen is stretched and distorted by the nitrogen and oxygen atoms making the positioning of the hydrogen nucleus from X-ray diffraction results educated speculation. Neutrons are sensitive only to the nuclei, which makes the placing of the hydrogen nucleus simple and unambiguous.

Diffraction

We have collected data on crystals of pyridine-3,5-dicarboxylic acid [PDA], which contains a short N··H··O hydrogen bond with an N···O distance of ~2.52 Å [2] (figure1), on D9 at 15 K and 300 K. At 300 K the proton in the hydrogen bond is observed 1.3 Å from the nitrogen atom and 1.2 Å from the oxygen atom; and at 15 K it is observed 1.2 Å from the nitrogen atom and 1.3 Å from the oxygen atom, a change of 0.1 Å over the temperature range. We have also observed this effect in 2:1 co-crystals of 4,4-bipyridine and benzene-1,2,4,5-tetracarboxylic acid [3] and it has also been seen in co-crystals of pentachlorophenol and 4-methylpyridine [4].

To investigate further this phenomenon we collected data on a crystal of PDA with the two carboxylic acid hydrogen atoms deuterated at 15 K, 150 K and 300 K. At 300 K the deuteron is 1.1 Å from the oxygen , at 150 K 1.35 Å from the oxygen and 1.4 Å from the oxygen at 15 K, an even more pronounced motion. The results are summarised in table 1.

	N···O distance (Å)	N-H/D distance (Å)	H/D-O distance (Å)
300 K - protonated	2.525(3)	1.308(6)	1.218(6)
15 K - protonated	2.523(2)	1.216(5)	1.309(5)
300 K - deuterated	2.564(3)	1.457(4)	1.108(4)
150 K - deuterated	2.532(3)	1.192(4)	1.342(4)
15 K - deuterated	2.538(3)	1.150(3)	1.389(3)

Table 1: Hydrogen bond parameters.

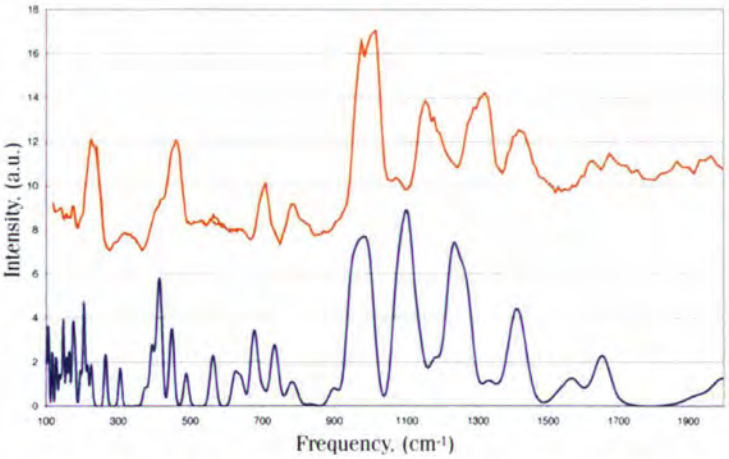

Figure 2: The inelastic neutron scattering spectrum measured at 20 K on IN1. The calculated spectrum is in blue and the measured spectrum in red. The measured spectrum has been offset vertically for comparison.

Incoherent Inelastic Neutron Scattering

The strength of the hydrogen bond modifies significantly the vibration frequencies of the associated molecular groups. In particular, on the formation of a strong hydrogen bond, out of plane proton motion (wagging of the N-H bond) moves to a higher frequency, from 400 cm^{-1} to ~1200 cm^{-1} and in-plane motion (stretching of the N-H bond) moves to lower frequency, from over 3000 cm^{-1} to 2000 cm^{-1} or below. The vibrational modes have been measured on IN1 (figure 2) for the fully protonated compound at 10 K. The analysis is based on solid-state quantum-chemistry calculations described below.

Density Functional Theory Calculations

We have used density functional theory calculations, in the codes CASTEP and VASP, to model the solid -state structure of PDA, from which we can calculate the shape of the hydrogen bond potential-energy well. From the low-temperature structure a broad asymmetric potential well is calculated with a single minimum close to the nitrogen atom (figure 3). The lowest eigenstate for a proton has an expectation value of position 1.19 Å from the nitrogen atom. The deuteron, which is heavier, lies lower in the potential well and the expectation value of position is 1.16 Å from the nitrogen, in agreement with our diffraction results.

The temperature dependent proton migration cannot be explained simply by this potential well. Although the expectation values of the proton position for the higher levels move across the well, the energy required to populate these levels corresponds to temperatures above 1000 K. The potential well must be modulated by increase in temperature so as to give a (meta-) stable minimum closer to the oxygen atom. A small modification of the average molecular structure is obtained in the simulation by forcing the proton to be closer to the oxygen atom and optimising the resulting structure. In reality the thermal motion causes an expansion of the unit cell and a weakening of the hydrogen bonds. By imposing a high-temperature unit cell in our calculations the most stable configuration has the proton bound to the oxygen.

Figure 3: The calculated potential-energy well and energy levels for the N··H··O hydrogen bond (black) and the calculated harmonic-approximation potential well and energy levels (blue). The harmonic approximation needs to be corrected to predict the vibrational frequencies.

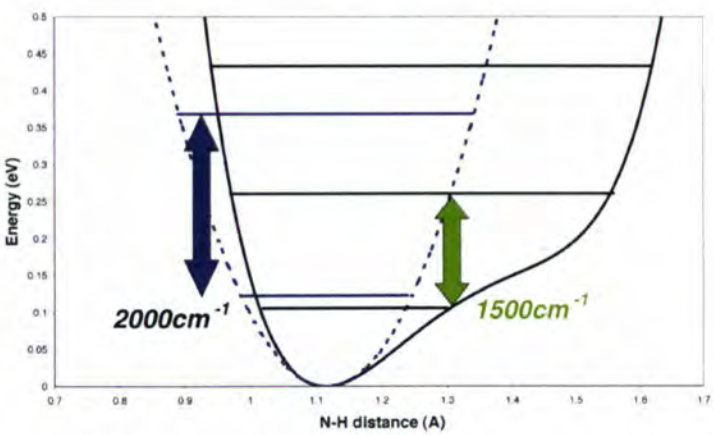

Finally the same total energy calculations have been used to calculate the vibrational spectrum in the harmonic approximation. The strongest bands between 1100 and 1500 cm^{-1} are the N-H and O-H wagging modes, the N··H··O bonds being stronger and giving the higher frequency bands. Our calculation predicts the N-H stretch to be at 2000 cm^{-1}, but the potential well (figure 3) is clearly not harmonic. The exact energy levels shown in the well indicate a vibration frequency of ~1500 cm^{-1}, in the region of other vibrational excitations. Neutron and Raman measurements on partially deuterated samples are being prepared to identify this mode and thereby quantify the strength of the hydrogen bond.

While the environment of the hydrogen bond in a crystal is different to that in a protein, these experiments and calculations begin to provide possible models for the mechanisms of proton transfer in enzymatic catalysis. The characteristic spectroscopic signatures of these hydrogen bonds could possibly be used to verify the existence of these hydrogen bonds in biological systems. ■

REFERENCES

[1] W.W. Cleland and M.M. Kreevoy, Science 264 (1994) 1887 • [2] F. Takusagawa, K. Hirotsu and S. Shimada, Bull. Chem. Soc. Japan. 46 (1973) 2292 • [3] A.J. Lough, P.S. Wheatly, G. Ferguson and C. Glidewell, Acta Cryst. B56 (2000) 261 • [4] T. Steiner, I. Majerz and C.C. Wilson, Angew. Chem. Int. Ed. 40 (2001) 2651.

The strong hydrogen bond in crystal engineering

● J.W. Steed, P.D. Prince and C. Wilkinson (King's College, London)

● S.A. Mason (ILL)

Oxonium ions, forms of the hydrated proton, have been known for many years [1,2] but their formation, isolation and study has often been a rather serendipitous process. Recent work [3,4] has shown that crown ethers may be used to selectively isolate particular oxonium ions from strongly acidic solutions, particularly aqua regia. Combined single crystal low-temperature X-ray and neutron crystallography reveal a wealth of synergistic, solid state interactions from highly covalent strong hydrogen bonds, through intermediate OH···O and OH···Cl-M motifs, down to weak CH···O interactions. Using neutron diffraction we have characterised the novel hydrogen bonded polymer $(H_7O_3)[AuCl_4]$·15-crown-5 (1) and the discrete complex $\{HNO_3 \cdot H_2O \cdot 18\text{-crown-}6\}_2$ (2).

The crown ethers (figure 1) display a marked hydrogen bond acceptor ability. Multiple, cooperative hydrogen bonds in labile crown ether complexes are frequently more important in determining overall structure in the solid state than direct interactions with metal centres [1]. This hydrogen bond acceptor ability (without significant hydrogen bond donor capacity) is also highly useful in binding species other than metal cations. Thus, crown ethers are remarkably effective in the isolation of strong hydrogen bond acceptors such as the hydrated proton (oxonium ion) [2]. We and others [3,4] have recently shown that H_3O^+, $H_5O_2^+$ and $H_7O_3^+$ among other species may be isolated from acidic solution by appropriate choice of crown ether. At King's College London we were able to show solid state and solution association of crown ethers and oxonium ions. However, in the most interesting case of all, $(H_7O_3)[AuCl_4]$·15-crown-5 **(1)** the X-ray data did not reveal the all-important hydrogen atom positions.

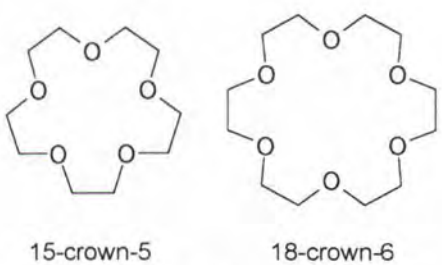

15-crown-5 18-crown-6

Figure 1: Crown ethers 15-crown-5 and 18-crown-6.

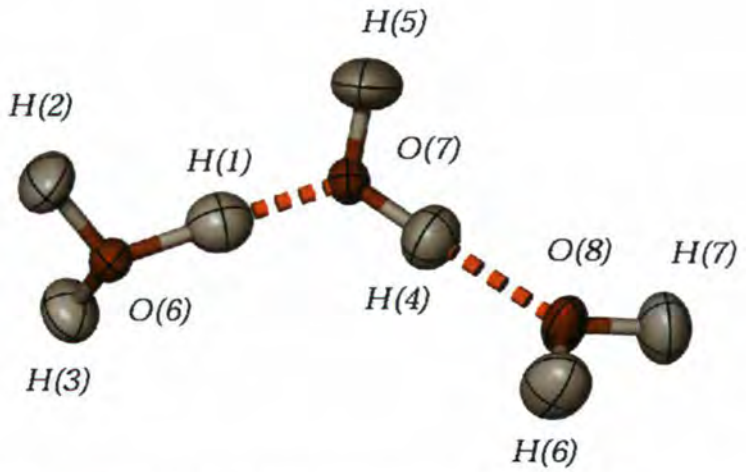

Figure 2: Thermal ellipsoid plot (70% level) of the $H_7O_3^+$ ion in the neutron structure of **1**.

Structure of $(H_7O_3)[AuCl_4]$·15-crown-5 (1)

The neutron study of 1 suggests that the $H_7O_3^+$ ion is unsymmetrical, possessing a significant contribution from an $H_5O_2^+ \cdot H_2O$ "resonance form" with one short O···O distance of 2.437(2) Å and one longer, 2.574(2) Å (figure 2). Notably, however, even the longer O···O separation is markedly shorter than that reported previously in a neutron study of *o*-sulfobenzoic acid trihydrate [5]. One proton, H(1), is situated asymmetrically along a line joining the shorter pair of oxygen atoms. The two O-H(1) bond distances are significantly longer than those found in isolated OH bonds. The anisotropic displacement ellipsoid relating to H(1) is also somewhat elongated along the O(6)···O(7) axis indicating that the proton interacts strongly with both centres. Interestingly, however, H(1) is not situated symmetrically between O(6) and O(7) and, lies closest to O(6), the terminal oxygen atom of the O(6)-O(7)-O(8) chain. This suggests that the positive charge of the oxonium ion is stabilised by interactions to the crown ether. These O(6)-H···O_{crown} interactions (figure 3) are typical of moderate strength electrostatic hydrogen bonds with the protons located close to the donor O(6). The hydrogen bond linking the central oxygen atom O(7) to O(8) is of intermediate length between the value expected for a strong and a moderate interaction. The H(4)···O(8) distance is longer, consistent with a description of O(8)/H(6)/H(7) as a very strongly hydrogen bonded water molecule, rather than part of the oxonium ion.

The last remaining oxonium proton H(5) forms a fascinating, nearly symmetrical

bifurcated interaction with the chloro ligands of the $[AuCl_4]^-$ anion. Such hydrogen bonds to coordinated chloride have been observed previously [6], although bifurcation is relatively uncommon and difficult to unambiguously identify.

Structure of $(HNO_3)_2 9(H_2O)_2 \cdot$18-crown-6 (2)

A further potentially oxonium-ion containing species is $\{HNO_3 \cdot H_2O \cdot 18\text{-crown-}6\}_2$ **(2)** which was examined by neutron diffraction on D9. Monitoring of a test reflection from room temperature all the way down to 20 K showed that the unusual change in cell dimensions (particularly of the crystallographic β angle) occurred gradually and continuously over the temperature range with β increasing from about 66.8° to 69.3°. Two data sets were collected at different temperatures (20 K and 250 K). The structure comprises an 18-crown-6 molecule in its customary D_{3d} symmetric conformation with two water molecules, hydrogen bonding to a total of four of the six ether oxygen atoms. Each water oxygen atom also accepts a much stronger, partially covalent hydrogen bond from a nitric acid molecule (figure 4). The short O···O distance in the $NO_3H \cdots OH_2$ unit and near-linear OHO angle are characteristic of strongly hydrogen bonded oxonium species (like $H_5O_2^+$) but the acidic proton resides firmly on the nitrate anion with an NO_3-H distance of 1.063(2) as opposed to the $NO_3H \cdots OH_2$ of 1.433(2) Å. The hydrogen bond distances involving the water protons and the crown ether increase significantly as the temperature rises. One of these interactions lies approximately along the crystallographic *c* direction while the other is along the *a/c* diagonal. The net result is to introduce a shear, *lowering* the crystallographic β angle. Because the change is correlated to the gradual increase in hydrogen bond length as a function of thermal motion there is no distinct phase change – just a smooth shift in unit cell parameters over the temperature range studied.

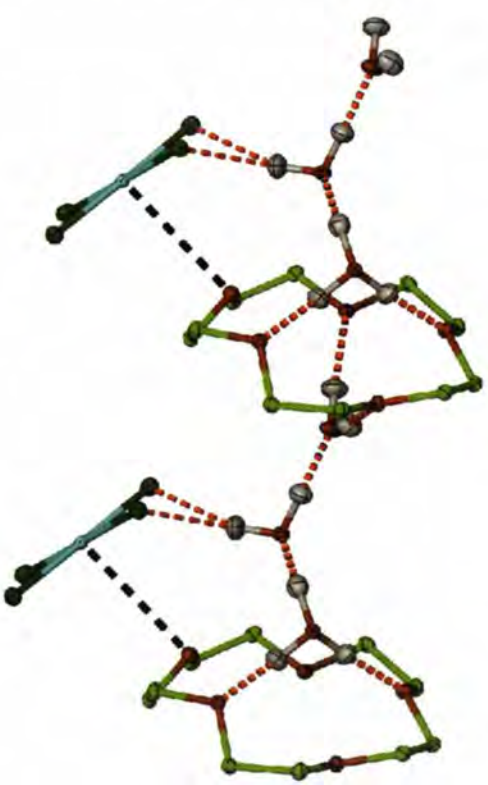

Figure 3: The hydrogen bonded chain structure in **1** showing the oxonium···crown interactions.

Figure 4: The 20 K neutron structure of $(HNO_3)_2 \cdot (H_2O)_2 \cdot$18-crown-6 **(2)** showing the proximity of the acidic proton to the nitrate anion and not the water molecule.

Conclusion

This study has shown that there is a well-defined interplay between supramolecular and covalent interactions with O-H bond distances being modulated by the characteristics of the acceptor atom. In this instance the $H_7O_3^+$ ion in **1** may best be described as a very strong $H_5O_2^+ \cdot H_2O$ hydrogen bonded unit with the asymmetry arising as a consequence of the better H-bond acceptor properties of the crown ether over the softer $[AuCl_4]^-$ anion. An unusual bifurcated OH···ClAu interaction has also been fully characterised in this compound. Complex **2** contains a nitric acid molecule very strongly hydrogen bonded to water. Thermal expansion of weaker hydrogen bonds in this system produces a marked shear in the unit cell as a smooth function of temperature. These results indicate how vectorial thermal expansion might be utilised to produce materials with anisotropic thermal response. ■

References

[1] J.W. Steed, Coord. Chem. Rev. 215 (2001) 171 • [2] C.I. Ratcliffe, D.E. Irish, in F. Franks (Ed.): Water Science Reviews 2, Cambridge University Press, Cambridge 1986, p. 149 • [3] M. Calleja, K. Johnson, W.J. Belcher, J.W. Steed, Inorg. Chem. 40 (2001) 4978 • [4] P.C. Junk, J.L. Atwood, J. Chem. Soc., Dalton Trans. (1997) 4394 • [5] R. Attig, J.M. Williams, Inorg. Chem. 15 (1976) 3057 • [6] G. Aullon, D. Bellamy, L. Brammer, E.A. Bruton, A.G. Orpen, Chem. Commun. (1998) 653.

Clathrate hydrates addressing questions from geology and chemical engineering

B. Chazallon, A. Klapproth, D. Staykova and W.F. Kuhs (Göttingen University)

Clathrate hydrates are non-stoichiometric inclusion compounds encaging small, usually apolar molecules in a framework of hydrogen-bonded water molecules. Often the embodied molecules are gaseous at normal conditions forming crystalline compounds in the presence of water or ice, compounds which are known also under the name of gas hydrates. They crystallise predominantly in two different structure types both with cubic symmetry, called structure I and structure II clathrate hydrate [1]. Known for almost 200 years they were established to exist in natural settings only a few decades back [2]. CH_4 hydrate can be found in marine sediments in huge amounts estimated to 10000 Gt which exceeds by far the other known fossil energy sources of coal, oil and gas. They will be of major economic interest in the future once techniques for their save extraction are established. It also is a nuisance in many gas and oil-pipelines where it causes blockages by a reaction of hydrocarbons with traces of water. CO_2 hydrates have found recently considerable interest as means of sequestering CO_2 in the ocean sea floor thus reducing the amount of CO_2 in the atmosphere. Moreover, it is likely that water on Mars is stored to a large extent in the form of CO_2 hydrate. Air hydrates, which can be found in the deeper parts of polar ice sheets, have been formed by a pressure induced transformation of closed-off air bubbles and carry important information on the air composition of the last one million years. Due to this wide-spread importance, a number of industrial countries have initiated large research efforts to better understand the physical chemistry and geology of gas hydrates.

Gas hydrates need high gas pressure and/or low temperatures to exist, conditions, which are met in the ocean sea floor from depths of a few hundred meters water pressure downwards or in permafrost regions. Likewise, experimental work needs to be done at non-ambient p-T conditions. Due to the complication of working at elevated gas pressures, a number of properties of gas hydrates were not well established. Several years back our group at the University of Göttingen has started to investigate gas hydrates in their field of stability. We have succeeded in preparing large amounts of clathrate hydrates in a self-organised process leading to a well crystallised meso- and macro-porous material [3] shown in figure 1. *In situ* neutron powder diffraction proved to be essential for their further investigation, backed up by molecular computer simulations to establish suitable crystallographic models for these disordered systems [4].

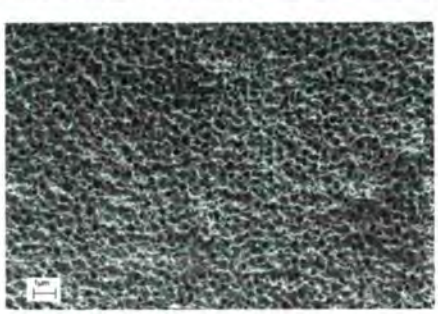

Figure 1: Field-emission scanning electron micrograph of CH_4 clathrate hydrate with regular submicron porous sponge-like structures.

One of the major unknowns in gas hydrate research in general and for CH_4 hydrate in particular is the occupancy of the small and large cages as a function of pressure and temperature. Until very recently it was assumed that the cage filling follows a Langmuir isotherm with increased pressure (fugacity). This assumption was never rigorously proven. Using in-situ neutron diffraction experiments on D2B (figure 2) we were able to establish the stoichiometry of a number of gas hydrates as a function of gas fugacity (figure 3). The results allow for the first time a completely assumption-free check of the widely used statistical thermodynamic theory (STT) for gas hydrates established by van der Waals & Platteeuw [5] and predicting a simple Langmuir isotherm. While there is undoubtedly a trend following these predictions, deviations exist for all investigated cases and in some cases the theory even completely fails. Coming as a complete surprise at first we found that the large cages in nitrogen hydrate were doubly occupied [6] violating one of the unquestioned basic assumptions of the theory. Still, one can modify the STT to accommodate double occupancy [7] as shown in figure 4. Yet, in other cases like for CO_2 hydrate the behaviour is strongly non-Langmuir and specific interactions between guest and host must be introduced into the model [8]. These findings are of major importance to chemical engineers since all computer programs for the calculation of gas hydrate stability and composition are build on the assumptions of STT.

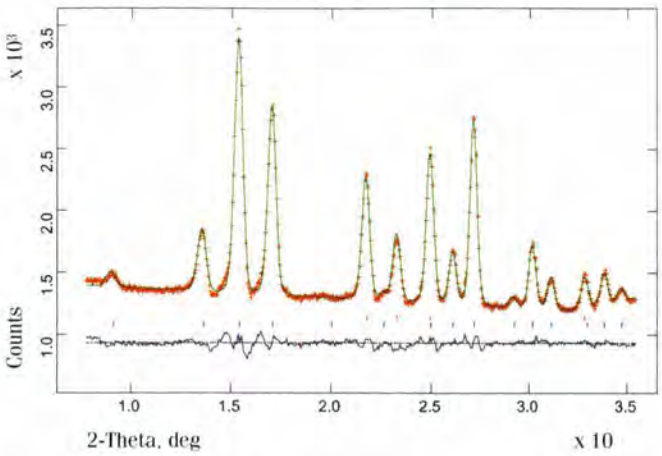

Figure 2: Rietveld refinement result for CH_4 clathrate hydrate at 100 bar and 0°C showing the low- angle data obtained on D2B. Clathrate hydrates form very small crystallites of a few µm size and are completely texture free thus forming ideal powders for diffraction studies.

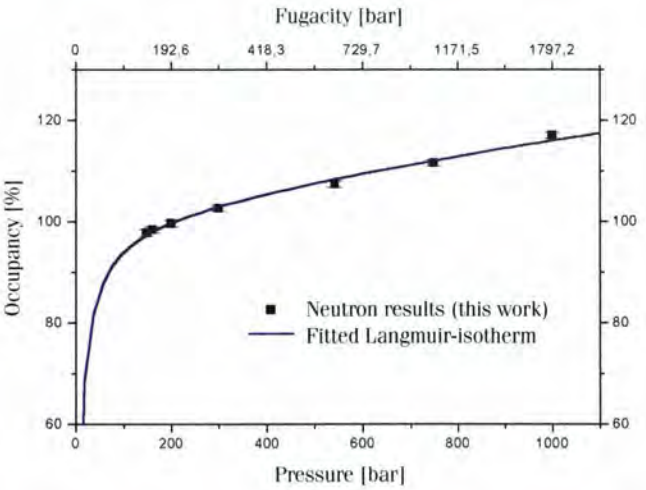

Figure 4: Experimental filling for the large cages in N_2 clathrate hydrate at 0°C as a function of pressure(fugacity). Using an extension of the statistical thermodynamic theory allowing for double occupancies a good fit to the experimental data can be obtained.

Another point of considerable interest is the compressibility of clathrate hydrates. Seismic profiling of the ocean sea floor is the most generally usable detection tool for submarine gas hydrates. A proper modelling of the seismic signals can be done only if certain physical parameters are known, most prominently the compressibilities. Here until very recently only very approximate data were available. We have for the first time established the isothermal compressibilities of a number of clathrate hydrates including CH_4 hydrate. It should be mentioned that the compressibilities of the deuterated and hydrogenated compounds are different. This shows that, while a number of questions in clathrate hydrates can be readily addressed using neutron diffraction techniques on deuterated samples, it will eventually be important to conduct experiments on the normal hydrogenated material too. However, it is fair to say that such experiments at elevated gas pressures performed by us at synchrotron sources are still somehow a *tour de force* as compared to the fairly straightforward neutron diffraction experiments.

A number of further questions concerning gas hydrates remain to be answered for which neutron techniques have proven to be very useful. Details of the formation and decomposition mechanism are unknown and some quite unexpected findings puzzle the community like the very much retarded decomposition below 0°C. First in-situ experiments for CO_2 and CH_4 hydrate were performed on D_2O. For the first time differences in the reaction rates for the two gases were established quantitatively which can be related to the systematically different sub-micron porosity of these two compounds [2,9]. Likewise, the transient formation of a metastable structure of CO_2 hydrate was found in the initial stage of formation, a quite unexpected result but helpful in understanding the molecular processes during clathrate formation.

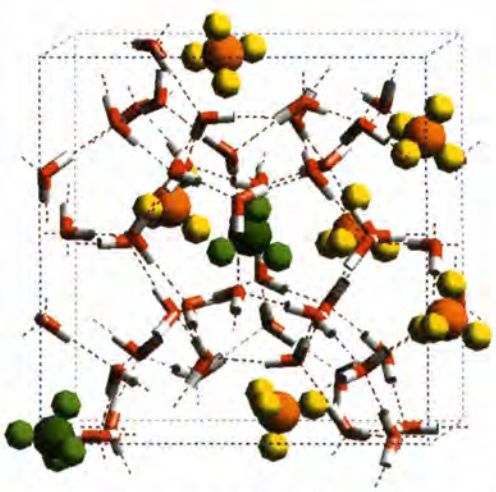

Figure 3: The structure of CH_4 clathrate hydrate. The water molecules are disordered in a H-bonded network. Methane molecules occupying small and large cages are shown in green and yellow colours respectively. At 60 bar and 0°C the statistical occupancy is 84% for the small cages and nearly 100% for the large cages.

Finally, it should be mentioned that gas hydrates merit considerable interest as model systems for gas-water and water-water interactions. A full understanding of these systems is far from being achieved and neutron scattering will undoubtedly be one of the major tools to study experimentally their structure and dynamics. As a matter of fact, all existing molecular interaction models are unable to reproduce the filling isotherms of gas hydrates experimentally established by neutron powder diffraction [10] thus providing critical tests for our theoretical understanding of the molecular interactions in these systems. ■

References

[1] M. von Stackelberg, Naturwissenschaften 36 (1949) 327 and 359 • [2] E.D. Sloan, Clathrate Hydrates of Natural Gases, Marcel Dekker, New York 1998 • [3] W.F. Kuhs et al., Geophys.Res.Lett. 27 (2000) 2929 • [4] B. Chazallon et al., AIP CP479 (1999) 74 • [5] J.H. van der Waals and J.C.Platteuw, Adv.Chem.Phys. 2 (1959) 1 • [6] W.F. Kuhs et al., J.Inclus.Phenom.29 (1997) 65; B. Chazallon and W.F. Kuhs, J. Chem. Phys. (2002) in press • [7] W.F. Kuhs et al., In Physics of Ice Core Records (Ed.T.Hondoh), Sapporo University Press, 2000 • [8] W.F. Kuhs et al., Rev. High. Press. Sci. Technol. 7 (1998) 1147. • [9] D. Staykova et al., Proceedings ICGH2002, Yokohama (2002) • [10] A. Klapproth et al., AIP CP479 (1999) 70.

Ti6Al4V welded components for aerospace technology: a residual stresses study

- T. Pirling (ILL)
- G. Bruno (ILL and University of Manchester)
- A. Carradò (University of Reims)
- B. Dunn (European Space Agency, ESTEC, Nordwijk)
- F. Fiori and E. Girardin (University of Ancona)

The effect of wall thickness of aerospace fuel tanks on the residual stress field induced by welding was investigated by neutron diffraction. For the comparison, a thick Ti6Al4V welded plate (thickness 6 mm), and a thin one (1.6 mm), were used. Experiments have been performed on the D1A diffractometer at the ILL. The unstrained interplanar distance d_0 has been evaluated with the plane stress hypothesis for each investigated gauge point. Large variations of d_0 have been found inside the heat affected zone and the weld pool, probably due to the large grain size, and some composition and precipitation gradients. In both samples the highest stresses have been found at the interface region between the weld pool and the heat affected zone. The hoop stress is always higher than the axial one, which is almost vanishing for both samples. Generally lower tensile stresses have been found in the thinner sample.

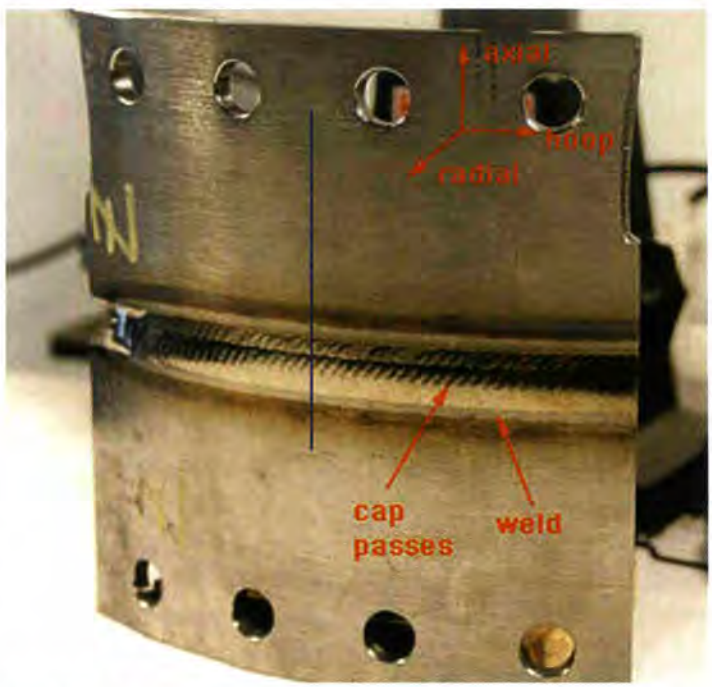

Figure 1: The 6 mm thick specimen. The orientation of the principal axes is also indicated.

Material, samples and experimental conditions

The Ti6Al4V alloy is a well established material for the construction of spacecraft fuel tanks [1]. From the micro-structural point of view, the alloy belongs to the mixed $\alpha+\beta$-Ti alloys, as Vanadium stabilises the presence of the β-phase (bcc structure) at room temperature. In the parent material, this implies the presence of globular α precipitates in a matrix of a finely dispersed α-phase embedded in residual β, and a lamellar mixed $\alpha+\beta$ structure in the heat affected zone and in the weld pool. In the weld pool, the grain size is considerably larger than elsewhere, and at the boundary between heat affected zone and weld pool it can reach 500 µm [2]. The volume fraction of the β-phase is slightly lower in the weld pool than in the parent material, where it is 6-7%.

Fuel tanks are built by joining two half-cylinders, first drawn and successive cold worked. The thickness of the half-cylinders is usually a few millimetres and their external diameter is of the order of 0.5-2 m. They are usually welded by TIG (Tungsten Inert Gas) welding. It is extremely important to determine the stress state in the weld region, in order to ensure safety during both storage on earth and launch, and to increase the vehicle lifetime. The stress state due to fuel pressure and weight can be easily calculated, and therefore the total stress evaluation needs the determination of residual stresses already present in the tank. We have investigated two specimens: a thick-walled welded sample (thickness 6 mm, shown in figure 1) and a thin one (1.6 mm). Experiments were performed at the D1A diffractometer of the ILL. The strain in α-Ti (011) lattice planes was measured, with a neutron wavelength of 2.99 Å. A gauge volume of 0.9×4×8 mm^3 was used for the 1.6 mm thick and 0.9×1×12 mm^3 for the 6 mm thick sample. For the thicker sample a gauge volume of 0.9×1×3 mm^3 was used in the direction parallel to the weld (longitudinal). 5 gauge points were investigated inside the weld pool, 5 in the heat affected zone and 1 far from the weld. Measurements were performed in three perpendicular directions (the scattering vector being oriented along them), namely the hoop, axial and radial (figure1), assumed to be the principal directions of strain and stress.

Results and Conclusions

As the geometry of the specimens suggests, the unstrained interplanar distance d_0 was evaluated with the *plane stress* hypothesis for each sample and in each investigated gauge point. Large changes of d_0 have been found [3], especially inside the weld, due to the variation of the grain size and some composition and precipitation gradients between the molten zone and the heat affected zone.

For the calculation of stresses from measured strains, the Young's modulus and the Poisson's ratio of the 011 reflection were used, as measured in [3] ($E_{(011)} = 98.9$ GPa, $\nu_{(011)} = 0.323$).

The results are plotted in figures 2-3. Higher stresses, in the hoop direction, are not (or not only) obtained inside the weld pool, but in the transition region between the weld pool and the heat affected zone. The measured stress values in the weld region (250/350 MPa in the hoop direction) are comparable to results from previous strain gauge measurements (180 MPa) [5]. The difference could be ascribed to texture, grain size effects and to the presence of 2nd order stresses, which are not detected by strain gauge methods. This kind of stresses are probably due to the presence of a β-phase[2].

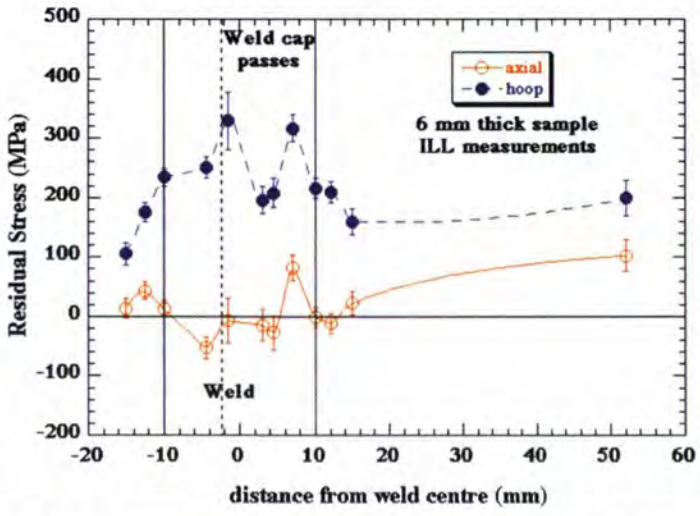

Figure 2: The axial and hoop stresses for the thick sample: values around 300 MPa are attained in the weld, but they decay rapidly outside. The far field level is not zero, but around 100-200 MPa.

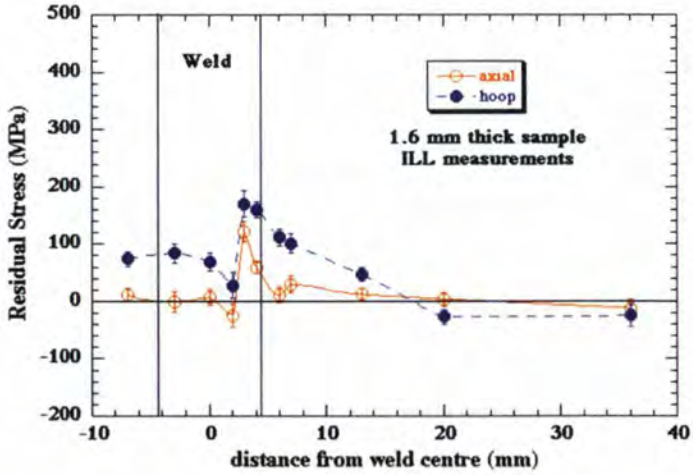

Figure 3: The axial and hoop stresses for the thin walled tank: lower values (max. around 180 MPa) are reached in the weld, and the far field level is zero.

For the thick sample a non-zero value is attained far from the weld. This far field stress state probably comes from the drawing process or the successive cold-working after welding. This is confirmed by the fact that the stress state is in-plane homogeneous, which is typical for drawn samples. There are some points in common between the investigated samples:

i) the stress profile is asymmetric with respect to the weld centre. This behaviour depends on the order of the weld passes, at least in the thick sample;

ii) the highest stress values are reached at the transition region between heat affected zone and weld pool;

iii) some oscillations appear in the stress profile, especially in the weld pool. This is due to the coarse-grain structure of the molten zone, but also to the effect of phase transitions, as shown in [6] and [7]. The last point applies to the specific alloy under investigation, and not only the investigated samples.

In conclusion, it can be remarked that, probably due to the overlap of the machining stresses, the weld stresses reach higher (and always tensile) values in the thick sample. The thin one seems to be relaxed or it may be thought that the freedom to straining brings to lower residual stress. The stress reaches asymptotic values far from the weld, so that the influence of the welding process extends only up to 12 mm from the weld centre line. ■

References

[1] T. Lorentzen, T. Leffers, in "Measurement of Residual and Applied Stress Using Neutron Diffraction", M.T. Hutchings & A.D. Krawitz Eds., Kluwer Academic Publ. (1992), p.253 • [2] G. Bruno, Ph.D. Thesis, Universities of Bologna and Ancona (1997) • [3] G. Bruno, A. Carradò, B. Dunn, F. Fiori, E. Girardin, T. Pirling, F. Rustichelli, Mat. Sci. For. 347-349 (2000) 684 • [4] G. Bruno, B.D. Dunn, Meas. Sci. & Techn. 8 (1997) 1244 [5] B.D. Dunn, private communication (1998) • [6] G. Albertini, G. Bruno, M. Ceretti, B.D. Dunn, F. Fiori, W. Reimers, F. Rustichelli, Proc. of the 26th National Congress of the Italian Association of Metallurgy (AIM), Milan 6-8/11/1996, AIM Publ., Milan (1996), p. 404 • [7] H. Wohlfahrt, HTM Beiheft, 31 (1976) 56.

Lubrication on the nanoscale:
spinning buckyballs *via* the intercalation of guest molecules

H. Schober and M.T. Fernandez-Diaz (ILL)

B. Renker (Forschungszentrum, Karlsruhe)

G. Roth (RWTH, Aachen)

Buckyballs are hollow, close-to-spherical molecules consisting of 60 carbon atoms. They possess a diameter of about one nanometer. When cooled down from the gas phase Buckyballs aggregate to form cubic crystals (figure 1). As the forces between these miniature balls are very weak they spin more or less freely at room temperature, leading to so-called plastic crystal properties. At around -20° C the balls finally realise that their structure deviates from that of a sphere and collectively lock into special orientations.
The temperature T_c of orientational ordering depends strongly on external pressure and intercalated guest molecules. Using neutrons it is possible to determine the mechanism by which the guest molecules facilitate the reorientational movement of the buckyballs.

The closer the balls are pressed together the harder it gets for them to reorient and therefore T_c increases. T_c equally reacts to the presence of guest atoms or molecules that may be intercalated easily into the rather large voids of the C_{60} host system. Alkali atoms like K or Rb act like grains of sand in the gearbox of the buckyballs. In systems like the superconducting K_3C_{60} the buckyballs stay orientationally locked up to very high temperatures. In contrast, the opposite behaviour is observed upon the intercalation of guest molecules like oxygen and nitrogen. As an example, T_c decreases by more than 30° C in N_2C_{60} with respect to pristine C_{60}. In a sense, the oxygen and nitrogen molecules act like a lubricant. Lubrication is an every day experience and consists in diminishing the efforts necessary to move a body in contact with its environment.

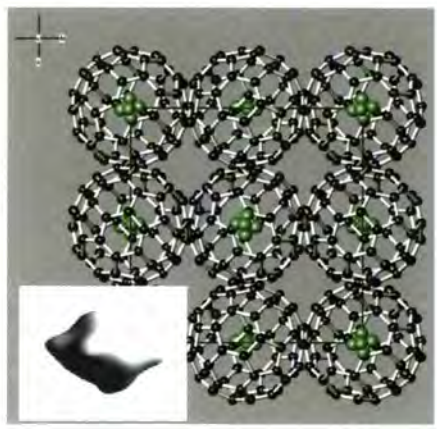

Figure 1: Refined low-temperature structure of N_2C_{60} for the space group P3. N_2 nitrogen molecules are found on the edges of a small octahedron (occupation probability shown as insert) centred on the octahedral sites of the host lattice (S6 symmetry).

High-resolution neutron diffraction experiments carried out on the instrument D2B at the ILL in combination with high resolution dilatometry measurements (figure 2) have shown that the intercalation of the guests leads to an expansion of the host lattice. The buckyballs are pushed apart by the intercalated molecular spacers. This is referred to as negative chemical pressure. Being further apart the corrugation of the charge density of the balls looses its potential to hinder reorientation. T_c decreases provided the spacers themselves do not constitute obstacles. A rather simple calculation shows, that the negative pressure effect alone cannot account for the observed decrease in T_c. The diffraction data, therefore, have to be analysed in more detail. It turns out that the guests do not only push the balls apart but also influence the way these lock into position. In pristine C_{60} below T_c the molecules are basically found in two competing orientations which differ only slightly in energy (figure 3). Close to T_c the balls are, therefore, distributed nearly

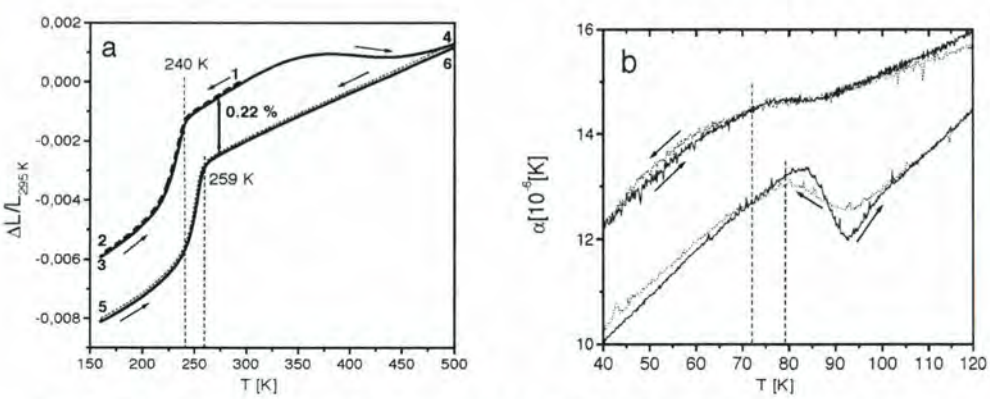

Figure 2: High resolution dilatometry measurements on N_2C_{60}. The cooling history is indicated by the arrows.
(a) Shown is the absolute linear expansion of the sample. The first order freezing of buckyball rotation (1 to 2) is accompanied by a strong lattice contraction. Upon heating above 350 K the N_2 molecules diffuse out of the sample (3 to 4) leaving behind pure C_{60}. Pure C_{60} shows a smaller lattice constant (6) and an upshift of the transition temperature from 240 K to 259 K.
(b) Suppression of the glass transition anomaly in N_2C_{60} (upper curves) and its recovery after annealing (loss of N_2 lower two curves) in pristine C_{60}.

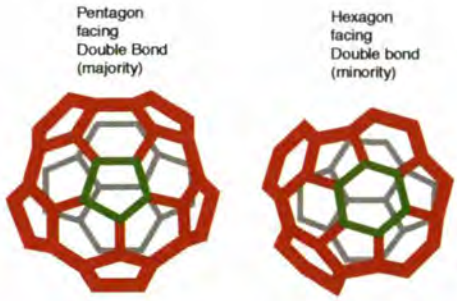

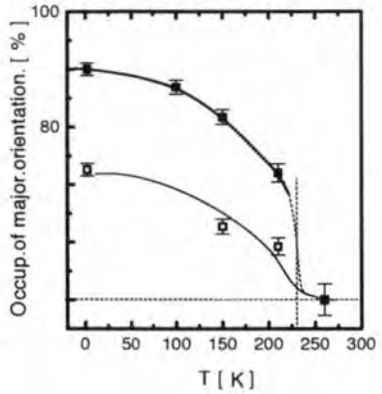

Figure 3: Occupation of the major orientation of C_{60} molecules (pentagon phase). Solid squares: N_2C_{60}; open squares reference C_{60}. In the majority orientation pentagons (green) of one buckyball face double bonds (grey) on the neighbours. In the minority orientation it is hexagons (green) facing double bonds.

equally between these two symmetrically inequivalent orientations. Switching from one orientation to the other, however, requires overcoming rather high energy barriers. Upon cooling these processes occur on increasingly long time scales. Below the so-called orientational glass transition temperature T_g part of the molecules (about 25 % in the case of powder samples; figure 3) are trapped in the energetically unfavourable orientation. In the intercalated systems the glass transition is, as our data show, more or less absent (figure 2). At very low temperatures we find practically all the balls (> 90 %) in the energetically favourable pentagon orientation (figure 3). This observation constitutes direct evidence for a modification of the energy landscape encountered by the buckyballs via the guest molecules. Lower effective barriers facilitate the reorientation of the balls leading to an orientationally more ordered state at low temperature. So even if the statement may sound counterintuitive, higher mobility actually favours ordering.

The guest molecules themselves are orientationally disordered (figure 2), which is to be expected, since the symmetry of the dumbbell shaped guests is not compatible with the symmetry of the crystallographic site on which they are intercalated.

Using the cold neutron time-of-flight instrument IN6 has allowed to monitor directly the dynamics of the molecules (figure 4). At low temperature, both guest and host molecules are performing small amplitude librations about their equilibrium orientations. The main band of the buckyball librations is found to be practically at the same frequency than in pristine C_{60}. This means that the forces necessary to slightly turn one ball with respect to the others are not weaker in the intercalated systems, an observation which comes as a surprise given the fact that the buckyballs are further apart from each other. This finding can only be attributed to the higher degree of order induced within the host via the intercalation of the guests.

When warming up, the librational band softens more quickly in the intercalated systems than in pristine C_{60}, indicating stronger anharmonicities. Already far below the transition temperature quasi-elastic scattering is observed, which indicates reorientations of isolated buckyballs. The average number of buckyballs participating in reorientation increases until it reaches 100 % when the system finally attains the plastic crystal phase. This happens some 20 to 30 degrees lower in temperature than in pristine C_{60}.

No quasi-elastic scattering which could be traced back to reorientation of the guest molecules can be detected, which implies that the orientational disorder of the guest molecules is static on the time scale of molecular vibrations. However, their librational movements are strongly anharmonic and coupled to the buckyball dynamics. They, therefore, cannot be completely ignored when analysing the transition mechanism. Large amplitude motion of the guest may provide the mobility necessary to prevent that the guests become obstacles for the reorientation of the balls.

In summary we find that the mechanism of T_c reduction in these rather simple systems is highly complex. The guest molecules do not only push the hosts apart but also influence the interactions between them. While this leads to increased orientational order and stiffer potentials at low temperatures it facilitates the passage towards nearly free rotations at higher temperatures. ■

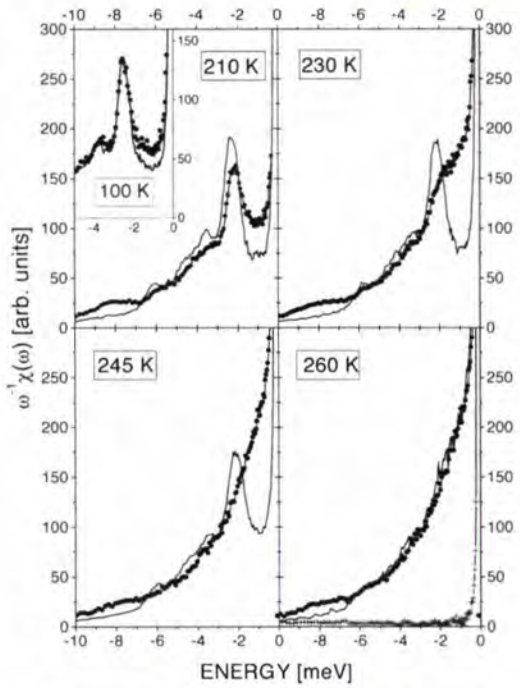

Figure 4: Generalised susceptibility of N_2C_{60} (dots) and a reference sample of C_{60} (line).The orientational freezing at T_c is characterised by the vanishing of C_{60} libron bands near 2 meV and the concomitant rise of quasielastic scattering (observable as a filling of the gap between the libron band and the elastic line).

References

[1] B. Renker, H. Schober, M. T. Fernandez-Diaz and R. Heid Phys. Rev. B 61 (2000) 13960 - [2] B. Renker, G. Roth, H. Schober, I. Nagil, R. Lortz, C.Meingast, P. Ernst, M. T. Fernandez-Diaz and M. Koza Phys. Rev B 64 (2001) 205 417.

Crystallisation of FeZr amorphous powders: bcc-Fe as a metastable phase?

P. Gorria (University of Oviedo, Oviedo)

J.S. Garitaonandia and R. Pizarro (University of País Vasco, Bilbao)

J. Campo (ILL)

Fe-Zr binary alloys display a complex magnetic diagram in the amorphous state, including ferromagnetic and re-entrant spin glass behaviour at low temperatures. After annealing above 850 K, crystallisation of the alloys takes place, leading to several FeZr phases. However, the crystallisation process of this system is not yet completely known, and some controversy exists concerning the different crystalline phases that appear. Three samples in the Fe-rich side have been obtained in powder form by means of mechanical alloying. An in situ kinetic study of the whole crystallisation process, by means of neutron diffraction, was performed on D1B for the three alloys. The most striking feature is that, while the beginning of the crystallisation process occurs at the same temperature, the crystallisation process evolves very differently for the three samples, including the appearance and disappearance of a bcc-Fe phase at intermediate temperatures in one of the samples.

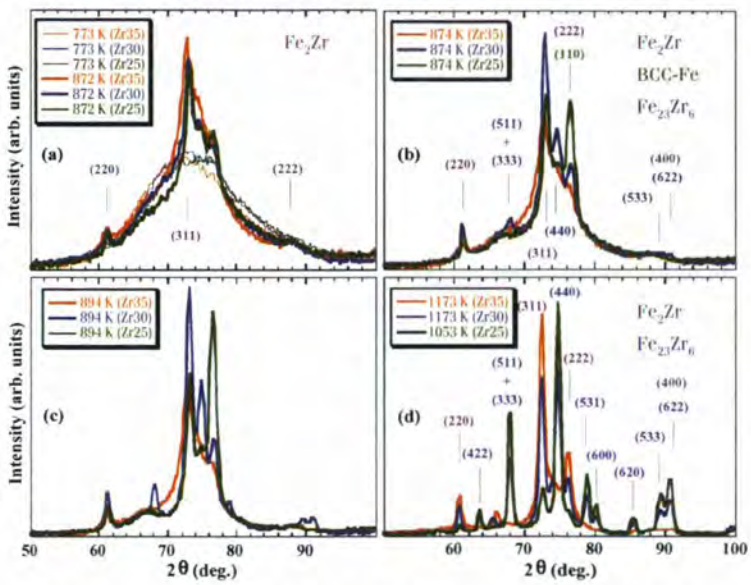

Figure 1: Evolution of the neutron diffraction patterns for the three samples during the crystallisation process. For easier reading, the same colour is used for each sample over all the spectra, (red for Zr35, blue for Zr30 and green for Zr25).

Over the last decade great efforts have been spent to obtain Fe binary and ternary amorphous alloys in powder form by means of mechanical alloying, given their two-fold interest, both fundamental and technological. In the case of Fe-Zr alloys, most of the samples studied have up to now been obtained in the form of ribbons, by means of the so-called rapid solidification technique. Nowadays, mechanical alloying presents several advantages over other fabrication methods: it is possible to obtain massive samples with a complete amorphous structure [1], and there is a broader range of compositions in which an amorphous structure can be obtained using this method (between 20 and 70 at. % of Zr and only 7 – 20 at. % of Zr using rapid solidification).

At low temperatures, Fe-Zr alloys become ferromagnetic; the magnetic properties, such as the ordering temperature T_c, present strong dependencies on the sample composition (T_c increases when the Zr content rises to 20 at. %, and then slowly decreases) [2]. As for their application, the production of nanocrystalline alloys by heating Fe-Zr-based amorphous alloys to adequate temperatures boosted enormous research activity during the '90s, mainly focussed on such technical applications as magnetic transducers, due to their soft magnetic behaviour. These alloys have also provided an exciting medium for the study of competing magnetic interactions between the small precipitated Fe-grains, as well as the respective roles of the remaining amorphous matrix and the nanocrystal-amorphous interfaces [3]. This report deals with structural properties only.

Three different crystalline phases are reported in the literature for alloys containing more than 65 at. % of Fe; two of them are the Laves phases Fe_2Zr ($Fd\bar{3}m$ and $P6_3/mmc$) and the third is $Fe_{23}Zr_6$ ($Fd\bar{3}m$) [4]. Some controversy exists about the third phase, and up to now it has not been clarified whether the composition of this phase is really $Fe_{23}Zr_6$ or Fe_3Zr [5].

Recent experiments performed on D1B have followed the whole crystallisation process of three samples, with compositions $Fe_{65}Zr_{35}$ (Zr35), $Fe_{70}Zr_{30}$ (Zr30) and $Fe_{75}Zr_{25}$ (Zr25).

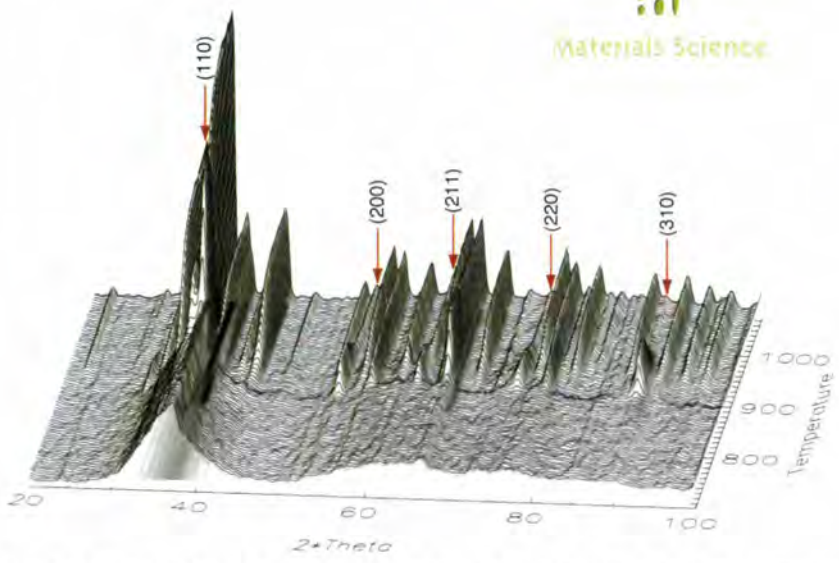

Figure 2: Neutron thermodiffractogram of the crystallisation process in a $Fe_{75}Zr_{25}$ alloy. The reflections corresponding to the bcc-Fe phase are indexed and marked with arrows.

using *in-situ* neutron diffraction for the first time. Samples were heated from room temperature to 1173 K, to ensure full crystallisation, and at a slow rate of 0.5 K/min, to distinguish all possible changes in the structure during the process. The most noticeable phenomena observed are the following.

At temperatures below 850-860 K the three samples remain in an amorphous state (figure 1a). They show only the characteristic halo typical of amorphous materials with no topological long range order: no reflections from impurities nor contamination during the fabrication process are observed. Above 850 – 860 K, a narrowing of the three amorphous haloes is clearly noticeable, marking the beginning of the nucleation of the first crystalline grains.

The first surprise appears with the spectra obtained at 872 K (figure 1a), where three reflections corresponding to a cubic $Fd\bar{3}m$ Fe_2Zr phase appear superimposed on the amorphous halo. These three patterns look very similar, providing evidence that, even if the composition of the samples is different, the onset of crystallisation takes place at nearly the same temperature, as previously observed in calorimetric measurements. If the temperature is raised only 2 – 3 K (figure 1b), it becomes clear that once the crystallisation starts, the process evolves in a very different way for the three compositions. In the case of the Zr35 sample only a slight rise in the peaks is observed, while in the case of the Zr30 sample reflections corresponding to a cubic $Fm\bar{3}m$ phase with $a \approx 11.7$ Å are evident; in the case of the Zr25 sample, no evidence of this latter phase is observed, but the development of the (222) reflection of the Fe_2Zr is clearly visible. This latter effect is only explicable if we consider that this intensity corresponds not only to this phase, but also to a small amount of $Im\bar{3}m$ bcc-Fe. As can be seen in figure 1c (894 K), this bcc-Fe phase grows quicker than the Fe_2Zr in the Zr25 sample; meanwhile, in the other samples only a small increase of the existing phases is observed.

The second surprising phenomenon takes place at temperatures above 894 K. The amount of bcc-Fe in the Zr25 sample remains almost constant up to 943 K, the temperature at which the above-mentioned $Fm\bar{3}m$ phase appears; this phase appears at a different temperature in the Zr30 and Zr25 samples. The amount of this phase continuously increases up to 972 K, where no evidence of bcc-Fe remains (figure 2). Furthermore, the intensity of the reflections corresponding to the Fe_2Zr phase also decreases, while the reflections of the $Fm\bar{3}m$ phase continue to increase up to 1012 K (figure 1d). Above 972 K, the structure of the sample does not vary; nor does it vary when the sample is cooled to room temperature. Figure 3 shows the X-ray diffraction pattern measured from Zr25 at RT. Only the reflections corresponding to the $Fm\bar{3}m$ phase are present; the composition of this phase must therefore be Fe_3Zr instead of $Fe_{23}Zr_6$, given the original composition of the powder.

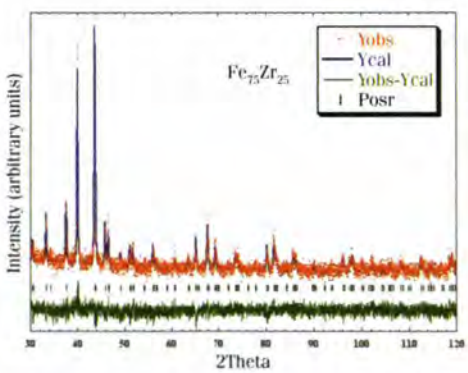

Figure 3: X-ray diffraction pattern together with the fit for the sample $Fe_{75}Zr_{25}$ fully crystallised and obtained at room temperature. Only reflections corresponding to one phase with a $Fm\bar{3}m$ structure are present.

These results have shown, for the first time, that a metastable BCC-Fe phase can appear at high temperatures, and also that the Fe_3Zr phase can be obtained as a result of the crystallisation of an amorphous Fe binary alloy. Mössbauer spectroscopy and magnetisation measurements will be performed in order to study the magnetic behaviour of these "new" phases.

This work has been supported by Spain's CICyT under projects MAT99-0667-C04-03 and MAT2000-1047. We wish to thank ILL and the CRG-D1B for its allocation of neutron beam time and SCT (Univ. Oviedo) for the XRD (High Resol.) facility. ■

References

[1] L. Schultz and J. Eckert in Topics in Applied Physics, Glassy Metals III, Vol. 72, H.J. Güntherodt and H. Beck (Eds.) Berlin: Springer (1994) 69-120 • [2] K. Fukamichi, T. Goto, H. Komatsu and H. Wakabayashi in Physics of Magnetic Materials, ed. W. Gorzowski, H.K. Lakowicz and H. Szymczak (World Scientific, 1989), 354 • [3] J.S. Garitaonandia, P. Gorria, L. Fernández Barquín and J.M. Barandiarán, Phys. Rev. B 61 (2000) 6150 • [4] P. Villars and L.D. Calvert, Pearson's Handbook of Crystallographic Data for Intermediate Phases (American Society of Metals, Cleveland, OH, 1985) • [5] F. Aubertin, U. Gonser, S.J. Campbell and H.-G. Wagner, Z. Metallkunde, 76 (1985) 237.

Magnetic multilayers studied by spin-resolved unpolarised neutron off-specular scattering

- V. Lauter-Pasyuk (TU München Garching, JINR Dubna and ILL)
- V. Ustinov and L. Romashev (Institute of Metal Physics, Ekaterinburg)
- H.J. Lauter (ILL)
- B.P. Toperverg (PNPI Gatchina and Forschungszentrum Jülich)
- A. Vorobiev (MPI für Metallforschung, Stuttgart and ILL)
- O. Nikonov (JINR Dubna and ILL)
- J. Major (MPI für Metallforschung, Stuttgart)

It is shown that unpolarised neutrons scattered from magnetic multilayers self-separate according to their spin state in the dynamical scattering regions of Yoneda scattering and superstructure Bragg-sheet scattering. Strong anomalies in the off-specular scattering originating from magnetic fluctuations in the multilayer are determined by the spin-flip selective process. A complete 2-dimensional model describes all experimentally observed features and gives a detailed picture of the multilayer magnetisation.

In exchange coupled multilayers, the interplay between the crystalline anisotropy, interlayer exchange coupling and external magnetic field strength leads to the result that the layer magnetisations in successive Fe-layers in each columnar domain [1] are oriented at a certain coupling angle with respect to each other as shown in figure 1. Here it is shown that even unpolarised neutron off-specular scattering can efficiently be used to determine the configurations of the atomic magnetic moments.

Reflectometry experiments have been carried out on the EVA-spectrometer with a wavelength of 5.4 Å and an external magnetic field of 500 G. The sample was a $([Cr(9\ Å)/^{57}Fe(68\ Å)]_{12}/Cr(68\ Å))$ multilayer on sapphire substrate grown with molecular beam epitaxy. The scattering geometry with specular and off-specular scattering and the sample composition are depicted in figure 1: here the layer magnetisation is decomposed into domains (figure 1 top view) with an antiferromagnetic interaction perpendicular to the layering (figure 2 side view). The exchange coupling angle α between the magnetisation directions in successive Fe-layers arising due to the external field H is shown in the inset of figure 1 top view. In figure 2a, the 2-dimensional intensity map of specular reflected and off-specular scattered neutrons is shown as a function of p_i and p_f, the perpendicular to the surface components of the incoming and outgoing wave vector, respectively. The specularly reflected intensity along the line $p_i = p_f$ shows the total thickness oscillations as well as the first order Bragg peak ($p_i = p_f = 0.041$ Å^{-1}) corresponding to the bi-layer thickness of 77 Å. The off-specular scattering originates from the domain structure of the multilayer. It appears as spin-flip Bragg-sheet scattering through the 1/2 and 3/2 order

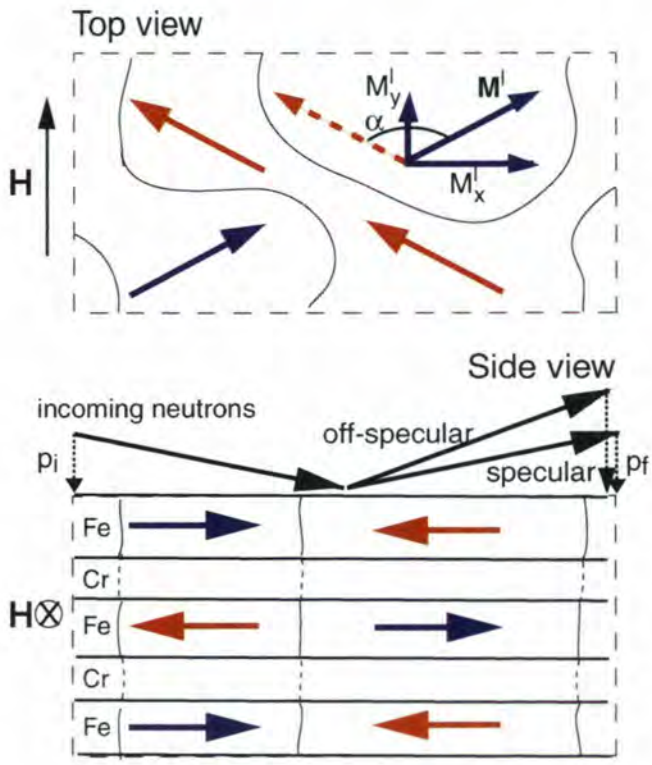

Figure 1: Schematic presentation of the multilayer sample in an external magnetic field H parallel to the sample surface (top and side view). In the side view the scattering geometry of specular and off-specular scattering is added and in the top view the layer magnetisation M^l is shown with the coupling angle α between the magnetisation vectors in successive Fe layers. The layer magnetisation M^l has two components M^l_x and M^l_y perpendicular and parallel to the external magnetic field, respectively.

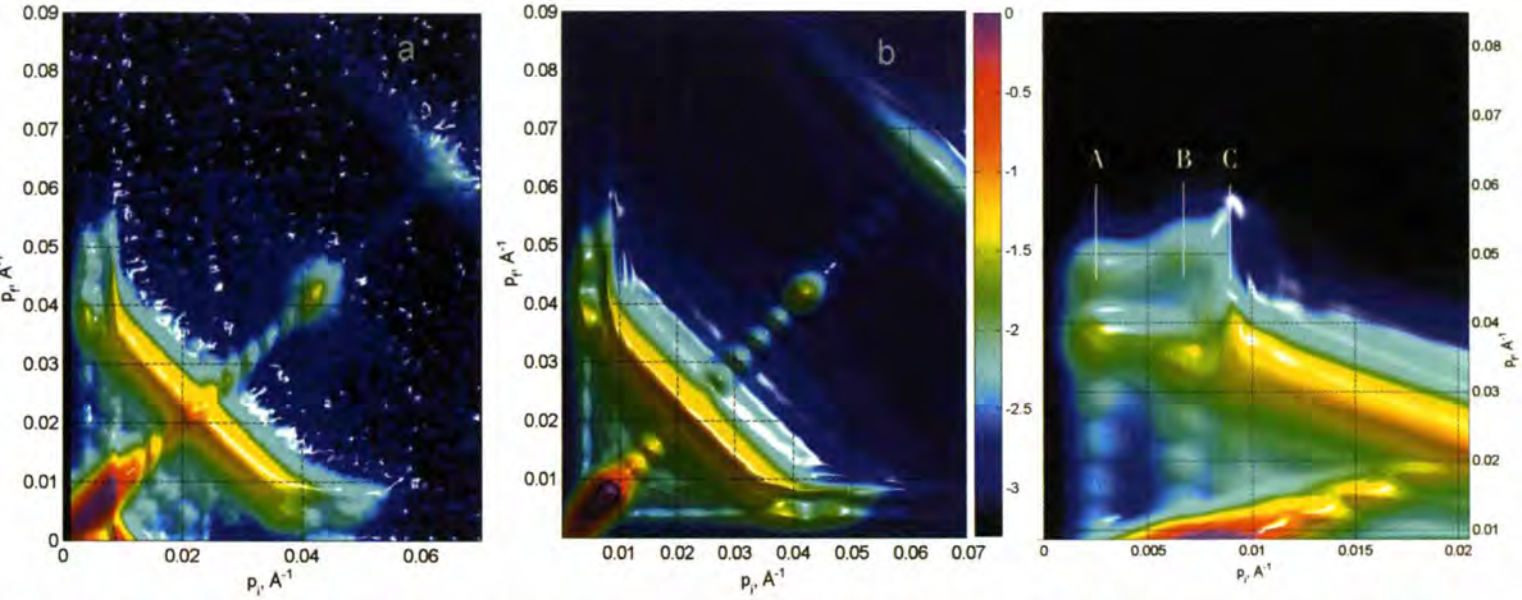

Figure 2: a) Experimentally determined 2-dimensional intensity map of a Fe/Cr multilayer as a function of p_i and p_f, the perpendicular components of the incoming and outgoing wave vector, respectively. The specular reflection is along the line $p_i = p_f$. The off-specular Bragg sheet scattering spreads from the 1/2 and 3/2 order Bragg peak positions perpendicular to the specular line. The first order Bragg peak position corresponds to the Fe/Cr bilayer thickness and does not show off-specular scattering.
b) Model fit of the 2-dimensional intensity map of a Fe/Cr multilayer shown in figure 2a.

Figure 3: Extended view on the region of the Bragg-sheet scattering crossing the Yoneda-scattering for experimental data. A and B mark the position of Yoneda scattering related to total thickness scattering. C is the position of the first critical angle which coincides with the position of the cut-off by the substrate potential.

Bragg peak positions ($p_i = p_f = 0.0205$ Å^{-1} and $p_i = p_f = 0.0615$ Å^{-1}, respectively) on the reflectivity line as well as along the spin-flip Yoneda scattering parallel to p_i and p_f (figure 2a). A proof of the spin-flip character can be made by spin-analysis of polarized neutrons being scattered from the multilayer [1]. But here it is visible directly through the intensity cut-off due to critical angles. The two critical angles are determined by the two scattering length densities $SLD_n \pm SLD_{mp}$ for the two neutron spin states. SLD_n is the nuclear contribution of the ^{57}Fe and SLD_{mp} is the magnetic contribution from the parallel to the external field component of the magnetic moments M^l_y (figure 1). So, one critical angle shows up in the units of momentum transfer along $p_i = 0.009$ Å^{-1} and also along $p_f = 0.009$ Å^{-1} due to the use of unpolarized neutrons. It is best visible in the characteristic spikes (marked with C in figure 3) where the Bragg-sheet scattering runs into the Yoneda scattering and intensity is cut for one spin-state. Any intensity below the mark C originates from the other spin-state. For the sample used in this experiment the other critical angle is imaginary because the difference of $SLD_n - SLD_{mp}$ is negative. Therefore, the off specular scattering extends down to the horizons along $p_i = 0$ and $p_f = 0$ which interferes also with the scattering arising due to the total thickness oscillations visible in modulated bands parallel to the horizons (*modified Yoneda scattering*) marked with A and B in figure 3. The positions of these *Yoneda-bands* depend on the value of the imaginary critical angle. These effects have been taken into account in the 2-dimensional model fit shown in figure 2b. Another critical parameter is given by the substrate potential, which leads to another cut of intensity. For the applied external magnetic field of 500 G this value coincides with the first critical angle marked with C. An extended view of the modelled intensity distribution is shown in figure 3.

With the model fit based on the distorted wave Born approximation [2] it is possible to describe all details of the off-specular scattering and to unravel the detailed composition of the layer magnetisation in the multilayers system. In particular, it has been possible to extract the two scattering length densities related to ^{57}Fe (SLD_n and SLD_{mp}) from the fit to the data obtained with unpolarised neutrons. The knowledge of SLD_{mp} is decisive to determine the coupling off-specular scattering angle α (figure 1) of the magnetic moments using for M^l the full atomic magnetic moment of Fe. Consequently, the mean coupling angle can be determined (as also a function of applied field) and related to the GMR effect [3]. ■

References

[1] V. Lauter-Pasyuk, H.J. Lauter, B. Toperverg, O. Nikonov, E. Kravtsov, M.A. Milyaev, L. Romashev, V. Ustinov, Physica B283 (2000) 194 • [2] B.P. Toperverg, O. Nikonov, V. Lauter-Pasyuk, H.J. Lauter, Physica B297 (2001) 169; B.P. Toperverg, Physica B 297 (2001) 160 • [3] H.J. Lauter, V. Lauter-Pasyuk, B. Toperverg, L. Romashev, M.A. Milyaev, E. Kravtsov, V. Ustinov, O. Nikonov, V. Leiner, V. Aksenov, ILL Millennium Symposium, April 2001, p.187 (http://www.ill.fr).

The structure of ferrofluids
in the vicinity of the interface with silicon

- A. Vorobiev (MPI Stuttgart and ILL)
- J. Major (MPI Stuttgart)
- G. Gordeev (PNPI Gatchina)
- B.P. Toperverg (PNPI Gatchina and Forschungszentrum Jülich)

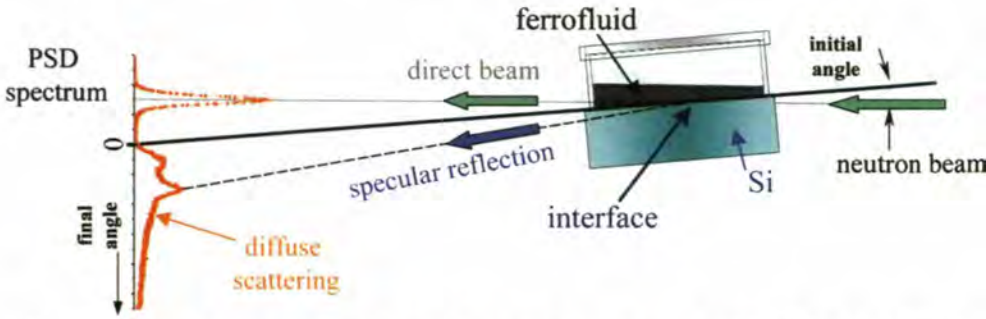

Figure 1: The setup of the experiment. The neutron beam reaches the interface through the Si block. The reflected, transmitted, and scattered intensities are recorded by a 1D position-sensitive detector (PSD). A homogeneous magnetic field up to 100 Oe was applied parallel both to the Si-ferrofluid interface and the incoming beam.

A combination of magnetic and non-magnetic interactions in ferrofluids, i.e. in colloidal solutions of ferromagnetic nanoparticles [1], results in a strong ordering tendency of the particle magnetic moments into various arrangements, e.g., (anti)-ferromagnetic or spin-glass-like structures, while the coupling between the rotational and the translational degrees of freedom may lead to various instabilities in their spatial order. The presence of an interface with another material brings new factors into the possible structuring of the ferrofluids. Here we show that ferrofluid particles order in the vicinity of a monocrystalline silicon interface, forming structures depending on their sizes and concentrations. The resulting layering can be influenced by the application of weak magnetic fields, and it is also shown that their reorganization is governed by a relatively slow kinetic process.

Ferrofluids are stable colloidal suspensions of fine, magnetic particles which are coated with a layer of nonmagnetic molecular surfactants that protects the system from irreversible aggregation. Due to their small sizes in the range of 100 Å, each particle represents a single magnetic domain. The point of our interest is the ordering phenomenon of the magnetic particles in external magnetic fields in the vicinity of a well-defined solid wall, in the present case near a flat monocrystalline silicon interface. The forces acting on the particle near the interface are equilibrated in a different way than in the bulk and this may result in interface structures which differ from the bulk structure.

Amongst a number of techniques used for studying ferrofluids, only the neutron reflectivity methods and the neutron diffuse scattering at grazing-incidence provide detailed microscopic information on the near-interface behaviour as well as on the interfacial properties. These methods have been used to study ferrofluids samples made at the Petersburg Nuclear Physics Institute (PNPI, Gatchina, Russia) by chemical deposition of dispersed magnetite (Fe_3O_4). The synthesised particles were coated with a surfactant ($C_{18}H_{33}NaO_2$) and selected by weight. Three D_2O-based samples with different particle sizes and concentrations have been studied :

sample	c	r [Å]
FF-2	0.02	23 ± 3
FF-3	0.03	50 ± 5
FF-7	0.07	50 ± 5

Samples' specifications: c is the volume concentration of the ferromagnetic cores; r is the effective particle radius, obtained from SANS experiments. The SLD of the magnetite core (Fe_3O_4) is $6.87 \cdot 10^{-6}$Å^{-2}, that of the surfactant ($C_{18}H_{33}NaO_2$) is $2.04 \cdot 10^{-7}$Å^{-2}, and $6.375 \cdot 10^{-6}$Å^{-2} for D_2O.

Room temperature reflectivity experiments have been carried out at the EVA evanescent wave diffractometer with a monochromatic neutron beam with wavelength of 5.5 Å [2]. The sample holder was a quartz frame glued onto a horizontal silicon monocrystal block. The neutron beam reaches the silicon-ferrofluid interface through the silicon monocrystal (figure 1). Such experiments provide with information on the depth distribution of the so-called scattering-length density (SLD) with nearly atomic resolution. The scattering length is a quantity which strongly differs for the various atoms involved.

Figure 2a shows reflectivity curves, obtained for the sample FF-2, after subtraction of the off-specular contribution. The corresponding SLD profiles along the z-axis (normal to the interface), determined by a standard fitting routine, are shown in figure 2d. These curves reveal a rather complex ferrofluid structure in the vicinity of the interface

(figure 2g), which clearly consists of four distinct layers. The thickness of the first (I) layer is smaller than the mean core diameter of the particles and therefore it can only be composed of surfactant in the $H = 0$ case and mainly of surfactant for $H = 100$ Oe. The second layer (II), whose thickness corresponds to the mean ferrofluid core diameter, can be composed of magnetite and D_2O. The third layer (III) is a somewhat thicker interlayer than I, consists mainly of surfactant, and the fourth layer (IV) possesses a magnetite concentration which is slightly larger than that in the bulk ($z > 250$ Å). The applied magnetic field does not influence the basic layering structure but its application results in the partial depletion of the range $z < 140$ Å (layers I to IV) from magnetite and/or D_2O.

Data obtained on the sample FF-3 are shown in figures 2b,e,h. The layering is similar to that in the sample FF-2. Layer I is probably missing, however, and layer II is much broader than in FF-2 and contains a large fraction of surfactant (note that the particles in this sample are much larger than in FF-2). The effect of the applied magnetic field is very weak.

Since diffuse scattering may significantly contribute to the signal in the specular direction, a clear separation of the specular component is not always straightforward. This is especially true if the in-plane fluctuations are strong and also correlated along the direction perpendicular to the interface studied. Such a case is revealed on the sample FF-7, as shown in figure 2c. The presence of the magnetic-field-dependent strong peak at $q_z > 0.55$ Å^{-1} is ascribed to such correlations which are clearly possible at the high concentration of this sample. Accordingly, the SLD profile shown in figure 2f was derived from the reflectivity data for $q_z < 0.55$ Å^{-1} only. The surface-induced ordering in this sample is obviously different from the layering in the low-concentration samples FF-2 and FF-3.

During these experiments the magnetic field effects were found to be affected by relaxation processes, with characteristic time of several hours. This delay time is much longer than the characteristic diffusion time of the ferrofluid particles, which leads to conclude that in the vicinity of the interface an additional strong coupling between the particles must exist. The steric (entropic) repulsion, which keeps the ferrofluid particles apart from each other in the bulk, appears to become ineffective under the influence of the silicon wall and makes the dense layering possible [3]. ■

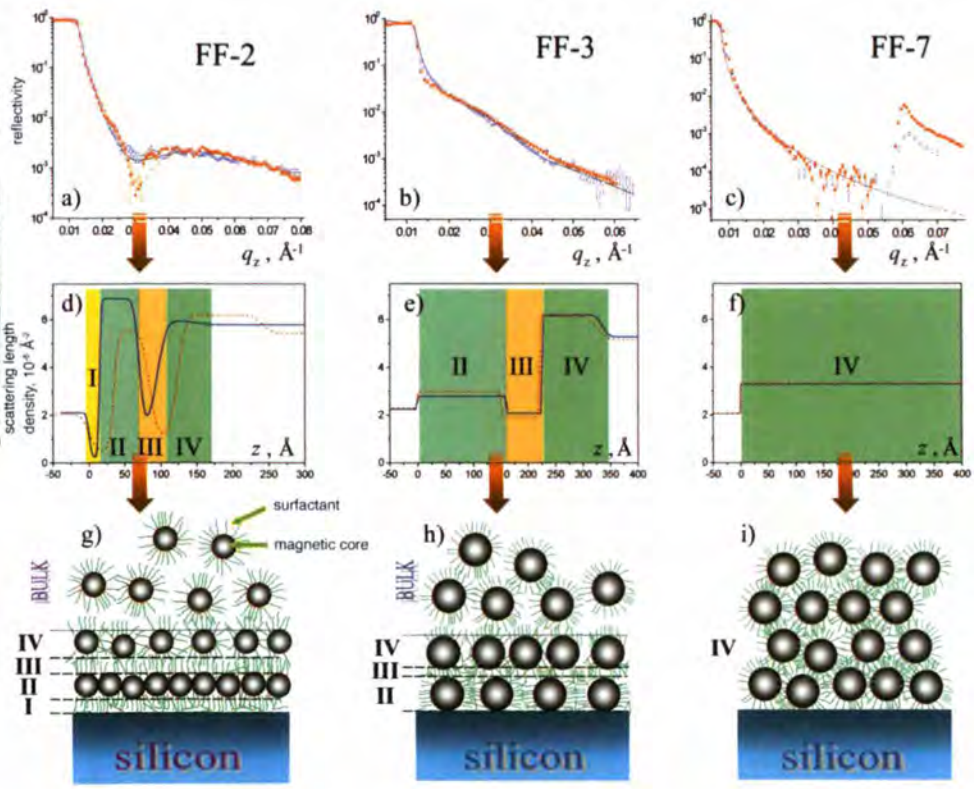

Figure 2: First row: reflectivity curves obtained on the ferrofluid samples. Second row: fitted z-profiles of the SLD. Third row: reconstructions of the ferrofluid particle distributions. (FF-2: a, d, g; FF-3: b, e, h; FF-7: c, f, i; points: experimental results corrected for diffuse scattering; lines: fitted (a, b, c) or calculated (d, e, f) results; blue colour: $H = 0$, red colour: $H = 100$ Oe.) The thickness of the obtained layers for FF-2 and FF-3 correlates with the mean particle size (see Table 1).

REFERENCES

[1] R. E. Rosensweig: Ferrohydrodynamics, Cambridge University Press, Cambridge, 1985 • [2] H. Dosch, K. Al Usta, A. Lied, W. Drexel, and J. Peisl, Rev. Sci. Instrum. 63 (1992) 5533 http://www.ill.fr/YellowBook/EVA/ • [3] A. Vorobiev, G. Gordeev, J. Major, B. P. Toperverg, H. Dosch, to appear in: Applied Physics A.

Quantitative textural analysis of geological low-symmetry materials:
amphiboles from the Sesia-Lanzo Zone (Italy)

M. Zucali and M. Dugnani (Milano University)

D. Chateigner (Laboratoire CRISMAT-ISMRA, Caen)

B. Ouladdiaf (ILL)

Quantitative texture analysis of geological low symmetry material from the Alpine chain, carried out at the D1B diffractometer, allows to compare neutron with X-rays data in the quantitative determination of multiphase geological textures and to define the relationship between microstructure and texture. Texture of amphiboles, deformed at 15-20 kbar and 550-600°C during the Alpine time, shows a pronounced crystallographic preferred orientation related to the rigid body rotation and dislocation creep components of the deformation mechanisms. [010] axis and (hol) planes axis are parallel to the mesoscopic mineralogical lineation. This study shows the neutron reliability compared to X-ray for quantitative texture analysis purposes in polyphasic rocks, which is the first step for the understanding of deformation mechanisms and mechanical proprieties of rocks during subduction.

The development of planar and linear fabrics in metamorphic rocks occurs under different physical conditions (temperature, pressure, stress, strain, strain rate, fluid-mineral grain boundaries interaction, etc.) and depends on the deformation mechanisms active within metamorphic minerals accommodating strain during each stage of mechanical and mineralogical re-equilibration. Microstructural analysis, using classical optical microscopes, even providing a complete description of the relationships between individual grains and subgrains and allowing the description of the multistage mechanical and mineralogical re-equilibration of rocks, remains inadequate for the quantitative analysis of textures (lattice preferred orientation). Scattering probes such as neutrons provide the necessary information. The investigated samples are hornblendites and eclogites from the Sesia-Lanzo Zone (Western Italian Alps). The Sesia-Lanzo Zone is a kilometre wide slice of continental crust subducted and exhumed during the Alpine orogeny [1]. The quantitative texture analysis of eclogite facies fabrics, developed at high pressure (15-20 kbar) and low temperature (550-600°C) allows investigating the deformation mechanisms of rock forming minerals within a subducting continental crust. The samples are made of recrystallised calco-sodic amphibole (98% of rock volume), chlorite and rutile. The preferred orientation of amphiboles defines the macroscopic mineralogical lineation. The texture of amphiboles with respect to the microstructure (lineation) has been studied in order to:

i) compare neutron data with X-rays in the quantitative determination of multiphase geological material textures;

ii) define the relationship between microstructure and texture;

iii) describe the active slip system(s) of amphiboles.

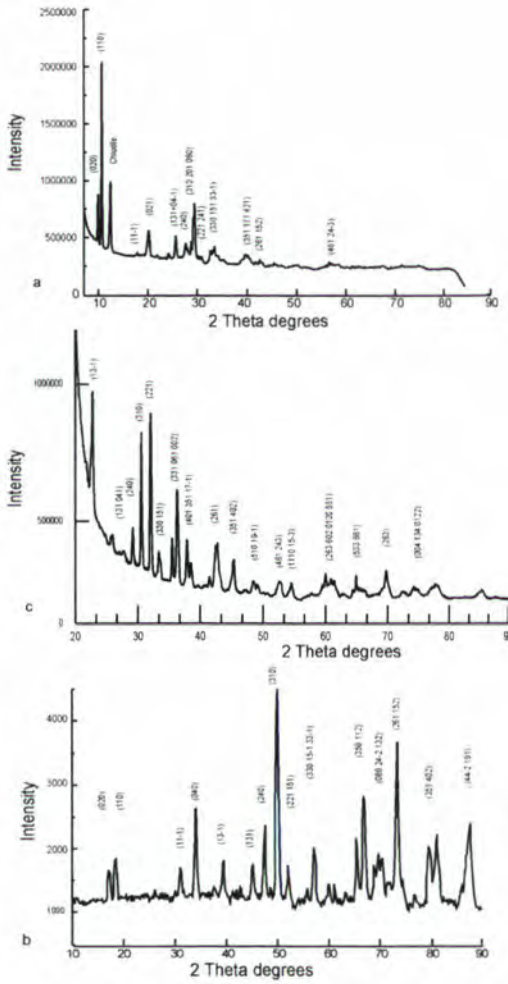

Figure 1: X-ray and neutron diffraction pattern of M26 hornblendite. a) sum of 1080 X-ray diffraction patterns with an incidence angle of 5.36°. b) sum of 1368 neutron diffraction patterns with an incidence angle of 20°. c) Summed X-ray diffraction pattern of 1080 scans with an incidence angle of 16°.

The D1B diffractometer has been chosen for its curved Position Sensitive Detector (PSD), comparable in angular span to the one used at our laboratory [2], and using a previously developed methodology [3]. Figure 1 compares the summed neutron and X-ray diffraction pattern of M26 sample for the 1368 and 1080 measured scans respectively. The defocussing effect

that occurs using flat specimens with X-rays makes high angular ranges (2theta and chi) comparatively less reliable. This effect is partly compensated for higher incidence (omega) angles (figure 1c). Orientation Distribution (OD) refinements for neutrons, X-rays (at 2 omega values) are compared in figure 2, using experimental and recalculated pole figures. While X-rays at low omega offer unreliable calculation of the OD, using a higher omega value permit a relatively better approximation of it. Neutrons data still show the best reliability (see R-factors), whereas several X-rays experiments on the same samples are needed to compensate the relatively low number of probed grains.

Recalculated pole figures (figure 2) show the concentration of the [010]* axis (a = 9.540 Å, b = 5.281 Å, c = 17.717 Å, γ = 103.770°) parallel to the macroscopic lineation (vertical direction in pole figures) and the dispersion of [001]* - [100]* directions within a plane perpendicular to the lineation and foliation. Those patterns reproduce the observation on naturally deformed amphiboles [4 and refs. therein]. In recalculated pole figures from neutron and X-ray experiments the same distribution of lattice axes occurs. It can be shown that the shape preferred orientation of amphiboles, marking the mesoscopic lineation/foliation, corresponds directly to the lattice preferred orientation of the [010]*directions, suggesting a component of rigid body rotation for the fabric development, and that the preferred orientation of the (*hol*) planes, parallel to the lineation, can be due to slip along [010](*hol*) systems.

The orientation of the [110]* and the [010]* directions with respect to the lineation and foliation can be interpreted as due to a dominant constrictional component of the finite strain [5]. The pronounced asymmetry of the [010]* directions can also be interpreted as developed during a non-coaxial deformation, where comparable asymmetries have been observed in other materials (e.g. calcite and quartz [6, 7, 8]). The comparison of the two techniques shows that X-ray data can produce semi-quantitative results, which reproduce the overall texture if a sufficient area of the sample, or different pieces of the same sample are scanned in similar conditions and that the neutron results are much more reliable as also shown by the RP values (16.5 for neutron-derived OD and 66.4 for X-ray derived OD). ■

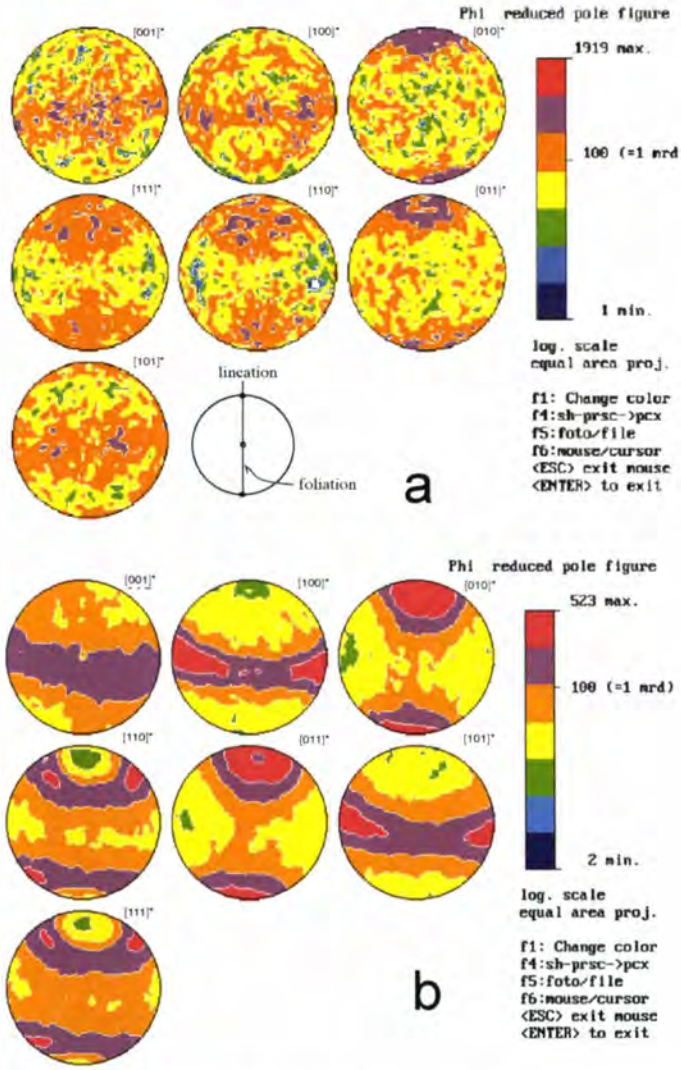

Figure 2: Recalculated pole figures for X-ray (a) and neutron (b) experiments.

REFERENCES
[1] R. COMPAGNONI, REND. SOC. IT. MINER. PETROL. 33 (1977) • [2] D. CHATEIGNER, H.R. WENK AND M. PERNET, TEXT. AND MICROSTR (1999) 33 • [3] J. RICOTE AND D. CHATEIGNER, BOL. SOC. ESP. CERAM. VIDRIO 38 (1999) 6 • [4] S. SIEGESMUND, K. HELMING AND R. KRUSE, J. OF STRUCT. GEOL. 16 (1994) 1 • [5] GAPAIS & BRUN, CAN. J. EARTH SC. 18, 995-1003 (1981) • [6] NICOLAS & POIRIER, WILEY, 440 (1976) • [7] GAPAIS & COBBOLD, TECTONOPHYSICS, 138/2-4, 289-309 (1987) • [8] LAW, GEOL. SOC. SPECIAL PUBB., 54, 335-352 (1990).

Sodium silicate melts:
structural changes, relaxation and ion diffusion

● A. Meyer (TU München)

● H. Schober (ILL)

● D.B. Dingwell (LMU München)

Silicate melts have great relevance both in earth science and technology: physical properties of magma (molten silicate rock) dominate many geological processes and technological glasses are synthesised from the molten state. These silicate melts, natural and technological, are multicomponent systems. A considerable effort has been made to investigate a wide range of silicate melts with the general aim of linking structural with physical properties and to develop an atomic level understanding of their structure and dynamics [1]. Nevertheless, experiments on the structure and microscopic dynamics in the viscous melt well above the conventional glass transition temperature T_g are scarse in part due to the high melting temperatures. Here, inelastic neutron scattering results on sodium disilicate melts are presented to show that at temperatures well above T_g significant structural changes occur that have a strong influence on the sodium ion transport. Such changes may very well be the cause for the weak temperature dependence of the viscosity at higher temperatures.

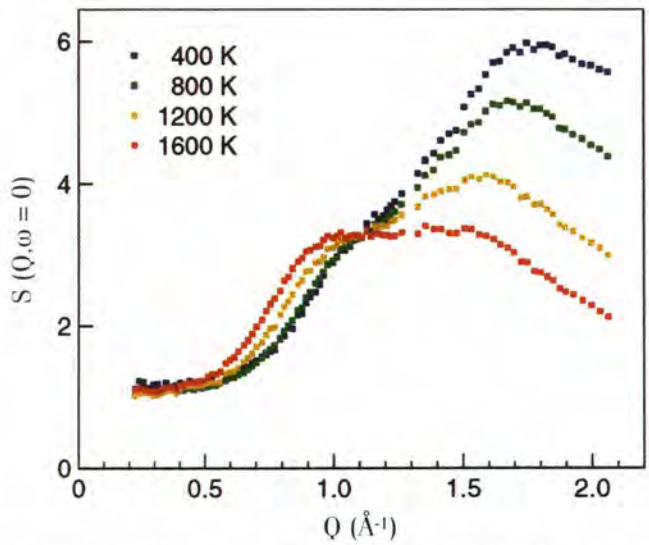

Figure 1: Elastic structure factor $S(Q,\omega = 0)$ of sodium disilicate: Toward small Q the signal is dominated by the incoherent contributions of the sodium atoms. The maximum around ≈ 1.7 Å^{-1} reflects the scattering of the partially disrupted tetrahedral Si-O network. With increasing temperature a pronounced shoulder is emerging at $Q \approx$ 0.9 Å^{-1}. The decrease in intensity at Q values larger than ≈ 1.1 Å^{-1} in turn mainly reflects the Debye-Waller factor.

Alkali silicates are a simplified analogue for most magmas and technological glasses. Compared to pure silica, with a caloric glass transition temperature T_g at ≈ 1500 K, the addition of Na_2O partially disrupts the SiO_2 network structure resulting in a considerable reduction of T_g. The experimental investigation of the melt is, therefore, compared to pure SiO_2 more accessible ($T_g \approx$ 700 K for sodium disilicate). In addition, sodium disilicate has been the subject of extensive molecular dynamics simulations [2,3]. Inelastic neutron scattering covers a dynamic range that gives insight both into dynamics on microscopic time scales and the medium range structure of silicate melts. In addition, the results can provide input for simulations used e.g. to model magma properties in volcanic activity and are an experimental test of molecular dynamics simulations.

Inelastic neutron scattering measurements have been performed on the time-of-flight spectrometer IN6 with the sodium disilicate sample encapsulated in a Pt sample cell. Spectra were measured in the glass at 400 K and in the viscous melt at 800 K and between 1200 K and 1600 K in steps of 100 K.

Figure 1 displays the elastic structure factor of glassy and viscous sodium disilicate. At $Q \approx$ 0.9 Å^{-1} a *pronounced prepeak* is emerging with increasing temperature. The molecular dynamics simulations on sodium disilicate melts [2] do indeed exhibit a shoulder in the static structure factor at $Q \approx$ 0.94 Å^{-1}. This shoulder is linked to regions where the SiO_2 network is disrupted and where the sodium concentration is enhanced. A recent molecular dynamics simulations study on sodium tetrasilicate [3] has suggested the existence of sodium rich channels having a distance of about 6-8 Å. The experimentally observed prepeak at 0.9 Å^{-1} corresponds to the distance between these channels. Figure 2 displays the location of the sodium atoms in the simulation box during a 1.4 ns run and

demonstrates the existence of these channels. A similar behaviour has been found in the simulations on sodium disilicate.

At temperatures up to $\approx 2 \cdot T_g$ the diffusive dynamics of the alkali atoms in silicate melts have been observed from the experimental data taken on the instrument IN6. It is appreciably faster than the structural relaxation [1] of the SiO_2 network which – as demonstrated by high-energy resolution backscattering spectra taken at the NIST Center for Neutron Research in Gaithersburg – takes place on a nanosecond time scale. Figure 3 displays the scattering law $S(Q,\omega)$ of sodium disilicate as determined on IN6. At Q = 0.5 Å^{-1} the signal is dominated by the incoherent scattering of sodium which in turn is dominated by elastic scattering. This indicates that at a given time only a fraction of the sodium atoms is participating in the fast diffusion. Beside the dominant elastic contribution, diffusive motion of sodium leads to a broad quasielastic signal on a 10 ps time scale. The lines in figure 3 are fits with

$$A\left(\int dt\, e^{-i\omega t} \exp\left[-(t/\tau_Q)^{\beta Q}\right] + B\delta(\omega)\right) \qquad (1)$$

where the δ function represents the elastic scattering contribution to the signal. A and B are the respective amplitudes of the quasielastic and elastic scattering.

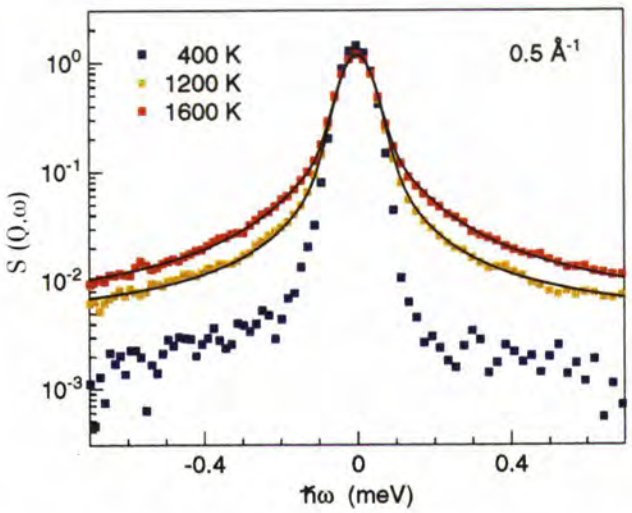

Figure 3: Scattering law $S(Q,\omega)$ at $Q = 0.5$ Å^{-1} measured on the neutron time-of-flight spectrometer IN6. The signal is dominated by the incoherent scattering of sodium which in turn is dominated by elastic scattering. This indicates that at any given time only a fraction of the sodium atoms is participating in the fast diffusion. Diffusion of sodium ions results in a broad quasielastic signal that is described by equation (1) with a stretching exponent β within [0.7,0.8] and relaxation times on a 10 ps scale.

Best fits have been obtained with a stretching exponent β within [0.7,0.8] in accordance with the molecular dynamics simulation result of $\beta = 0.77$. τ_Q is the Q-dependent relaxation time. Prior to the fit the theoretical function is folded with the instrument resolution $R(Q,\omega)$.

The present data [4] represent experimental evidence for the existence of regions that exhibit an enhanced sodium concentration as predicted by the molecular dynamics simulations [2,3]. The concentration of sodium in these channels implies that the Si-O network is less disrupted in the rest of the system leading to a higher viscosity of the entire system and thus may equally explain the weak temperature dependence of the viscosity in sodium silicate melts at high temperatures.

Inelastic neutron scattering combined with modern simulation techniques thus proves an interesting tool to investigate modern questions of molecular motion pertaining to the geosciences. ■

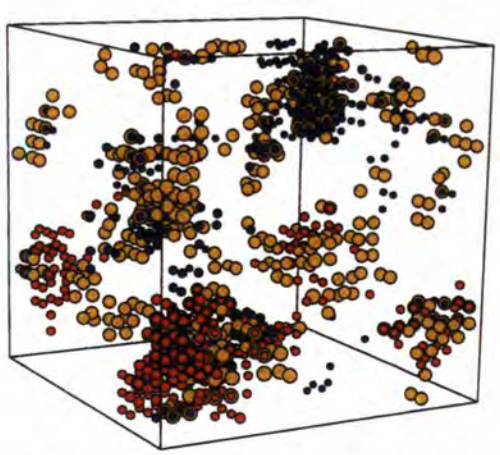

Figure 2: Molecular dynamics simulations on sodium tetrasilicate [3]: diffusion of sodium ions during a 1.4 ns run at 2000 K. Yellow circles: regions where more than 10 different sodium ions passed. Blue and red circles mark the trajectories of two individual sodium ions. The figure shows the existence of sodium rich channels. The distance between these channels is typically 5-8 Å causing a prepeak in the static structure factor around 0.9 Å^{-1}.

References

[1] For an overview see: Rev. Mineralogy 32, Structure, Dynamics and Properties of Silicate Melts, (1995) edts: J.F. Stebbins, P.F. McMillan, D.B. Dingwell; Chem. Geol. 174, 6th Silicate Melt Workshop, (2001) edts: Y. Bottinga, D.B. Dingwell, P. Richet. • [2] J. Horbach, W. Kob, K. Binder, Phil. Mag. B 79 (1999) 1981; Chem. Geol. 174 (2001) 87 and references therein. • [3] P. Jund, W. Kob, R. Jullien, Phys. Rev. B 64 (2001) 134303 • [4] A. Meyer, H. Schober, D.B. Dingwell, submitted to Phys. Rev. Lett.

The solvation structure
of lithium in ammonia

● J.C. Wasse, S. Hayama and N.T. Skipper (University College, London)

● H.E. Fischer (LURE Orsay and ILL)

● P. Palleau (ILL)

Neutron diffraction has been used in conjunction with $^{6}Li/^{nat}Li$ and $^{nat}N/^{15}N$ isotope substitution to measure the microscopic structure of saturated metallic solutions of lithium in ammonia (21 mole percent metal). Isotopic labeling allows us to obtain detailed information on the coordination environment around the solvated metal Li^{+} cations, and around the nitrogen atoms of the solvent molecules. We find that the solutions are highly structured over both short and intermediate length scales, and that the local coordination around each Li^{+} cation consists of a well-defined solvation shell containing an average of 3.5 ammonia molecules.

Alkali metals dissolve readily in liquid ammonia without chemical reaction, producing solutions that have been the subject of numerous experimental and theoretical investigations [1]. This is primarily due to their fascinating electronic properties, being either metallic or non-metallic depending on temperature and alkali cation concentration. For example, the metallic solutions studied here, comprising completely solvated Li^{+} cations and delocalised excess electrons, have electrical conductivities exceeding those of liquid mercury at room temperature. Alkali-ammonia solutions are also the lowest-temperature metallic liquids, and have the lowest densities known for any non-cryogenic liquid [1].

Metal-ammonia systems have been well characterised by thermodynamic, transport, spectroscopic and computational techniques [1,2]. However, interpretation of these results is impeded by the dearth of high-resolution structural data [3]. This is in part a consequence of the immense challenge posed by the sample preparation: the solutions are metastable; they react with almost anything, including gold!

In this work, we have conquered the experimental challenges associated with the sample preparation, and are able to report high-resolution structural data for saturated metallic lithium-ammonia solutions [4]. Indeed, the logistics of this experiment made it, arguably, the most complicated ever to be performed during the last 10 years on the D4 instrument at the ILL. The solution samples were made *in situ* at the beamline, and the technique of isotope substitution in neutron diffraction was employed. This technique exploits the contrast in the neutron scattering lengths found for different isotopes of a particular species, e.g. $^{6}Li/^{nat}Li$ and $^{nat}N/^{15}N$. Therefore by performing neutron diffraction experiments on samples that are identical apart from the isotopic composition of a particular species, the subtraction of the measured total structure factors yields difference functions containing information about the microscopic structural environment of the substituted species [4].

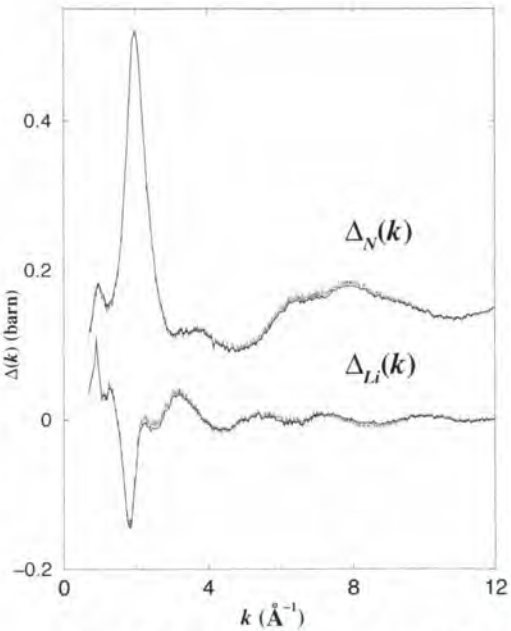

Figure 1: The first order difference functions $\Delta_{Li}(k)$ and $\Delta_N(k)$ for saturated metallic lithium-ammonia solutions at 235 K. The measured data points are given by the error bars and the solid line is the back-Fourier transform, obtained from the solid line in figure 2.

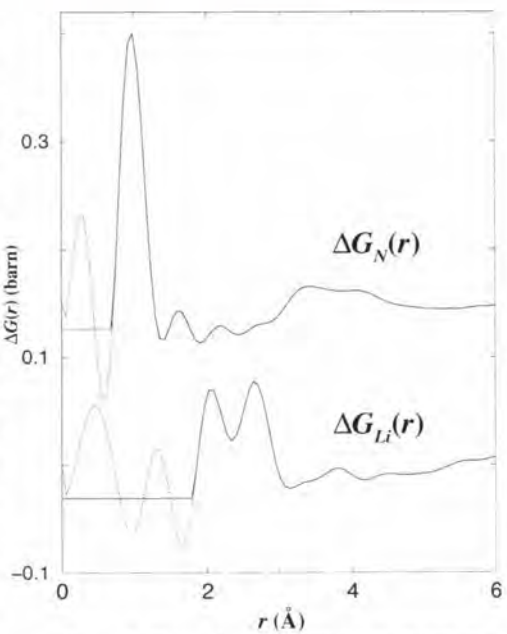

Figure 2: The real space partial pair distribution functions $\Delta G_{Li}(r)$ and $\Delta G_N(r)$ for the saturated metallic lithium-ammonia solutions at 235 K (shifted vertically for clarity).

Figure 1 shows the first-order difference functions $\Delta_{Li}(k)$ and $\Delta_{N}(k)$ measured at 235 K. Here, we note the presence of a pre-peak at approximately 1 Å^{-1} in both data sets. This indicates immediately that intermediate range ordering is present in the solutions, having a contribution from both Li^{+}- and N-centred correlations and therefore consistent with contact between ammonia and solvated lithium ions.

The real-space functions of figure 2 correspond to the data sets presented in figure 1, and are proportional to the probability of finding a species "x" around the substituted species. The real-space partial pair distribution $\Delta G_{Li}(r)$ is characterised by two intense overlapping peaks at 2.06(2) and 2.64(2) Å. These features are assigned to correlations between the lithium cations and solvent molecules (nitrogen and hydrogen, respectively), yielding an average of 3.5 ammonia molecules solvating the Li^{+} cations. It should be noted that the ammonia molecules direct their dipole moments away from the cation, and are undistorted relative to those of the pure solvent. The presence of the broad intermolecular N-N peak centred at 3.40(3) Å in $\Delta G_{N}(r)$ confirms that the Li+ cation solvation is based upon a *distorted* tetrahedral geometry, i.e. $r_{N\text{-}N}/r_{Li\text{-}N} = 1.65$. These data for $r_{Li\text{-}N}$ shows that the electrons are dissociated from the cations in the first solvation shell.

Figure 3 depicts a snapshot of the arrangement of ions and molecules in metallic lithium-ammonia solutions. The extraordinarily low density is clearly visible, due to the presence of excess delocalised electrons in solution. Note the cations lying at the centers of the distorted tetrahedral solvation shells of ammonia molecules.

The high stability of the detectors of the D4 instrument proved invaluable to the success of this experiment, which again highlighted the importance of the isotope substitution technique in neutron scattering to obtain specific structural information of disordered materials [4]. The present observations will help guide the development of structural models used in computer simulations for this class of non-aqueous solutions [2]. This experiment was a pre-cursor to neutron diffraction studies of *dilute* nonmetallic lithium-ammonia solutions, recently carried out on the upgraded version of the D4 instrument: D4C. The combined results should help shed light on the mechanisms of the fascinating metal-nonmetal transition exhibited by these exotic solutions on the temperature-concentration phase diagram. ■

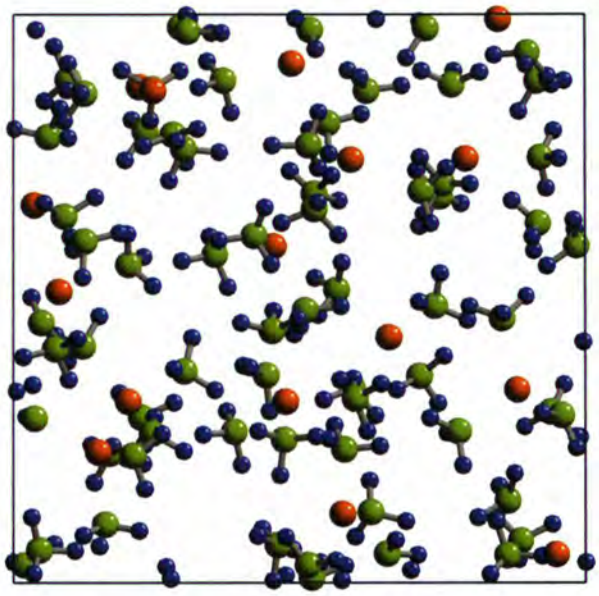

Figure 3: A snapshot of the system at 21 mole percent metal presented for visualisation purposes. It is taken from a classical Monte Carlo simulation of lithium cations in ammonia at 235 K. The lithium cations, nitrogen and hydrogen atoms are denoted by the red, green and blue circles respectively in the box of dimensions 16 x16 x 16 Å^{3}.

References

[1] J.C. Thompson, Electrons in Liquid Ammonia (Clarendon, Oxford 1976); P.P. Edwards, Adv. Inorg. Chem. R. 25 (1982)135; P.P. Edwards, J. Superconductivity 13 (2000) 933 • [2] Z. Deng, G.J. Martyna and M.L. Klein, Phys. Rev. Lett. 71 (1993) 267; Z. Gurskii, S. Hannongbua and K. Heinzinger, Mol. Phys. 78, (1993) 461; T. Kerdcharoen, K.R. Liedl and B.M. Rode, Chem. Phys. 211 (1996) 313 • [3] P. Chieux and H. Bertagnolli, J. Phys. Chem. 88 (1984) 3726 • [4] J.C. Wasse, S. Hayama, N.T. Skipper and H.E. Fischer, Phys. Rev. B 61 (2000) 11993.

Influence of the interface
for the structural ordering in sheared liquids

● M. Wolff and A. Magerl (University of Erlangen-Nürnberg)

● H. Zabel (Ruhr University, Bochum)

● B. Frick (ILL)

Neutrons are characterised by a very large penetrating power through many materials used in engineering sciences. As such they are a powerful tool for in-situ investigations under complex sample environments. A special shear device for neutron reflectivity measurements has been developed to investigate the adhesion properties of sheared liquids to different solid interfaces. Neutron reflectrometry experiments have shown that sheared polymer solutions exhibit distinct wetting behaviour on coated silicon wafers and characteristic structural changes in the bulk.

Lubrication has been a long standing problem in physics with important industrial implications. It is estimated that about 6% of the gross national product of the United States are wasted due to friction and wear [1]. Therefore a better understanding of lubrication processes is strongly desirable. In this context, neutrons may come to play a particular role because of their high penetration power for many engineering materials making it possible to investigate samples *in-situ* even if they are contained in heavy and complex environments such as shear cells. Additionally, the high scattering cross section of hydrogen, found in practically every liquid lubricant, eases a study of such samples. Following these lines, it has been shown that the macroscopic flow of sheared liquids can be well explored by neutron backscattering. Distinguished velocity distributions of the macroscopic flow have been found for different interfaces [2, 3]. To allow for a closer inspection of this important region of the solid/liquid interface, a shear cell has been constructed which meets the special requirements of neutron reflectivity instruments. The cell shown in figure 1 during an experiment at ADAM can be used in any orientation, either horizontal or vertical. The plate-plate shear device is sealed by a standard radial shaft packing, consisting of Viton and an O-ring, making an operation possible for shear rates up to 5000 s^{-1} and for temperatures between 10 and 80 °C. The fixed disk of the shear device is made by an interchangeable hydrophilic or hydrophobic coated polished silicon wafer (to the standards of the semiconductor industry) with a thickness of 11 mm. Neutrons proceed through this wafer from one edge to the interface where they get reflected back into the wafer exiting at the opposite edge before they finally reach the detector (figure 1). The path length of the neutrons in the silicon is about 200 mm which results in a modest reduction of flux (absorption coefficient in silicon is about 0.025 cm^{-1}).

Figure 1: Shear device designed for neutron reflectivity studies mounted at ADAM. The white arrows mark the neutron path way.

An experiment has been performed on EVA with this shear device to investigate the interface properties of a solution of the polymer P85 (33% in weight). It consists of a polypropylene core (hydrophobic for tem-

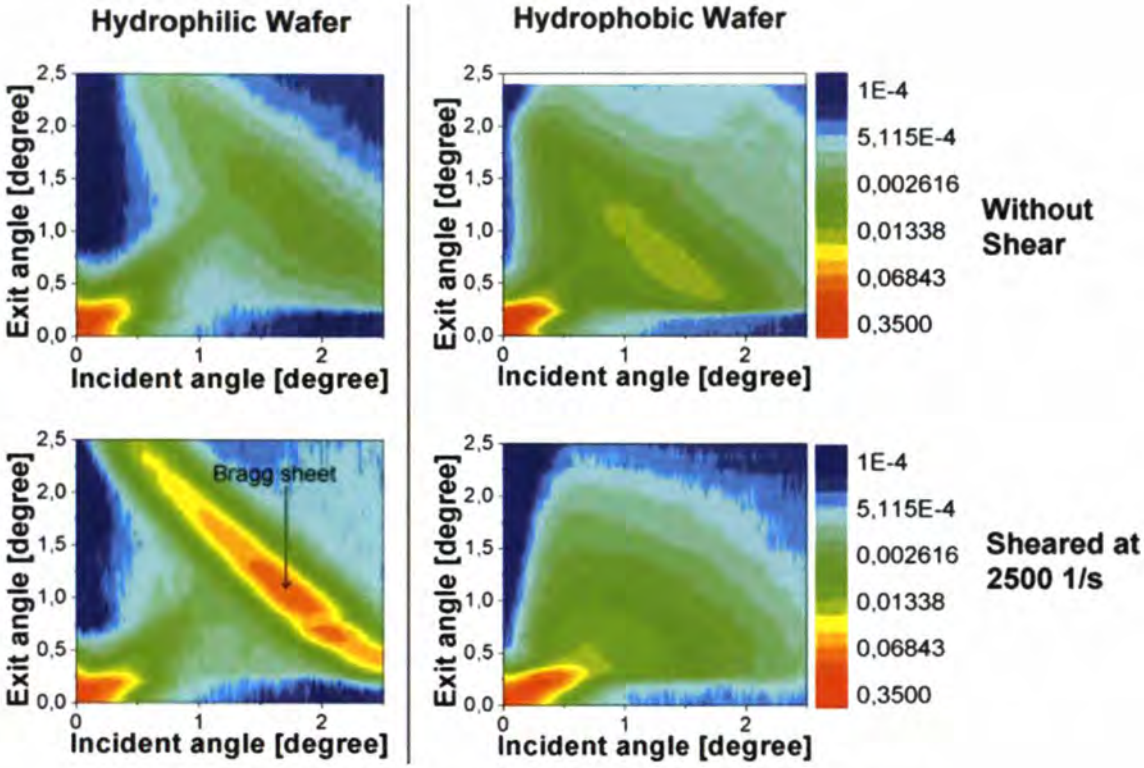

Figure 2: Contour maps of the intensity for a sample of a 33% (in weight) solution of P85 in deuterated water as a function of the incident and exit angle. Data for the interface with a hydrophilic and a hydrophobic coated silicon wafer are shown left and right, respectively. The top and bottom panels are without shear and sheared at 2500 s^{-1} at a temperature of 18 °C. The Bragg sheet representing structural ordering in the bulk medium becomes enhanced under shear for the hydrophilic disk while it is diminished for the hydrophobic disk.

peratures above 15 °C) with polyethylene end groups (hydrophilic in the investigated temperature range). Structural properties of this sample have extensively been studied by Small Angle Neutron Scattering (SANS) and different phases reaching from unimers to lammelar have been found depending on temperature, polymer concentration and shear [4]. The scattering length density of P85 ($0.44 \cdot 10^{-6}$ Å^{-2}) is very different to that of deuterated water ($5.77 \cdot 10^{-6}$ Å^{-2}) and of silicon ($2.1 \cdot 10^{-6}$ Å^{-2}) yielding a good contrast between the components. In this measurement the polymer concentration right at the surface, as deduced from the angle of total reflection, was found to vary dramatically between 12 and 52 % for different shear rates and temperatures [3]. As a perhaps even more striking result we find that these changes at the interface influence strongly the structure deeper in the bulk of the medium.

Figure 2 shows a contour map of the intensity as a function of the incident and exit angle for the hydrophilic as well as for the hydrophobic coated Si-disc at a temperature of 18 °C. A Bragg reflection caused by structural orderings in the bulk medium, which is already visible without shear, becomes more pronounced when shearing the sample against a hydrophilic disc. With a hydrophobic disk, the situation is reversed with the Bragg reflection becoming less pronounced under shear. At a higher temperature of 73 °C, this Bragg reflection vanishes completely in the hydrophobic case whereas with the hydrophilic coated disc the Bragg peak remains at nearly the same strength irrespective of temperature [3].

This demonstrates a strong relationship between the structural ordering in the bulk of a liquid and the properties of the solid/liquid interface layer. ■

References

[1] B.N.J. Persson, Sliding Friction (Springer Verlag, Berlin, Heidelberg 1998) • [2] A. Magerl et al.: Appl. Phys. Let. 74 (23) (1999) 3474 • [3] M. Wolff et al.: Proceedings, The ILL Millennium Symposium (2001) 100 • [4] K. Mortensen, J. Cond. Matt. 8 (1996) A103.

Model biological membranes
supported in anisotropic microporous alumina

D. MARCHAL (UNIVERSITY PARIS VII)

B. DEMÉ (ILL)

Biological membranes encapsulate cells and structures within cells and play a major role in living processes like enzymatic catalysis involving insoluble compounds (lipophilic substrates and co-enzymes, membrane proteins). They also play a key function of selective transfer between compartments, e.g. between extracellular liquids and the cytoplasm, the cytoplasm and the nucleus. They consist of a fluid hydrophobic layer made of self-organised lipids, sugars, proteins, and complex macromolecules such as glycolipids and glycoproteins. Some of these complex macromolecules also contribute to specific recognition processes, others are responsible for the specific binding of soluble proteins of the cytoskeleton. In both cases they participate to the membrane stability and to its dynamic.

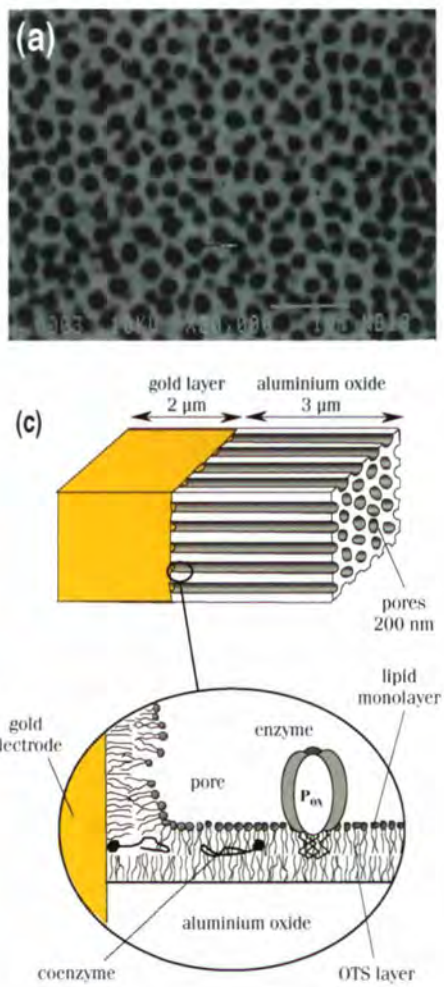

Figure 1: Front view (a) and side view (b) of a 60 µm thick alumina membrane, and (c) a detail of the microporous electrode used to investigate catalytic kinetics of redox membrane enzymes.

Because of the structural complexity of their environment, these membrane processes are not easy to study. Therefore, there is a general attempt to make simple models of the membrane that specifically simulate the conditions of a reaction or the environment suitable for the stability of a given molecular structure. Here, the reaction of interest is involved in bacterial respiration - in which the enzyme pyruvate oxidase carries out the catalysis of its substrate, pyruvate, with the help of a coenzyme, quinone Q_8. This 'redox' reaction involves the transfer of electrons and the general aim of this work is to understand the precise mechanism and kinetics by which this occurs in a 2-dimensionnal medium. To study the catalysis reaction by following the 'redox reaction', a bilayer confined in porous alumina is placed in contact with a gold electrode which can supply electrons for the reaction. The enzyme is then attached to the lipid layer inside the pores and the coenzyme commutes between the enzyme and the gold/alumina interface by lateral diffusion in the membrane - as shown in figure 1. An important prerequisite for the study of such a reaction is a careful characterisation of the solid surface that supports the molecular self-assembly and of the assembly itself. The model membrane used is a hybrid bilayer that consists of a layer of a long-chain hydrophobic material (octadecyltrichlorosilane, OTS), chemically bound to porous alumina (aluminium oxide, Al_2O_3), on top of which a second layer is added by fusion of small unilamellar vesicles (1,2-diacyl-*sn*-glycero-3-phosphocholine, DMPC).

In the present report, Small-Angle Neutron Scattering (SANS) is shown to be a unique tool to characterise the confined Hybrid Bilayer Membrane (HBM) at the interface between alumina and water (figure 1a and 1b). Indeed, SANS is the only technique that allows the *in situ* study of this interface at different contrasts, starting from bare alumina and proceeding step by step, as the complexity of the biomimetic self-assembly increases.

Measurements were performed at the instruments D11, D22 and D16. Figure 2a shows the scattering of a membrane-free, 60 µm thick, alumina support wet by

pure D_2O. The thin alumina sheets are in the coaxial orientation, that is with their pores oriented parallel to the beam axis. A perfect Q^{-4} decay of the intensity is produced by the porous material indicating a perfectly smooth interface. The solid line is a fit to the data (step profile shown in the insert) in the exceptionally wide Porod regime observed for this material. The dashed line is a simulation of the Porod law calculated with the same parameters plus a gaussian roughness of 5 Å.

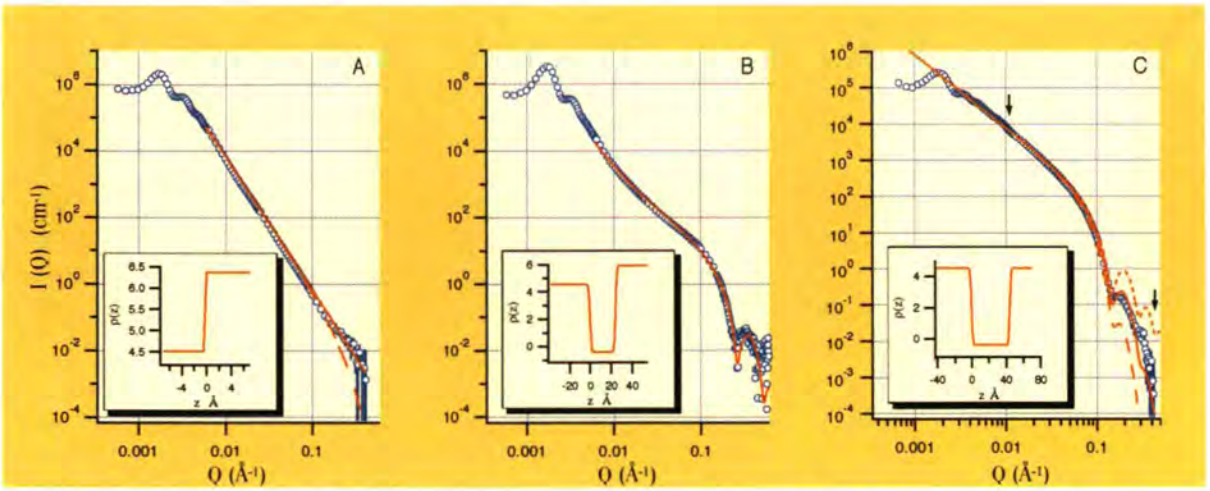

Figure 2: Small-angle neutron scattering by bare porous alumina (a), the OTS-grafted alumina (b) and the full membrane (c). The solid lines are fit to the data according to equation 1 which simplifies to a single Porod term in (a) and a flat membrane form factor in (c) (equation 2). The inserts show the corresponding scattering length density profiles. In (a) the fit showing a perfectly sharp interface is compared to the simulation of a rough interface with 5 Å roughness. In (c) the fit to the data in the regime delimited by the arrows yields a roughness of 6 Å. It is compared to a simulation of a sharp interface (dots) and to a rough interface with 10 Å roughness.

Figure 2b shows the scattering of the OTS layer chemically bound to the alumina and wet by deuterated methanol (CD_3OD) giving the contrast shown in the insert. Here again, thanks to the high specific area of alumina and to the contrast, SANS data have been collected over an exceptionally wide Q-range ($6x10^{-4}$ - 0.5 $Å^{-1}$) which covers the structure of the oxide at large scale, the Porod regime (leading the total membrane area Σ), and the membrane form factor, representing a range of 9 decades in intensity. Here, the intensity is the sum of the material scattering (the Q^{-4} decay shown in figure 2a) and that of the film scattering (Q^{-2} decay followed by oscillations). The solid line is a fit to the data in the q-range of interest for the OTS layer using the relation:

$$I(Q) = \left[2\pi\sum(\Delta\rho_{1,3})^2 \frac{1}{Q^4} + 2\pi\sum(\Delta\rho_{2,3})^2 \frac{1}{Q^4}(1-\cos Q2t) - 4\pi\sum(\Delta\rho_{1,3})(\Delta\rho_{2,3}) \frac{1}{Q^4}(1-\cos Q2t)\right] e^{\sigma^2 Q^2} \quad (1)$$

where t is the membrane thickness, $\Delta\rho_{1,3}$, $\Delta\rho_{1,2}$ and $\Delta\rho_{2,3}$ are the solid-solvent, solid-film and film-solvent contrasts. In the particular case where the two sides of the film are matched to one another, that is the solid and water, $\Delta\rho_{1,3} = 0$ and the Porod and cross contributions (respectively 1st and 3rd term) vanish both. Equation 1 then simplifies to the scattering of a freely suspended film:

$$I(Q) = 2\pi\sum(\Delta\rho_{2,3})^2 \frac{1}{Q^4}(1-\cos Q2t)e^{\sigma^2 Q^2} \quad (2)$$

The fit to the data yields a film thickness t = 24 Å and a roughness σ = 2.5 Å.
Finally, the scattering of the Hybrid Bilayer Membrane is shown figure 2c. Here the contrast of the alumina and of the solvent are matched to one another. Thus the scattering results from the film scattering only characterised by a perfect Q^{-2} decay followed by the oscillations of the membrane form factor (equation 2). A fit to the data yields the membrane thickness (44 Å), the membrane roughness (6 Å) and its average scattering length density ($-0.4x10^{-6}$ $Å^{-2}$). Two simulations with a perfectly sharp interface (dots) and 10 Å roughness (dashes), show the sensitivity of the wide-angle signal to this parameter.

This new approach in the characterisation by SANS of a supported membrane in a porous material provides information on the homogeneity, the specific area, the roughness, the thickness and the density of the membrane. HBMs are the first step in the study of fully reconstituted phospholipid membranes loosely bound to their support. They are compatible with the electrochemical detection method *via* the coupling to the gold electrode. The next step is to carry out similar but more difficult experiments on a pure lipid bilayer which is more fluid and not directly attached to the alumina but more like a real biological membrane. Eventually we hope to incorporate a membrane enzyme and study the whole system *in situ* with SANS. This will mean deuterating the enzyme - a difficult task that will require special preparation facilities but will be an exciting challenge for the future. ■

References

D. Marchal, J. Pantagny, J.M. Laval, J. Moiroux, C. Bourdillon. Biochemistry 40 (2001) 1248-1256 • D. Marchal, C. Bourdillon, B. Demé. Langmuir, 17 (2001) 8313-8320.

Super-cooled water flows at 200 K between biological membranes

M. Weik (IBS Grenoble)

U. Lehnert (IBS Grenoble, ILL and MPI für Biochemie, Martinsried)

G. Zaccai (IBS Grenoble and ILL)

Confined water is of considerable current interest owing to its implication in biology, food and earth science. It can be studied in its amorphous or super-cooled state in the temperature range 150 K - 235 K, in which bulk water crystallises. A neutron diffraction study on D16 of flash-cooled amorphous solid deuterium oxide (D_2O) confined in stacks of native biological membranes showed that, upon heating to 200 K, the water adopts liquid-like behaviour and flows out of the inter-membrane space. Since this temperature is close to the one where protein motions display dynamical transitions, these results will contribute to the understanding of protein-water dynamical interactions.

The behaviour of water confined to biological or mineral structures is of considerable current interest owing to its implication in biology, food and earth science. It is also important for a fundamental understanding of water because it can be studied in its amorphous or super-cooled state in a temperature range in which bulk water crystallises. Water can be in a super-cooled, liquid state at temperatures below 0 °C if crystallisation is prevented, but necessarily crystallises into ordinary hexagonal ice when approaching 235 K, at atmospheric pressure [1]. If the temperature is lowered rapidly (flash-cooling) to below e.g. 100 K, amorphous ice is formed with a structure similar to liquid water, but with infinite viscosity [2]. Amorphous bulk water undergoes a glass transition upon heating to 136 K, where the molecules gain mobility. Subsequent warming leads to crystallisation at about 150 K. Experimental studies on super-cooled bulk water in the temperature range between 150 and 235 K, the so-called 'No-man's land' [2], are therefore quasi-impossible .

The study of confined water allows to enter the 'No-man's land' experimentally, because interactions with the confining medium prevent crystallisation [3]. Water confined to biological structures is an important subject of study because of its importance for biological processes and for cryo-preservation of tissues. Purple membranes (PM) are part of the cell membranes of certain organisms that live in very high salt conditions such as salterns or the Dead Sea. Their structure and hydration-dependent dynamics have been extensively characterised, including by neutron diffraction and scattering (reviewed in [4]), and they represent an excellent opportunity to study the behaviour of water confined to biological membranes. Drying a suspension of PM fragments leads to a stacking, the spacing of which can be varied from 49 Å (the thickness of the dry membrane, i.e. no inter-membrane water) up to 69 Å (that is 20 Å of water between adjacent membrane fragments) by equilibration under different ambient relative humidity. Slowly lowering the temperature of a hydrated stack of PM below 0 °C has been shown to result in super-cooling of the confined water and a subsequent dehydration when water leaves the inter-membrane space to crystallise outside the stack of membranes [5]. A minimal spacing of 54 Å has indicated that about two layers of water remained in the inter-membrane space, each in direct contact with a membrane surface. The experiments described here show that more inter-membrane water can be trapped in an amorphous state by rapid flash-cooling and that it displays liquid-like behaviour upon warming at 200 K.

Flash-cooling PM stacks by rapid plunging into liquid nitrogen leads to a decrease in lamellar spacing to ~ 58 Å – that is 3-4 layers of water in between adjacent membranes – irrespective of the initial value determined at room temperature that ranged from 59 to 69 Å and to concomitant formation of cubic ice. The decrease is attributed to the flow of water out of the inter-membrane space, where crystallisation is hampered, towards less confined regions in the sample, where it can crystallise. The fact that only 3-4 water layers (that is two 'first hydration layers' in direct contact with the membrane surface and 1-2 'second hydration layers') can be vitrified at the cooling rates employed in our experiments is in line with observations that the water mobility increases abruptly beyond the second hydration shell. Upon slow-heating the lamellar spacing remains constant up to 200 K and decreases abruptly upon further heating to reach a minimum value of 54 Å (corresponding to about 2 water layers) at 260 K (figure 1). Concomitantly, heating from 200 to 260 K, leads to a constant increase in intensity of diffraction originating from cubic ice. Above 260 K the lamellar spacing increases again and reaches at 280 K the initial value determined at room temperature prior to flash-cooling. At ~ 260 K cubic ice re-crystallises

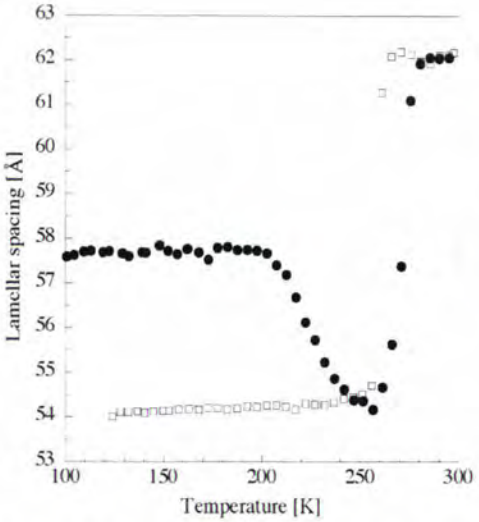

Figure 1: Lamellar spacings of stacks of purple membranes as a function of temperature. Closed circles show the lamellar spacing after flash-cooling upon heating from 100 to 300 K, open squares represent the one during subsequent slow-cooling from 300 to 120 K. Errors in lamellar spacing were estimated to be about 0.2 Å. The time interval between successive data points was about 28 min.

into hexagonal ice which melts upon further heating as seen by vanishing diffraction intensity. It can be concluded that water beyond the first hydration layer displays liquid-like behaviour at 200 K. It is the prevention of crystallisation by the 1D-confinement that drives water out of the inter-membrane space, which, in turn, represents a direct proof for long-range translational diffusion in the 'No-man's land'.

Upon slow-cooling inter-membrane water becomes super-cooled (figure 1) as already has been reported [5] yet the abrupt change in lamellar spacing at 200 K was not reversible. In order to gain insight into the relaxation times involved the temperature was increased stepwise after flash-cooling with sufficiently long time intervals at constant temperature so as to allow the lamellar spacing to become stable (figure 2). Dehydration of the flash-cooled membrane stacks above 200 K and rehydration above 260 K are processes that seem to involve the same intermediate spacings, *viz.* 54.5 (corresponding to about 2 water layers) and 56.5 - 57 Å (corresponding to about 3 water layers). This indicates that individual inter-membrane water layers display differential dynamical characteristics, which translates into differential glass transition and crystallisation temperatures. Dehydration is a slow process with relaxation times between 67 and 105 min depending on the temperature, whereas rehydration is instantaneous on the time scale of our experiments (about 30 min per data point in figures 1 - 3).

One might object that the sudden decrease in lamellar spacing at 200 K may not be due to a decrease in the thickness of the inter-membrane water layer but rather be a consequence of a structural change *within* the membrane plane which could affect the lamellar spacing as well. This was ruled out by observing the temperature-dependence of the in-plane unit cell parameter *a* of the two-dimensional hexagonal PM lattice, which does not display a sudden change at 200 K (figure 3). In fact, the temperature dependence of the unit cell parameter *a* is strikingly reminiscent of the one displayed by the dynamics of thermal motions in PM as measured by elastic incoherent neutron scattering, both showing a transition at about 230 - 240 K [4]. This suggests that the onset of liquid-like behaviour of the second hydration layers does not trigger directly the dynamical transition in the membrane.

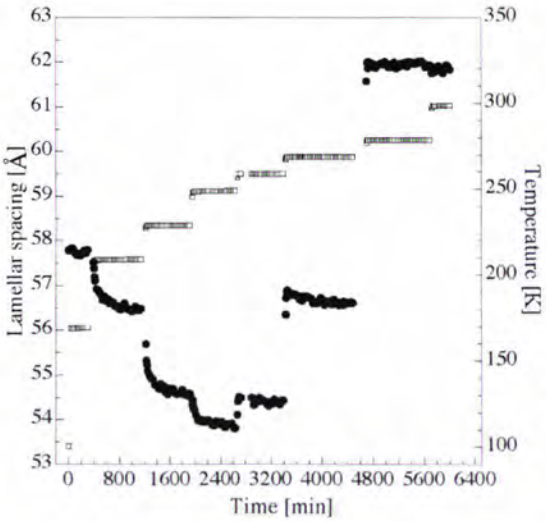

Figure 2: Lamellar spacing (closed circles) of flash-cooled stacks of purple membranes as a function of experimental time. The temperature (open squares) was increased stepwise from 100 to 300 K after flash-cooling. Errors in lamellar spacing were estimated to be about 0.2 Å. The time interval between successive data points was about 29 min.

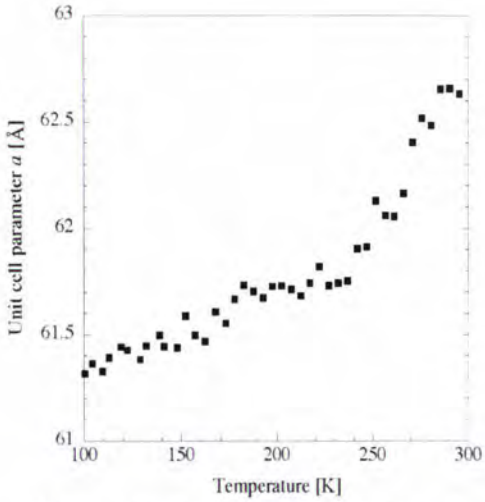

Figure 3: Unit cell parameter *a* of the two-dimensional PM lattice as a function of temperature. Closed squares show *a* after flash-cooling upon heating from 100 to 300 K. The error in *a* was estimated to correspond to approx. 0.1 Å. The time interval between successive data points was about 28 min.

In summary, we addressed the behaviour of amorphous water confined to thin films by native biological membranes. The second hydration layers showed long-range translational diffusion upon heating at 200 K as seen by a decrease in lamellar spacing, which is attributed to draining of water molecules from the inter-membrane space. This showed that amorphous water confined to one dimension by biological membranes transforms into an ultra-viscous liquid above its glass transition prior to crystallisation. Our result showed that the glass transition of the second hydration shell does not occur at the same temperature as the dynamical transition of the membrane, which may contribute to the understanding of the coupling between solvent and protein dynamics. ■

References

[1] H. Kanno, R.J. Speedy, C.A. Angell, Science 189 (1975) 880 • [2] A. Mishima, H.E. Stanley, Nature 396 (1998) 329 • [3] R. Bergman, J. Swenson, Nature 403 (2000) 283 • [4] G. Zaccai, Biophys. Chem. 86 (2000) 249 • [5] R.E. Lechner, J. Fitter, N.A. Dencher, T. Hauss, J. Mol. Biol. 277 (1998) 593.

Dewetting of model membranes

● L. Perino-Gallice and G. Fragneto (ILL)

● U. Mennicke and T. Salditt (University of the Saarland, Saarbrücken)

● F. Rieutord and J.F. Legrand (CEA, Grenoble)

Multilamellar bilayers of the neutral lipid dimyristoyl phosphatidilcholine (DMPC) deposited on solid substrates, were found to become unstable upon hydration. Both neutron reflectivity and atomic force microscopy were used to study these assemblies formed by less than ten bilayers spin-coated on hydrophilic silicon wafers, both alone and in presence of the peptide Alamethicin.

Lipid bilayers have attracted the interest of physicists for many years and have been extensively studied with the aim to understand the behaviour of cell membranes [1]. The most common model systems consist of multilamellar vesicles in aqueous medium, stacked bilayers in controlled humidity environment, monolayers on the liquid surface and single bilayers on solid substrates. All of these systems have advantages and drawbacks and the search for a fully satisfying model is still in progress. Stacked multibilayers have the disadvantage that it is difficult to prepare them in fully hydrated medium and only an average of the behaviour of the thousands bilayers is determined. Single adsorbed bilayers interact strongly with the substrate.

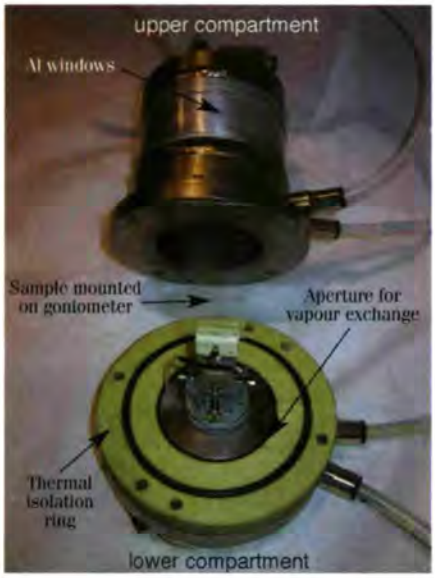

Figure 2: Picture of the D16 humidity chamber.

Salditt and co-workers have succeeded in the preparation of only few lipid bilayers, typically less than ten, on silicon wafers and started their characterisation with X-rays [2]. Those systems are such that the characteristics of each bilayer may be determined alone by techniques able to give structural details in the Å scale like specular and off-specular reflectivity. The deposition is made at room temperature by spin coating (figure 1).

Here, results are presented from this new membrane model [3] as well as of the interaction of DMPC bilayers with the anti-microbial peptide Alamethicin. Unlike the conventional antibiotics that have specific protein targets, antimicrobial peptides like Alamethicin have been shown to exert their activity directly on the lipid bilayer of the cellular membrane. Extensive in vitro and in vivo studies have established that binding of peptide monomers to the surface of the target cells causes disruption, permeabilisation or disintegration

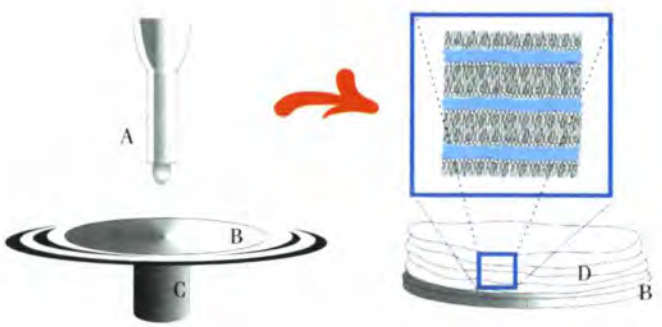

Figure 1: Schematic representation of sample preparation by spin coating. A is a drop of solution containing the lipids or lipids+peptide; B is the silicon wafer; C the spin coating device; D the deposited bilayers.

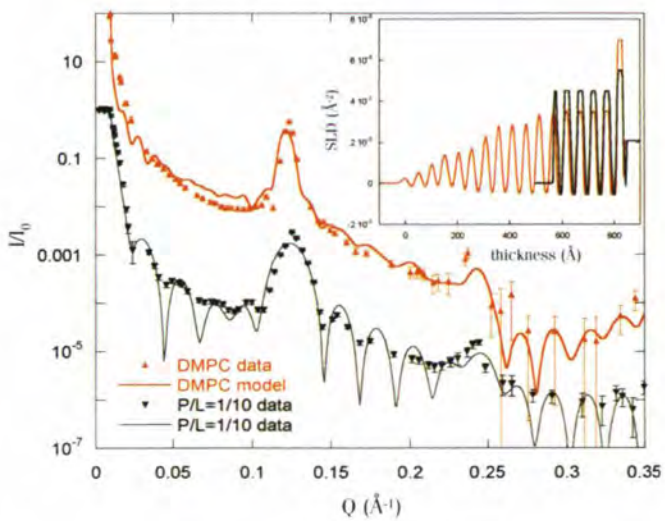

Figure 3: Neutron reflectivity profiles and best fits of data from a sample formed by d-54 DMPC in H_2O water vapour (red points and line); and a sample formed by d-54 DMPC and Alamethicin in the ratio P/L=1/10 in H_2O water vapour (black points and line). In the inserts are the corresponding scattering length density profiles from the models used to fit the data.

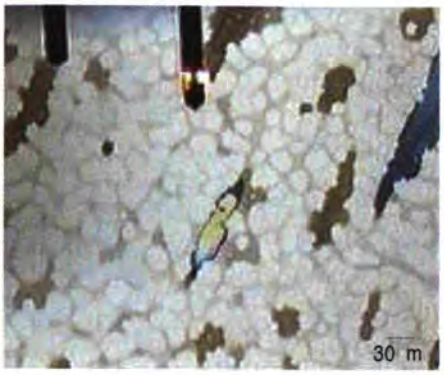

Figure 4: Optical microscopy image of a d-54 DMPC sample fully hydrated at 45 °C.

of cytoplasmic membranes. The primary mechanism by which bacteria are killed has not been clarified because of the current lack of understanding of lipid/peptide interactions. Specular neutron reflectivity measurements were taken from samples made from several isotopic compositions of DMPC, in ~ 100% relative humidity and temperature of 45 °C on 2" diameter silicon wafers. Samples containing Alamethicin in the peptide/lipid molar ratios (P/L) of 1/200, 1/100, 1/25 and 1/10 were also measured. Data were collected on the small angle diffractometer D16 specially adapted for reflectivity measurements [4]. Samples were hydrated in the humidity chamber shown in figure 2 [5]. Reflectivity data were analysed by model fitting using the optical matrix formulation of reflectivity [6]. Two of the measured reflectivity profiles are shown in figure 3, one is a sample made of chain deuterated DMPC (from now on referred to as d-54 DMPC) in H_2O vapour and the other is from a sample made by deuterated DMPC and Alamethicin with P/L=10. Inserts show the scattering length density profiles obtained from the best fits to the data. While in the case of pure bilayers there is a decrease in the layer densities as the system gets further away from the substrate, when Alamethicin is present, the lowering of density is constant for all layers after the one adjacent to the substrate. No in-plane information is available from these data.

Atomic Force Measurements (AFM) were additionally performed to determine the in plane features of the surface. Figure 4 shows an optical microscopy image and figure 5 shows AFM images of fully hydrated bilayers in the fluid phase with and without Alamethicin. In all cases, the presence of a high percentage of holes on the surface is observed, with very thick islands appearing on parts of the surface. While in the case of pure bilayers one can observe the formation of steps with quantity of material decreasing further away from the substrate, in the presence of a big amount Alamethicin the diameter of the holes stays constant along the depth except for the fact that the first bilayer covers a bigger part of the surface.

The AFM measurements showed also that while before hydration pure DMPC samples were relatively uniform with a few holes of diameter 2 to 6 mm and depth of 130 to 330 Å, hydration led to dewetting and the phenomena was faster at 45 °C, that is above the gel to fluid phase transition (that occurs around 23 °C), than at 20 °C, just below the transition. In the presence of peptide, already at 20°C hydration leads to a considerable amount of dewetted surface suggesting that probably the transition temperature is lower for the mixture. Moreover, the system appears stable after less than 4 hours while many more hours are needed when the lipids are alone. The patterns observed on the dewetted surfaces are very similar to those observed on the dewetted surface of liquid crystal films [7] and interpreted by spinodal dewetting, that is fluctuation induced dewetting. We suggest that the observed dewetting may have the same origin, due to the presence of the solid/liquid and liquid/air interfaces which reduce the fluctuations and change the equilibrium distance between the layers [8]. Both the reflectivity and AFM data for the samples at high peptide content are consistent with an assembly of Alamethicin around the walls of the holes as a preferred configuration with respect to the peptide inserted, for example, in the lipid headgroups. It may be considered as a further confirmation of the fact that at high P/L ratios Alamethicin stabilises pores in the cell membrane which are believed to cause the death of the cell [9]. ■

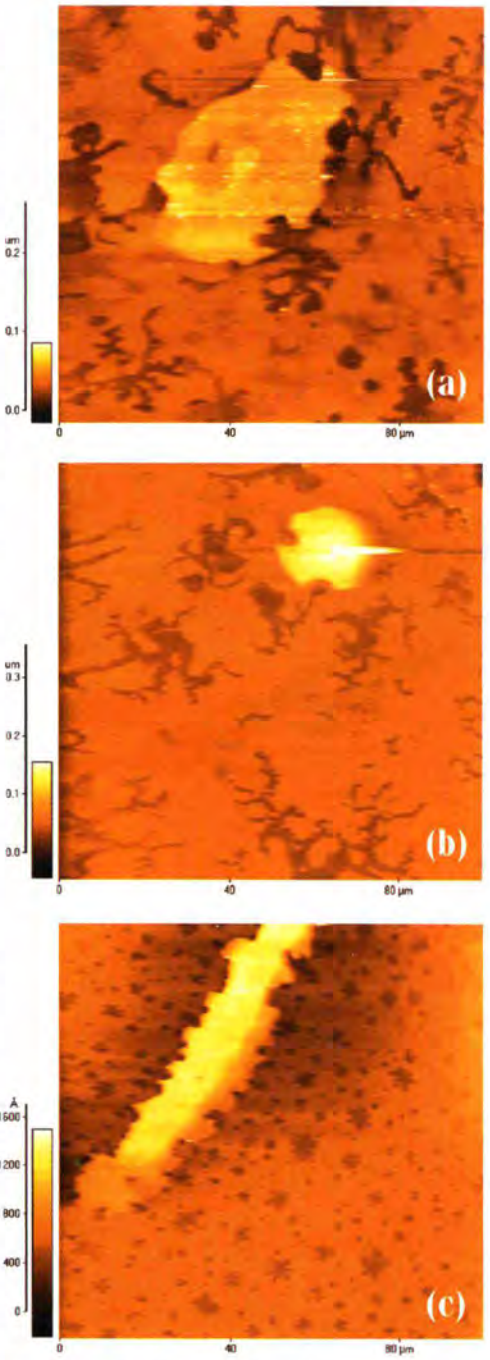

Figure 5: AFM images from (a) a sample formed by d-54 DMPC in H_2O water vapour in the fluid phase; (b) a sample formed by d-54 DMPC and Alamethicin in the ratio P/L=1/100 in H_2O water vapour; and (c) a sample formed by d-54 DMPC and Alamethicin in the ratio P/L=1/25 in H_2O water vapour.

References

[1] E. Sackmann, Science 271 (1996) 43 • [2] U. Mennicke and T. Salditt, submitted to Langmuir • [3] L. Perino-Gallice et al., submitted to Eur. Phys. J. • [4] T. Charitat et al., Eur. Phys. J. B 8 (1999) 583 • [5] ILL News, June 2001 • [6] M. Born and E. Wolf, Principles of Optics (1989) Pergamon Press, Oxford • [7] S. Heminghaus et al., Science 30 (1998) 916 • [8] R. Podgornik and V.A. Parsegian, Biophys. J. 72 (1997) 942 • [9] S. J. Ludtke et al., Biochemistry 35 (1996) 13723.

The deuteration laboratory
a new user facility

● M. Haertlein, J.B. Artero, V.T. Forsyth, I. Parrot and P.A. Timmins (ILL)

● M.Th. Dauvergne, F. Meilleur, D.A. Myles (EMBL)

Why deuteration ?

Neutron scattering experiments provide important information in structural biology that is not accessible by X-ray scattering alone. At low resolution the contrast variation technique is particularly powerful both in solution and in crystals. In its simplest form it can be performed by varying the H_2O/D_2O content of the solvent to match alternately protein, nucleic acids, or lipids. However, if deuterium labelling of the constituent macromolecules is available, much more sophisticated experiments can be carried out. It becomes, for example, possible to investigate the shape of a single labelled protein within a multi-subunit protein complex or to measure the distance between two labelled sub-units within a complex. At medium to high resolution, the ability to determine and distinguish H/D positions in membranes, fibres and single crystals provides unique information and insight into catalysis, protein-ligand interactions and the protein-solvent interface.

A dedicated laboratory for deuteration

Although the benefits of sample deuteration have been widely appreciated for some time, it has never been easy for individual biologists to deuterate their systems in a routine way that allows best use to be made of valuable central facility resources. The expertise required is rather specialised and individual requirements vary quite considerably. The development of a deuteration laboratory within the infrastructure of the ILL and the EMBL Outstation will have a critical impact on the quality and speed of neutron experiments, in protein crystallography, fibre diffraction, small-angle scattering and inelastic scattering, and will bring new science to the ILL in each of these areas. Access to the laboratory is open to all users (and potential users) of the ILL's neutron scattering facilities by way of a proposal system (detailed information can be found on the ILL web site at http://www.ill.fr/pages/science/User/UProposals.html).

Fermentation equipment in the Deuteration Laboratory

Preparation of deuterated biological samples

Deuterated macromolecules such as proteins and nucleic acids can be isolated from micro-organisms grown in a D_2O-containing medium. Recombinant DNA technology including bacterial and yeast expression systems are often used when large quantities of a deuterated material are needed. Before the expression systems can be used to produce deuterated macromolecules the host organism has to be adapted to growth in 100% D_2O.

The use of a bioreactor (fermentor) allowing the control of parameters such as aeration, pH, fed rate etc. is important to obtain high cell density cultures. Given the high costs for deuterated carbon sources (glucose, succinate, glycerol) and D_2O, fermentors are an essential piece of equipment in the deuteration lab because they allow to obtain high yields of biomass per volume of culture.

Laboratory activities

The laboratory is currently focussing on developing methods for both per- and selective deuteration.

Perdeuteration of proteins and DNA expressed in E. coli

Cultures of the deuterium adapted BL21 (DE3) strain have been produced and used for the production of rat γ-crystallin-C and γ-crystallin-E. The aim is to grow large crystals to carry out neutron crystallographic studies on the surface structure of these proteins and in particular the role of hydrogen atoms. It is planned to also adapt strains of the yeast *Pichia pastoris* to compare expression in this system. Deuterated cytochrome P450CAM from *Pseudomonas putida* has also been expressed in *E. coli* and purified in order to carry out crystallographic studies. Perdeuterated DNA has been produced for fiber diffraction studies.

The development of fermentation protocols for High Cell Density Cultures in D_2O has been started.

Specifically labelled proteins

Rat γ-crystallin has also been produced with specific deuterium labelling of the tryptophans (Trp). This was done using the Trp-auxotrophic *E. coli* strain KS463 after site-specific integration of the T7-RNA polymerase gene via the prophage λDE3 into its chromosome. The resulting strain was transformed with the expression vector pET26a carrying the cDNA for the rat γ-crystallin under control of a T7 promoter and a kanamycin resistance marker. ■

Icosahedra:
a new shape in surfactant self-assembly

● C. Vautrin, M. Dubois and T. Zemb (CEA, Saclay)

● T. Gulik-Krzywicki (CNRS, Gif-sur-Yvette)

● B. Demé (ILL)

Self-assembled structures having a regular hollow icosahedral form are extremely rare and have not hitherto been observed with organic components such as surfactants, although predicted theoretically [1]. It is, however, well known that certain lipids or surfactants form bilayers that can fold into a variety of distinct geometric forms: vesicles, random bilayers, ordered stacks of flat or undulating membranes, etc. Here, we show that such bilayers made of two oppositely charged single-chain surfactants can self-assemble into hollow aggregates with a regular icosahedral shape [2]. The icosahedron is known to have the lowest curvature energy in the family of polyhedra. One of the fascinating feature of these supramolecular aggregates is the presence of pores located at the 12 vertices. The resulting icosahedral structure has a size of about one micrometer and mass of 10^{10} Daltons, making them larger than any known icosahedral protein assembly or virus capsid.

Combined small-angle neutron and light scattering (SANS and SALS, figure 1) provide independent proof that closed unilamellar objects of well-defined size are formed upon cooling a suspension of vesicles. As in the case of lipid microtubules, the aggregates are formed by cooling the sample through a first-order phase transition [3]. The exact decay of the scattering as the second power of the scattering vector (Q) and over an exceptionally wide range of scattering vectors covered by light and neutron scattering is the signature of a perfectly flat (extremely rigid) membrane. This is due to the fact that icosahedra are made of locally perfectly flat triangles (20) connected by 30 edges. As for carbon nanotubes, the persistence length is in the micrometer range. Thus the elastic Young's modulus of the walls is extremely high for a surfactant assembly, of the order of 100 MPa, as for the nanodiscs previously described [4]. The size and mass of the aggregates derived from these experiments coincide with those found by freeze-fracture electron microscopy (we evaluate that on average, $2x10^7$ surfactant pairs form one aggregate, which therefore has a molar mass close to 10^{10} Dalton). The fit to the SANS data yields a bilayer thickness of 40 Å, close to the thickness of individual nanodiscs [4].

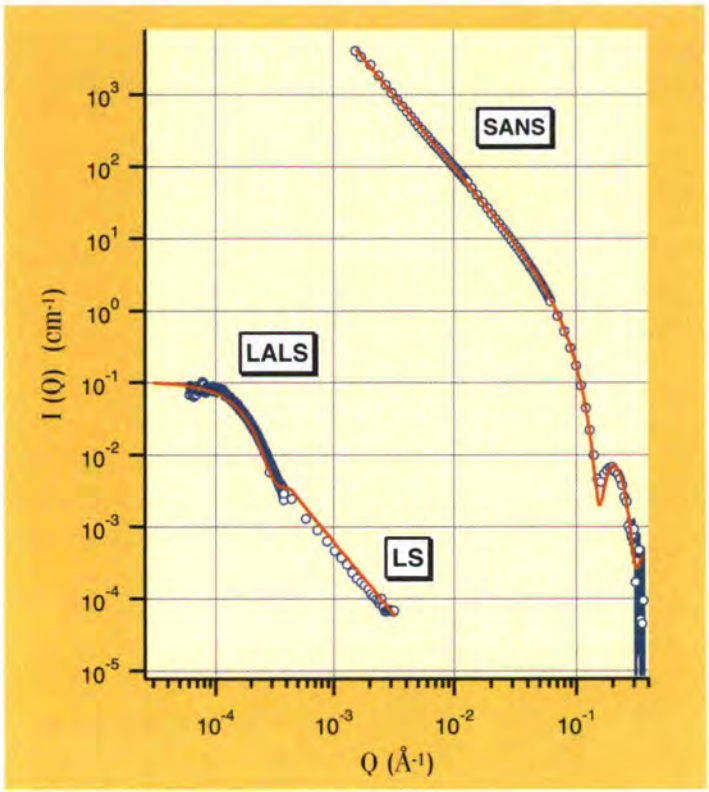

Figure 1: Combination of small-angle neutron scattering to light scattering showing the exceptional regime dominated by the scattering of perfectly flat aggregates on 3 decades in scattering vectors. This regimes corresponds to the flat triangles forming the icosahedra. The Guinier range seen at low Q with light scattering yields the size of the aggregates while the sharp minimum at wide angles in the neutron curve indicates the absence of thickness fluctuations. The fit to the neutron data gives the membrane thickness (40 Å).

As can be seen in figure 2, the pentagonal contour shape observed in freeze-fracture electron microscopy (figure 2a) differs from the hexagonal symmetry apparent in cryo-TEM (transmission electron microscopy, figure 2b). The icosahedron is the only possible shape consistent with these two images. At high magnification, a crucial feature appears: vertices of icosahedra consist of pores. The only topology to evacuate excess charges - that is curvature - from a perfectly flat 2-D crystal, is to segregate them in edges or in pores. This is a way for the system to self-assemble by minimising its curvature energy. During cooling down (figure 3), chain crystallisation produces a two-dimensional

array of alternated positive and negative charges responsible for the local to long-range in-plane cohesion. A small part of the component in excess which is not miscible in the two-dimensional crystal is expelled laterally. The amount of excess anionic component is such that 12 pores per vesicle are formed during crystallisation. If the density of pores is too low or too high, icosahedra cannot form and planar fragments are found. The structure that minimises the bending energy with the electrostatic constraints is thus, as expected, a regular icosahedron.

The microstructure of these complex aggregates is sketched in figure 3. The self-assembled two-dimensional crystalline shell is similar in shape to the structure initially proposed for viruses by Watson and Crick [6]. In icosahedra, subunits are combinations of oppositely charged surfactant pairs. Although in viruses the number of subunits is smaller, the type of aggregates described here should obey a similar topology control mechanism: a locally hexagonal lattice folds into 20 equivalent triangles. What is interesting about polyhedra is that the curvature is locally concentrated in edges, which is also the case for the pores. The edges are line singularities in the curvature, whereas the vertices are point singularities of the curvature. What does the Helfrich bending energy in the vicinity of a line or point singularity? It appears that the structure of the objects can handle a line singularity, but not a point singularity. Hence, a second explanation of the generation of pores is that their presence acts to eliminate this singularity in the curvature, rather than providing a place for the excess anionic surfactant. In other words, the anionic surfactant stabilises this structure by removing a singularity in the curvature. For regular icosahedra, there are relationships between the number of faces, edges and vertices given by Euler's formulas. The count of 12 pores per structure seems like it might be related more to the topology than the amount of excess surfactant, and may dictate why only certain ratios of anionic to cationic surfactant work.

There is a large demand for intelligent encapsulation procedures in many areas of medicine, pharmacy, cosmetics and materials areas like printing. Consequently, there is also a large demand for encapsulation procedures that are simple and versatile. The merit of the present system is the development of a fascinating self-assembly method to prepare capsules of defined geometry. A special feature is that the wall structure can be controlled with submolecular precision. This means that also the structure of defects can be well controlled, that is pores and instabilities have precise definitions which may become important for controlled release of drugs with specific size and conditions. In addition, although made of soft matter and non resistant to the addition of even small quantities of salt, the capsules appear very tough. This property would be important for controlled drug or DNA release. ■

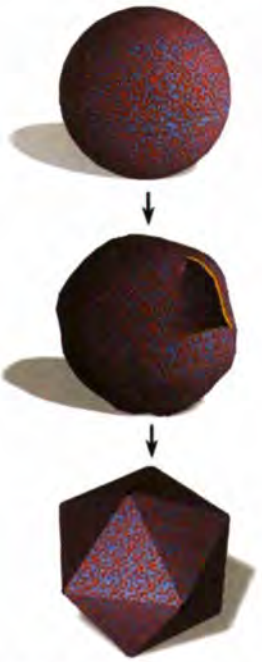

Figure 3: Sketch of an icosahedron and sequence resulting from cooling of vesicles prepared above the chain melting transition of the surfactant mixture.

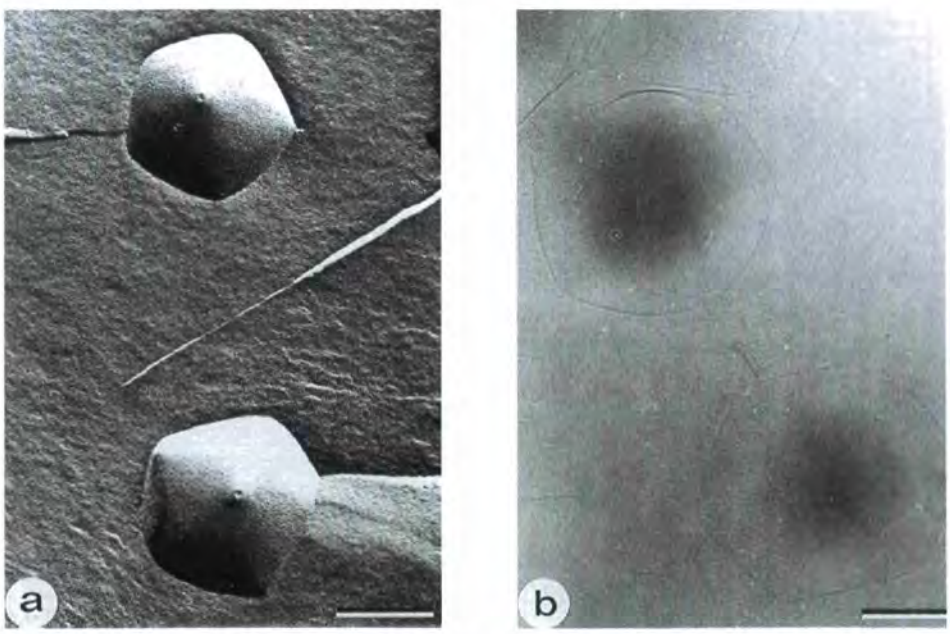

Figure 2: Freeze-fracture EM and cryo-TEM of icosahedra showing the pentagonal shape of two aggregates crossed by the fracture (a) and the hexagonal shape resulting from the projection as seen in transmission (b).

References

[1] T. C. Lubensky, J. Prost. J. Phys. (France) II, 2, 371-382 (1992) • [2] M. Dubois, B. Demé, Th. Gulik-Krzywicki, J.-C. Dedieu, C. Vautrin, S. Désert, E. Perez, Th. Zemb. Nature 411, 672-675 (2001) • [3] Thomas, B. N., Safinya, C. R., Plano, R. J. & Clark, N. A. Science 227, 1635-1638 (1995) • [4] Th. Zemb, M. Dubois, B. Demé, & Th. Gulik-Krzywicki. Science 283, 816-820 (1999) • [5] A. Klug, D.L.D. Caspar. Adv. Vir. Res. 7, 225-325 (1960) • [6] F. H. Crick, J. D.Watson. Nature 177, 473-475 (1956).

Soft Matter

Stabilisation of thin polymer films

- P. Müller-Buschbaum and W. Petry (TU München)
- O. Wunnicke and M. Stamm (IPF Dresden)
- R. Cubitt (ILL)

The stabilisation of thin polymer films is of great importance for many applications. The addition of copolymer represents one possible route for enhanced stabilisation. The stabilising effect is obtained from a thermally activated copolymer brush created at the interface. Above a critical concentration of the copolymer the density of the brush is high enough to prevent dewetting.

A large number of recent technological applications makes use of thin and continuous polymer films. One major problem is the thermal stability of these polymer films on semiconductor or polymer surfaces. As a result of miniaturisation, spatial dimensions are reduced ("shrink technology") which gives rise to instability of polymer layers. Below a certain film thickness polymer films are typically metastable. The thermal load in processing can act as an annealing step above the glass transition temperature of the polymer. Therefore, small perturbations can be followed by a complete destabilisation of the originally continuous film. The film tears up and a drop structure sets in. This so called dewetting process will prevent any further use. As an example, tearing-off of an insulting polymer layer would destroy any electronic device built on it.

To focus on the process of film stabilisation, we have investigated a model system: two polymer layers (polystyrene and polyamide) on top of a semiconductor surface (silicon). The topmost polystyrene layer is blended with a copolymer (styrene maleic anhydride acid). In the bulk, this copolymer is successfully added to blends of polystyrene and polyamide for improved adhesion (reactive compatibilisation) [1]. Figure 1 shows a schematic picture of the sample system. The thermal load is modelled by annealing above the glass transition temperature of the topmost layer. Without the added copolymer the polystyrene film dewets on top of the polyamide layer. The stabilising effect of varying amounts of added copolymer of up to 30% is determined in this investigation.

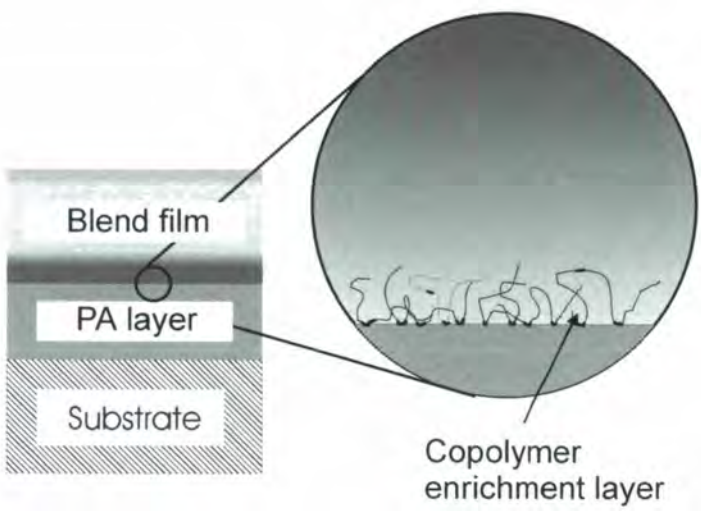

Figure 1: Schematic side view of the polymer bilayer film on top of the substrate. The grey scaling in the blend layer depicts the copolymer content. With increasing copolymer amount a darker colour is chosen.

Experiments were performed with neutron reflectometry as well as with grazing incidence small angle neutron scattering (GISANS) [2]. Thus the density profile perpendicular to the sample surface and the lateral morphology were addressed. The measurements were carried out on the instruments D17 and D22 at ILL. Figure 2a shows an example of reflectivity data from annealed samples. The solid lines correspond to fits to the data calculated from the scattering length density profiles which are shown in the inset. After annealing for longer than 300 hours, the bilayer polymer films with a copolymer concentration of 5% or larger still exhibit a smooth surface. No sign of dewetting is detectable: the polymer system is stabilised. The reduced density between both polymer layers results from the enrichment of copolymer at the interface. In contrast, the addition of 1% copolymer is not sufficient to suppress a destabilisation. After annealing a structure is still observable on the surface. This surface is well described by one dominant in-plane length scale. In the GISANS data this surface heterogeneity gives

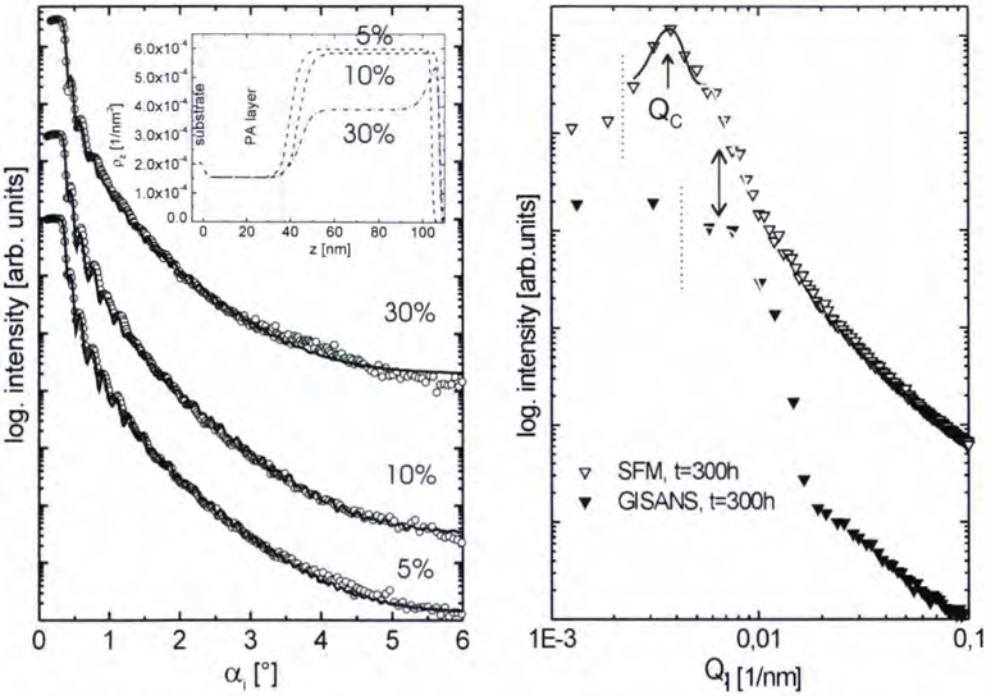

Figure 2: (a) Reflectivity data from annealed samples with increasing amount of copolymer (from bottom to top 5, 10 and 30%). The inset shows the resulting density profiles. (b) Comparison between GISANS data and data obtained with SFM (copolymer 1%). The dotted line indicates the resolution limit. The position of characteristic peaks are marked. The data are shifted for clarity.

rise to well pronounced peaks. Figure 2b compares data measured with GISANS with data obtained from scanning force microscopy (SFM). Both depict the film destabilisation.

The combination of scattering methods, reflectivity and GISANS, has yielded results which enable the adaptation of the model used in the bulk system to thin film geometry [3]. Copolymer molecules are considered to be connected to the polyamide layer via hydrogen bonds. Those connected copolymers stick to the interface and give rise to an enrichment layer. During annealing further copolymers diffuse to the interface which results in an increase of the enrichment layer. The thickness of the enrichment layer is of the order of the radius of gyration of the copolymer. Thus only copolymers which are connected via hydrogen bonding stay near the interface. Parts of the copolymer chain, which are not directly connected with the polyamide layer, create a brush-like interface (figure 1). This reduces the possible movement of polymer chains in the top layer. Above a critical concentration, e.g. 5 % of copolymer added, this movement is suppressed completely. Consequently in this regime the stabilisation is observed. Below the critical concentration, e.g. at 1% added copolymer, the density of the brush is not high enough and the destabilisation is only retarded. After sufficiently long annealing first holes occur.

To summarise, the addition of a copolymer which can form bonds with the underlying polymer layer is well suited to improve thin film stability. ■

References:

[1] K. Dedecker, G. Groeninckx, T. Inoue, Polymer 39 (1998) 5001 • [2] P. Müller-Buschbaum, J.S. Gutmann, R. Cubitt, M. Stamm, Colloid Polym Sci. 277 (1999) 1193 • [3] O. Wunnicke, C. Lorenz-Haas, P. Müller-Buschbaum, V. Leiner, M. Stamm, Applied. Phys. A, in press.

Soft Matter

Study of vesicle formation by means of highly time-resolved stopped-flow experiments

● D. Gräbner and M. Gradzielski (University of Bayreuth)

● I. Grillo (ILL)

The formation of unilamellar vesicles was studied by means of the stopped-flow technique. The high neutron flux, on the small-angle scattering instrument D22, allows to study the formation process with a temporal resolution of 200 ms, thereby reaching the current limits of such structural investigations. Vesicles were formed by mixing a Na oleate surfactant solution with the cosurfactant octanol. After mixing emulsion droplets of octanol are present from which it diffuses into the micellar aggregates. By this simple diffusion mechanism first a growth of rod-like aggregates is induced which is followed by a two-dimensional growth at larger times. After about 2 mins formation of vesicles is observed. During the next 20-30 mins these unilamellar vesicles grow in size and become more monodisperse until a final state is reached. This shows that in this system by simple diffusion well-defined, monodisperse vesicles are formed by a process of self-organisation. The stopped-flow technique has allowed the observation of the various stages in this complex, multi-step reorganisation process with a good time-resolution.

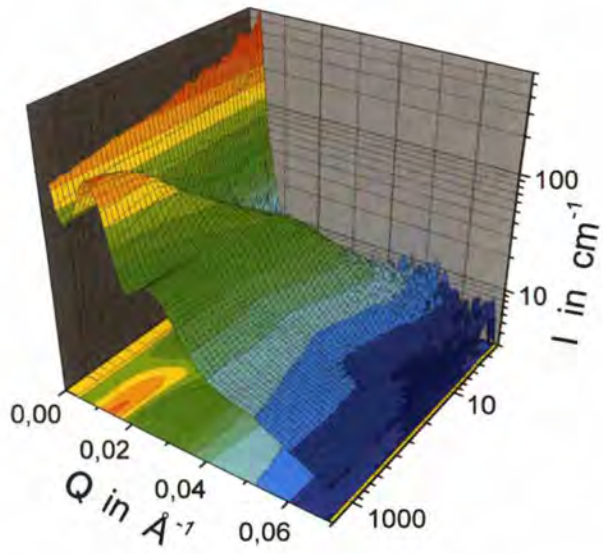

Figure 1: I(Q) as a function of time after mixing a 100 mM Na oleate solution with 3.5 wt% octanol.

Vesicles are closed bilayers of amphiphilic molecules – as for instance present in biological membranes. They can be unilamellar or multilamellar ('onions') and vary largely in size, with radii ranging from 50 Å to several µm. Not only are they of interest as models for biological membranes but also have widespread application in formulations in cosmetics, pharmacy etc. Therefore, the formation process of vesicles is of much interest both for fundamental as well as for applied research. Vesicles can be formed in a large variety of amphiphilic systems [1]. The chosen aqueous system consists of a conventional soap molecule, sodium oleate, and 1-octanol as a cosurfactant. Here, vesicles can be formed by simple mixing of a micellar solution with the corresponding amount of octanol. For low concentrations (50-150 mM Na oleate) isotropic vesicle solutions are found. For higher concentrations (150-250 mM Na oleate) a stiff gel of densely packed vesicles is obtained [2, 3]. The details of the formation process with high temporal resolution could be studied by using the stopped-flow technique [4] and mixed a 100 mM Na oleate solution with 3.5wt% octanol. The mixing process was followed by SANS experiments with time channels down to 200 ms over a total time of 40 mins. In order to have sufficient statistics for the short time intervals at the beginning the mixing process was repeated 10 times and the resulting data sets have been summed.

The obtained scattering curves as a function of time are shown in figure 1 together with the scattering curve of the pure 100 mM surfactant solution. Immediately after mixing the micellar correlation peak is still visible, in the pure micellar solution. In addition, the scattering intensity is found to increase at low Q, which is due to the initially formed emulsion droplets of octanol. As time passes on, the correlation peak moves to lower Q, thereby indicating a growth of the micelles. It should be noted that initially the micelles and in the final state, the formed vesicles, both of which are charged, exhibit spatial correlations. The final scattering pattern possesses very

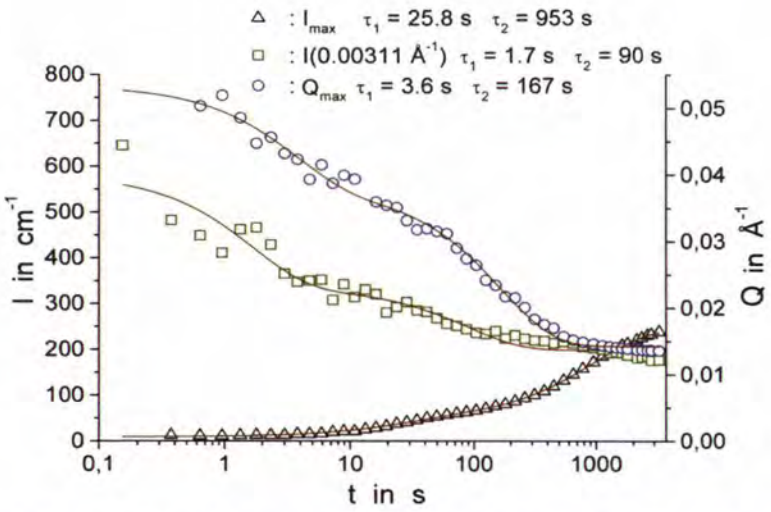

Figure 2: Change of position and intensity of the scattering maximum, and of the intensity at the lowest q-value a as a function of time.

pronounced minima and maxima which are oscillations of the form factor. They can be described well by the scattering of shell like particles, i. e. vesicles, with a radius of 140 Å, a shell thickness of 22 Å, and a polydispersity of 15%.

The temporal change of the experimental scattering pattern can be characterised by the change in position and intensity of the correlation peak, as displayed in figure 2. Both changes can be well described by a bi-exponential function with the time constants given in figure 2. It is interesting to note that the shift of the maximum occurs significantly faster than the increase in intensity. This indicates that the average size of the aggregates changes faster than the ordering in the system. In addition also the change of intensity at the lowest measured Q (= 0.00311 Å^{-1}) is given. The intensity at the Q-value, is an indication of the presence of emulsion droplets as well as a measure of the degree of ordering in the system. From its variation one can deduce that the initial emulsion droplets disappear with a time constant of 1.7 s, whereas the subsequent ordering process takes place with a time constant value of 100-150s, similar to that for the shift of the Q-value of the maximum.

Analysis of the time-dependent scattering curves shows that in the first 10 s the micellar growth is mainly unidimensional (related to τ_1 of I_{max} and Q_{max} of figure 2), i. e. growth of rodlike micelles, and that with increasing time, more and more bidimensional growth takes place (related to τ_2 of Q_{max} of figure 2), i. e. here bilayers are formed. After about 2 mins the scattering pattern of unilamellar vesicles can be discerned and these vesicles grow in size and become more monodisperse. At the end, i. e. after about 30-60 mins a very pronounced scattering pattern is observed that is characteristic for well-defined, relatively monodisperse vesicles with a radius of about 150 Å.

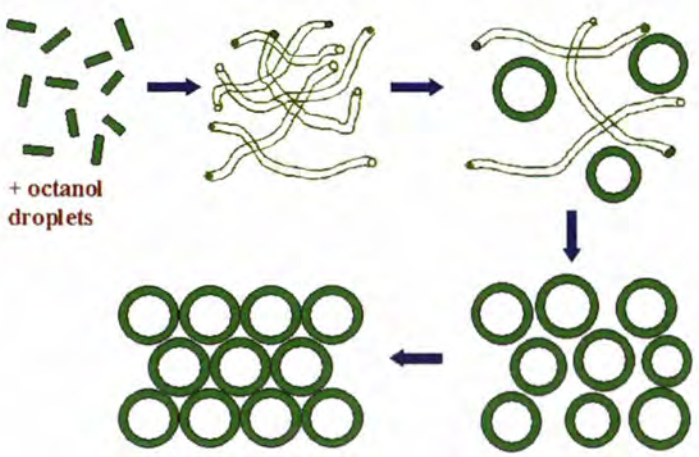

Figure 3: Schematic picture of the structural changes that take place upon mixing Na oleate solutions with octanol.

Putting all this information together, a schematic picture (figure 3) can be drawn for the structural changes that take place upon mixing the Na oleate solution with the cosurfactant octanol. In the beginning emulsion droplets of octanol in the surfactant solution are present. Then very quickly octanol diffuses into the micelles thereby leading to a growth of rod-like micelles. Once a sufficient amount of octanol is incorporated into the micelles the formation of bilayer structures sets in. They close and form unilamellar vesicles. In a much slower process, these vesicles "ripen" and become more monodisperse and somewhat larger in size. It can be mentioned that for samples of higher concentrations - where the vesicle gel is formed - a still much slower ordering process takes place where the initially present densely packed glassy state becomes transforms into a highly ordered final gel state of vesicles.

This experiment demonstrates that by mixing two simple liquids one can obtain by purely diffusive processes of self-organisation well-defined vesicles (or even a highly ordered vesicle gel). This process of self-organisation proceeds in a relatively complex way over different intermediate structures, where the time constants for the individual transformation processes vary from the seconds range to the hours range. ■

References:

[1] Vesicles, M. Rosoff (Ed.), Surfactant Science Series, 62, Marcel Dekker Inc.: New York, 1996 • [2] M. Gradzielski, M. Müller, M. Bergmeier, H. Hoffmann and E. Hoinkis, J. Phys. Chem. B 103 (1999) 1416 • [3] M. Gradzielski, M. Bergmeier, H. Hoffmann, M. Müller and I. Grillo, J. Phys. Chem. B 104 (2000) 11594 • [4] http://www.ill.fr/YellowBook/D22/D22_info/D22_stopped_flow/html/D22_SF_title.html.

The neutron as a quantum object

H. Rauch and Y. Hasegawa (Atominstitut Wien)

M. Baron and R. Loidl (Atominstitut Wien and ILL)

Quantum optics of material particles has become a rather topical field of research during the last decades. Almost forgotten is the fact that the neutron is just an ideal tool for such experiments. Neutron interferometer and neutron spin-echo systems are the basic instruments for such investigations. Various fundamental experiments in this field of physics have been performed long before experiments with other matter waves became feasible. The observation of the 4π-symmetry of spinor wave functions, the coupling to the Earth gravitational and rotational field, the neutron Fizeau effect and various Aharonov-Bohm phenomena are typical examples of such experiments which have been summarised in a recent book [1].

In an interesting publication, mentioned in the ILL Annual Report 2000, F. Pistolesi and N. Manini [2] showed that, in addition to the dynamical phase, which causes the above-mentioned 4π-symmetry of the spin wave function and the geometrical Berry phase, an additional topological phase exists when a physical system is transported differently in both beam paths of a split-beam interferometer set-up. In this case diagonal and off-diagonal geometrical phases occur, which can be visualised when the start and the end points of the spin excursion on the Poincaré sphere are connected by the related geodesics. Figure 1 shows the physical situation and the scheme of the experiment recently performed at the thermal neutron interferometer S18 where the polarisation has been oppositely rotated in both beam paths. In this case, an additional phase factor of π is expected which has been verified by experiment (figure 2) [3]. The results show that the neutron carries much more information than used in most experiments. This gives hope that the neutron can be used in future as a much more powerful and sensitive tool for phase-sensitive investigation. The realisation of this experiment within a rather short time is also a good example of an efficient cooperation of the ILL Theory Group and CRG experimentalists.

Another neutron quantum-optical experiment deals with the reconstruction of non-classical neutron quantum states that exist in interferometer and spin-echo systems when wave functions, separated in space, overlap. These phenomena can be descri-

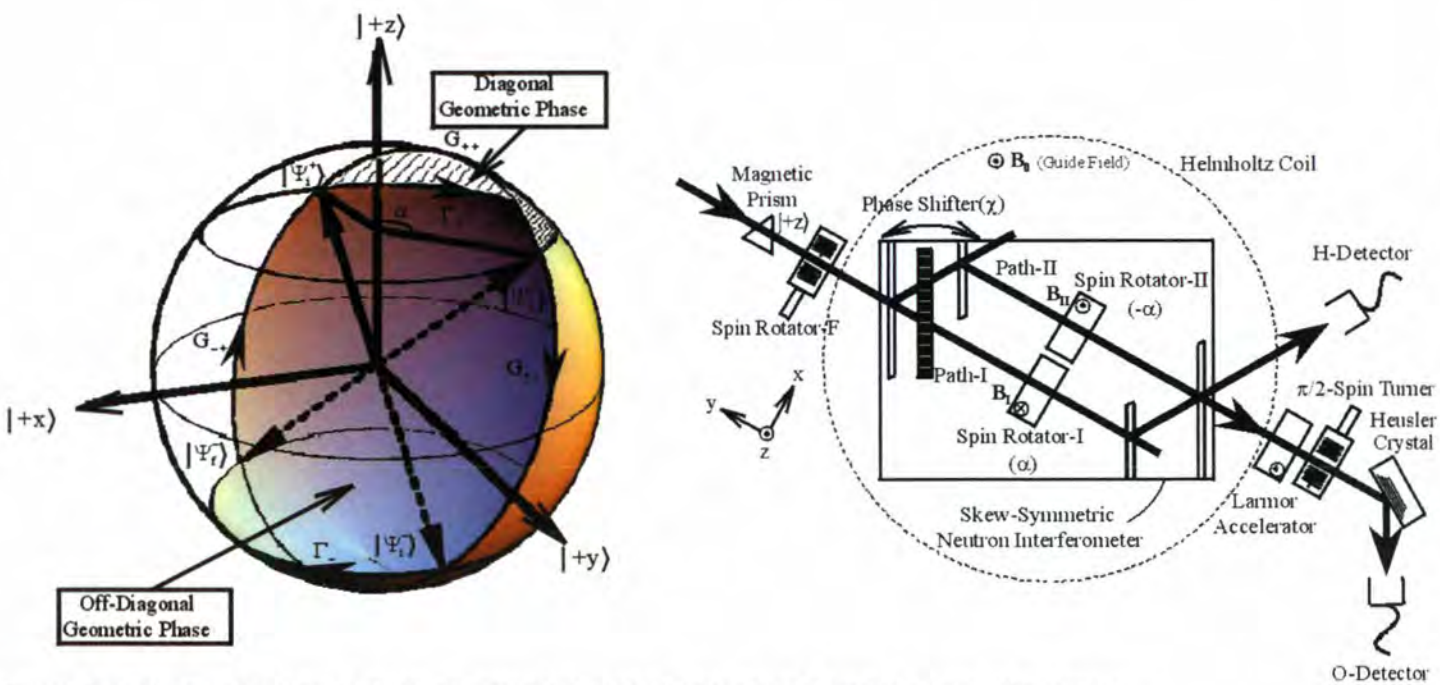

Figure 1: Poincaré sphere representation (left) and experimental set-up (right) for diagonal and off-diagonal geometric phase analysis.

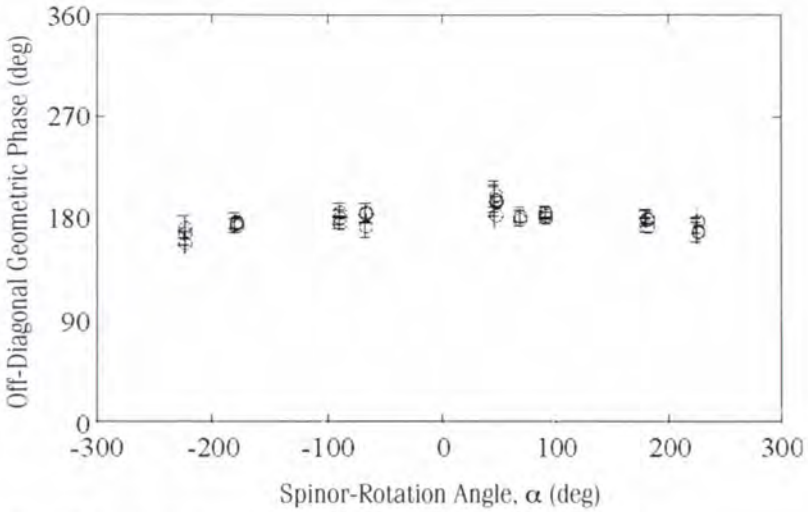

Figure 2: Experimental results of off-diagonal geometric phase measurements.

bed by Wigner functions which are constructed from the wave function and which are equivalent to it. Figure 3 shows such a quantum state in a double-loop interferometer.

This enables the simultaneous measurement of the momentum and space component of the Wigner function and provides the key for a quantum state reconstruction which has similarities to a tomographic reconstruction of a material object [4]. Since these quantum states are very fragile and sensitive against various dissipative effects they may be used in future for highly sensitive condensed matter research and may provide an access to higher order correlation functions. ■

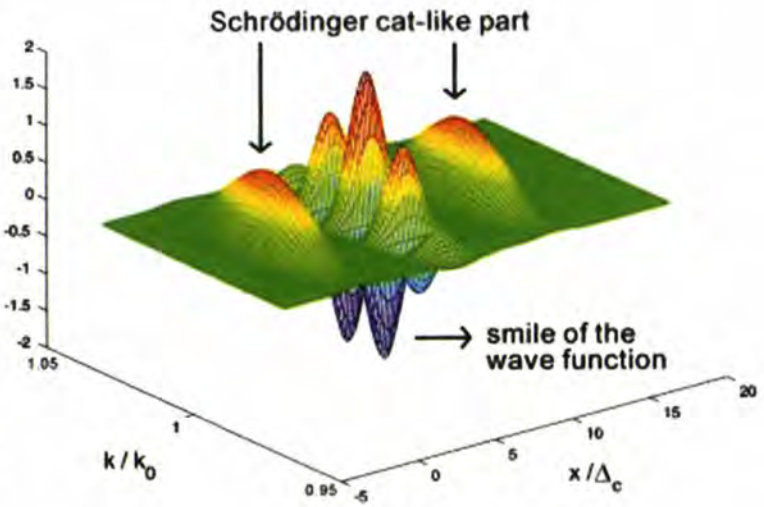

Figure 3: Non-classical Schrödinger cat-like states as they exist in interference and spin-echo instruments, which can be reconstructed on a quantum basis.

REFERENCES

[1] H. Rauch, S.A. Werner, "Neutron Interferometry". Clarendon Press, Oxford 2000 • [2] N. Manini, F. Pistolesi, Phys. Rev. Lett. 85 (2000) 3067 • [3] Y. Hasegawa, R. Loidl, M. Baron, G. Badurek, H. Rauch, Phys. Rev. Lett. 87 (2001) 070401 • [4] M. Baron, H. Rauch, M. Suda, Appl. Phys. A (in print)1.

Neuton β-decay, quark mixing and the question of unitarity

H. Abele, S. Baessler and J. Reich (Physikal. Institut, Heidelberg University)

V.V. Nesvizhevsky and O. Zimmer (ILL)

The combination of neutron β-decay experiments at the Institut Laue-Langevin challenges the Standard Model of elementary particle physics: A last measurement of the β-asymmetry A_0 and the world average of the neutron lifetime τ can be used to determine the first element $|V_{ud}|$ of the quark mixing matrix. With these values and the particle data group values for $|V_{us}|$ and $|V_{ub}|$, the unitarity condition for the first row of the CKM matrix deviates from unity by Δ = 0.0083(28), which is 3.0 times the stated error and conflicts with the prediction of the Standard Model of particle physics.

Matter is built from two types of fundamental fermion, called quarks and leptons (see Table). Quarks occur in several varieties or flavours labelled u=up, d=down, c=charm, s=strange, t=top and b=bottom. The strong interaction glues the quarks together and these quarks are considered to be quantum mechanical mass eigenstates. Neutrons are built from two d-quarks and one u-quark, whereas protons are built from two u-quarks and one d-quark: ddu=n (neutron), duu=p (proton). A neutron is unstable. The decay process is governed by the weak interaction converting a d-quark into an u-quark. Thus, a neutron decays into a proton, an electron and an electron antineutrino with an energy release of 782 keV and a lifetime τ of 885 s:

1st family	2nd family	3rd family
Quarks		
u	c	t
d	s	b
Leptons		
ν_e	ν_μ	ν_τ
e	μ	τ

Table: Elementary particles: Leptons and Quarks in three families.

$$n \rightarrow p\, e\, \overline{\nu}_e \qquad (1)$$

One parameter characterising an interaction is its strength. For example, the strength of the electromagnetic force is governed by the universal fine-structure constant α. In a similar way, a strong coupling constant a_s has been defined for the strong interaction. Weak interaction seemed to be different. The weak coupling strength responsible for nuclear β-decay is not identical with the coupling for μ-decay. The difference is about 2%. In the past, this flaw in the universality of the weak interaction has led to the development of a new model of the very basic part of quarks: The quark eigenstates of the weak interaction do not correspond to the quark mass eigenstates. A weak decaying quark is a mixture of different flavours of mass eigenstates. The weak eigenstates (primed) are related to the mass eigenstates (unprimed) as:

$$\begin{pmatrix} d' \\ s' \\ b' \end{pmatrix} = U_{Quark} \begin{pmatrix} d \\ s \\ b \end{pmatrix} \quad , U_{Quark} = \begin{pmatrix} V_{ud} & V_{us} & V_{ub} \\ V_{cd} & V_{cs} & V_{cb} \\ V_{td} & V_{ts} & V_{tb} \end{pmatrix} \qquad (2)$$

with unitary CKM-matrix U_{Quark}. All the mixing is expressed in terms of U_{Quark} operating on d, s and b quarks. As a consequence, the d'-quark that is responsible for neutron β-decay, is a linear superposition of d-, s-, and b-mass states: $d' = V_{ud} \cdot d + V_{us} \cdot s + V_{ub} \cdot b$. The basic idea of U_{quark} is that what is perceived to be several independent couplings is expressed as a single force. Now, if every quark gives as much as it takes in this mixing, then the quark-mixing-CKM-matrix has to be unitary.

Unitarity requires that the sum of the squares of the matrix elements for each row and column is unity. So far precision tests of unitarity are only possible for the first row of V, namely:

$$|V_{ud}|^2 + |V_{us}|^2 + |V_{ub}|^2 = 1 - \Delta \qquad (3)$$

The Standard Model requires unitarity, that is Δ = 0. A violation of unitarity in the first row of the CKM matrix is a challenge to the three generation Standard Model. A deviation Δ has been related to concepts beyond the Standard Model, such as couplings to exotic fermions, to the existence of an additional Z boson or the existence of right-handed currents in the weak interaction.

In the Standard Model, two free parameters describe the neutron β-decay. One parameter is the first entry V_{ud} of the CKM-matrix. The other one is λ, the ratio of the vector coupling constant and the axial vector constant. The observables for determining V_{ud} are the neutron lifetime τ and a measurement of one of the angular correlation coefficients e.g. the β-asymmetry coefficient A_0. The β-asymmetry A_0 is linked to the probability that an electron is emitted with angle J with respect to the neutron spin polarization $P = \langle \sigma_z \rangle$:

$$W(\vartheta) = 1 + v/c\, P\, A \cos(\vartheta) \qquad (4)$$

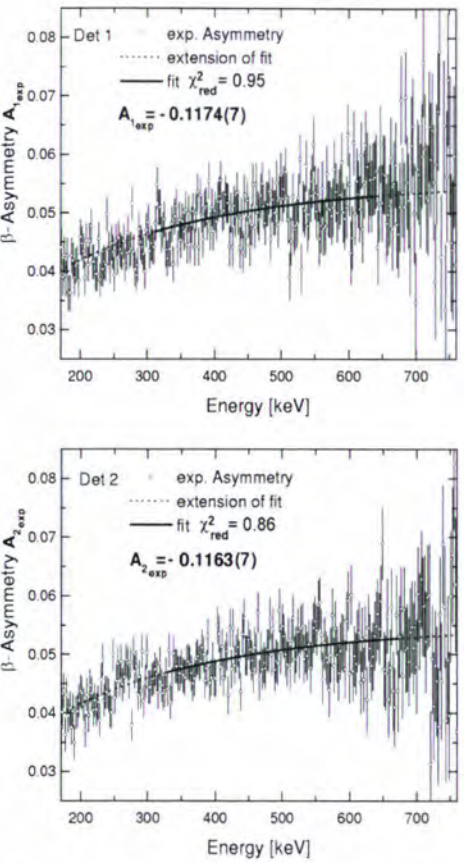

Figure 1: Fit to the experimental asymmetry A_{exp} for detector 1 and detector 2. The solid line shows the fit interval, whereas the dotted line shows an extrapolation to higher and lower energies.

where v/c is the electron velocity expressed in fractions of the speed of light. Neglecting order 1% corrections, A is a simple function of λ.

For a measurement of β-asymmetry A_0, the instrument PERKEO was installed at the PF1 cold neutron beam position at the High Flux Reactor at the Institut Laue-Langevin, Grenoble. The neutrons are polarized by a 3 x 4.5 cm² supermirror polarizer. The degree of neutron polarization was measured to be P = 98.9(3)% over the full cross section of the beam.

The main component of the PERKEO II spectrometer is a superconducting 1.1 T magnet in a split pair configuration, with a coil diameter of about one meter. Neutrons pass through the spectrometer, whereas decay electrons are guided by the magnetic field to either one of two scintillation detectors. The detector solid angle of acceptance is $2x2\pi$. The measured electron spectra $N_i^\uparrow(E_e)$ and $N_i^\downarrow(E_e)$ in the two detectors (i=1,2) for neutron spin up and down, respectively, define the experimental asymmetry $A_{iexp}(E_e)$ as a function of electron kinetic energy E_e and are shown in figure 1. $A_{iexp}(E_e)$ is directly related to the asymmetry parameter A_0. After a 2% correcting for small experimental systematic effects we obtain:

$$A_0 = -0.1189(7) \text{ and } \lambda = -1.2739(19) \text{ [1,2]} \quad (5)$$

Earlier experiments with larger corrections on A_0 [3-5] gave significantly lower values for λ. With our value only, and the world average for τ = 885.7(7) s, we find that $|V_{ud}|$ = 0.9713(13). With $|V_{us}|$ = 0.2196(23) and the negligibly small $|V_{ub}|$ = 0.0036(9), we obtain:

$$|V_{ud}|^2 + |V_{us}|^2 + |V_{ub}|^2 = 1\text{-}\Delta = 0.9917(28) \quad (6)$$

This value differs from the Standard Model prediction by Δ = 0.0083(28), or three times the stated error. For comparison, information about $|V_{ud}|$ and λ are shown in figure 2. The bands represent the one sigma error of the measurements. The β-asymmetry A_0 in neutron decay depends only on λ, while the neutron lifetime τ depends both on λ and $|V_{ud}|$. The intersection between the curve, derived from τ and A_0 (5), defines $|V_{ud}|$ within one standard deviation, which is indicated by the error ellipse. Other information on $|V_{ud}|$, derived from nuclear β-decay and higher quark generation decays assuming CKM-unitarity are shown, too. As can be seen from figure 2, both the nuclear β-decay result [6] and the neutron β-decay differs from this unitarity value by more than one sigma level.

In summary, $|V_{ud}|$, the first element of the CKM matrix, has been derived from neutron decay experiments in such a way that an unitarity test of the CKM matrix can be performed based solely on particle physics data. With this value, we find a 3 σ standard deviation from unitarity, which might conflict the prediction of the Standard Model of particle physics. ■

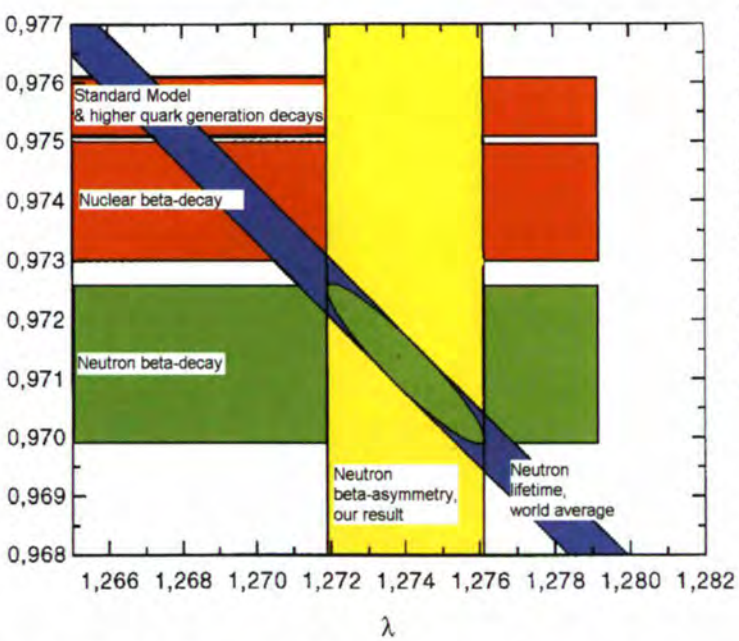

Figure 2: $|V_{ud}|$ vs. λ. |Vud| was derived from Ft values of nuclear β-decays, higher quark generation decays, assuming the unitarity of the CKM matrix, and neutron β-decay.

REFERENCES
[1] H. Abele et al., Phys. Lett. B 407 (1997) 212 • [2] H. Abele et al., submitted to Phys. Rev. Lett. • [3] B. G. Yerozolimsky et al., Phys. Lett. B412 (1997) 240 • [4] K. Schreckenbach et al., Phys. Lett. B 349 (1995) 42; P. Liaud et al., Nucl. Phys. A 612 (1997) 53 • [5] P. Bopp et al., Phys. Rev. Lett. 56 (1988) 919 • [6] J. Hardy et al., nucl-th/9812036.

Phase modulation of a neutron wave
and diffraction of ultra-cold neutrons by a moving grating

- A.I. Frank and I.V. Bondarenko (FLNP, Dubna)
- S.N. Balashov and S.V. Masalovich (Kurchatov Institute, Moscow)
- P. Høghøj and P. Geltenbort (ILL)

A neutron diffraction experiment was performed with a moving grating on the gravity spectrometer for ultra-cold neutrons (UCN) using interference filters (Fabry-Perot interferometer for neutrons). The results have shown for the first time that the phase modulation of the neutron wave induces a discrete splitting of the neutron energy spectrum.

In general, quantum experiments are performed for a better understanding of quantum mechanics and to demonstrate the validity of its conclusions. But their importance is not only limited to the undoubtedly great pedagogical role: such experiments can also stimulate the development of new methods and devices based on quantum principles. In particular, the new non-stationary quantum experiment described below has become possible only after the development of a dedicated spectrometer based on principles of quantum mechanics. In contrast to devices most commonly used in optics, non-stationary devices change the energy of a neutron.

Probably the simplest way to vary the neutron energy is to introduce a time modulation of the neutron wave since a periodical modulation of any wave leads to a splitting in its frequency spectrum. In the case of matter waves, the splitting of the frequency line is equivalent to a discrete spectrum of the particles energy.

Let us assume that a plane wave $\psi(x,t) = e^{i(kx-\omega t)}$ is propagating along the positive x-direction. A modulator device is located at the origin of the reference frame. The action of this modulator results in a periodic variation (period T) of the amplitude or phase of the primary wave. Then, at small distances away from the modulator, the wave function will have the form

$$\psi(x,t) \cong f(t)e^{i(kx-\omega t)} \qquad (1)$$

where f(t) is a function of period T. Representing f(t) in the form of a Fourier series, $f(t) = \sum_{n=-\infty}^{\infty} a_n e^{-in\Omega t}$, one obtains that the wave function in any distance from the modulator is:

$$\psi(x,t) = \sum_{n=-\infty}^{\infty} a_n \exp[i(k_n x - \omega_n t)] \qquad (2)$$

$$\text{with} \quad \omega_n = \omega + n\Omega, \quad k_n = k(1 + n\gamma),$$

$$\Omega = \frac{2\pi}{T}, \quad \gamma = \Omega/\omega << 1. \qquad (3)$$

Equations (2) and (3) show that due to the modulator, the transmitted state is a superposition of coherent waves with a discrete frequency spectrum. For matter waves, the resulting frequencies ω_n correspond to the particle energies $E_n = \hbar(\omega + n\Omega)$, where $\hbar$ is the Planck constant. The intensities of the partial waves are $I_n = |a_n|^2$ where a_0 is the amplitude of the wave with the initial energy.

Now let us assume that a periodic structure, a grating with a spatial periodicity 2a is moving with the velocity V across the neutron beam. Assume further that different elements of the grating have different properties, so that the waves, which are transmitted through different parts of grating differ in their intensities or phases. In the simplest case, one half of each grating element fully transmits neutrons while the other half completely absorbs them. It can be easily seen that such a moving grating will modulate the transmitted wave in each point of the beam cross section with the frequency $\Omega = \pi V/a$. As a consequence, the spectrum of the transmitted waves will be discrete.

The most promising experimental set-up uses a phase π-grating where the phase difference of waves transmitted through adjacent elements amounts to π, while their intensities are unaltered. In such a case the amplitudes of the partial waves are

$$a_n = \frac{2}{i\pi n} \qquad \text{with} \quad n = 2s - 1 \qquad (4)$$

where s is an integer. It must be stressed, that the line with the initial energy $\hbar\omega$ (n = 0) is absent in the final state. In the

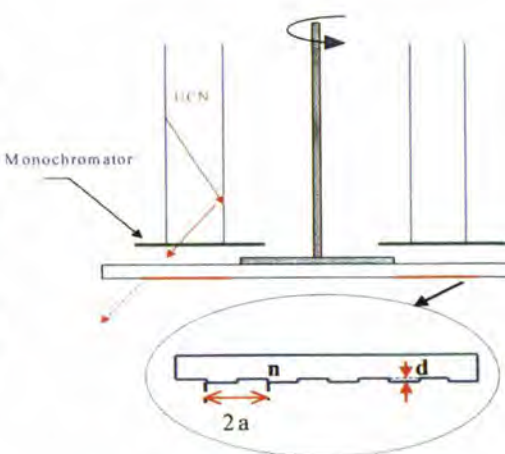

Figure 1: Principle of the experiment. A phase grating is prepared on the surface of a silicon disc. When the disc is spinning, each point of the monochromatic UCN beam is crossed by the moving grating.

experiments described below the energy spectrum of ultra-cold neutrons after diffraction by a moving phase π-grating have been measured for the first time.

As proposed earlier [2], the primary neutron monochromatisation of UCN as well as the analysis of the diffracted spectrum were performed by means of Neutron Interference Filters [3,4] (NIF), a quantum device, which is analogous to the Fabry-Perot interferometer for light.

The principle of the experiment is shown in figure1. The rotating grating was manufactured at the surface of a silicon disk of 150 mm diameter and 0.6 mm thickness. On its peripheral region the radial grooves were made by lithographic techniques. The angular period of the grating was 3.325×10^{-4} rad^{-1} corresponding to a spatial periodicity of 20 μm at a diameter of 120 mm. The grooves cover about half of the period. UCN reach the grating through an annular guide. Between the exit of the collimator and the grating the NIF–monochromator is placed. Only UCN with vertical velocities around 4.52 m/s (narrow spectrum with FWHM of about 0.085 m/s) pass the monochromator and reach the grating. (Note that such a velocity corresponds to an energy of 107neV). Due to refraction in the silicon, neutron waves, which passed through different elements of the grating, have different phases. The phase difference is $\Delta\varphi = k(1 - n)d$ where k is the neutron wave number, n is the refractive index and d is the depth of the grooves. The depth d was chosen to be about 0.14m which corresponds exactly to a phase shift $\Delta\phi = \pi$ for 107neV neutrons refracted by silicon.

The experiment was performed at the PF2/TES beam position of the ILL. The major component of the set up is an UCN gravity spectrometer with interference filters as described in detail in Ref. [4,5]. UCN

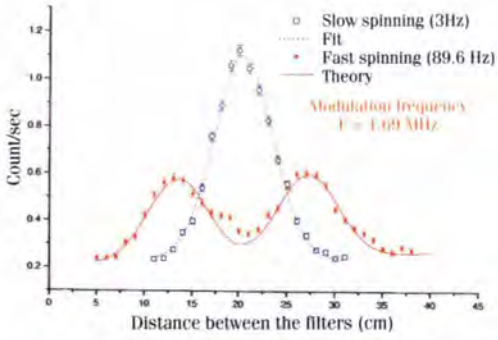

Figure 2: Measured energy splitting after the diffraction of UCN in a moving grating due to phase π-modulation of the neutron wave.

fed the spectrometer through a neutron guide. Then, UCN fall down the annular collimator. The grating was located just below the filter-monochromator (NIF). It was spun around the vertical axis up to 6000 rpm. UCN which are transmitted through the filter and the grating, fall further down in a mirror-like neutron guide of glass of 40 cm height. Doing so, the UCN are accelerated in the Earth's gravitational field and gain in energy 1neV per cm of free fall. This glass guide contains a second NIF which acts as an analyser. By changing the position of this analysing filter, the energy of the transmitted neutrons can be scanned. The resonant energy of the second filter was 127neV to compensate the change in energy due to gravity. Finally, the transmitted neutrons are counted with a ^{3}He gas detector.

The neutron count rate as a function of the analyser position was measured for two very different grating rotation frequencies: 180 and 5400 rpm (figure 2). In the case of slow spinning the effective modulation frequency $\Omega = \pi V/a$ is small, and the corresponding energy splitting $\Delta E = \hbar\Omega$ is much less than the width of initial energy spectrum of the UCN. Therefore, the scanning curve is simply a convolution of the monochromator and analyser spectral functions. The experimental results are shown in figure 2 as open dots. The dash curve represents a fit using a Gaussian with a dispersion $\sigma \cong 6.2$ neV, corresponding to the energy resolution of the spectrometer of about 7.3 neV (FWHM).

The fast rotation regime (5400 rpm) corresponds to a linear velocity of the grating $V \approx 36$ m/sec and a modulation frequency Ω around 1.07×10^7 rad/sec. The scan in figure 2 clearly shows a discrete spectrum. The spectrum of neutrons, which passed through the grating, can be written as $\Phi(E) = \sum_n |a_n|^2 f(E + n\hbar\Omega)$. According to equations (2) and (3) the scanning curve is then given as $F_2(z) = \sum_n |a_n|^2 F_1(Ez + n\hbar\Omega)$, where $F_1(z)$ is a Gaussian resolution function. A "theoretical" scanning curve is calculated using the values of and the resolution function $F_1(z)$ as obtained in the measurements with a slow grating rotation. It is shown in figure 2 (solid curve) and compared with the results of the measurement (solid dots). It can be seen that the intensities $|a_{\pm 1}|^2$ of the first satellites as well as the energy splitting are all in a good agreement with theory.

As already noted in ref. [2], all tentatives to explain these results by using real forces, which may change the neutron energy have failed. For the interpretation of this purely quantum effect, however, the concept of quasi-energy [6], as well as the uncertainty principle $\Delta E \Delta t \cong \hbar$ itself are much more appropriate. These effects, which have been observed for the first time, can be exploited in other experiments to modify the neutron energy. The idea of neutron time focusing, which was proposed recently in [7], looks now more realistic. ■

References

[1] A.I. Frank, V.G. Nosov, Phys. At. Nucl., 57 (1994) 968 • [2] A.I. Frank, V.G. Nosov, Phys.Lett. A 188 (1994) 120 • [3] A. Steyerl, W. Drexel, S.S. Malik, E. Gutsmiedel, Physica B, 151 (1988) 36 • [4] I.V. Bondarenko, A.I. Frank, S.N. Balashov et al., NIM A 440 (2000) 591 • [5] I.V. Bondarenko, A.I. Frank, S.V. Masalovich et al., ILL Annual Report (1999) 86 • [6] Ya.B. Zel'dovich, Zh.Eksp.Teor.Fiz. 51 (1966) 1492 • [7] A. Frank and R. Gähler, Phys. At. Nucl., 63 (2000) 545.

Single wall carbon nanotubes:
from one to two-dimensional adsorption

- M. Muris and M. Bienfait (CRMC2-CNRS, Marseille)
- P. Zeppenfeld (Linz University)
- N. Dupont-Pavlovsky (LCSM - University H. Poincaré, Vandœuvre-les-Nancy)
- P. Wass and M. Johnson (ILL)
- O.E. Vilches and T. Wilson (University of Washington, Seattle)

The structures formed by CD_4 and D_2 adsorbed on single wall carbon nanotube bundles at low temperatures have been determined by neutron diffraction as a function of gas dosing. Both molecules, at low coverages, form one-dimensional chains in the bundle grooves and in the interstitial channels. With increasing coverage, they cover completely the outer surface of the bundles to form a quasi-hexagonal two-dimensional layer.

Much attention has focused recently on the problem of gas adsorption within bundles of single-walled carbon nanotubes (SWNT). Those nanotubes are made of graphene sheets wrapped around themselves into tubes with a diameter of 1-2 nm and a length of a few μm. The tubes are capped at both ends and are hexagonally packed in bundles with a typical diameter of about 10 nm.

SWNT's have potential application in gas storage and provide a linear arrangement of adsorption sites which may be considered as a physical realisation of one-dimensional matter. Such one-dimensional adsorption sites are located in the interstitial channels between the tubes within a bundle and in the grooves separating two adjacent tubes on the outer surface of a bundle (see box in figure 1). In addition, two-dimensional like sites are located on the graphene outer surface.

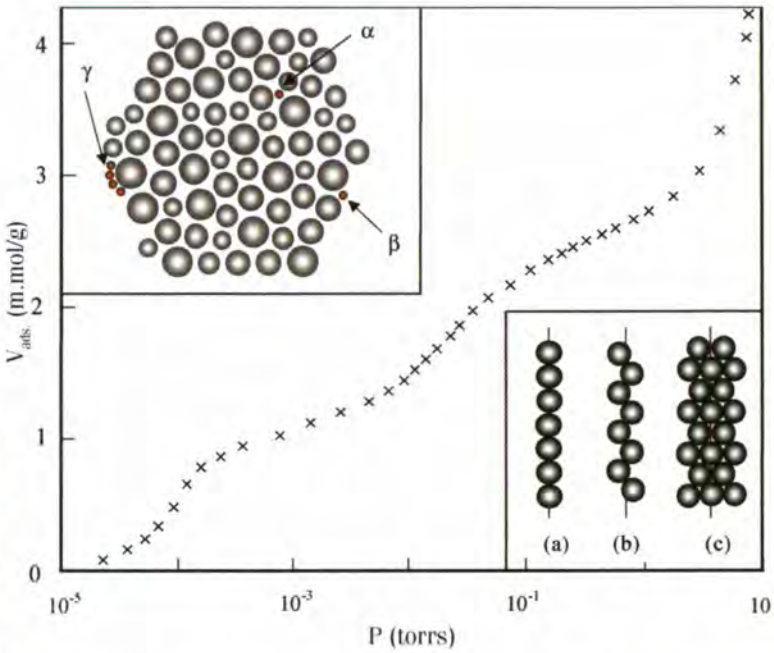

Figure 1: Adsorption isotherm at 77K of CH_4 on 26.6 mg single wall carbon nanotube bundle. The bundle section is schematicaly represented (top left) with the three adsorption sites, interstitial channels (alpha), grooves (beta) and outer part of the surface (gamma). The different structures, along the nanotube strands, deduced from the diffraction spectra(bottom right) are either one-dimensional (linear or zigzag) or two-dimensional hexagonal.

In the work reported here we show the evolution from one to two-dimensions of the adsorption as a function of gas uptake. Our SWNT substrate was provided by C. Journet from Montpellier and the adsorbate molecules methane and hydrogen, were chosen because of the large coherent scattering lengths of their deuterated compounds.

The study combines thermodynamic [1] and neutron diffraction [2] measurements with computer simulations.

The thermodynamic characterisation is performed by volumetric measurements [1]. The so-called adsorption isotherms are obtained by recording at constant temperature the amount of adsorbed molecules as a function of pressure. A typical example is represented in figure 1; it exhibits two risers corresponding to the successive population of two fairly uniform adsorption sites. The variation of the vapour pressure of the two "steps" as a function of temperature yields the corresponding heat of adsorption. The obtained values for the first step (190 meV) and the second step (115 meV) are respectively larger and smaller than the heat of adsorption on the (001) graphite surface (154 meV). The more attractive adsorption sites are assigned to the grooves and to the widest interstitial channels (figure 1) and the less attractive ones to the convex part of the outer surface.

The diffraction experiments [2] were performed on the D1B diffractometer for CD_4/SWNT's and on the D20 and D1B diffractometers for D_2/SWNT's.We observe common features upon CD_4 and D_2 adsorption. There is no big change of the nanotube

background diffraction pattern. This implies that the overall hexagonal arrangement of the nanotubes into bundles is preserved during the adsorption.

The main modification of the spectra upon CD_4 and D_2 adsorption is the appearance of a new broad peak at about 1.7Å^{-1}, represented in figure 2 for two uptakes.

This peak results from two contributions [2]. One is centered at about 1.6 Å^{-1} and corresponds to a lattice parameter of about 4.17 Å, the distance of methane molecules in its solid phase. The shape of the peak can be fitted with a linear chain model as sketched in figure 1 (bottom right). The peak persists up to the highest uptake when the outside surface of the SWNT bundles are covered with a single layer of methane molecules. It is interpreted as arising from linear rows of 4 to 7 molecules adsorbed in the grooves and into the widest SWNT interstitials channels [2]

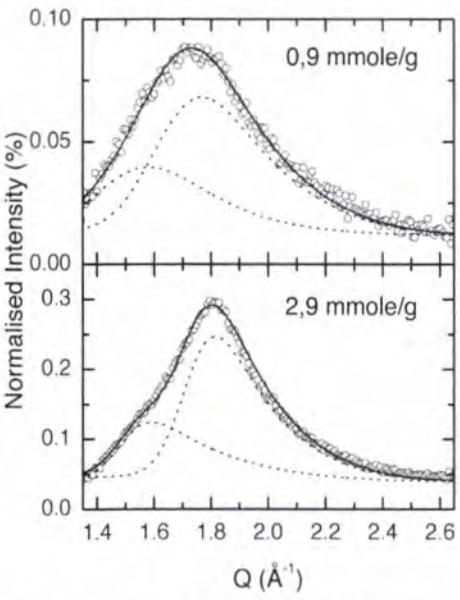

Figure 2: Difference spectra (after subtraction of the bare nanotube spectrum) of CD_4 adsorbed on 660 mg of single wall carbon nanotubes at 77 K for two doses. Best fits (solid lines) to CD_4 diffraction profiles assuming two contributions (dotted lines), one from linear chains, (see figure 1a), and the other one from zigzag chains or hexagonal stripes shown in figure 1b and c.

The second peak , whose width decreases as a function of CD_4 concentration , is centered at about 1.8 Å^{-1} ; itcorresponds to a periodicity a_0 of 3.75 -to 3.6 Å and can be assigned to a zig-zag packing located in the irregular shaped voids (figure 1) at small uptakes and to a quasi hexagonal packing on the outer part of the surface at larger methane concentration.

The results obtained for D_2 adsorption are qualitatively similar except for the observation of a large compressibility of this quantum molecule as a function of uptake. Force field-based simulations [3] offer clear insight into the adsorption of methane. While real bundles of SWNT's contain several tens of tubes, a computationally-tractable model of three tubes, periodic along the tube axis, has been used, the triangular bundle having the three adsorption sites of interest. Binding sites are probed using a Monte Carlo search routine at fixed temperature and variable pressure. At the lowest pressures in the simulation (10^{-3} Torr), the groove sites are always occupied, and as pressure increases from 10^{-2} to 10^{-1} Torr (as in the measurement), a step in the calculated isotherm is observed, corresponding to populating the curved graphene surface. The interstitial channel is never occupied in this type of simulation.

Binding energies for single methane molecules in the three sites are calculated from the loaded structures: –243±10 meV for the grooves, –121±10 meV for the curved graphitic surface and +104±10 meV for the interstitial channel. For comparison, the corresponding calculated value for planar graphite is –143±10 meV.

While the simulations on triangular bundles are consistent with the diffraction data, they are in conflict with the measured isotherms. The heights of the two plateaux give the relative numbers of two binding sites, approximately 1:1. Scaling-up from triangular to realistic hexagonal bundles gives a limiting ratio for groove:curved-graphite sites as 1:4. However, in hexagonal bundles, the problem of packing different diameter tubes results in voids of different shapes and sizes, many of which will be populated at the lowest pressures. The binding energy of methane in the interstitial channel is extremely sensitive to the shape and size of this void, a small increase in size allowing a site to evolve from being the least to the most stable.

Finally we come to the following adsorption scenario. Initially the adsorption of CD_4 or D_2 takes place as linear chains in the grooves and in the wide enough interstitial channels and by filling the irregular shaped voids with zig-zag chains. The initial binding of these quasi one-dimensional solids is stronger than for graphite. Subsequently, additional chains are adsorbed to form stripes of hexagonally ordered molecules along the grooves of the outer surface of the bundles until this surface (a single wall of graphite-like carbon atoms providing less binding than graphite) is completely covered by a single two-dimensional layer of CD_4 or D_2. Hence, neutron scattering is able to show a progressive transition from 1D to 2D adsorption on the carbon nanotubes as a function of the adsorbate concentration. ■

References

[1] M. Muris, N. Dufau, M. Bienfait, N. Dupont-Pavlovsky,Y. Grillet and J.P. Palmari, Langmuir 2000, 16, 7019-7022. M. Muris, N. Dupont-Pavlovsky, M. Bienfait and P. Zeppenfeld, Surf. Sci. 2001, 492, 67-74. T. Wilson, A. Tyburski, M.R. DePies, O.E. Vilches, D. Becquet, M. Bienfait, J. Low. Temp. Phys., in press • [2] M. Muris, M. Bienfait, P. Zeppenfeld, N. Dupont-Pavlovsky, M. Johnson, O.E. Vilches and T. Wilson, Applied Phys. A, in press (Spring 2002) • [3] see www.msi.com.

Order-disorder transition in acetylacetone
driven by coupled quantum dynamics

● A. Geis and H.P. Trommsdorff (Joseph Fourier University, Grenoble)

● N. Jones and A.J. Horsewill (University of Nottingham)

● M.R. Johnson (ILL)

In acetylacetone, the proton transfer between the two oxygen atoms is accompanied by a 60° rotation of two methyl groups. These three wide-amplitude motions are therefore coupled but can still take place at low temperatures by tunnelling and they determine the phase behaviour of crystals. Intermolecular coupling leads to an ordering of the proton positions and methyl group orientations below 100 K, and lowers the crystal symmetry. This ordering is not only deuteration dependent, but also very sensitive to the presence of impurities in the crystal. A combination of structural, spectroscopic, and numerical studies leads to a consistent picture of the observed quantum dynamics and order-disorder transition in this system.

At room temperature acetylacetone is a liquid and exists as a 25/75 % equilibrium mixture of keto and enol forms (figure 1). In powder samples, prepared by rapid cooling of the liquid, keto and enol forms coexist, as shown in calorimetric measurements, where two melting peaks are observed. Similarly neutron powder diffractograms show two sets of reflections, one of which disappears after annealing the sample under reduced pressure at a temperature that lies between the melting

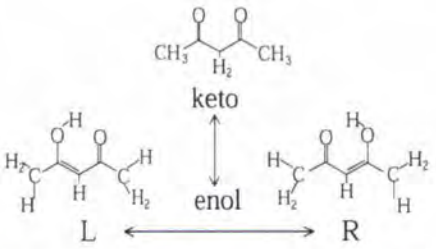

Figure 1: The molecular structures of the keto and enol forms of acetylacetone. The two tautomers of the cyclic enol form interconvert by proton transfer in the hydrogen bond. The non-equivalent methyl groups of the enol form have equilibrium positions shifted by 60° and experience different potential barriers.

points of the enol and keto forms. Structural information is also obtained from inelastic neutron spectra, recorded on IN10, of a non-annealed and an annealed powder sample at 5 K (figure 2). In this spectral region, tunnelling transitions of the methyl groups are observed. In addition to the disappearance of the peak at 4 μeV in the annealed sample, the transition around 40 μeV narrows and shifts to lower frequency. The peak at 4 meV, thus assigned to the keto phase, has an instrument limited width, while the enol peak is considerably broadened, indicating disorder. Its width, even after annealing, exceeds the instrument resolution. The second methyl group of the enol molecule has a tunnel splitting that is just too small to be resolved, but the dynamics of this rotor are clearly observed in quasielastic measurements.

Raman spectra recorded in the phonon region up to 120 cm^{-1} show similar linewidth effects, the lines of non-annealed powder samples being considerably broadened at 7 K. In order to follow the crystal ordering and to identify a phase transition, Raman spectra of pure single crystals of the enol form were recorded at temperatures between 7 K and 140 K (figure 3). On cooling, a spectacular narrowing of the lines between 50 to 70 cm^{-1} is observed, indicative of ordering in the crystal. In addition, the lines shift to higher frequency at ~90 K and resolve in to two lines upon further cooling. An analogous evolution was observed in the temperature dependence of the crystal unit cell parameters, as determined from D2B and D1A diffraction data (figure 4).

The crystal structure of the enol form of acetylacetone was first reported in 1998 from a single crystal X-ray study at 110 K and 220 K [1]. At these temperatures, a mirror plane relates the two halves of a symmetric molecule, which is the average of the enol L and R tautomers, occupying the crystal sites at random. Our data on dynamics in acetyl acetone and solid state first principles calculations (see below) show that this high temperature symmetry is not due to quantum delocalisation of the protons in individual molecules. The average symmetry, due to disorder, cannot sur-

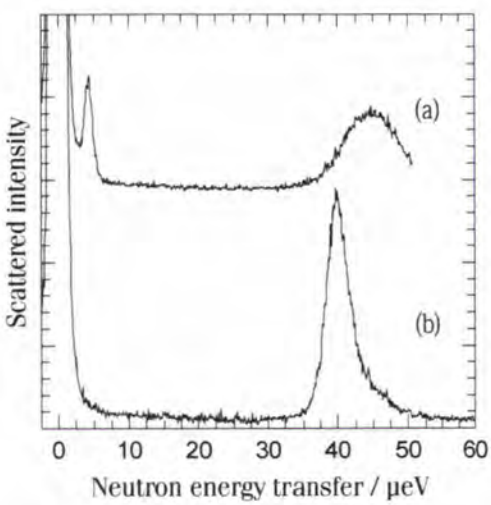

Figure 2: The inelastic neutron scattering spectra recorded of acetylacetone at 5 K on IN10 in the range 0 – 60 μeV; a) non-annealed sample, b) annealed sample. The center of the inelastic peaks corresponds to the methyl tunnelling splittings.

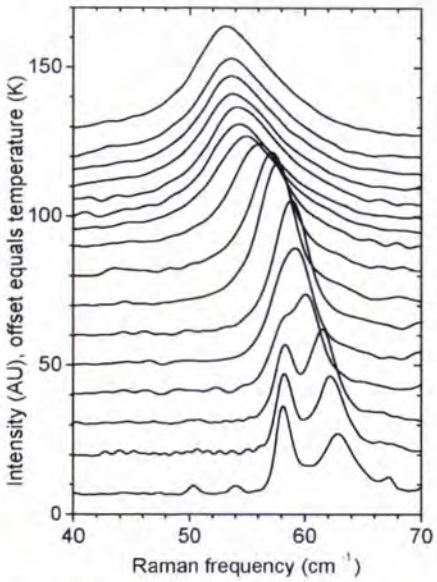

Figure 3: Raman spectra of fully deuterated acetylacetone as a function of temperature in the region of lattice modes. The vertical offset of the spectra is proportional to the temperature.

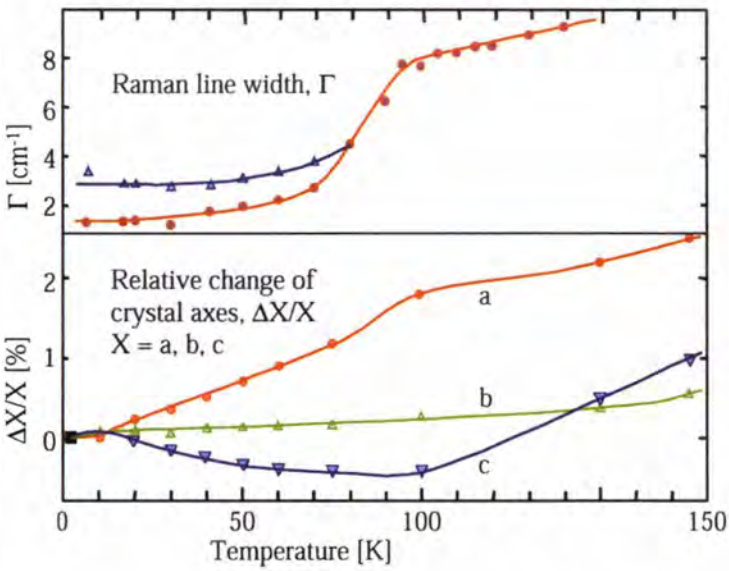

Figure 4: Evolution of the Raman line widths (top) and of the unit cell parameters (bottom) of fully deuterated acetylacetone as a function of temperature.

vive at lower temperatures when the energy difference between different tautomer distributions in the crystal exceeds the thermal energy. Coupled proton tunnelling dynamics allow relaxation from meta-stable tautomer states to the ground state. On cooling, ordered domains of enol molecules grow, but this process is limited by the growth of other, differently ordered domains or by the presence of defects, like embedded keto molecules. Tunnelling transitions are a sensitive local probe of potentials, while phonons, observed in Raman transitions, probe a longer length scale, to a degree that is given by the ratio of the intermolecular coupling to the energy of disorder. The observed linewidths suggest that ordering is limited to not more than a few tens of unit cells. In view of this situation it is not surprising that the analysis of the low temperature diffraction data from D1A has presented some difficulty. The best refinement of the low temperature phase was obtained in the $Pn2_1a$ space group, a polar subgroup of the high temperature space group Pnma, in which the mirror plane of the molecule is eliminated. Solid state quantum chemistry calculations, based on density functional theory (DFT - CASTEP and VASP codes), give quantitative insight into the structure and dynamics in acetyl acetone. Initially stable proton positions, prior to Rietveld refinement, were determined by optimising the crystal structures with different orientations of the methyl groups and positions of the hydrogen bond proton. The structures shown in figure1 are ~30 meV more stable than any structure with eclipsed methyl groups. Rotational potentials and the energies of different conformers are calculated in a supercell, composed of two unit cells, for a molecule which is surrounded by ground state, molecules. The rotational barriers are ~20 meV and ~60 meV for the methyl rotors bonded to the C=O and C-OH group, respectively, consistent with the experimental values of the tunnel excitations [2,3]. Transferring the hydrogen-bond proton in one molecule increases the supercell energy by ~ 42 meV, and rotating both methyl groups in addition causes an energy increase of ~70 meV. These last two values characterise the energies needed to create an isolated disordered molecule in an ordered lattice. Since these energies are in excess of the temperatures at which disorder prevails (90 K ≈ 8 meV), aggregates of disordered molecules must exist in the high temperature phase.

Measurements and calculations of structure and dynamics in acetyl acetone have enabled an order-disorder transition in the enol phase to be characterised. On cooling, coupled proton tunnelling dynamics allow metastable tautomers to relax into a ground state composed of ordered domains. Remaining questions concern the possibility of a further lowering of crystal symmetry below 60 K, as suggested by the line splitting observed in the Raman spectra, and the collective nature of excitations in the onset of disorder. These questions will be tackled, respectively, with single crystal diffraction measurements and molecular dynamics simulations using a calibrated force field. ■

References

[1] R. Boese, M.Y. Antipin, D. Bläser, K.A. Konstantin, J. Phys. Chem. B 102 (1998) 8654 • [2] S. Clough, A. Heidemann, A.J. Horsewill, J.D. Lewis, M.N.J. Paley, J. Phys. C: Solid State Phys. 15 (1982) 2495; A.J. Horsewill, A.M. Alsanoosi, C.J. Carlisle, J. Phys. C : Solid State Phys. 20 (1987) L869; M.R. Johnson, A. Aibout, A.J. Horsewill, J. Williams, J. Phys.: Condens. Matter 5 (1993) 7375 • [3] M.R. Johnson, N.H. Jones, A. Geis, A.J. Horsewill and H.P. Trommsdorff, J. Chem. Phys (in press) and unpublished results.

Rotational tunnelling in phase III:
a step forward in understanding methane

● M. Prager (Institut für Festkörperforschung, FZ Jülich)

● W. Press and B. Asmussen (University of Kiel)

● J. Combet (ILL and CNRS/ICS, Strasbourg)

Rotational tunnelling of tetrahedral molecules is a sensitive probe of site symmetries and site multiplicities. However, the complexity of overlapping tunnelling patterns can render a model free description of data impossible. Only on the basis of the recently determined low temperature crystal structure of phase III of methane the high resolution tunnelling spectrum of 1.5% CH_4 in CD_4 could be quantitatively explained. The analysis is based on tunnelling matrix elements and includes line positions and intensities. Barrier heights and disorder obtained with high accuracies will allow to refine pair interaction potentials. Level specific spin conversion times show up in the intensities of tunnelling transitions.

Methane is the simplest organic molecule. Nevertheless, it is of fundamental importance to understand interactions between methane molecules for the comprehension of organic materials. Like many supposedly simple molecular materials, methane has a rich phase diagram with at least seven known phases. However, the crystal structures of the two cubic phases I and II only have been fully solved [1]: phase I is an orientationally disordered plastic phase while in phase II 75% of the molecules become orientationally ordered. The structure of phase II was predicted on the basis of octupole-octupole interaction of methane tetrahedra [2] where the octupole moment was calculated from pair interaction potentials [3]. Very recently, the structure of phase III – known to exist since 1937 – has been determined using high resolution neutron powder diffractometry. In disagreement with predictions [4] it is not a subgroup of phase II but the cell is very slightly orthorhombic with all molecules ordered on two types of sublattices of m and 2 site symmetries, respectively, and equal occurrence probabilities [5].

The solution of the crystal structure of phase III [5] has provided a solid basis for the analysis of tunnelling spectra. It is based on the model of single particle rotation with the overlap matrix elements as the appropriate parameters [6]. In the general case the ground state multiplet is a quintet (A, T_1, T_2, T_3, E) with nine allowed tunnelling transitions. With increasing site symmetry T_i-levels become degenerate and the number of transitions is finally reduced to 2 for tetrahedral environment. In the present case, the results for 2-and m-local symmetries are needed.

Tunnelling spectra were measured on IN10. A wide range of energy transfers $-7\ \mu eV \leq E \leq 180\ \mu eV$ at ~1 μeV energy resolution is obtained using the *KCl*[200] and *NaCl*[111] variable temperature monochro-

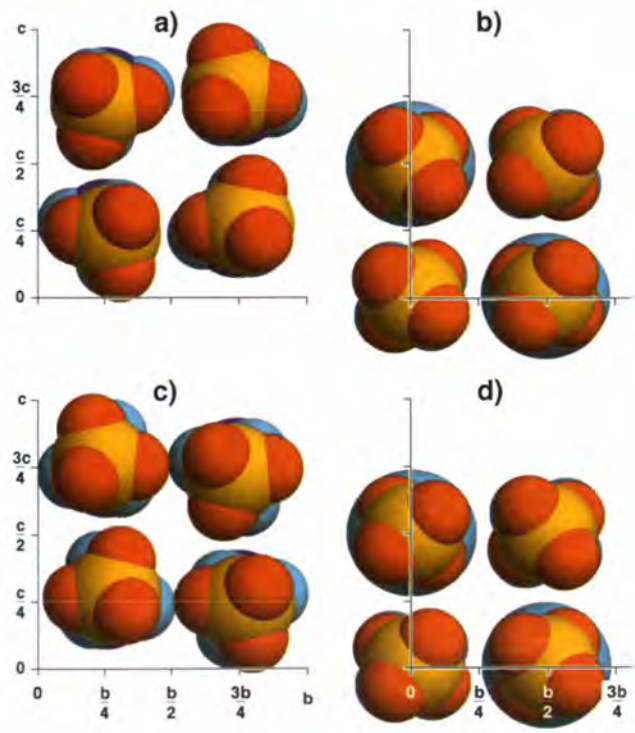

Figure 1: Arrangement of the methane molecules in the b-c-plane of the *Cmca* space group of phase III. a) and c) show cuts through the planes at $x = 0, \frac{1}{2}$ with m molecules, b) and d) represent planes $x = \frac{1}{4}, \frac{1}{2}$ with 2-site molecules. The underlying blue colour represents orientations in phase II (measurements at HRPD, ISIS).

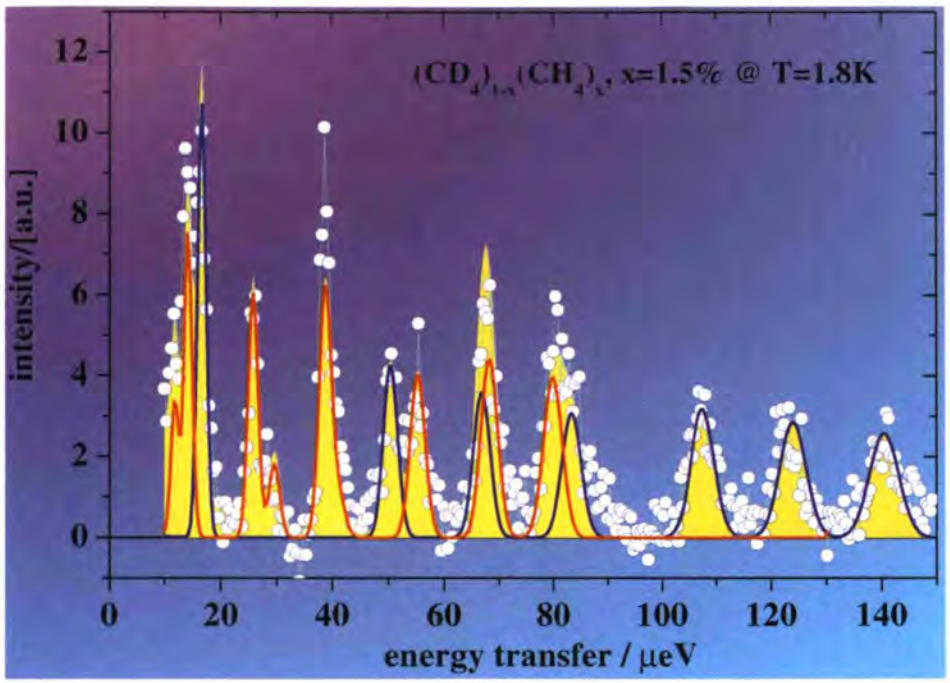

Figure 2: Neutron spectrum of 1.5% CH_4 in CD_4. Energy resolution about 1 μeV. Sample temperature T = 1.8 K .Experiment: open circles; red line: CH_4 on m-sites; blue line: CH_4 on 2-sites; yellow area: sum of both.

mators. The lattice spacings of both monochromators allow only downscattering processes to be observed. The pen symbols in figure 2 show a composed spectrum representing 100h of counting time. A constant background is subtracted. The high energy resolution reveals many new details especially at low energy transfers. The signal to noise ratio is limited by the low concentration of guest molecules, the high resolution and the large number of transitions distributed over the energy range of ±150 μeV.

The spectrum is further modified by inhomogeneous line broadening. Despite the concentration of guest molecules was reduced to 1.5% disorder and the corresponding distribution of rotational barriers is still significant. Inhomogeneous line broadening is proportional to the energy transfer, $\Gamma(T)=\Gamma_{res}(1+\frac{0.018}{\mu eV}\hbar\omega)$, and thus reduces the quality of a spectrum especially at large energy transfers.

The three equidistant lines of equal intensities at energy transfers > 100 μeV are identified as the $T_i \rightarrow$ A transitions of the site with 2-fold symmetry axis. This assignment and a small 180° matrix element H determine all other transitions of this site. Final parameters are $h_1 = h_3 = -19.99$ μeV, $h_2 = h_4 = -11.82$ μeV, $H = 0.80$ μeV with levels $0(A^{(2)})$, $107(T_1^{(2)})$, $124(T_2^{(2)})$, $140(T_3^{(2)})$, $190(E^{(2)})$ μeV.

The remaining inelastic intensity is explained by transitions of methane molecules at m-sites. Starting with attributing the largest unexplained inelastic intensity to the T_3 to A transition, a number of combinations of lines was explored under the usual restrictions. Final parameters are $h_1 = -2.09$ μeV, $h_2 = -16.55$ μeV, $h_3 = h_4 = -6.33$ μeV, H = 0.056 μeV with levels $0(A^{(m)})$, $39(T^{(m)})$, $68(T_2^{(m)})$, $79(T_3^{(m)})$, $91(E^{(m)})$ μeV.

Intensities are calculated for equal population of the tunnel sublevels. The very good fit (yellow area figure 2) supports the new crystal structure [5]. The potential of molecules at 2-sites is ~16.6 meV and significantly weaker than that of m-sites with 21.5 meV. This could be a residue of partial orientational disorder on this sublattice in phase II. Both potentials are stronger than that at the ordered sites in phase II. The rotational potentials show a distribution of less than 1%, δV=0.12(0.13) meV, due to chemical and excitational disorder.

The description with matrix elements is a first phenomenological step only. Next, the overlap matrix elements have to be related via the wave functions with the rotational potential $A(\omega_E)$, ω_E being the Eulerian angles. $A(\omega_E)$ must follow from the crystal structure and the intermolecular atom-atom potentials. Eventually, such a refinement may lead to improved pair potential parameters beyond those of Bartell [3] which were successful for phases I and II.

A transition within the tunnelling multiplet requires a nuclear spin flip. This prevents immediate equilibration with the phonon bath. Spin conversion times τ are of the order of days and usually different for different levels. This leads to differences in population. The fit shows a mismatch of intensity around 39 and 67 μeV of m-site methane. We are led to conclude that the involved T_1 level converts faster, the T_2 level more slowly than the average.

After long stagnation the solution of the structure of phase III of CD 4 gives a new impact towards understanding dynamics and interactions of the simplest organic material. The field is again open for interesting new research. ■

References

[1] W. Press, J.Chem.Phys.56 (1972) 2597 • [2] H.M. James, T.A. Keenan, J.Chem.Phys.31 (1959) 12 • [3] L.S. Bartell, J.Chem.Phys.32 (1960) 827 • [4] K. Maki, Y. Kataoka, T. Yamamoto, J.Chem.Phys.70 655(1979) • [5] M. Neumann, W. Press, C. Noeldeke, B. Asmussen, M. Prager, R.M. Ibberson, submitted • [6] W. Press, Single Particle Rotations in Molecular Crystals Springer Tracts in Modern Physics, Vol.81, Springer, Berlin 1981.

Long-range electron transfer
in periodic nucleotide base stacks

D.J. Bicout and E. Kats (ILL)

A simple model for charge transfer in one-dimensional donor (D) - bridges (B_n) -acceptor (A) systems is proposed. The model describes the charge transfer as the conjonction of two non-dichotomic competiting mechanisms: coherent direct D - A tunneling and incoherent hopping. An analytical expression of the charge transfer rate k_{ET} is derived for this model, and seemingly contradictory observations of a strong followed by a weak influence of D - A distance on k_{ET} are readily reproduced.

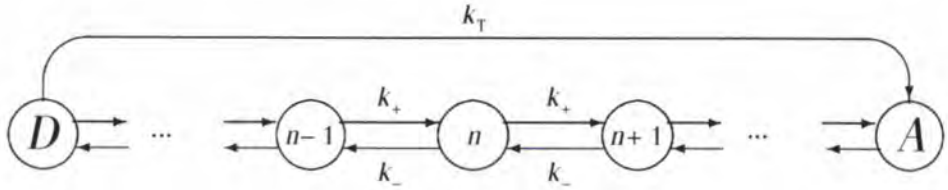

Figure 1: Schematisation of electron transfer routes in a model of DNA. The donor and acceptor correspond to $n = 0$ and $n = N$, respectively. k_T denotes the tunnelling rate and k_+ and k_- the forward and backward hopping rates, respectively.

Molecular electron transfer (ET) is one of the most relevant processes observed in chemistry. Moreover, considerable experimental work has been reported on a number of systems in which the charge transport is effectively confined to one dimension. The particular example of long-range electron transfer in nucleotide base stacks has been a recurrent hot topic during the past decade [1-3]. However, mechanisms leading to such charge transfer processes are not fully understood and thus have been heavily debated. In particular, many relevant factors (e.g., molecular environment, counterions, thermal vibrations, and so on) can influence the electron transport in materials such as DNA, which are very hardly to control in real experiments. In such a case it seems reasonable and worthwhile to put forward a simple, but yet non-trivial, model which can provide experimentally testable consequences under relatively weak assumptions. In this spirit, this attempt is inspired by the experimental work by Giese *et al.* [3] where the charge transfer rate between guanine base pairs of DNA separated by adenine - thymine bridges of various lengths has been measured. These authors have found that the rate of charge transfer decreases exponentially only for small distances (i.e., up to about three base pairs, i.e. $3a \approx 10.5$ Å), while the decay is considerably weak when the bridge length increases showing hence a transition from coherent tunnelling for $N \leq 3$ to thermally induced hopping for $N > 3$, where N counts the number of base pairs in the bridge. For comparison, the standard Marcus-Levich-Jortner [4] theory predicts an exponential decay of the electron transfer rate, k_{ET} with the donor-acceptor distance Na as, $k_{ET} \propto \kappa_0 e^{-\beta Na}$, where a denotes the base pairs interspacing, κ_0 si prefactor (see [4]), and the falloff factor β may range from 0.5 Å^{-1} to 1.2 Å^{-1}. One finds that some works (see e.g. [5]) can be described by the Marcus theory, but many others [6] are not and indicate very weak decay of, k_{ET} for large donor-acceptor distance.

This paper aims at demonstrating that although simple, the proposed model already reproduces a number of features found in long-range electron transfer in DNA, i.e. an exponential decay of the electron transfer rate k_{ET} with the donor-acceptor separation at small distance, and the slow algebraic decay of k_{ET} for large donor-acceptor separations.

Below the rate of the charge transfer process between donor and acceptor species is calculated for separate sites of a large molecule (e.g., DNA with specially designed base sequences [3]). The electron transfer from a donor to an acceptor is illustrated below in figure 1. The donor D is attached to the site $n = 0$, the bridges B_n consist of $N - 1$ identical segments (denoted $n = 1, 2, \ldots, N - 1$), and the acceptor A is attached to the site $n = N$. The electron transfer may proceed by two non - dichotomic processes: either by direct unistep superexchange tunnelling from the donor to the acceptor with the rate k_T or following the multisteps hopping process with forward and backward rates k_+ and k_-, respectively. Although phenomenological, the three relevant quantities k_T and $k_\pm$ are related to microscopic energetic of the processes.

The calculated rate $k_{ET}(N)$ for different values of the parameters (κ_0, $k_\pm$) is represented in the figure 2. The rate k_{ET} as a function of N is shown to exhibit a transition from tunnelling to hopping regimes. The rate k_{ET}

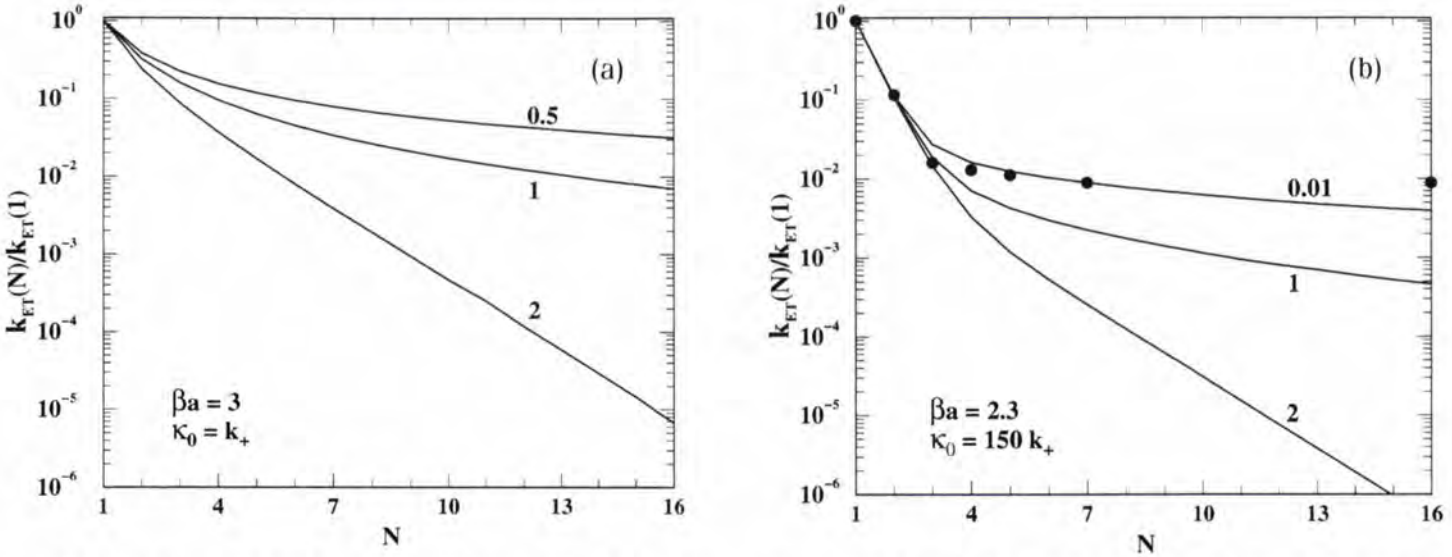

Figure 2: Reduced rate, $k_{ET}(N)/k_{ET}(1)$, as a function of the reduced length N. Quoted numbers correspond to the ratio k_-/k_+. (a): $k_{ET}(1)=1.05\ \kappa_0$. (b): $k_{ET}(1)=0.107\ \kappa_0$. Filled circle are data from [3].

decreases exponentially with N for short N while the decay is weaken and becomes non-exponential as N gets larger. It clearly appears that the ratio κ_0/k_+ measures the relative magnitude of the contribution of tunnelling versus hopping to the ET rate whereas k_-/k_+ is the control parameter for different of the ET rate with N in the hopping limit.

As an illustration, the experimental data from Giese *et al.* [3] are reported on panel B of figure 2. The agreement between experiment and the theory is rather spectacular. The model suggests that the magnitude of tunnelling is about hundred times lager than the hopping in these experiments [3]. The exponential decay at short N ($N \leq 3$) corresponding to the tunnelling regime with $\beta \approx 6.5$ Å^{-1} is common to the three curves. In the hopping regime at large N, the data are well described by the curve quoted $k_+ = 100\ k_-$, i.e. almost ballistic hopping. ■

References

[1] P.J. Dandliker, R.E. Holmin, J.K. Barton, Science, 275 (1997) 1465 • [2] H.W. Fink and C. Schonenberg, Nature, 398 (1999) 407 • [3] B. Giese, J. Amaudrut, A-K. Kohler, M. Spormann, S. Wessely, Nature, 412 (2001) 318 • [4] R.A. Marcus, Annu. Rev. Phys. Chem., 15 (1964) 155 [5] F.D. Lewis, T. Wu, Y. Zhang, R.L. Letsinger, S.R. Greenfield, M.R. Wasielevski, Science, 277 (1997) 673 • [6] D.B. Hall, R.E. Holmin, J.K. Barton, Nature, 382 (1996) 731.

Instrument personalities

◀ Benoit Malard and the detector bank of the high resolution powder diffractometer D2B.

Gwenaelle Rousse and the D20 pyrolitic graphite monochromator reflecting a sample holder. Normally neutrons reflect from the monochromator on to the sample. ▼

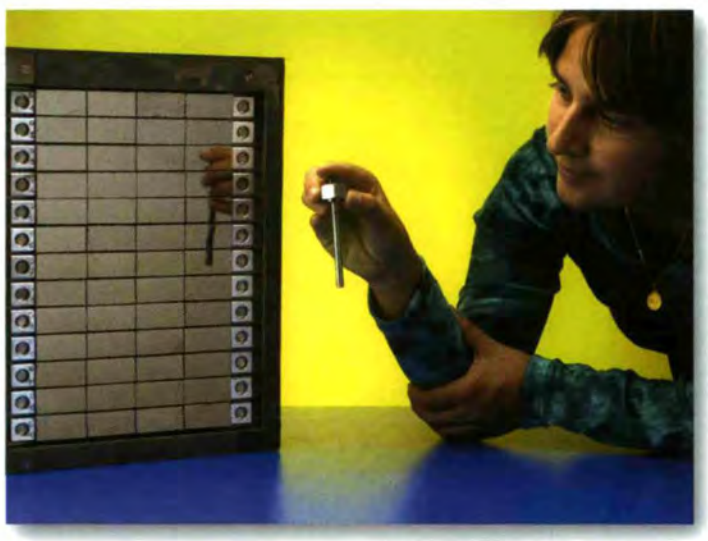

▲ Christopher Ling positioning a sample on the Eulerian Cradle of the hot neutron four-circle diffractometer D9.

Roland Gandelli during the assembly of the new collimation mechanism for ▶ D11.

millennium programme and technical developments

Launched on 1st January 2000, the first day of a new century and a new millennium to all except a few purists, the ILL's Millennium Programme is now a central theme in ILL's daily life. The aim of the Millennium Programme was to set in place an accelerated and continuous programme of instrument and infrastructure renewal which would increase the data rate of each and every instrument by a factor of between ten and twenty and perceptibly improve the service to users. The ILL's reactor was rebuilt in the early 90's resuming full operations in 1995. This operation totally absorbed the Institut's budget with the result that the modest investment in instrumentation possible in the late 90's and currently now reaching fruition ended a period of famine for instrument upgrade at ILL which lasted a full decade. The Millennium Programme will reverse that decline. Five instruments were rebuilt in the late nineties from within the Institut's own budget and a sixth instrument was rebuilt using external funding from Spain and in addition the H113 ballistic guide was installed, funded from Germany. The Millennium Programme currently contains a further nine instrument projects with the rebuild of two neutron guides underway and the renewal of the ageing vacuum pump park (54 oil diffusion pumps !) now 25% achieved. This intense activity has required a refocussing of working practices and project management to which the ILL staff has responded admirably, but it is becoming clear that there is a need to redeploy staff in key areas. This process is taking place in an organic manner.

Details of progress on individual projects are given on the following pages.

Overview of the ILL's Millennium Programme

C.J. CARLILE (ILL)

The D4 liquid and amorphous diffractometer with its microstrip detectors is now in routine operation with a significant improvement in detector stability, and a five times increase in solid angle. Users (and instrument scientists) eagerly await the installation of the new hot source in April 2002.

The Mark-II microstrip detector on D20 has operated for 18 months with no signs of any degradation in performance. Improvements to the design and manufacture appear to have paid off and talk from the diffraction group is of a Mark-III detector. The dead time between stop-start of runs is only 80 ms which makes this high intensity diffractometer ideal for kinetic experiments. The ability to increase the take-off angle for the monochromator to 120° presently being implemented will significantly enhance the resolution.

The D17 reflectometer has been fully functional now for over a year. There were some tricky problems in the early days of the commissioning phase with the electronics of the 2-D detector which have been overcome and the instrument now boasts the highest intensity in its class.

Thomas Hansen and the Mark-III detector of D20.

The primary spectrometer of **the IN5 time-of-flight instrument** has been completely rebuilt with a new focussing supermirror guide. The multiple chopper system with magnetic bearings from Jülich is now nearing completion. First neutrons are expected during summer 2002.

At that stage the design of a new secondary spectrometer using a new type of 2-D He^3 gas detector will start.

The high-intensity **triple-axis spectrometer IN8**, built in collaboration with Spanish researchers, took its first neutrons in November 2001. Intensities on the sample position, reflected off the three-faced doubly focussing monochromator, are sufficiently high that Bragg reflections from the sample position pose a potential radiological hazard. Hot spots are now being shielded against.

The refitting of **the IN4 spectrometer** with horizontal axis choppers is now complete and the commissioning of the small-angle detector is underway. Time-of-flight data on single crystal samples look very promising as they do on IN6.

The installation of the 2-D 26 cm square wire detector on **the D16 long wavelength detector** took place in February 2002 and it is performing beautifully. Overall the data rate on the instrument has risen by fifteen times.

The polarisation analysis triple-axis spectrometer IN20 has benefitted from a total rebuild of the primary spectrometer with a "virtual source" and a large area doubly focussing Heusler monochromator, built in-house, which results in a 10 times increase in flux on the sample position but, as importantly, a doubling of the accessible energy transfer range.

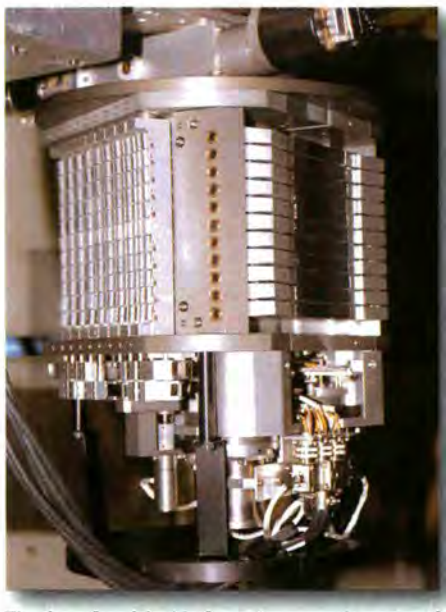

The three-faced double-focussing monochromator of the thermal three-axis spectrometer IN8C. One face consists of eleven horizontally bent sandwiches composed of perfect Si111 crystals. The two other faces (one is hidden) consist of 9 x 11 elements equipped with PG002 and Cu200 crystals, respectively.

The D3 spherical polarimeter is moving steadily towards completion. Various components are now in place – including the polarisation sensitive detector and a total rewrite of software with sophisticated optimisation processes for this complex instrument. Cryopad Mark III, a 4-circle single-crystal device inside a zero magnetic field cavity inside a cryostat, is in manufacture due for delivery in 2002.

The thermal beam **single-crystal image plate diffractometer Vivaldi** is now fully operational – the first totally new instrument of the Millennium Programme – and it is producing high quality data in short collection times – recent data from vitamin B12 look particularly impressive.

The Strain Imager – another totally new instrument, built in collaboration with the University of Manchester – is well underway. Site excavation is complete and the sophisticated sample support table – marble floor, granite table and hexapod orientation device – is now the subject of a design study in collaboration with a Grenoble robotics research laboratory. It will support samples up to one tonne in weight with 50 µm accuracy.

The D16 two-dimensional wire detector.

The high speed 2-D SANS detector for **the D22 small-angle camera** has progressed faster than expected. 7.5 mm diameter linear position sensitive detectors, 1 m long with a spatial resolution of 5 mm have been developed. 128 of these will be assembled into a single detector and installed during 2002. Together with fast read-out electronics newly developed, the specified count rate of 2 MHz at less than 10% dead-time losses will be far exceeded. This development will now be applied to D2 and D11 as well as the three time-of-flight instruments IN4, IN5 and IN6 which will benefit from a further development to encase all linear detectors in an integrated double-manifold. This design has been patented.

The high resolution powder diffractometer D2B (the only instrument to retain its trailing letter!) will benefit from a total rebuild of its secondary spectrometer followed by a new monochromator. The 128 linear position sensitive detectors have been received and the same number of fine Soller collimators are mid-way through the manufacturing process.

The Lohengrin fission fragment spectrometer has been furnished with 2 Eurogams germanium detectors on loan with coincidence electronics and anticoincidence scintillator shields for prototype studies of short-lived isotopes close to the neutron dripline. The sensitivity of the instrument will improve very significantly as early results have shown. The beam stop area of Lohengrin has been totally rebuilt to provide an intense beam for kinetic radiography and tomography.

The rebuild of **the polarisation analysis time-of-flight spectrometer D7** has begun with the installation of a new incident beam polariser providing a 2.5 times increase in flux on the sample. The prototype spin analyser which has negligible extraneous material in the beam path is undergoing tests prior to the mammoth task of sputtering the many square metres of supermirror for the new analyser banks.

The BRISP Brillouin scattering spectrometer located on one of the thermal inclined beams has become a significant presence in the reactor hall. After rigorous earthquake simulations of the platform and the instrument itself, the build phase is progressing apace. First tests are planned for early 2003.

The quarter century old collimation system and neutron guide for **the small-angle scattering instrument D11** has now been replaced between the rebuilt velocity selector position and the instrument. The upstream section will be installed in summer of 2002. We plan to replace the detector following on from the D22 detector renewal programme.

The fibre and single crystal diffractometer D19, being rebuilt in collaboration with a UK consortium of universities, will benefit from a much larger area detector which will deliver a 20 times improvement in data rate. Prototype area detectors, both traditional wire and microstrip versions, have been tested and show impressive results. Manufacture of the large detector itself will start soon ready to take data before the end of 2003.

So there's a lot going on and we haven't touched upon the deuteration laboratory, part of the proposed Partnership for Structural Biology with ESRF and EMBL, or the facility for Materials Engineering FaME built in collaboration with the University of Salford and ESRF.

We look forward to the new neutron sources around the world being operational, but the older ones are not standing still.

Partial array of the Lohengrin MINIBALL detectors (courtesy of the University of Cologne).

A strain imager at the ILL

S. Rowe and T. Pirling (ILL)

W. Hutt, G. Bruno
(University of Manchester, ILL)

As part of the Millennium Programme the ILL, in collaboration with the University of Manchester, is constructing a neutron Strain Imager, partly funded by an EPSRC grant. Its design and construction is expected to be completed in 2003. After a one-year commissioning period during 2004 it will become a full ILL instrument.

The Strain Imager Team. From left to right: Steven Rowe (draughtsman), William Hutt and Philippe Decarpentrie (instrument technicians), Thilo Pirling (project leader, ILL), Giovanni Bruno (project leader, Manchester).

A short description of the new instrument

The instrument and the principle of strain determination has been described already in the ILL Annual Report 2000 [1,2]. Therefore we give only a short summary of its operation here. A neutron strain imager determines the stress distribution in a component with a lateral resolution of typically 1 mm^3. This is done by measuring the variation of the lattice spacing of the crystallites inside the material. This method applies to measurements in welds, composite and hardened materials and many more applications in engineering and materials science, as well as industrial testing. The advantage of the neutron strain imaging method is that it is applicable to real engineering components. Therefore the range of sample dimensions and weight is quite large: from millimetres to metres in length and from grams to several hundred kilograms in weight. The challenges for the construction of the instrument are a high neutron flux to enable penetration of large samples, and at the same time high resolution to determine stresses precisely.

Our solutions to achieve this goal are the development of a double focussing monochromator using bent Silicon crystals. A new super mirror guide (m = 2) will provide at least 3 times more flux than today. A special feature is the sample table which is a Stewart Platform (known from flight simulators). It allows us to tilt, rotate and translate samples to within 50 µm accuracy. This gives a unique flexibility in sample positioning and the capability to set up nearly every type of specimen. The load capacity will be more than 500 kg. The Stewart platform will slide on a large base plate in order to extend its range of action, so that samples up to 2 metres in length can be measured. Collimating optics will allow high lateral resolution and a variable take-off provides a wavelength range from 0.13 to 0.45 nm. The development of the instrument will be in close contact with the FaME project for the coordination and preparation of stress experiments. This will result in standardised sample holders and sample environment, and standard file format for data interchange.

Progress during 2001

The winter shutdown 2000/2001 saw the excavation of the Strain Imager zone, where an estimated 55 tons of material were removed. The area was then consolidated with concrete including the foundation block required for the 1 000 kg crane.

The area around the guide housing and the casemate has temporarily been rebuilt to the pre-excavation height, in order to allow the old guide, guide protection and casemate to be replaced. This is a stop-gap measure until the new guide, guide protection and casemate are ready at the end of 2002.

The H22 guide between D1A/D1B and the Strain Imager will be increased from the current 125 x 30 mm² to 200 x 30 mm² supermirror guide. This is linked to the proposed replacement of the H22 guide from the reactor, onwards.

The replacement guide between D1A/D1B to Strain Imager is currently out for tender with the contract for manufacture, due to be placed in early November. Delivery and installation on site is planned for the 2002/2003 winter shutdown.

The new casemate will house a 3-monochromator selector table. The 3 monochromators will comprise a silicon variable double focussing monochromator which will have a focus range in both planes of infinity down to 1.4 m, a flat graphite monochromator for broad bandwidth imaging applications, and a fixed focus copper monochromator. This combination will provide the required high-intensity, high-resolution beam adaptable for different applications.

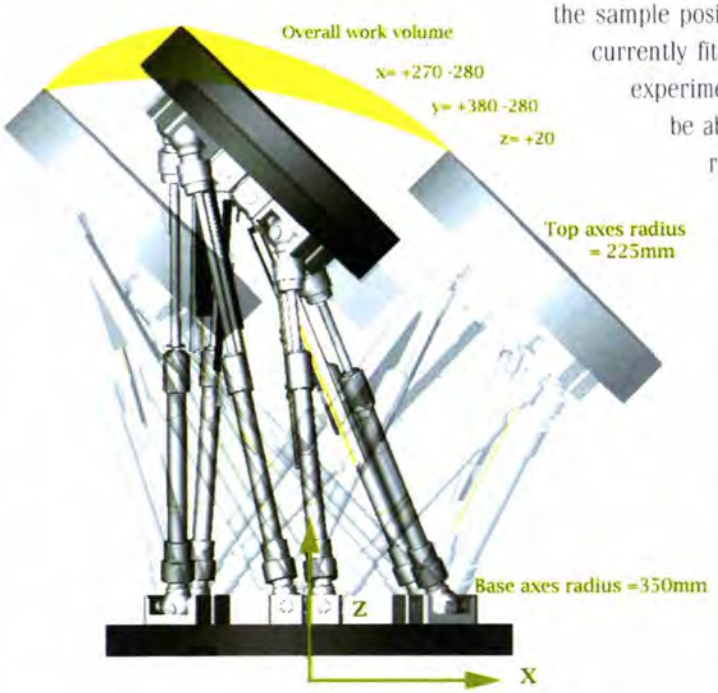

The sample holder of the Strain Imager, the Stewart Platform, in tilt position. The range of the x,y and z movement is indicated, together with the 3D working space.

The initial design for the double focussing monochromator has been produced. Due to its complexity it has been decided to manufacture a prototype with 3 segments. The final version will consist of a 13 segments. Each individual crystal is 180 mm wide, 15 mm high and 2 mm thick with each segment consisting of 5 crystals.

The specifications for the graphite and copper monochromators will be produced in early 2002. These monochromators are of a standard design and construction, with delivery expected at the end of 2002. The Health Physics Service has completed the initial casemate calculation, which indicates that 750 mm of heavy concrete will be required to provide adequate shielding adjacent to the monochromator.

The sample scan position is fixed at 2 m from the monochromator. A variable take-off angle is possible between 55 to 125 degrees, giving a wavelength range of 0.13 to 0.45 nm. The results will be collected using a bi-dimensional micro-strip Position Sensitive Detector, placed 1 m away from the sample position - this detector is currently fitted on D1A for stress experiments. The detector will be able to be removed and replaced with an alternative set-up, if required.

In order to be able to analyse a wide selection of samples both in size and weight (more than 500 kg), we have decided to use a parallel robot (Stewart platform) for the sample positioning. The initial design of the parallel robot has been produced, with a study of the proposed mechanical configuration being carried out by Jean-Pierre Merlet at INRIA Sophia-Antipolis. It has been proved that it is possible to construct a system that will provide the 6 degrees of freedom with accuracy greater than that of conventional units. INRIA is now continuing to determine the optimum geometry for maximum performance and safe operation.

Collaboration with the University of Manchester

The Strain Imager is fortunate in benefiting from its collaboration with the University of Manchester (led by Professor Withers), not only with the EPSRC funding but also with the experience and knowledge they bring to the project. The funding has also provided two additional co-workers at the ILL: one technician, William Hutt, and a dedicated physicist Dr. Giovanni Bruno, who joined the group in October 2001 when the ILL hosted the first Management meeting with representatives of the EPSRC, Manchester University, the ILL and the U.K. users community. Management meetings will take place every 6 months.

Conclusion

2002 looks to be an exciting year, which will see further development of the parallel robot and control system, manufacture of the monochromator, delivery of the guide, guide protection and casemate with installation over the winter shutdown 2002/2003. This puts the instrument on target for its first test cycle in 2003. ■

References

[1] T. Pirling, S. Rowe, A strain imager at the ILL, ILL Annual Report 2000, 84-85 • [2] T. Pirling, Optics for strain imaging: radial collimators or slits? ILL Annual Report 2000, 86-88.

Upgrade of the IN20 high-flux polarised neutron three-axis spectrometer

- J. Kulda, P. Courtois, M. Enderle, M. Thomas, and P. Flores (ILL)
- J. Šaroun (ILL and Nuclear Physics Institute, Řež, Prague)

The three-axis spectrometer IN20 has received the first part of its upgrade, aiming at a substantial increase in its data collection rate for inelastic scattering experiments with polarised neutrons. The in-pile collimation has been remodelled, and a new large, double focussing Heusler alloy monochromator/polariser has been installed, illuminated through a heavy-input slit (virtual source) of adjustable width. In combination with a horizontally focussing Heusler analyser of similar design implemented in spring 2000, the data collection rate in polarisation analysis mode has increased by a factor 30 - 50 compared to the original IN20.

IN20 was designed for excitation studies in the 10-60 meV range using polarised neutrons; it represented the state of the art in its domain in the 1980's and 1990's. The experiments carried out on IN20 involve elastic and inelastic scattering with 1D [1] and 3D (CRYOPAD) [2] polarisation analysis, as well as the thermal beam spin-echo technique (TASSE) [3]. In reality the energy scale of excitations covered on IN20 extended only to about 35 meV due to a severe cut-off of the monochromatic flux at incident neutron energies higher than 60 meV, caused by the small size of the original Heusler monochromator. Even at lower neutron energies the data acquisition rate often proved insufficient for the proposed experiments.

Figure 1: The new IN20 Heusler monochromator ready to be installed.

To match the increasing demand on inelastic polarised neutron studies (spin dynamics in low-dimensional quantum magnets and strongly correlated electron systems, spin-lattice coupling) it was imperative to increase the luminosity of the spectrometer by relaxing its momentum resolution while maintaining good energy resolution and signal-to-noise ratio. In practical terms this means employing a monochromatic focussing geometry on both the monochromator and analyser, increasing the neutron source width, and placing a heavy input slit upstream of the monochromator to serve as a virtual source, whilst keeping the background at an acceptable level. The exact beam geometry has been optimised using a Monte-Carlo ray tracing code (RESTRAX [4]), validated by simulations of the existing ILL TAS instruments on an absolute scale [5]. The major technological achievement of the renewed primary spectrometer is the new double focussing Heusler monochromator with an active area 230 mm wide and 150 mm high (displayed in figure 1). It consists of 75 crystal plates arranged in 15 columns, each pivoting around a vertical axis to allow for variable horizontal focussing. In addition, the 5 plates in each of the columns are cut in such a way as to provide fixed vertical focussing, optimised for the neutron wavelength of 1.4 Å. The saturating field, optimised by detailed 3D finite-element calculations (ANSYS), is produced by NdFeB permanent magnets mounted into a C-shaped iron yoke closing the magnetic circuit on the rear of the monochromator. This solution provides the neutron beam with unlimited lateral access neutron to the monochromator crystals.

The exchange of the beam tube was performed during the 2000/2001 winter shutdown followed by the installation and preliminary testing of the new monochromator in the March/April reactor cycle. From May 2001, IN20 was again available to external users. The polarised monochromatic flux delivered at the sample position (figure 2) closely follows the project curves, aiming at a gain factor of 5 - 10 in the higher thermal energy range. Thanks to the monochromatic horizontal focussing the increase in neutron flux results in no loss of energy resolution. The typical energy widths (FWHM) at the graphite filter wavenumbers k_f = 2.66 Å^{-1} and 4.1 Å^{-1} are 0.82(3) meV and 3.05 (15) meV, respectively. Good beam polarisation (about 90%) has been confirmed across most of the neutron energy range [6].

Measurements of the vanadium scattering intensity, including measurements of sensitivity to inelastic scattering, permit to follow the evolution of the instrument performance achieved with the modifications

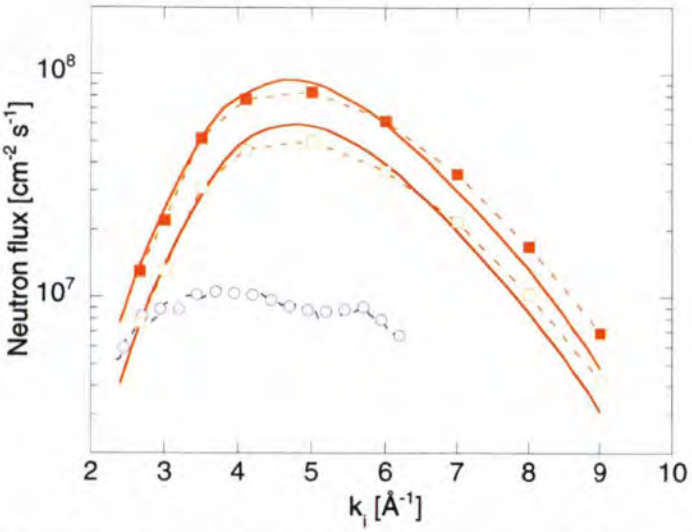

Figure 2: The polarised neutron flux at the sample position of the new IN20 (full and empty squares corresponding to input slit widths of 30 and 15 mm respectively) together with the project curves (full line). The open circles represent the flux measured in the old set-up.

introduced in recent years. At standard conditions and at unchanged energy resolution IN20's peak count-rate at $k_i = 4.1$ Å^{-1} rose from 3 cts/s with vertically focussing geometry in 1998 to 15 cts/s after implementation of the horizontally focussing analyser in 2000 and achieved about 100 cts/s with the new monochromator in 2001. The background level has increased at the same rate as the monochromatic flux, with almost no change in the signal-to-noise ratio.

Since May 2001, IN20 has been available to external users in all of its operation modes. The power of the renewed instrument in the conventional three-axis mode is illustrated by the first direct polarised neutron study of the multi-magnon continuum in a two-dimensional quantum (spin-1/2) Heisenberg antiferromagnet. Combining scattering data from CFDT (copper formate tetra-deuterate) [7] collected with neutron polarisation direction along each of the three principal axes, sufficient intensity is achieved to distinguish the strong single-magnon dispersion branches (mainly transverse - figure 3a) from the multi-magnon continuum filling the space between them (mainly longitudinal - figure 3b).

The performance of the CRYOPAD has been enhanced by new spin nutators, avoiding parasitic scattering at the increased beam divergence. Its performance was tested on a single crystal of MnF_2, a well-known collinear antiferromagnet. A polarisation close to 90% was confirmed for all diagonal components on a nuclear Bragg peak, on a magnetic Bragg peak, and on a purely transverse magnetic excitation ($q \| Q$). The off-diagonal polarisation components should vanish in MnF_2 – indeed zeros within the statistical error were found in all three cases. In the TASSE mode (spin-echo) a systematic study of temperature and mass disorder effects on phonon line width in isotopic Ge crystals has become possible, with a significant gain in the data collection rate due to an increase in the monochromatic flux and the possibility of working at higher incident neutron energies.

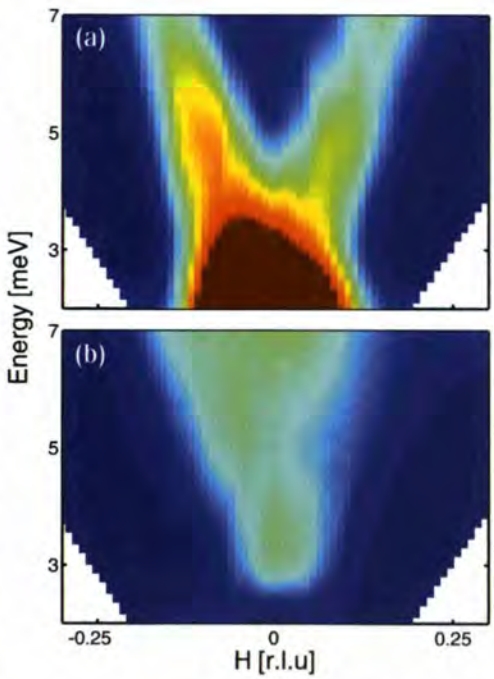

Figure 3: Quantum spin excitations in the 2D-antiferromagnet CFTD: transversely polarised single-magnon signal (a) vers. longitudinally polarised multi-magnon continuum (b) resolved by neutron polarisation analysis on IN20.

The implementation of horizontal focussing is only a first step in the IN20 upgrade. The result is that experiments of the same quality as in the past can now be performed much faster. The next step is a reduction of the background level to enhance further the sensitivity of the instrument. In order to cut the fast neutron background, increased by the opening up of the in-pile collimation, the monochromator shielding will be reinforced and the incident white beam filtered. A second monochromator will also be added using elastically bent Si (111) crystals [8]. The main advantage of this will be the suppression of $\lambda/2$ contamination in the incident beam at wave-vectors of 2.66 – 4 Å^{-1}, which is otherwise responsible for a significant part of the sample-related unpolarised background. In this case an alternative neutron polarisation technique, a ^{3}He filter or a multilayer bender, will be employed. ■

References

[1] G. Aeppli, T.E. Mason, S.M. Hayden, H.A. Mook, J. Kulda, Science 278 (1997) 1432 • [2] C.M.E. Zeyen, J. Phys. Chem. Solids 60 (1999) 1573 • [3] P.J. Brown, J.B. Forsyth, F. Tasset, Proc. R. Soc. Lond. A442 (1993) 147 • [4] J. Saroun, J. Kulda, , Physica B 234-236 (1997) 1102 • [5] J. Saroun, J. Kulda, A. Wildes, A. Hiess, Physica B 276-278 (2000) 148 • [6] J.Kulda., J. Saroun, P.Courtois, M. Enderle, M.Thomas, P.Flores, Proceedings ICNS 2001, Munich • [7] N.B. Christensen, H.M. Ronnow, D.F. McMorrow, M. Enderle, A. Harrison, unpublished (2001) • [8] J. Kulda, J. Saroun, Nucl. Inst. Meth. A379 (1996) 155.

Coping with increased data rates on SANS machines

P. Van Esch (ILL)

Resistive charge division is a position encoding technique well suited to neutron detection in gas detectors. However, it puts severe demands on the read-out electronics, as not only hit/no-hit information has to be conveyed but an accurate signal amplitude has to be measured within a short time if high count rates are to be achieved. Front end electronics has been successfully developed in the framework of the Millennium SANS-2MHz project. It consists of a fast low-noise preamplifier, a Gaussian shaping circuit and a noiseless baseline correction.

Principle of resistive charge division

The idea of resistive charge division is to use a distributed resistive electrode as detecting element, terminated at both ends with a low impedance. The charges collected at both ends encode for the position of the impact along the electrode. This technique is well-suited to the readout of neutron gas detectors, because the signal provided by these detectors is inherently "slow": the time of charge collection lasts from a few hundred nanoseconds up to a microsecond and sometimes even longer depending on the detector topology. On this time scale, a distributed resistor can be considered fairly ideal, a fact which is primordial to the functioning of resistive charge division.

This technique is the readout principle of the new detection elements for the SANS-2MHz project [1,2]. In that project, the anode wire in a cylindrical 1 metre long detector is the resistive electrode.

Spatial resolution and electronic noise: preamplifier

In many cases (especially in large detectors), the determining factor of the spatial resolution in charge division is the electronic noise added to the signals. This noise has two different kinds of sources: on one hand, there is the noise due to the preamplifiers, on the other hand there is the thermal Johnson noise due to the resistive anode wire itself. The calculation of the relative contributions to the spatial resolution is detailed in [2]. The ability to calculate those contributions (which are found to be in excellent agreement with actual measurements) enables us to optimise the choice of the preamplifier such that the essential term (the Johnson noise of the resistive electrode itself) is the dominant one.

The preamplifier is a current amplifier with a very large bandwidth: it is configured as a first order system with a time constant that can be as low as 12 ns. Indeed, the presence of a finite resistance in the detection element does away with the low noise advantages of an integrating charge amplifier. The advantages of a current amplifier are that there is no pile up at high counting rates, that no pole-zero compensation is necessary and that the input impedance (important in our case) can be much lower.

Counting rate issues and noise: shaper

The total dead time (and hence the counting rate) of one detector tube will be essentially determined by the total pulse width of the shaping circuit. In order to optimise this pulse width and to limit at the same time the spectral width of the pulse, a Gaussian shape is optimal. We implemented a 4th order active filter

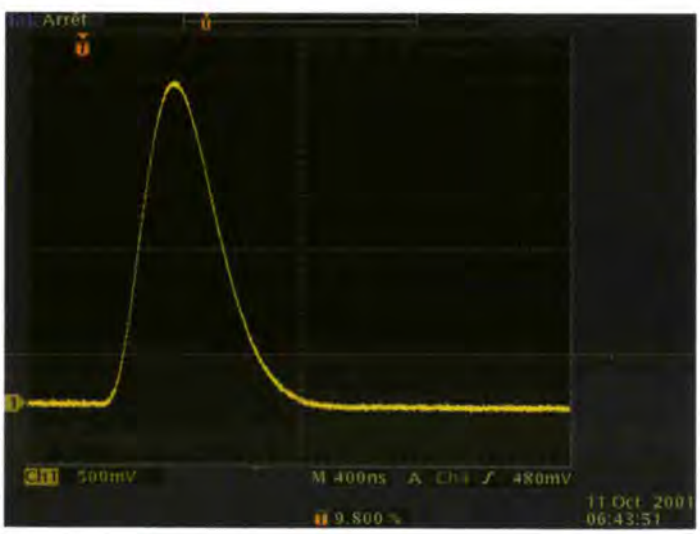

Figure 1: Impulse response of amplifier with a pulse width slightly larger than 1 µs. This is the shaping that we intend to use for the SANS-2MHz project.

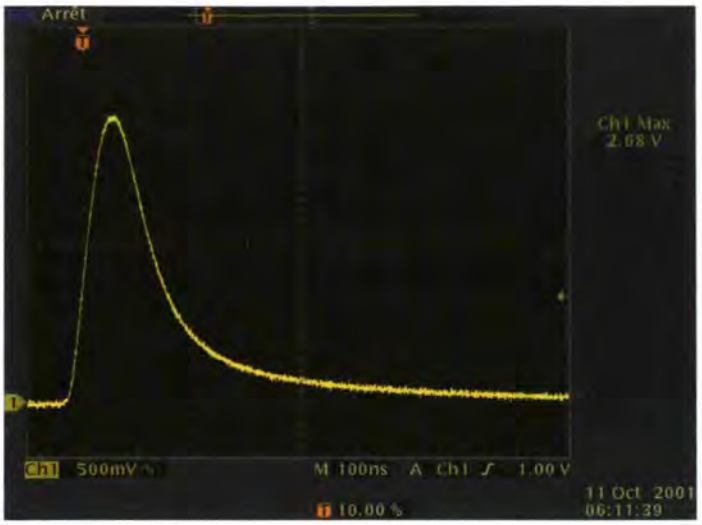

Figure 2: A typical detector signal (on the 10 mm diameter prototype multi-tube detector at low pressure) after shaping with a Gaussian filter of total width about 200 ns. The trailing signal at the end is not a result of the shaping, but due to the residual ion movement in the detector.

approximation of that shape. We have demonstrated, within the same circuit topology, filters of which the 1% pulse width can vary from 100 ns up to 2 ms (and more). The time scale of the pulse can hence be adapted to the need of a particular detector. Unipolar shaping has two advantages: the obvious one is that the duration of the pulse is of course twice as short as for bipolar shaping. The less obvious advantage is that the noise bandwidth is about 40% lower than what can be achieved with bipolar shaping. The signal shape of the Gaussian shaper intended for use with the SANS-2MHz project is shown in figure 1. A fast shaped detector signal (about 200 ns) is shown in figure 2.

Noiseless baseline correction

The disadvantage of unipolar shaping is that at high count rates, the "baseline" shifts down. We have developed a simple baseline correction circuit that filters out the shifted baseline, passes it through a low pass filter (eliminating essentially all noise on the baseline) and adds the shift to the original signal so as to restore the baseline. The advantage of this approach over the more traditional "clamping" approach is that this does not add any noise to the signal. The effect of the baseline correction is shown in figure 3.

Conclusion

We have developed a complete analogue amplification chain, adapted to fast counting neutron gas detectors using the principle of charge division to extract position- sensitive information. A careful analysis allowed us to design a circuit topology that does not add any significant limits on the detector performance concerning count rate or spatial resolution. Initially this work has been developed in the framework of the Millennium SANS-2MHz project in order to achieve (and supersede) its goals (6 mm spatial resolution on 1 m active length, 140 KHz count rate at 10% dead time correction per detector element). As charge division is a quite promising technique, its applications in neutron detection will not be limited to that project only. The range in time constants and gain factors demonstrated covers a wide range of potential applications. ■

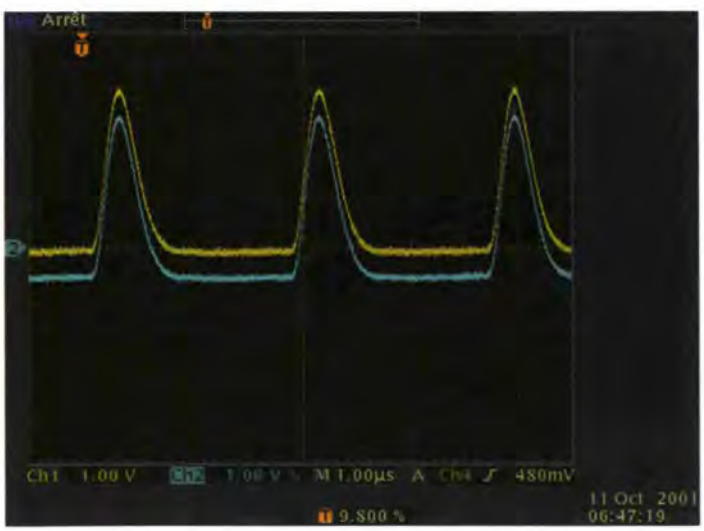

Figure 3: Effect of the baseline correction: with (yellow) and without (blue) baseline correction, at high count rates.

References

[1] The Millennium Programme: Proposals for ILL's 5-year development progamme. ILL Scientific Council, April 1999. SC99-1 • [2] High Count Rate Detectors for Small-Angle Neutron Scattering, The Millennium Symposium, April 2001.

Neutron nano-beam production
using a thin film waveguide

- F. Pfeiffer (ILL and University of Saarbrücken)
- V. Leiner (ILL and University of Bochum)
- P. Høghøj (ILL and XENOCS)
- I. Anderson (ILL)

We have experimentally demonstrated that planar neutron waveguide structures can be used as resonant beam coupling devices to efficiently produce a coherent neutron line source with cross-sections in the sub-micrometer range. The Fraunhofer farfield diffraction pattern of the resonance modes was measured and found to be in excellent agreement with the theoretical model.

Neutron diffraction, spectroscopy and imaging, using beam sizes in the submicrometer range, are rapidly evolving fields of research. Progress is fueled not only by the availability of novel neutron optics, such as microcollimators, supermirrors or focussing monochromators and neutron lenses, but also by the urgent need for characterisation tools that meet the demands of the advances in biochemical and semiconductor nanoscience.

The simple use of slits to define a submicrometer neutron beam width in the range of 100 Å - 5000 Å is, however, both difficult and inefficient for various reasons. Firstly, suitable slit materials (like for instance B_4C or Cd) cannot be processed with the required accuracy. Secondly, the use of slits would also be extremely inefficient, since only a small fraction of the original beam could then be used. Similarly, focussing neutron optics, like for instance Fresnel lenses, microcollimators or bend crystal optics are limited by the achievable structural sizes of current nanolithographic techniques, general neutron optical properties of the materials or the quality of fabrication.

Alternatively, and analogous to the application of prism film couplers to couple visible light into fiber-optical systems, a resonant beam coupling device (RBC) can be used for neutrons. With this RBC device (in the following simply called 'waveguide') neutrons can be coupled into a thin guiding layer, guided, and then decoupled at the end [1,2].

Figure 1 (insert) shows a schematic diagram of such a waveguide structure consisting of a guiding layer of a material with a low neutron scattering length density (such as carbon) sandwiched in between a comparably thin cap layer and a rather thick bottom layer of a material with a high neutron scattering length density (such as nickel). Typical values for the thickness of the cap layer, the guiding layer and the bottom layer are 30 Å - 100 Å, 200 Å - 5000 Å and, 500 Å - 1000 Å, respectively.

To gain an understanding of the mode excitation and waveguide properties, we have calculated the internal (and external) neutron wavefunction $|\Psi(\alpha_i,z)|^2$ as a function of structural and geometric parameters by a transfer matrix algorithm similar to the one used in the case of optical waveguides [3].

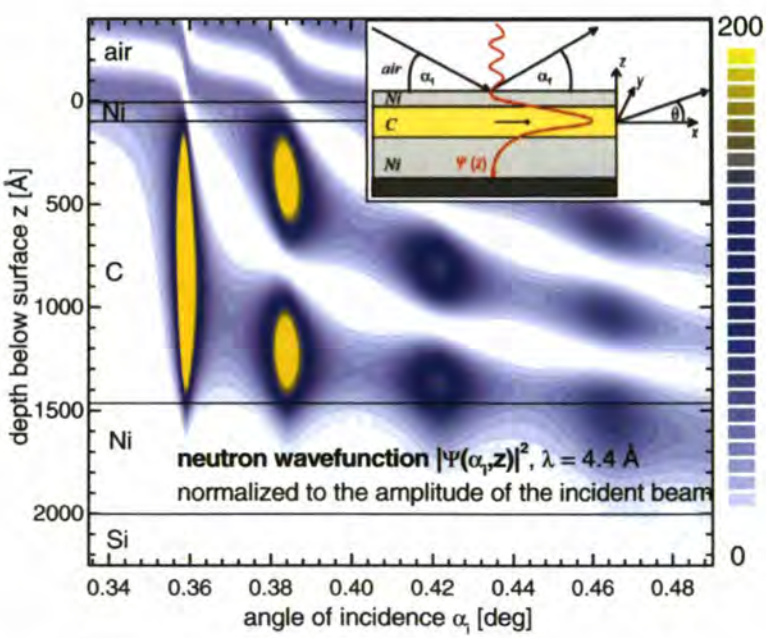

Figure 1: Insert: A sketch of a neutron resonant beam coupling waveguide device (RBC). The impinging neutron beam excites a resonance mode inside the structure. Main Figure: Linear contourplot of the calculated neutron wavefuntion $|\Psi(\alpha_i,z)|^2$ in a 52 Å Ni/ 1410 Å C/ 490 Å Ni/ Si neutron waveguide as a function of the angle of incidence α_i and the depth below the surface z.

In figure 1 the resulting neutron wavefunction $|\Psi(\alpha_i,z)|^2$ for a wavelength of $\lambda = 4.4$ Å is shown. As expected, the excitation of the resonant modes appears for a set of nearly discrete values of α_i in a range between the critical angle of the guiding layer and the critical angle of the cap/bottom layer. Importantly, the resonant enhancement of $|\Psi(\alpha_i,z)|^2$ with respect to the amplitude of the incident beam can reach a factor of more than two orders of magnitude when the angle of incidence matches the excitation angle of a resonance.

At the end of the structure, the neutrons trapped in the guiding layer exit the thin film structure, leading to a coherent beam with a vertical width (in the z-direction) corresponding to the thickness of the guiding layer and a divergence given by the FWHM of the Fourier transform of the excited standing wave-function. The divergence and shape of the exiting guided mode, the angular acceptance and the absolute number of supported modes, can be all controlled by the structural and geometric parameters and varied within a certain range [4]. Finally, the farfield-pattern $I(\theta)$ of the different modes can be obtained by applying classical optical diffraction theory (Fraunhofer diffraction) to the previously calculated complex neutron wavefunction of the different modes.

To demonstrate the effects calculated above experimentally, a series of differently designed neutron waveguides were fabricated at one of the sputtering facilities at the ILL by using a DC magnetron sputtering process. The samples were measured on the ADAM neutron reflectometer using a pyrolitic graphite monochromator adjusted to give a neutron wavelength of 4.4 Å with an energy-spread of $\Delta\lambda/\lambda \cong 0.7$ %.

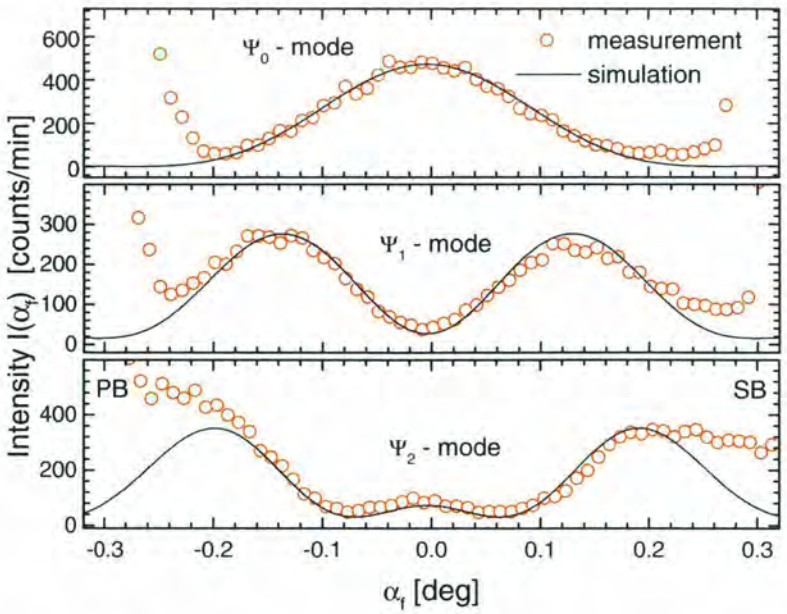

Figure 2: Measured (circles) and calculated (line) farfield-pattern of the excited Ψ_0, Ψ_1, and Ψ_2 - modes. The rise of the measured intensity towards greater values of α_f is due to the tails of the primary beam (PB) and the specular reflected beam (SB), having their maxima at $\alpha_f = \pm \alpha_i$.

The Fraunhofer diffraction pattern of different excited modes has been studied by measuring the intensity as a function of α_f for angles of incidence corresponding to the excitation of the different modes. Figure 2 shows these results (open circles) together with the calculations (line) based on the previously mentioned diffraction theory [5].

Importantly, the only fitting parameter used was the maximum intensity, from which information about the efficiency or gain can now be deduced. The latter value is defined by the ratio between the integrated flux exiting the waveguide (directly measurable by integrating over the divergent farfield-pattern) and the flux that one would obtain using a pair of hypothetical slits to prepare a neutron beam with the same cross section as the thickness of the guiding layer and a divergence corresponding to the angular acceptance of the excited mode. Our most efficient waveguide yielded a gain value of 17 ± 3.

Furthermore, since our simulation is based on a fully coherent beam propagation, the fact that the simulation matches almost perfectly with the measured data confirms the high degree of transverse coherence of the exiting wavefunction (in the direction perpendicular to the surface of the guide). For an additional assessment of the degree of coherence we fabricated waveguides comprising several guiding layers and thus incorporated the coherent source and a diffraction grating into one device. In a simplified view, low order excitation modes of such a multiple guiding layer waveguide can be considered as a source of several, distinct, coherent beams emerging from different guiding layers [6]. We measured the resulting farfield diffraction pattern (figure 3) of such a device (with ten 469 Å carbon guiding layers) and observed high contrast interference fringes, which did not show any significant broadening within the first few orders. Clearly, this again confirms the high degree of coherence of the exiting mode, particularly since the number of measured fringes was not limited by their intensity but rather by the surface area of the two-dimensional detector used.

technical developments

In conclusion, we have shown that using the resonant beam coupling principle for thin film neutron waveguides allows for the efficient production of a coherent neutron line source with a beam cross section in the sub-micrometer range. Many applications using these devices for sub-micrometer spatially resolved coherent micro-diffraction, (phase-contrast) projection microscopy or static and time-resolved coherent speckle experiments can be envisioned and are of interest to a broad user community in biochemical and semiconductor nanosciences. Further progress is expected from improved material compositions combined with adapted prefocussing optics. The application of these devices at next generation neutron sources may then lead to efficient two-dimensional focussing devices in the future.

We thank W. Graf, K. Ben-Saidane, and V. Schönherr for their technical help and T. Salditt for a series of fruitful discussions. ■

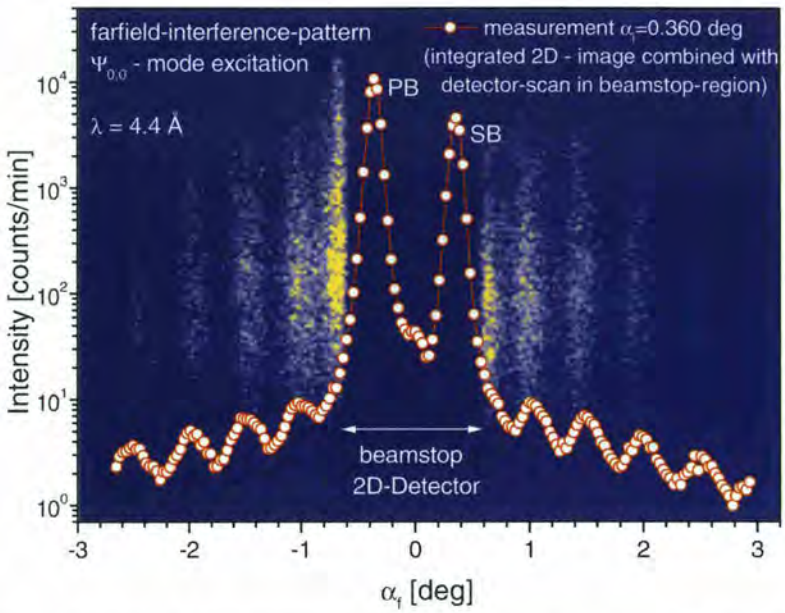

Figure 3: Front: Measured farfield interference pattern of a multiple guiding layer waveguide. The high degree of transverse coherence is confirmed by the number and the contrast (logarithmic scaling!) of the clearly visible interference fringes. Back: 2D-Detector image with beamblock in the middle to reduce diffuse background.

References

[1] Y.P. Feng, C.F. Majkrzak, S.K. Sinha, et al., PRB 49 (1994) 10814-10817 • [2] P.K. Tien and R. Ulrich, J. Opt. Soc. Am. 60 (1970) 1325 • [3] M.R. Shenon, K. Thyagarajan K., and A. K. Gatah, J. Lightwave Tech., LT-6 (1988) 1285 • [4] F. Pfeiffer, Diploma thesis: X-ray waveguides, LMU München, Sektion Physik (1999) • [5] D. Marcuse, Theory of Dielectric Optical Waveguides, Academic Press, New York (1974) • [6] F. Pfeiffer, T. Salditt, P. Hoghoj, I. Anderson, PRB 62, (2000) 16939 • [7] F. Pfeiffer, V. Leiner, P. Høghøj, I. Anderson, SPIE Proceedings 4109, in print.

1.8 K closed-cycle refrigerator
for the 4-circle diffractometer D9

S. Pujol, X. Tonon and F. Thomas (ILL)

The ILL Sample Environment Laboratory has developed a Joule-Thomson low-cooling-power stage to extend the temperature range of commercial cryocoolers from 10 K to 1.8 K. As this new set-up is very compact and insensitive to orientation, it will also be used on the Eulerian cradle of the diffractometer D9.

Over the last decades great progress has been made in neutron sample-environment techniques. For low temperatures the Orange Cryostat is widely used at most neutron sources around the world, making 1.5 K a temperature routinely achievable.

Nevertheless, in the case of 4-circle diffractometers, measuring a sample below 10 K (the base temperature of a small commercially available cryocooler) is still the privilege of a happy few. The two main reasons are:

- cryocoolers working below 10 K are big machines. Typically the cold-head itself weights 20 kg, measures 200 mm in diameter and is 500 mm long. Therefore, installing such a device on an Eulerian cradle would be a real *tour de force*.
- helium-flow cryostats working below 4.2 K in a 4-circle geometry are extremely difficult to build and maintain. They can only be run by users with a strong background in cryogenics. The ILL has developed such cryostats for D9 and D10 in the past and their success can be put down to the expertise of the ILL scientists in charge.

In order to democratise 4-circle diffraction experiments below 10 K, we have developed a Joule-Thomson low-cooling-power stage that can be fitted on a 2/9 Ricor™ cryocooler cold-head. The stage is a classic Joule-Thomson capillary together with a counter-flow heat exchanger. The stage is shown in figure 1. Special attention has been paid to achieve a very compact design: the overall dimensions of the stage are only 35 mm in diameter and 65 mm in height.

Figure 2 shows the complete four-circle set-up. In addition to the modified cryocooler system, a 10 m³/h primary pump is required to reach temperatures below 4.2 K, as well as a helium-gas bottle ensuring an input pressure in the 10 bar range and a liquid-nitrogen trap to purify the helium gas. The overall length of the modified cold-head is typically 350 mm, the diameter remaining unchanged by the addition of the third stage.

In such a design the helium flow through the Joule-Thomson stage can be adjusted via the input pressure. Increasing this flow increases the cooling rate and the cooling power below 20 K, but increases the base temperature too. Classically, the base temperature would be given by the vapour pressure of the liquid helium at the end of the Joule-Thomson capillary, i.e. 16.6 mbar at 1.8 K. In our case, the counter-flow heat exchanger is partly filled with liquid helium, rendering irrelevant the classic relationship between base temperature and the vapour pressure of the liquid helium. Experimentation has shown that the best compromise is a helium gas flow of 5 m³/week STP. This leads to a base temperature of 1.8 K, a cooling power at 2 K of 10 mW and a cooling time of about 3 hours from room temperature to 1.8 K. This new set-up is available on D9 for the ILL users. ■

Figure 1: Photo of the Joule-Thomson stage. A: Counter-flow heat exchanger. B: Joule-Thomson capillary. C: 1.8 K plate. D: 10 K plate.

Figure 2: Photo of the complete set-up. A: Joule-Thomson stage. B: cryocooler cold-head. C: Eulerian-cradle. D: helium-gas bottle. E: liquid-nitrogen trap. G: temperature controller. H: cryocooler compressor.

Imaging with a neutron lens

C.D. DEWHURST AND I. ANDERSON (ILL)

R. BEGUIRISTAIN (ADELPHI TECHNOLOGY, PAOLO ALTO, USA)

The word 'optics' naturally brings to mind the image of a lens used to focus or defocus a beam of light. In neutron optics refractive lenses are rarely, if ever, used – why?

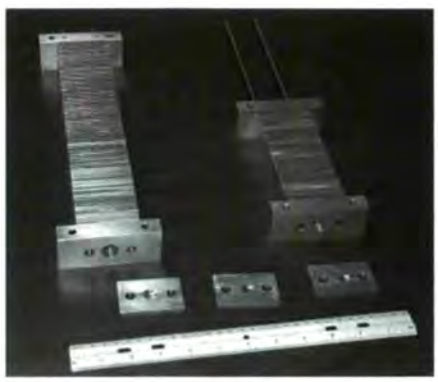

Figure 1: Aluminium compound refractive lens.

The answer lies in the low scattering power of most materials for neutrons, a characteristic that we normally consider an advantage!

Writing the refractive index for neutrons as:

$$n = 1 - \delta - i\beta$$

the decrement $\delta = (\lambda^2/2\pi)Nb_{coh}$ is typically of the order of 10^{-6}. It follows that the refractive index is less than 1, contrary to our experience with light optics. Hence concave lenses must be generally used to focus neutron beams and the focal lengths,

$$f = R/2\delta$$

where R is the on-axis radius of curvature, are prohibitively long. For example, a bi-concave lens with on-axis radius of curvature 1.27 cm made of aluminium ($\delta = 4 \times 10^{-5}$ for 10 Å neutrons) will have a focal length of 159 m. Reducing R, in order to reduce the focal length to practical values, would severely limit the lens aperture. A more reasonable approach involves stacking together a number of lenses. A series of N aligned lenses, with negligible distance between each lens has a focal length:

$$f = R/2N\delta$$

The factor 1/N reduction in focal length of a so-called Compound Refractive Lens (CRL) allows for a reasonable value for the radius, R, of each element. Spherical surfaces make imperfect lenses and

Material	density [g/cm³]	μ [m⁻¹]	δ	δ/μ [m]
O	1.14	0.00425	1.28E-06	0.000302
CO_2	2.15	0.0191	1.60E-06	8.4E-05
C	2.26	0.051	3.88E-06	7.62E-05
Be	1.85	0.116	4.95E-06	4.27E-05
F	1.11	0.0365	1.02E-06	2.80E-05
Bi	9.73	0.118	1.23E-06	1.04E-05
MgO	3.58	1.28	3.62E-06	2.83E-06
Pb	11.3	0.573	1.6E-06	2.78E-06
MgF	3.18	0.471	1.24E-06	2.62E-06
SiO_2	2.2	0.441	1.05E-06	2.37E-06
ZrO_2	5.89	0.812	1.6E-06	1.98E-06
Mg	1.74	0.615	1.19E-06	1.94E-06
Si	2.32	0.796	1.06E-06	1.34E-06
Zr	6.49	1.2	1.55E-06	1.29E-06
Al	2.69	1.38	1.06E-06	7.73E-07

Table 1: Density, linear absorption coefficient, $\mu = 4\pi\beta/\lambda$, and figure of merit of selected materials at a wavelength of 1.8 Å.

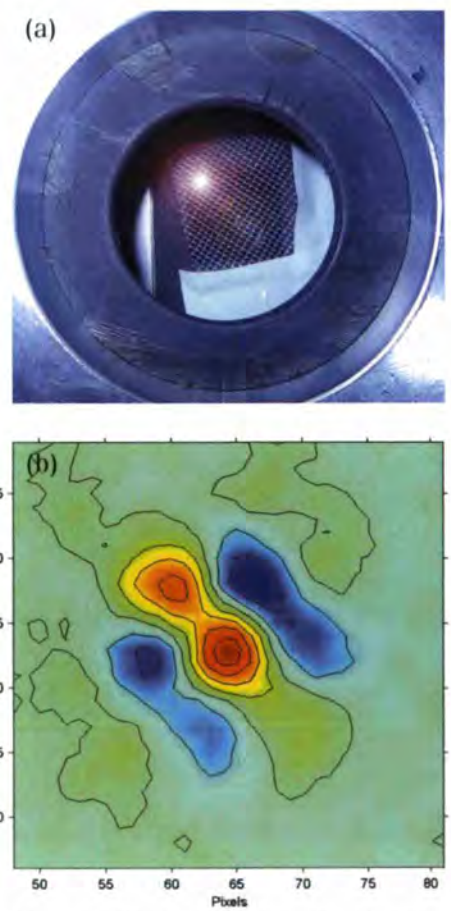

Figure 2: (a) Plastic mesh at the lens object position and (b) corresponding magnified neutron image.

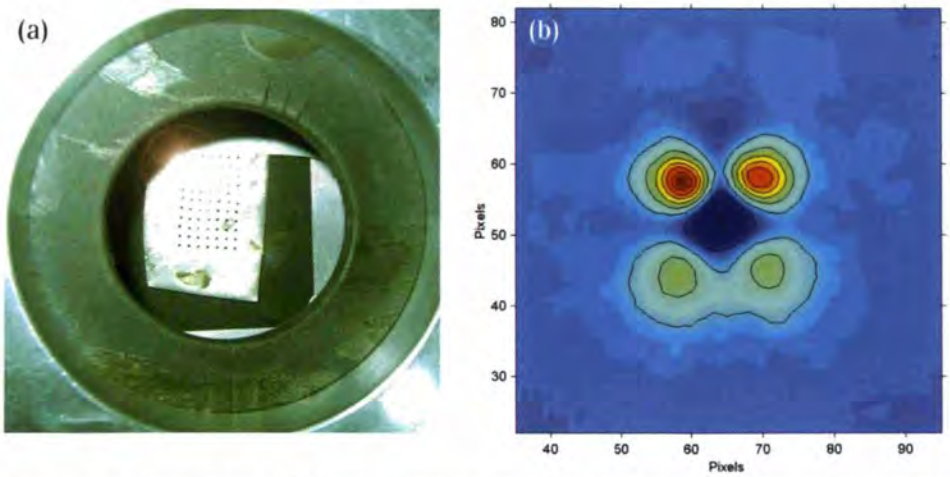

Figure 3: (a) Rectangular array of holes in cadmium at the lens object position and (b) corresponding magnified neutron image.

only the central, paraxial region of these approximate the paraboloid of resolution surface of ideal lenses.

Suitable materials for neutron lenses should have a large value of δ, low absorption, μ, and incoherent scattering, β, and show little small angle scattering. In Table 1 we show the figure of merit δ/μ of some common materials that may be considered for neutron lenses.

Refractive neutron lenses could be used in a number of applications: focussing or collimation of a neutron beam for example in small-angle scattering experiments, wavelength filtering due to their large chromatic aberration or imaging. Here we report on experiments performed on D22 to evaluate the imaging properties of an aluminium CRL.

The lens system was made up of 105 individual bi-concave spherical lenses with 1.27 cm radii of curvature and 1.2 cm aperture (figure1). The tests were made at a wavelength of 20 Å for which the lens has a theoretical focal length of 0.46 m and a transmission of 25 %. Various objects placed 0.5 m in front of the lens were imaged onto the D22 detector placed 17.6 m behind the lens giving a theoretical magnification of 35. Note that the detector pixel size is 7.5 mm.

Initial images were obtained using: (1) a plastic mesh with grid spacing of 1.5 and 2 mm in the two perpendicular directions (figure 2) and (2) a rectangular array of 0.5 mm holes drilled into cadmium with a hole-to-hole distance of ~ 2.5 mm (figure 3). The detector images obtained confirmed the imaging properties of the lens with a magnification of ~ 35 times.

Finally the lens was used to make an image of a steel spring, 16 mm long, 6 mm in diameter with a pitch of 2 mm. Due to the restricted field of view of the Al CRL, the full image (figure 4) had to be constructed by scanning the lens in horizontal and vertical directions in steps of 0.5 mm and recombining the individual images. The result is convincing, the lens produces a clear magnified image of the spring!

The next step: a neutron microscope? ■

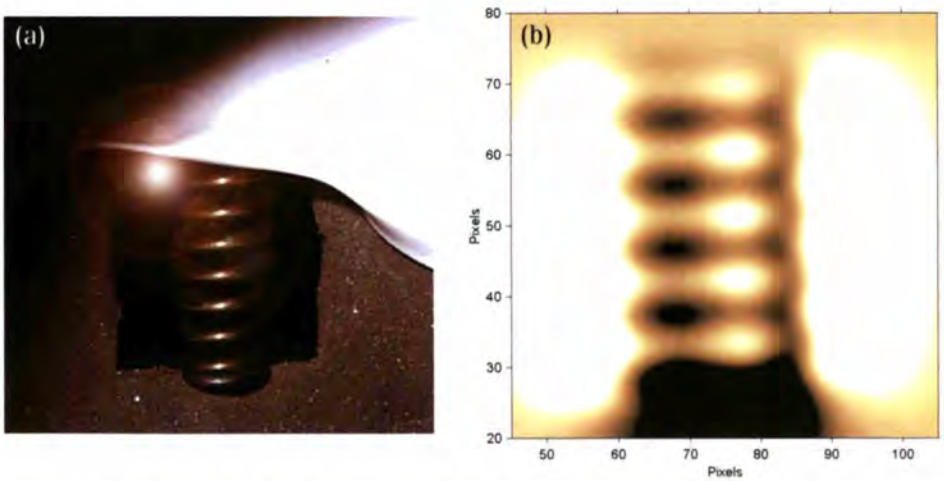

Figure 4: (a) Steel spring at the lens object position and (b) corresponding magnified neutron image.

Fast neutron multi-detectors
for new instrumental conditions

B. GUÉRARD (ILL)

The SDN (the Neutron Detectors Service) of the ILL participates in the Millennium project with the development of several gas detectors. Two of them are pushing back the limits of the current technology. One is the large area Micro Strip Gas Chamber (MSGC) two-dimensional detector. The other is a very fast (2MHz) multi-detector with an active area of 1 m² consisting of 130 small-diameter position-sensitive (PS) counter tubes. In parallel to the development of these gas detectors, different configurations of scintillator detectors have also been studied and are briefly presented.

Global or individual channel position measurement with gas detectors

The capture reaction of a neutron by a nucleus of ^{3}He is followed by gas amplification of the charge created by the two emitted particles (proton and triton). Using charge amplifiers to integrate the avalanche current provides a signal with a pulse height proportional to the energy deposited in the gas after the nuclear reaction has taken place. Detectors based on this principle are stable in time, with counting variations less than 10^{-4} of the mean.

The localisation is performed either by individual or global readout. With a *global readout*, the sensitive electrodes are interconnected inside the detector by passive electronic components (R for charge division, and LC for delay lines) that encode the centre of gravity of the primary charges. With an *individual readout* the position of a neutron is given by the channel with the maximum pulse height. It requires more electronics than global readout, but allows much higher counting rate[1]. Our MSGC 2D detector Bidim80 described in [3] uses a charge division global method. Several of these detectors have been installed at ILL, the first one on D1A [4], and more recently on D10 [5] as well as on several other instruments (T13A, T3, D15). A resolution of 1 mm has been recently demonstrated [6].

SANS_2MHz

For 2D multi-detectors, the most common method is to detect neutron signals with two orthogonal planes of individual cells. For the case of a distributed irradiation over the detector, the counting rate is mainly limited by the time of the XY coincidence, around 200 ns. The highest counting rate capability available today with 2D gas detectors is obtained using a multi-detector consisting of a large number of independent parallel counter tubes with double ended wires read out by charge division. The SANS_2MHz Millennium project plans to deliver such a detector in 2003 for D22. It required a careful design of the charge amplifier and electronics cards to convert analogue signals into position. 5 prototype PS counter tubes (1 m long, 7.9 mm diameter) have been fabricated according to our specifications and extensively studied. The position resolution along one tube specified for D22 (7.5 mm FWHM) has been obtained at a count rate up to 100 KHz/tube, with less than 10% counting correction. The spatial response does not require any correction for non-linearity effects.

Figure 1: The multi-tube prototype mounted on a gas handling system. It includes 33 tubes, 30 cm long with a diameter of 10 mm.

In parallel to this study, the SDN has recently fabricated a multi-tube detector which differs from independent PS counters only by the fabrication[2]. It is made of several tubes (30 cm in length) in contact side by side, soldered on a common flange on both ends (figure 1). Detector elements are therefore sharing the same counting gas. A position resolution of 1.7 mm FWHM has been measured along the wires. A gas amplification gain of 10^4 has been measured, a factor of 10 higher than the limit we obtained with commercial PS counters. Thanks to its simplicity and ease of mounting, the multi-tube could be an extremely cost-effective future solution for large area 2D detectors. We are already considering its use for the large time-of-flight spectrometers.

The two-dimensional MSGC detector Bidim200

With a sensitive area of 192 mm x 192 mm, the Bidim200 is the largest MSGC 2D detector ever built (figure 2). The first

(1) The counting rate capability is defined as the maximum counting rate which induces less than 10% of missing events. Compared to global readout, Individual channel readout of XY crossed cell improves the counting rate only when the irradiation is not concentrated on one single cell of the detector.
(2) French patent application 0115898 filed on December 2001.

detector out of 8 foreseen for the D19 project, started its operation in April 2001 [7], and is now running on D19 for routine experiments. Only materials known for their low outgasing properties were used in the fabrication of internal pieces. Baking out at 150°C under ultra-high vacuum (10^{-8} mbar) was applied during 2 weeks under the control of a mass spectrometer. The substrate is made of semi-conducting Schott glass, known for its long-term stability [8]. A "virtual cathode" layout is used, with anode strips on the upper side, and cathode strips on the rear side, perpendicular to the anodes. This layout allows very high gas amplification gain, which is an additional guarantee for the robustness of the detector in long-term operation. The pitch of the electrodes is 3 mm in both directions, and contacts are gold-plated. Each electrode is connected individually to a charge amplifier and a discriminator. Signals from the discriminator output are filtered by the CLET electronics which select the channel with the maximum pulse height. The following stage is the MCC encoding module which performs the X and Y coincidence, and converts the 64 X lines and 64 Y lines into a 12 bits pixel address. For applications requiring a position resolution better than 3 mm, we are investigating a new set-up of this detector which will benefit from the development made for the SANS_2MHz project: by connecting both ends of each anode strip of the Bidim200 to a charge division electronics, a position resolution of 1.3 mm has been measured along the anode direction. Beside the advantage of a better position resolution, the MSGC is also simpler because the cathode layout of the rear side can be replaced by a uniform metallization.

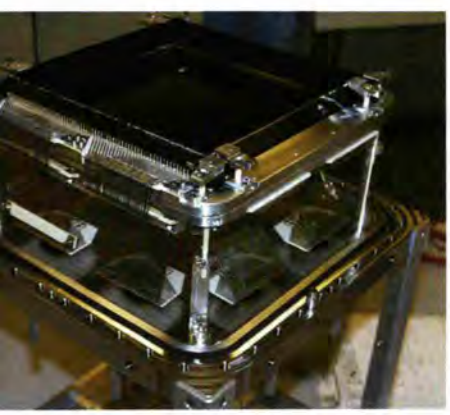

Figure 2: Internal view of the bidim 200 MSGC detector. Anode connectics are seen on the left, and cathode connectics on the right. The sensitive area of the detector is limited by 4 vertical guard electrodes which guarantee the uniformity over the whole sensitive area.

Scintillators

Instead of ^{3}He, a thin converter layer can also be used in gas amplification devices. The main drawback is that their detection efficiency is limited between 10% and 20% by self-absorption (in thick converters, ionising particles created after neutron capture may lose all of their energy before reaching the gas medium). Scintillating converters are more efficient because they are transparent to their scintillation light. Active gas scintillators work like a standard gas chamber, except that the detection signal is given by the light emitted during the avalanche, instead of the charge. Figure 3 shows the light integrated during 100 ms with a CCD camera coupled with the glass window of a multi-step gas electron multiplier detector with ^{3}He [10]. Proton-Triton tracks are visible. Their apparent length depends on the variable angle of the track projection. This promising detector combines two advantages: the low gamma-sensitivity and the fact that there is no need for electrical connections. For time-resolved measurements, the CCD readout can be replaced by a position-sensitive photo-multiplier.

Scintillators can also be coupled to multi-anode photo multipliers by means of wavelength shifting (WLS) fibres. We are studying a prototype based on this principle. It consists of a 128 mm x 128 mm ^{6}Li glass, 1 mm thick, sandwiched between two layers of 256 square WLS fibres. The blue light emitted by the ^{6}Li glass is reemitted isotropically in the green region by WLS fibres. The dimension of the fibres, 0.5 mm, allows high-position resolution (0.5 mm has been measured with a first design), and reasonably low scattering of neutrons. The PM signals are read out by the amplifiers and discriminators and the XY address is encoded on 12 bits. The aim of this prototype will be to demonstrate the following expected features : 85% efficiency at 2.5 Å, counting rate > 1 MHz, and low sensitivity to gamma-rays.

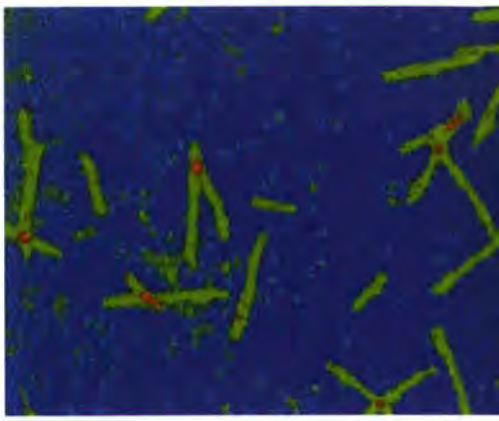

Figure 3: Light measured with a CCD camera, induced by the proton-triton tracks inside a multistep GEM gas scintillator.

Conclusion

Fast and accurate multi-detectors are being developed for the ILL instruments to fully benefit from the neutron flux of the high-flux reactor. New challenges of neutron detection imposed by the future spallation sources will reinforce the interest in these detectors. ■

References

[1] The ILL Millenium Symposium & European Users Meeting, 6-7 April 2001, 332-334 • [2] The ILL Millenium Symposium & European Usersr Meeting, 6-7 April 2001, 313-315 • [3] ILL Annual Report 96, 86 • [4] ILL Annual Report 97, 87 • [5] ILL News for reactor users n. 34, December 2000 • [6] International Workshop on Position-sensitive detectors, Berlin, Germany, June 28-30, 2001 • [7] ILL News for reactor users n. 35, June 2001 • [8] "Operation of sealed microstrip gas chambers", J.F. Clergeau et al., IEEE, TNS, Vol 48, No 4, August 2001 • [9] ILL Annual Report 99, 76 • [10] CCD readout of "GEM based neutron detectors", F.A.F. Fraga et al., submitted to Nucl. Instr. and Methods.

The IN5 project: optimisation of chopper disk design and manufacturing

M. Thomas, P. Malbert, H. Casalta, J. Ollivier and H. Schober (ILL)

The SMAE, the Mechanical Service of the Experimental Halls, has developed 3 pairs of disks for the choppers of the new IN5 time-of-flight spectrometer. The new primary spectrometer will use the full height of the H16 neutron guide to achieve a maximal flux increase. The beam is compressed vertically from 20 cm at the entrance to 5 cm at the sample. 6 disks, mounted in pairs, will be used along the beam axis. The height of the guide sections to be covered implies rather large disk diameters with correspondingly deep windows (see Photo 1). The development of these disks and their manufacture is a technical challenge pushing material properties and state-of-the-art design methods to their limits. The process is outlined here and has been entirely managed by the ILL, profiting from its excellent knowledge of chopper disks and the preliminary testing of prototypes. TMM and FZ Jülich are in charge of the other components: the power supply for the chopper system, magnetic bearings, motors, housings and electronics.

Functional specifications

- Diameters: $\Phi = 750$ mm for the first two disks and $\Phi = 690$ mm for the others.
- Windows (two per disk at 180°): fully open and up to 200 mm high and 30 mm wide.
- Operating speed: 7 000 to 17 000 rpm.
- Coated with a neutron absorber.

Design

The disks have been fully modelled by finite element analysis in order to define the optimum profile, taking into consideration the stresses, the link to the motor shaft and the required overspeed testing. Prototypes have been designed, manufactured and tested in order to validate the different concepts. Meeting the functional specifications (see insert above) is a technological challenge even when using a very sophisticated high strength aluminium alloy (7000 family). The angular opening of the windows results in stress concentration at their narrowest point, i.e. at the point where the windows connect to the full disk. The actual design problem consists in limiting the stresses in this area as much as possible. We solved this by :

- optimising the thickness profile (figure 1a and figure 1b)

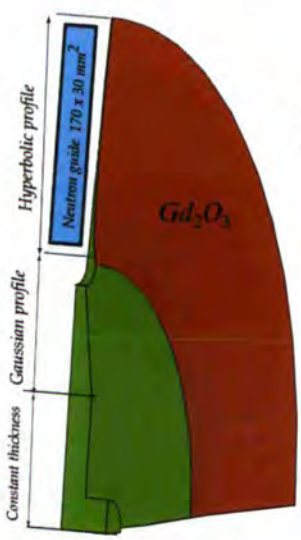

Figure 1a: Thickness profile optimisation (Disks 1 and 2).

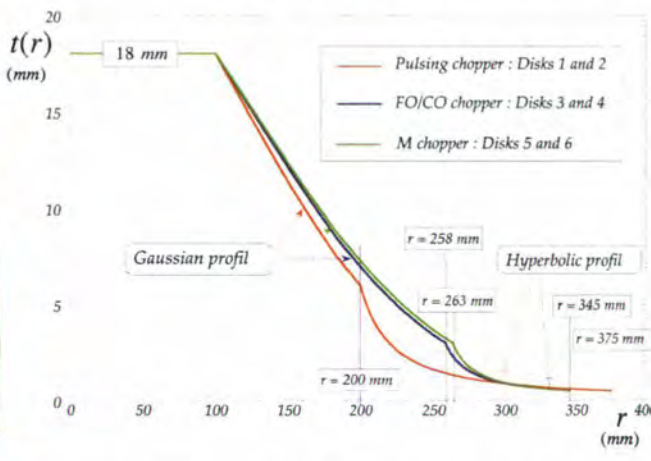

Figure 1b: Thickness profile t(r) of the disks.

Photo 1: 200 mm high window on a P disk.

- using the traditional technique of self hardening.

The principle involved in crossing the elastic limit via controlled overspeed runs in this very local area, to obtain a permanent strain ($\varepsilon_{plastic} > 0$) and in consequence a preconstrained state ($\varepsilon_{residual} < 0$) at zero speed (figure 2). Each of the 3 disk families has its own hardening protocol depending on window shape. To prevent any destructive unbalance, the steel motor shaft and aluminium disks must stay in contact whatever the speed, despite the different stiffness of

Photo 2: Marc Locatelli and one of the FO/CO disks.

the two materials. We achieved this by applying the principles schematically outlined in figure 3. The disk is fixed to the shaft by means of a central screw and a centering shoulder designed to prevent any play between the two pieces; this results in excellent stability during operation.

Manufacturing and testing

The manufacture of the disks is no trivial affair. Tolerances are extremely tight for such a large object. The disks were manufactured to specification on a conventional vertical lathe at YVES SANTI, Annecy, France, according to a protocol defined in close collaboration with the ILL.

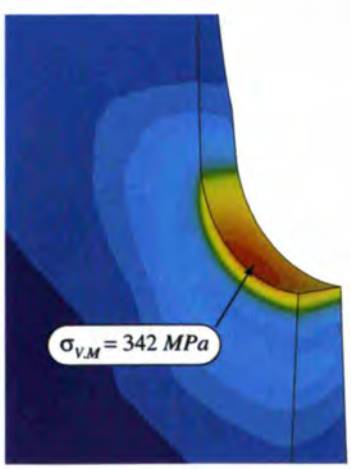

Figure 2: Residual Von-Mises stresses (in compression) at 0 rpm after a hardening overspeed at 21000 rpm (Disks 1 and 2).

Technical specifications

- The disks are made of one of the best high strength aluminium alloys available (yield strength σ_{YS} = 500 Mpa), chosen for its resistance and stability during machining.
- Mass: about 12 kg per disk, thickness at the periphery of the disks: only 1 millimeter.
- The tolerances asked for are : Concentricities within 0.01 mm - Centering on the shaft within 5 µm - Parallelism between the two faces within 0.02 mm.- Warping less than 1 mm.
- The disks are balanced according to G1 level (*residual unbalance ≈ 10 g.mm*).

These extremely tight manufacturing tolerances are crucial for the perfect reliability of the choppers over the long-term.

The disk profile follows exactly the curve determined by calculation. After manufacture the disks were balanced and hardened at the ILL using a dedicated test jig[1]. During the controlled overspeed operation (between 21000 and 24000 rpm depending on the disk family) we exceeded the yield limit at the bottom of the windows thus creating the desired pre-constrained state. The disks were then dismounted and sent to SICN in Annecy who were responsible for the neutron absorber coating. The neutron absorber is a Gd_2O_3 layer about 0.15 mm thick, deposited by plasma projection. Both faces are coated to maintain the mirror plane of the disk.

The ILL had carried out preliminary tests at SICN to determine the coating procedure with the best adhesion. The special gadolinium powder used is made at the CEREM in Grenoble according to ILL's specifications. Finally the disks were remounted on ILL's test jig to be balanced and spun at the nominal speed of 17000 rpm before shipping to FZ Jülich. ■

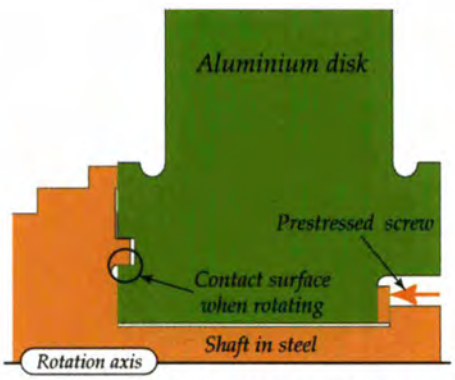

Figure 3: Interface between the disk and its shaft.

Photo 3: Claude Gomez and Ian Sutton with one of the Pulsing disks (ø = 750 mm) mounted on the ILL's test jig[1].

Project team

- Project manager: **ILL** (H. Casalta, H. Schober and J. Ollivier)
- Technical coordination: **ILL** (M. Thomas and P. Malbert)
- Design and finite element analysis of the disks: **ILL** (M. Thomas)
- Interface with the shaft: **ILL** (M. Thomas, M. Locatelli) and **TMM**, Germany
- Manufacturing drawings: **ILL** (I. Sutton/M. Locatelli)
- Manufacturing: **Y SANTI**, Annecy
- Gd_2O_3 coating: **CEREM** Grenoble, **SICN** Annecy (processes defined in collaboration with the ILL)
- Design and calculation of the test jig: **ILL** (P. Malbert, M. Locatelli, I. Sutton)
- Balancing and self hardening of the disks: **ILL** (C.Gomez, M. Locatelli, P. Thomas)

(1) The test jig (Photo 3) is based on high speed ceramic bearings from SNFA and a powerful brushless motor from PARVEX. It can spin disks up to 800 mm in diameter at 28000 rpm. For safety reasons it operates in a special casemate also designed at the ILL.

"Bending" gamma rays: high resolution index of refraction measurements at short wavelengths

M.S. Dewey, A. Henins and E.G. Kessler, Jr (NIST, Gaithersburg)

H.G. Börner, M. Jentschel and P. Mutti (ILL)

C. Petrillo and F. Sacchetti (University of Perugia)

Theoretical calculations of the index of refraction of light in matter differ in their predictions of the high-energy limit. In order to help resolve these differences, we are using the GAMS4 double crystal gamma ray spectrometer to measure the index of refraction of 184 keV gamma rays in silicon by measuring the deflection that occurs when gamma rays pass into and out of a wedge-shaped silicon artifact. No other facility in the world brings together the prerequisites for a measurement such as this one, namely an extremely intense source of gamma rays and an ultra-high resolution spectrometer. A movable collimator allows us to record deflected and undeflected rocking curves simultaneously thereby greatly reducing our sensitivity to small angular drifts.

Snell's law specifies the change in direction that electromagnetic radiation undertakes when it passes from one medium into another in terms of the index of refraction n of the materials. An example familiar to everyone is the way in which visible light bends when it passes from air ($n \sim 1$) into water ($n \sim 1.33$). Theoretical descriptions of the index of refraction differ in their predictions of the high-energy limit [1, 2]. These differences are thought to be due to the way in which relativistic contributions are included.

From the above it is apparent that accurate experimental measurements of the high-energy limit of n are needed to test the various theoretical descriptions, and that one way to do this would be to measure the angular deflection of gamma rays as they pass into and out of some material. At gamma ray energies the index of refraction is close to but slightly less than one and the angular deflections are very small. For a prism-shaped sample of silicon whose apex angle is 160 degrees (figure 1), and radiation of 184 keV, the angular deflection that occurs when radiation enters parallel to the base of the prism is 161 nrad. The accuracy required on $1 - n$ for a sensitive test is ~ 0.1%, which means that the angular deflection must be measured to ~ 0.2 nrad.

The GAMS4 double crystal gamma ray spectrometer with its high angular resolution is uniquely suited for this type of measurement [3]. Recently we have begun to carry out this measurement in silicon by placing the device shown in figure 1 between the two diffracting axes of GAMS4. A similar technique has been used for measurements in silicon at much lower energies [4]. In our case an intense beam of 184 keV gamma rays produced in the reaction $^{167}\mathrm{Er}(n,\gamma)^{168}\mathrm{Er}$ passes through an entrance collimator, is deflected slightly as it passes through a silicon prism, and then passes through the exit collimator (figure 1). The gamma ray beam is roughly twice the height of the prism. The height above the floor of the

Figure 1: Photograph of the apparatus used to measure the index of refraction. The silicon prism has an apex angle of 160 degrees and sits on top of a precision indexing table that can be rotated in one degree steps. Lead collimators on both ends of the prism define the incident gamma ray beam in the horizontal direction.

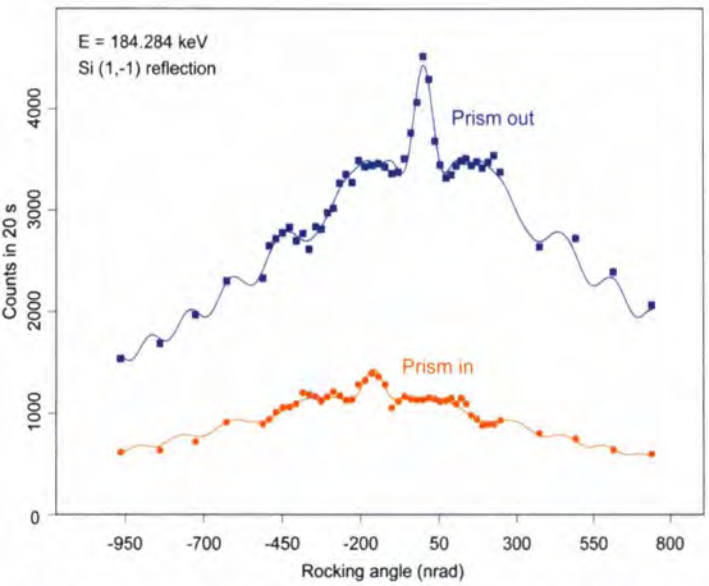

Figure 2: Prism-out and prism-in reflexes. The spectrometer was tuned to 184.284 keV and a (1,-1) reflection. At these energies there is significant absorption of the radiation in the prism-in configuration. The lineshapes show pronounced oscillatory behaviour with a narrow peak in the center. This is caused by interference effects of gamma rays in GAMS4's nearly perfect diffracting crystals analogous to a two slit interference pattern. Their existence has nothing to do with the index of refraction apparatus.

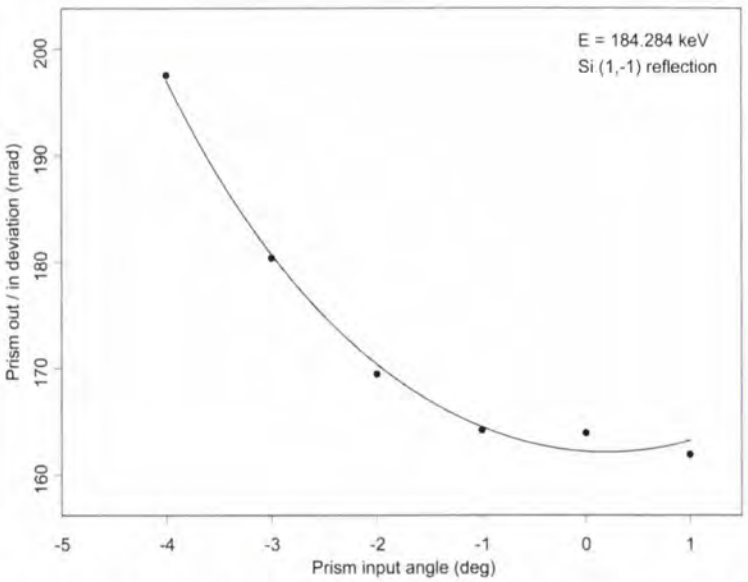

Figure 3: Difference between the prism-in and prism-out centroids as a function of the input angle of the prism. A fit to this curve yields the index of refraction and the input angle offset.

prism is arranged so that half of the beam goes through the prism while the other half misses it. A movable collimator containing two holes (not shown in the figure) sits between the prism and the gamma ray detector. It can be used to select either the undeflected or deflected beams. In the usual fashion, one axis of GAMS4 is rotated in order to obtain a rocking curve (for this experiment GAMS4 is tuned to a narrow reflection to maximise the resolution). At each rotation angle, counts are accumulated for each of the two states of the movable collimator. Thus a pair of rocking curves, one having been deflected and attenuated by the prism and the other not, are simultaneously acquired minimising sensitivity to small angular drifts (figure 2). The fitted centroid differences constitute our data.

The magnitude of the observed angular deflection depends on the wavelength-dependent index of refraction of silicon, the apex angle of the prism, and the input angle of the gamma ray beam. The apex angle can be measured accurately offline, but the other two quantities are more easily obtained in a fit to angular deflection versus input angle. In order to vary the unknown input angle in a precise way, the prism is mounted on a precision indexing table. The indexing table allows the prism to be rotated in one degree steps. The results of these measurements are shown in figure 3. Each point in this graph represents 16–42 paired scans taken over several days. The accuracy obtained on $1 - n$ from a fit to these data was 0.36%.

We have demonstrated the feasibility of this technique for measuring the index of refraction of gamma rays in materials such as silicon. Additional data will be needed to reduce the error to the 0.1% level. Our most important systematic uncertainty is due to a nonzero centroid difference that occurs between the two beams even when the prism is absent. It comes about because the GAMS4 diffracting crystals are not perfect. This difference, or offset, can be measured by carrying out similar measurements with the prism device removed. No other facility in the world brings together an extremely intense source of gamma rays and an ultra-high resolution spectrometer, making this the only place where such measurements can be done. We hope to use this technique to measure n at still shorter wavelengths and in other materials such as germanium where the experimental data are intriguing. ■

References

[1] D.T. Cromer and D. Liberman, J. Chem. Phys. 53 (1970) 1891 • [2] D.Y. Smith, Phys. Rev. A 35 (1987) 3381 • [3] E.G. Kessler, Jr., et al., Nucl. Instr. Meth. A457 (2001) 187 • [4] M. Deutsch and M. Hart, Phys. Rev. B 30 (1984) 640, Phys. Rev B 30 (1984) 643.

Ultra-cold neutrons at PF1:
creation and detection of "superthermal" UCN for a new generation neutron Electric Dipole Moment experiment

- C.A. Baker, K. Green, M.G.D. van der Grinten, P.S. Iaydjiev and S.N. Ivanov (Rutherford Appleton Laboratory, Chilton)
- J.M. Pendlebury, D.B. Shiers and M.A.H. Tucker (University of Sussex)
- H. Yoshiki (University of Kure)
- J. Butterworth and P. Geltenbort (ILL)

At PF1 ultra-cold neutrons (UCN) have been produced by means of a superthermal UCN source and have been detected in situ by a cryogenic neutron detector system specially developed to operate within superfluid helium. These results form a very successful start of a programme developing a new generation electric dipole moment (EDM) experiment that will require a high intensity UCN source at ILL.

PF2 is the world's most intensive UCN source and it is feeding the world's most sensitive EDM experiment. The EDM experiment, developed by the RAL/Sussex/ILL group, is currently probing many of the favoured theories for physics beyond the Standard Model [1]. The value of the neutron EDM is of great importance for particle physics and cosmology because of its direct bearing on the baryon asymmetry of the universe: why does the universe have more matter than anti-matter? Future progress in this area of physics will require significant changes in the techniques used to measure the neutron EDM. In particular it will require the development of new UCN sources and it requires a new generation of detectors capable of detecting UCN within superfluid helium. The work carried out in spring 2001 was aimed at this and was extremely successful in both: we have now produced UCN at the H53 PF1 beamline by downscattering cold neutrons in superfluid helium and also we have now cryogenic UCN detectors operational at temperatures of 430 mK.

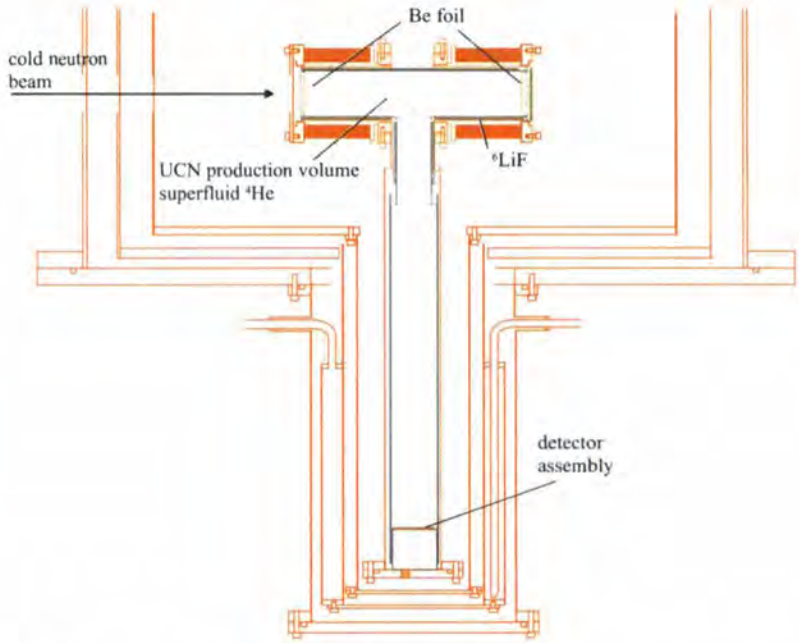

Figure 1: The UCN production and detection volume in the cryostat.

Experimental set-up and techniques

The UCN production in a superthermal source relies on the downscattering of cold neutrons to UCN energies by phonon and roton interaction with superfluid helium [2,3]. The cryostat used is part of a prototype cryogenic EDM apparatus, originally manufactured and assembled in Japan, but which has been modified to house a UCN production volume and storage cell containing 1.2 litres of isotopically pure ^{4}He at 0.5 K. Figure 1 shows the production and detection volume in the cryostat. The isotopically pure ^{4}He is made within the cryostat by forced flow through a super-leak. The cold neutrons are downscattered to UCN energies and pass, after storage in the beryllium coated horizontal guide section, through a small aperture in the guide and fall under gravity into a UCN detection system operating within superfluid helium. This *in situ* UCN detection is a tremendous improvement compared with techniques employed in the past where UCN were extracted from the helium, suffered from massive attenuation losses, and were then detected at room temperature outside the superthermal production region.

The detectors consist of solid-state silicon devices detecting the energy deposited by the charged particle reactants from the interaction of neutrons with ^{6}Li ($n + {}^6Li \rightarrow \alpha + {}^3H$).

The ^{6}Li atoms are contained in a thin converter film placed at the active surface of the silicon diodes. This reaction has an extremely large cross section (300 kb) at UCN energy and results in a neutron conversion efficiency approaching 100% with very thin conversion layers. A 2500 Å aluminium layer has been deposited directly onto the detector surface on top of which a layer of 600 µg/cm^2 of ^{6}LiF has been deposited. The 2500 Å aluminium layer has been used to improve the adhesion of the ^{6}LiF to the detector. A protective layer of 50 Å of aluminium has been evaporated on top of the ^{6}LiF. This converter configuration has been applied to various solid state detectors and has been proven to be efficient and stable [4]. These detectors have been mounted onto an assembly and placed in the cryostat within the liquid helium. Figure 2 shows the solid state silicon detector with the converter layer. The signal from the detectors is lead to a preamplifier situated outside the cryostat at room temperature.

Results and conclusions

The experiment was run in pulsed mode, with the beam on for 40 s and then shut off for the next 70 s. This cycle was repeated many times and the counts in the cryogenic neutron detectors recorded as a function of time. The detectors show a clean triton signal well separated from the noise. The detectors have been operating within the superfluid helium for a period of 30 days. At no moment the detectors have showed any sign of degradation. Figure 3 shows the number of detected neutrons at two temperatures: with the superfluid helium at a temperature of 430 mK and at 2.03 K. The figure shows that as the cold neutron beam passes through the superfluid helium in the cryostat, not only neutrons are scattered in the liquid helium but there is build-up of neutron counts as UCN are produced and stored within the liquid helium. When the incident beam is turned off at 40 s the signal from the scattered neutrons disappears and UCN leaving the storage cell are detected. At a temperature of 2.03 K a similar rate of scattered neutrons is seen but there is no built up of counts and no UCN are stored as they are immediately lost by upscattering from the helium. The normalised UCN production at base temperature is measured in this experiment to be considerably in excess of what one would expect for UCN production from the main production channel only *i.e.* single phonon emission from 8.9 Å neutrons.

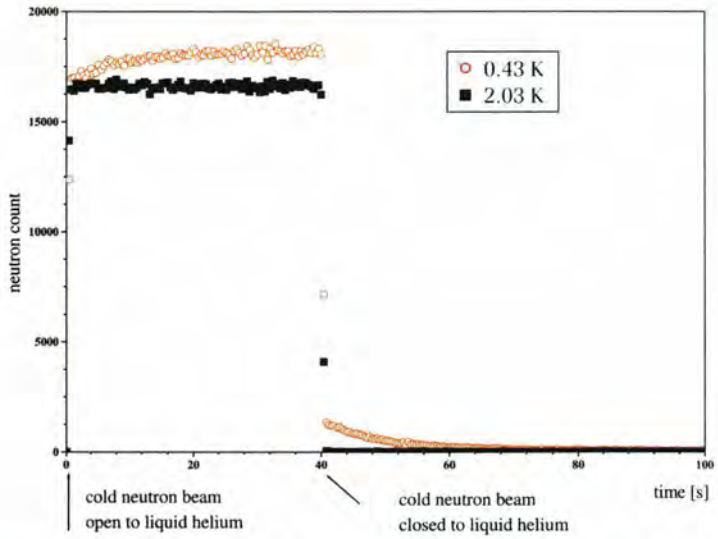

Figure 3: UCN build-up in superfluid helium (0.43 K) as the production volume is open to the cold neutron beam, and emptying of the production chamber after closing the cold neutron beam. At higher temperatures (2.03 K) UCN are immediately lost by upscattering in the helium.

Figure 2: The solid state silicon detector with its ^{6}LiF converter layer deposited directly to the active surface. The detector assembly has been operating within superfluid helium at temperatures of 430 mK.

In conclusion one can say that we have taken an important step in producing a new high-intensity UCN source for a new generation EDM experiment at the ILL. We have developed cryogenic UCN detectors that play a crucial role in this R&D phase of the project and these will continue to play a key role in the design of the new generation experiment. ■

References

[1] P.G. Harris, C.A. Baker, K. Green, P. Iaydjiev, S.N. Ivanov, D.J.R May, J.M. Pendlebury, D. Shiers, K.F. Smith, M. van der Grinten and P. Geltenbort, A New Experimental Limit on the Electric Dipole Moment of the Neutron, Phys. Rev. Lett. 82, 904 (1999) • [2] R. Golub and J.M. Pendlebury, Phys. Lett. 50A, 337 (1977) • [3] H. Yoshiki, K. Sakai, M. Ogura, T. Kawai, Y. Masuda, T. Nakajima, T. Takayama, S. Tanaka and A. Yamaguchi, Phys. Rev. Lett. 68 (1992),1323 • [4] C.A. Baker, K. Green, M.G.D. van der Grinten, P. Geltenbort, P.S. Iaydjiev, S.N. Ivanov, P.G. Harris, J.M. Pendlebury and D.B. Shiers. Accepted by Nucl. Instr. Meth . (2002).

GEORGE: dynamic experiment control at the ILL

D. RICHARD (ILL)

Instrument control on most ILL instruments involves a software called MAD driving instrument set-up and data acquisition. Predefined sequences of scans based on empirically determined counting times can be executed as a batch job, enabling instruments to run autonomously over long periods of time. In a recent development, an interface has been created between MAD and IDL, a powerful Fortran-like computing language with comprehensive graphics and interface-building routines, allowing instrument control parameters to be calculated from data analysis and passed to the instrument control program. In this way, counting times can be optimised on data quality criteria, and instrument parameters such as resolution or sample temperature can be calculated and set according to a search algorithm. The IDL program, in which scientists can develop intelligent control routines, is called GEORGE – General Experiment, Organisation, Response and Guidance Executive. By exporting data snapshots and instrument parameters to the BARNS web server, flexible data visualisation is available from any web browser and also personal communication devices such as mobile, WAP telephones.

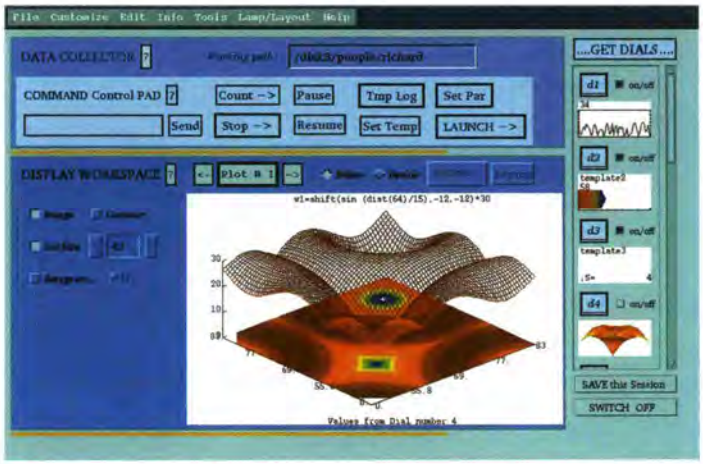

Figure 1: The graphical user interface of GEORGE showing the central display window, the small dial displays on the right and the PAD.

Neutron scattering is generally regarded as a low flux experimental technique, counting times traditionally ranging from hours to days, so that scientists could always arrange to be at the instrument at critical times with respect to directing the experimental investigation. Since the restart of the reactor in 1995 instruments and neutron guides have been and are being upgraded with a view to maximising the use of the ILL neutron flux by increasing counting rates, allowing shorter counting times and the detection of weaker scattering. One aspect of this policy of "maximising the use of ILL neutrons" is optimising counting times and experimental strategies. When counting times become of the order of the time required to initialise each scan (for example change temperature) considerable gains are to be made by counting on statistics and not on time. Directly in measured data, "statistics" means signal-to-noise ratio, but the physical quantities of interest are the parameters extracted by fitting the data, in which case "statistics" means the standard deviations of the refined parameters. In both cases, data analysis must be performed on-line, during the measurement, and a decision must be made to stop the scan and set new experimental variables (such as sample temperature). Dynamic or intelligent experiment control is defined here as decision making and implementation as a result of on-line data analysis.

On most instruments at ILL, instrument control software called MAD, running on UNIX work-stations, determines the instrument set-up and controls data acquisition. Each scan requires manually entering the parameters for set-up and acquisition and series of scans can be programmed in a batch file. For intelligent experiment control, two functions are missing from this kind of batch file, conditional flow (if no measurable signal then change the set-up) and passing parameters calculated on-line. Calculated instrument parameters are determined from data analysis and this requires a high-level computing language, which enable large data arrays to be manipulated easily and rapidly. Traditionally, such programs would be Fortran or C, but these have been complemented in the scientific computing domain by languages such as Matlab and IDL, which combine numerical and graphics routines with interface-building tools. With a view to developing intelligent experiment control, a MAD-IDL interface has

been created on the instruments, allowing IDL programs to communicate with MAD. Data visualisation and analysis can be performed on many instruments using the IDL-based, Large Array Manipulation Program called LAMP. All ILL data can be read and visualised in LAMP, data analysis is performed by writing macros in the Fortran-like language and a large number of macros now exist for different applications. For intelligent experiment control, the interface GEORGE (figure 1) has been developed from LAMP, offering scientists a familiar environment and access to the existing LAMP macros. In addition GEORGE allows for a new kind of macro, called a DIAL, which communicates with MAD using a library of 11 functions (figure 2). A dial has particular attributes, notably a frequency, which determines for example how often data is retrieved from MAD, and allows many dials to run simultaneously. Dial output is either text or a bitmap image, which is displayed in the small dial windows or in the central display window. Another feature of the GEORGE interface is the PAD, allowing direct, format-free execution of those MAD commands that the instrument scientist makes available to the user. In addition to multiple measurement scans, the ability to perform a sequence of scans is useful for setting-up the instrument, particularly where a number of non-independent rocking curves have to be measured (for example in monochromator alignment).

An internal dial in GEORGE can also be run, which exports the output of all operating dials to the web server BARNS [1], where html pages are created with a JAVA module. By connecting to BARNS with Netscape or Internet Explorer, the current state of the data acquisition can be seen, refreshed at the frequency of the dials. By giving the same password as that entered on the instrument control computer, dials can be stopped and new dials started, allowing flexibility in remote monitoring – visualisation is not limited to those dials started while at the instrument. Finally WML cards can also be exported from the web server, which can be visualised on WAP devices such as portable telephones.

Currently GEORGE can be run on the instruments D7, D17, D20 and D22 and it is being developed for the time-of-flight spectrometers IN5 and IN6. GEORGE is an IDL module, which is independent of the instrument control software. The software can be obtained as part of the LAMP distribution (see ftp://ftp.ill.fr/pub/cs/).

Acknowledgements

The MAD-IDL interface was designed in a joint project involving Franck Cecillon of the Instrument Control service (SCI) and Anita Schober from Computing for Science. We are grateful to Daniel Erb of the informatics service (SI) for his assistance in maintaining the BARNS web-server. ■

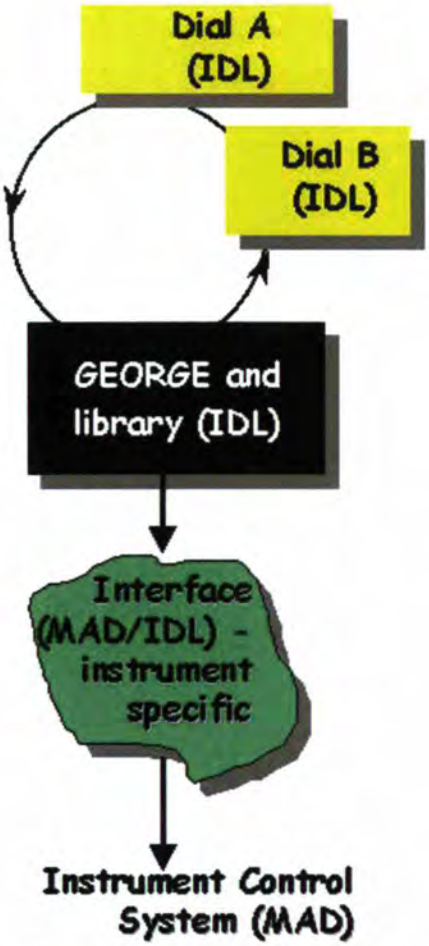

Figure 2: Schema illustrating the communication between dials in GEORGE and the instrument control program.

Figure 3: (a) The web-browser interface of GEORGE and (b) a dial output image as viewed on a portable telephone.

(1) (Web) GEORGE is one of many applications running on the web-server BARNS (http://barns.ill.fr). ILL data recovery, visualisation and treatment software is available on BARNS, enabling scientists to finish data analysis via the web, without downloading and compiling programs locally.

GRAS$_{ans}$P: Graphical Reduction and Analysis SANS Program

C.D. DEWHURST (ILL)

A new suite of software for the analysis of small-angle neutron scattering (SANS) multidetector data has been developed. The Graphical Reduction and Analysis SANS Program, GRAS$_{ans}$P, is designed for use with the SANS instruments D22 and D11, the small-angle diffractometer D16, together with the possibility of treating data from SANS or multidetector-based instruments at other neutron sources. Developed and running as a script language under Matlab™, an already comprehensive suite of data inspection and analysis tools can be enhanced or customised with the addition of 'User Modules' and 'Fitting Functions'. Compiled versions for several computing platforms allow the main GRAS$_{ans}$P package to be distributed as stand-alone and licence-free software. GRAS$_{ans}$P offers an easy access to analysis and display of SANS data via a modern style graphical user interface (GUI).

Modern GUI based packages such as Matlab™ and IDL™ offer a high-level computing language complete with easy matrix manipulation, comprehensive graphics and interface building routines [1]. Both Matlab™ and IDL™ programs are able to be compiled into stand-alone, licence-free, runtime code and are commonly used within the ILL. In this paper a new software package, *GRAS$_{ans}$P*, is presented developed using Matlab™ and designed for the graphical inspection, reduction and analysis of multi-detector data produced by SANS instruments [2,3].

The main *GRAS$_{ans}$P* GUI is shown in figure 1. The main interface shows the display of 2D multidetector data with the displayed image properties controlled by a panel at the right-hand side or from tool-bar or main-menu items. Data entry into *GRAS$_{ans}$P* and control over the displayed scattering data and background subtractions is achieved using the data-selectors below the main display. The data-selectors allow access to a large array of workspace storage areas indexed by Worksheet: Number: Depth; in a sense, a three-dimensional array of 2D

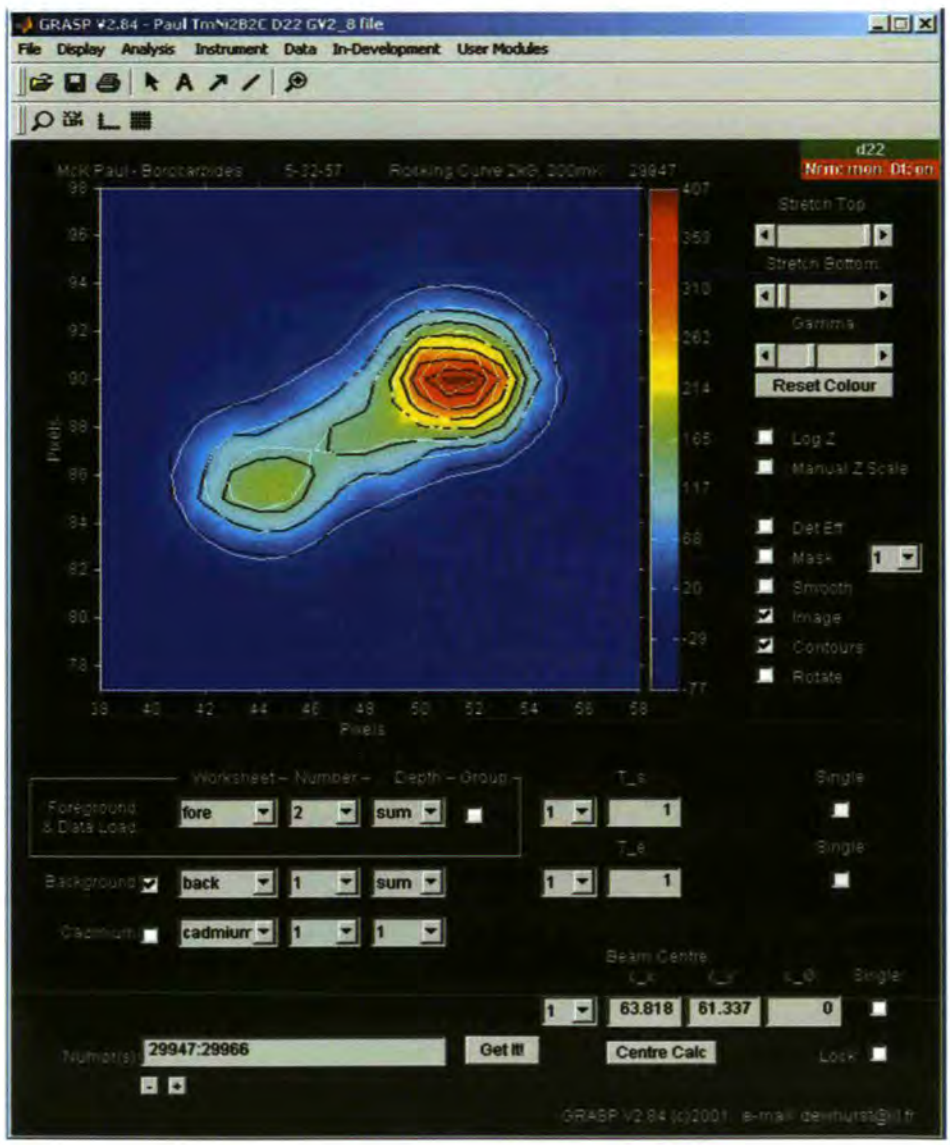

Figure 1: The main *GRAS$_{ans}$P* interface showing the main display window, displayed image control panel, data selectors and load control. Dropdown menus allow access to the numerous multidetector analysis tools, project, data, instrument, program options and controls.

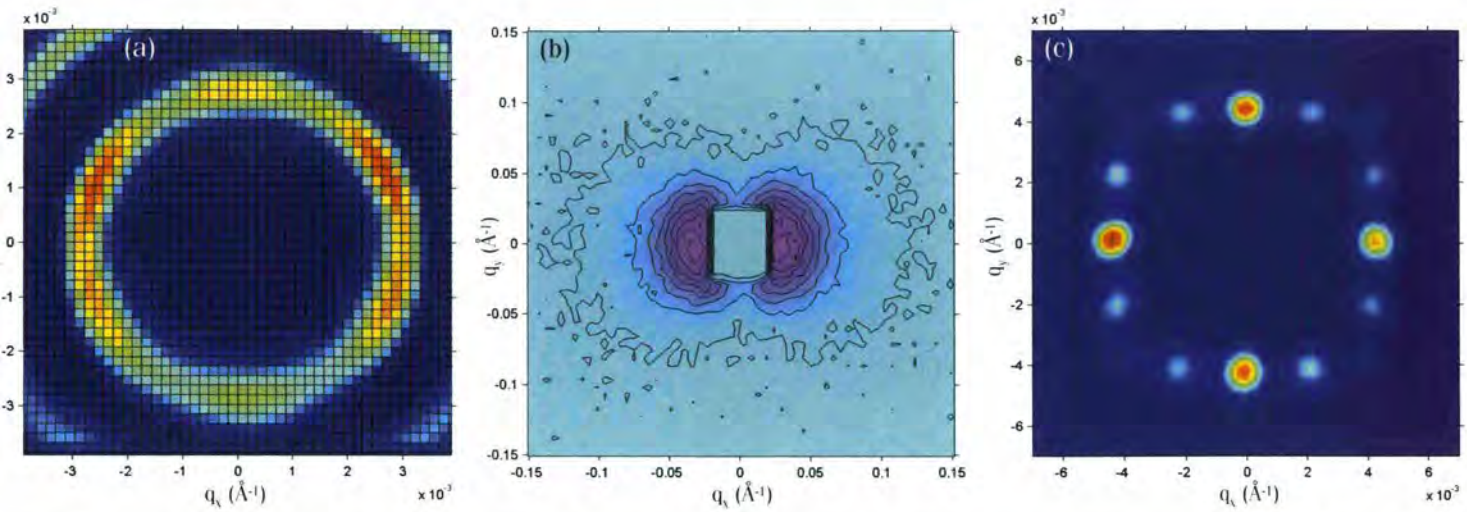

Figure 2: Example data treated, analysed and output using *GRAS$_{ans}$P*. (a) Colloidal crystals (Hellweg et al., D11). (b) Magnetised metallic ribbon (Badurek et al., D11). (c) Vortex lattice (Levett et al., D22).

data storage. The 'worksheet' and 'number' area allows several storage areas for generic classes of data such as foregrounds, backgrounds, transmission measurements etc. The 'depth' property allows many individual data files, for example on the same sample but with varying experimental conditions, to be collected together but stored separately under a single worksheet number. Whole sequences of data comprising a larger measurement can hence be analysed easily as a function data file or a changing sample environment parameter (e.g. temperature, magnetic field, sample angle etc.). Cross-referencing of selected areas of the multidetector data (e.g. intensities within boxes, strips, sectors, cuts at constant q, or 2D curve fit parameters) through a sequence of data files is one of the key features of *GRAS$_{ans}$P*. Examples of 2D anisotropic data corrected, analysed and graphically exported using *GRAS$_{ans}$P* are shown in figure 2. In figure 2(a) scattering from colloidal crystals shows a quasi-ordered hexagonal lattice structure. Analysis here might proceed by extracting an average I vs. $|q|$ or I vs. ψ (angle around the detector) about selected sectors or annuli of detector pixels using the Sectors and Averaging tools from the Analysis menu items. In figure 2(b) SANS from a magnetised ferromagnetic ribbon shows an approximately cosine-squared variation in I vs. ψ due to the absence of magnetic scattering for directions with a component of q parallel to the magnetisation direction (vertical). Individual fits to I vs. ψ as a function of $|q|$ could be performed manually using the Sector and Averaging tools. *GRAS$_{ans}$P*'s Ancos^2 [4] procedure separates non-magnetic from magnetic scattering and gives the cos^2 phase (magnetisation direction) as a function of $|q|$. In figure 2(c) sharp Bragg peaks from the magnetic vortex lattice in a superconducting sample are shown. Rocking curves, I vs. θ (sample angle), of a particular Bragg peak can be extracted from a sequence of measurements, collected together in the *GRAS$_{ans}$P* worksheet areas, using the Box and Sector tools. The 2D Curve Fitting option allows multiple functions to be fitted to the background corrected multidetector data (figure 1 main display). These are just examples of the kinds of analysis, data and graphics output that can be performed using *GRAS$_{ans}$P*.

GRAS$_{ans}$P currently accepts data from the ILL instruments D22, D11 and D16 as well as SANS data from SINQ, PSI in both uncompressed and compressed formats. Addition of data-read modules for other sources of SANS or multidetector data that could benefit from the treatment and analysis procedures offered by *GRAS$_{ans}$P* are envisaged or could be developed upon request.

GRAS$_{ans}$P 'm-code' (script) will work on any of the platforms supported by Matlab™ including PC windows, Linux, SGI and HP and Digital Unix [1]. We can currently provide compiled run-time versions for PC windows, Linux and SGI. Further information, software and manual download can be found on the ILL web site [2].

Acknowledgements

The existing suite of ILL SANS software created and maintained by Ron Ghosh (ILL) and co-workers has served as a benchmark standard during testing of *GRAS$_{ans}$P* [4]. Don McK Paul (Univ. Warwick) provided the initial impetus and highlighted the requirement for a graphical software package tailored for anisotropic or diffraction-based SANS measurements. Bob Cubitt, Giovanna Fragneto, Simon Levett, Ross Stewart and Johannes Zipfel (ILL) have carried out further testing and gathering of user feedback. ■

References

[1] "The Mathworks: Matlab" web site: www.mathworks.com • [2] "GRASansP" web site: www.ill.fr/lss/grasp/ • [3] "GRASansP: Graphical Reduction and Analysis SANS Program for Matlab™", User Manual, C.D. Dewhurst, ILL (2001) • [4] "A Computing Guide for Small-Angle Scattering Experiments", R.E. Ghosh, S.U. Egelhaaf and A.R. Rennie, ILL98GH14T (2000).

Simulation of neutron guides and instruments by means of Monte-Carlo packages

E. Farhi and J. Ollivier (ILL)

J. Šaroun (Nuclear Physics Institute, Řež, Prague)

With the increasing complexity of modern neutron scattering instruments, the need for powerful tools to optimise their geometry and physical performances (flux, resolution, divergence, etc.) has become essential. As the usual analytical methods (phase-space theory...) may sometimes reach their limit of validity in the description of fine effects, the use of Monte-Carlo simulations, that can handle these effects, has become widespread.

The McStas and Restrax programs were initially developed at Risø National Laboratory and the Nuclear Physics Institute Řez respectively in order to provide neutron scattering instrument scientists with efficient and flexible tools for building Monte Carlo simulations of guides, neutron optics and instruments. They are now also maintained and developed at the Institut Laue-Langevin. To date, the McStas and Restrax packages have been extensively used at the ILL for various studies including cold and thermal guides with ballistic and super-mirror geometries, diffractometers, triple-axis, back-scattering, and time-of-flight spectrometers.

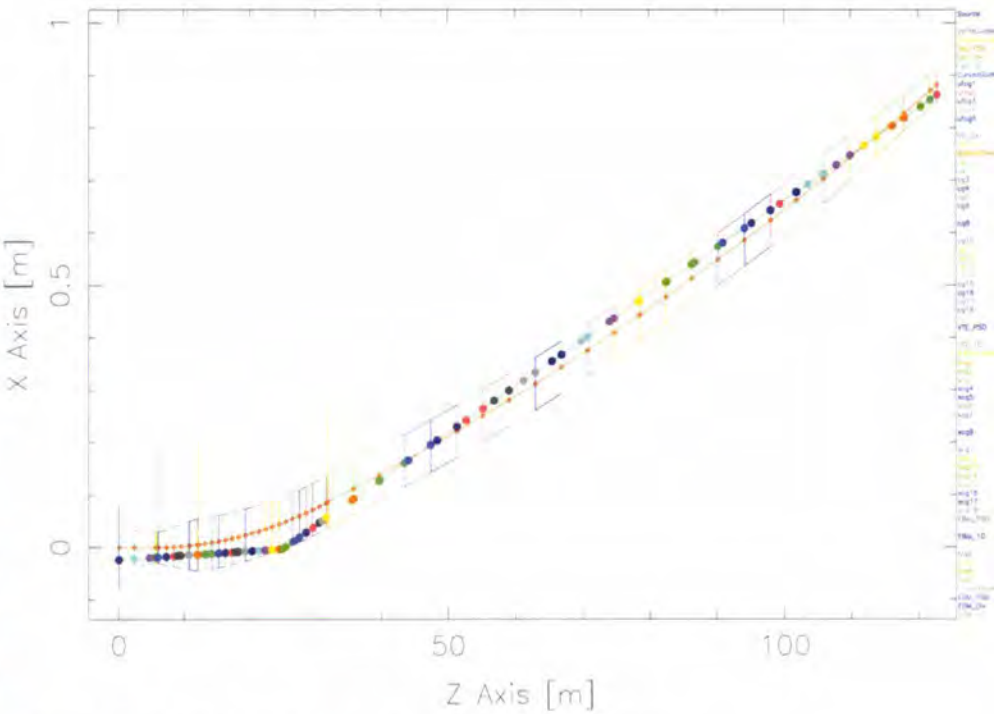

Figure 1: Top view of a curved ballisitic guide, showing a neutron trajectory.

It is a known fact that the neutron physicist always feels like increasing as far as the possible the available neutron flux reaching his instrument, in order to be able to perform original experiments. This can be done either by improving existing guide systems and instruments, or by building entirely new devices from scratch. Reasonable studies should then be carried out in order to estimate the new expected characteristics. The choice of the 'good' solution then usually comes from a careful compromise between the flux gain and the resolution. Other points such as the radiation and background levels, the financial cost, as well as the time and staff necessary to implement a solution, should also be estimated. Until recently, such studies were carried-out using analytical and numerical approximations of guides and instrument models [1]. Their efficiency is validated a posteriori by the mere existence of the high quality instruments installed on the available neutron sources world-wide. However, such methods can hardly describe fine effects resulting from the increasing complexity of all the elements composing existing and future guides and instruments. As a complement to the usual analytical methods, the Monte-Carlo method enables to simulate whole neutron systems from the source to the final detectors, and to compute all the beam characteristics at any point of the instrument (including phase-space diagrams as in [1,2]).

The *McStas* Monte-Carlo neutron ray-tracing program, initially developed at the Risø National Laboratory [3] as well as the *Restrax* program, developed at the ILL and the NPI [6], are now part of the daily tools used at the Institut Laue-Langevin for the design and optimisation of neutron devices [4]. Most existing guide systems installed in the main guide hall at ILL are now suffering from misalignment, dust and radiation damage. The annual capture flux measurements since 30 years show a continuous

decrease, now reaching about 30 %. This affects the 29 operational or commissioning main guide hall instruments. The renewal of the two guide systems H1 (cold) and H2 (thermal) has then become desirable. In the frame of the ILL Millennium programme, extensive guide simulations were performed with *McStas* and *Restrax* in order to find out the more suitable solution among super-mirror guides, wide guides and ballistic guides [5]. Furthermore, instrument models may then be positioned along and at the end of the simulation, in order to estimate the influence of the different geometries on the experimental measurements (flux, resolution...). Other constrains (moving older instruments, changing guide elements, necessary staff, cost of operations) must also be taken into account before decision.

In a *ballistic* geometry, the width of the guide is higher in some part of it, in order to lower the mean number of neutron reflections on side walls (figure 1). The resulting flux may be comparable to the one obtained with super-mirror coatings, and can range from a factor 2 up to a factor 5, depending on the instrument position, the wavelength and the guide peculiarities. Anyway, as most instruments hardly cope with large neutron beams, it is necessary to focus the guide output horizontally by means of a funnel. Unfortunately, the usage of such devices often creates unexpected beam shapes and degrades the effective resolution. Thus, ballistic geometries appear to be relevant for high flux/low resolution instruments, especially with focussing optics (e.g. bent monochromators and mirrors).

The new Strain Scanner and the VIVALDI Laue diffractometer will be installed soon at the end of the H22 thermal guide, next to the already existing D1A and D1B diffractometers. But the renewal of the guide elements with super-mirror coatings will affect differently each of these instruments, both in flux and in resolution. The delicate choice of the guide geometry and coatings was settled when looking at Monte-Carlo simulations carried out both with *McStas* [3,4] and ResTrax [6]. The figure 2 shows the simulated Laue pattern of an adrenaline crystal positioned in the VIVALDI sample chamber. Each diffraction spot takes into account the modelled resolution function, as shown for instance in the figure 3 for the simulated <222> YBa_2Cu_3O Bragg peak on the same instrument.

Thus, at the ILL, testing next generation guides and instruments within numerical models becomes part of their normal design process simultaneously with their physical and mechanical studies. ■

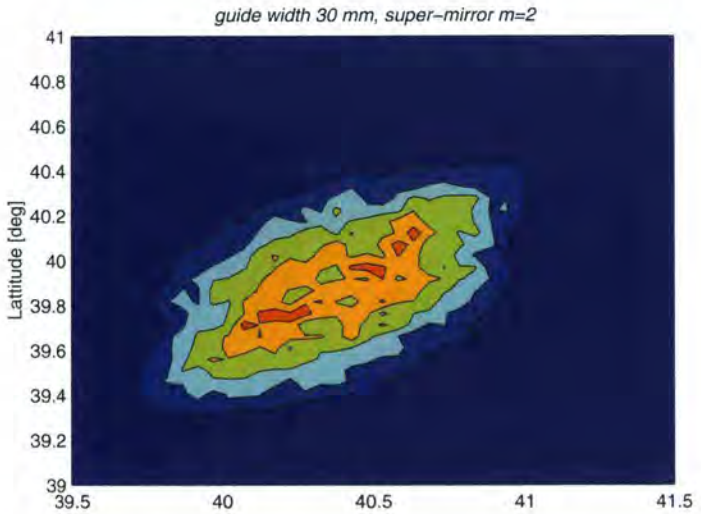

Figure 3: Simulated YBa_2Cu_3O <222> Bragg peak measured on the Vivaldi cylindrical detector at the end of the H22 thermal guide.

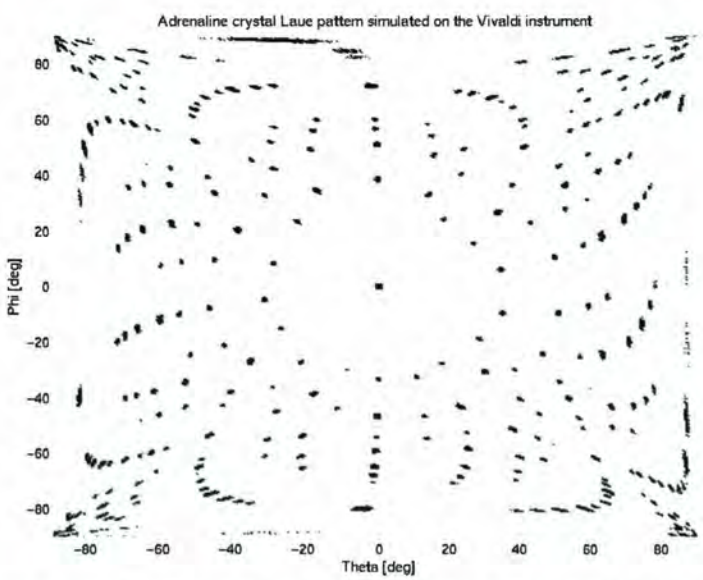

Figure 2: Simulated Adrenaline Laue Pattern (slightly misaligned) obtained at the end of the H22 guide on the Vivaldi instrument.

References

[1] D.F.R. Mildner, Nucl. Instr. Meth., A290 (1990) 189. See also J.R.D. Copley, J. Neutr. Research, 2 (1993) 21. • [2] L. D. Cussen, J. Appl. Cryst. 33 (2000) 1393. See also ibid p. 1399. • [3] K. Nielsen and K. Lefmann, Physica B, 283 (2000) 426. See also http://neutron.risoe.dk/mcstas/ • [4] See http://www.ill.fr/tas/mcstas/ and the McStas ILL internal reports therein. • [5] E. Farhi, T. Hansen, A. Wildes, R. Ghosh and K. Lefmann, J. Appl. Phys, in press. • [6] J. Saroun and J. Kulda, Physica B, 234 (1997) 1102. • See also http://omega.ujf.cas.cz/restrax/.

Teams teaming up

From the left: Christian Vettier, Efim Kats, Philippe Nozières, Paolo Carra and Bill Stirling during the Theory Group Open day, on 5 December. ▼

The BRISP Team (Brillouin Spectrometer, Italian CRG under construction) gathering during one of the project meetings. From the left: Anton Heidemann, Fabrizio Barocchi (University of Firenze); Francesco Sacchetti (University of Perugia), Caterina Petrillo (Politecnico of Milano), Sandro Jahn, Eddy Lelièvre-Berna, Fréderic Descamps, Eleonora Guarini (University of Firenze), Hannu Mutka, Ferdinando Formisano, Colin Carlile. ▼

▲ Seventeen of the ILL's PhD students during their second annual clip session, held on 6 December. It was aptly (and confidently!) entitled "We are the future".

The tenth anniversary of 'La Fête de la Science', the France-wide science festival, was held ▶ this year from the 15 to 21 October. Its objective is to make science accessible to everybody. From the left: Ingeborg Te Groen, Hubert Humblot, Alain Filhol, Isabelle Grillo and Andrew Wildes (the organiser) ready to welcome the visitors to the ILL stand.

workshops 2001

Workshops in which the ILL was a major player in 2001:

Protons in proteins	Organised by Peter Timmins (ILL) and Dean Myles (EMBL)	ILL and EMBL	25-27 January
Workshop on environmental studies using neutron and synchrotron radiation	Organised by Åke Kvick (ESRF), Alan Hewat (ILL), José Baruchel (ESRF), Peter Lindner (ILL), Anatoly Snigirev (ESRF), Jean Susini (ESRF)	ILL and ESRF	20-21 February
Perfect Crystal Neutron Optics (PECNO)-TMR	Organised by Matthias Baron (ILL) and Helmut Rauch (Atominstitut, Vienna)	ILL and Vienna	1-4 March
The ILL Millennium Symposium and European User Meeting	Organised by the ILL Direction	ILL	6-7 April
Collective Aid for Nomadic Small-Angle Scatterers	Organised by ILL, EMBL and ESRF	ILL, EMBL and ESRF	17-19 May
Colloquium in honour of Bruno Dorner	Organised by R. Currat and C. Vettier (ILL)	ILL	15 June
Self-Assembled Fibrillar Networks (in Chemistry, Physics and Biology)	Organised by Pierre Térech (CEA-CNRS, Grenoble) and Bruno Demé (ILL)	ILL	24-28 November
Workshop in honour of José Dianoux	Organised by C. Vettier and H. Schober (ILL)	ILL	6 December

Protons in proteins: biological applications of neutron diffraction

Hydrogen atoms are important in mediating biological structures and functions, but they are difficult to pinpoint in biological structures. A workshop organised by the ILL and the EMBL and co-sponsored by the EU Neutron Round Table was held in Grenoble to discuss how the complementary techniques of nuclear magnetic resonance (NMR) and neutron or X-ray protein crystallography can help in this respect.

On the first day a number of speakers discussed the role and particular achievements of neutron scattering in biology, stressing that neutrons should continue to focus upon important biological problems. Recent advances and applications using synchrotron X-ray crystallography and NMR were also described.

The new generation of neutron protein crystallography instrumentation was also reviewed in a dedicated session that highlighted the state of the art in neutron protein crystallography; this included LADI at the ILL, BIX-3 at JAERI and the newly completed TOF Laue diffractometer at LANSCE.

Talks in the afternoon focussed on low-resolution neutron crystallography, where contrast variation techniques have been used to locate detergent and lipid components in membrane proteins. A lively poster session was then followed by a conference dinner, during which many new theories were exposed on the powerful influence of protein/solvent interactions on biological systems.

The second day's agenda contrasted the use of X-rays and neutrons in the location of protons in proteins. A number of beautifully illustrated talks on enzyme structure emphasised that, even at atomic (1 Å) X-ray resolutions, crucial hydrogen atom positions often cannot be seen at all. For the enzyme endothiapepsin on the other hand it was shown that these problems can be resolved using neutron diffraction to locate hydrogen atom positions in the catalytic site. The final session saw the presentation of work at the frontier of X-ray and neutron protein crystallography.

A friendly discussion between Nobuo Niimura (JAERI), Joe Zaccai (IBS, Grenoble) and Don Caspar (University of Tallahassee, Florida).

The workshop finished with a round table chaired by Peter Lindley of the ESRF discussing the achievements and future prospects of neutron diffraction in biology. Key points to emerge were that:

- it is important to work on well-chosen important biological problems where neutrons can make unique or truly complementary contributions;
- such work should be more widely disseminated to the biology community;
- improved techniques and instrumentation were crucial to new (ESS & SNS) and upgraded neutron sources;
- the improvement in instrumentation and sample preparation facilities (e.g. for selective deuterium labelling) will bring solutions to hitherto intractable problems, in partially ordered systems, coherent inelastic scattering, protein crystallography, and small-angle neutron scattering for example.

A particularly exciting area to watch will be the complementary experiments with synchrotron radiation and neutrons on proteins which diffract to high resolution - it is already clear that, where some important parts of the structure are less well-ordered, neutrons will give unambiguous information on key H atoms.

In summary it was agreed that neutrons have played, and will continue to play, a significant role in structural biology, and that their complementarity with X-rays should be stressed and exploited.

ESRF/ILL workshop on environmental studies using neutron and synchrotron radiation

The ESRF and the ILL organised a joint Workshop on Environmental Studies on 20-21 February, attracting over 100 participants from Europe, the USA and Australia. These heard 19 invited lecturers and discussed a large selection of posters. Many of the lecturers had an opportunity to describe the practical importance of their work at a press conference attended by half a dozen journalists. The plenary lecture discussed new lithium-zeolites used for heavy-metal recovery from industrial and nuclear waste. It is now possible to study the crystal chemistry of these new materials using a combination of synchrotron and neutron diffraction techniques, including in-situ chemical synthesis.

Other speakers described neutron and X-ray structural research on the potential for developing the storage of hydrogen in metal alloys, thus improving the capacities of new lithium and NiMH batteries. Beautiful examples of real-time electro-chemistry in neutron and synchrotron beams were shown. An interesting application of electrochemistry, to thin film gas detectors was described. Neutron reflectometry is used to study the spatial distribution of material in the film used to selectively sense molecular species in the environment.

Diffraction measurements are also needed to understand the structure and stability of ice and clathrate materials under particular conditions. Antarctic ice apparently holds a record of changes to the earth's atmosphere over thousands of years, while clathrates (which remain stable under the pressure and temperature of the oceans' depths) may have the capacity to store waste carbon dioxide. Natural clathrates are also seen as a potential source of methane fuel.

A number of talks were given on the detection of heavy metals in geological formations, in water and in soil, using, for the most part, synchrotron methods. Participants were reminded how sensitive neutron activation analysis can be for detecting trace elements. It was agreed that the ILL is the best-placed neutron source to take up such work again. Finally a proposal was presented from the French CEA for the transmutation of nuclear waste using special reactors or accelerators; the mini-INCA experiment at ILL - designed to explore such possibilities - was described. Indeed it has been proposed that the new European Spallation Source might also operate as a nuclear waste incinerator.

Altogether a very enjoyable meeting at which the ESRF and ILL discovered that they were contributing more to the study and improvement of the environment than they might have imagined, confirming that they share not only a user community in common but a number of overlapping scientific interests as well.

Hervé Jobic (CNRS/IRC, Villeurbanne), Olivier Isnard (CNRS, Grenoble) and Gwenaëlle Rousse (ILL) enjoying the coffee break.

The ILL Millennium Symposium and european user meeting

About 320 participants attended the ILL Millennium Symposium and European User Meeting on 6 and 7 April in Grenoble. The objective of this initiative was to debate the future use of neutrons at the ILL and the relevance of neutron methods to emerging scientific and technological fields. Time was also devoted to the complementarity of neutron technology with other investigative techniques of similar potential, including X-ray technology, nuclear magnetic resonance, muon spectrometry, and microscopy techniques.

The Millennium Symposium was, most notably, an opportunity to present ILL's Millennium Programme, the ambitious pro-

gramme launched in January 2001 for the further development of ILL's instruments and infrastructure: No less significant however was the distribution to the participants of the "ILL Roadmap", a document produced by ILL management, serving as a springboard for discussion of the choices that have to be made on instrument development and the very future of the Institute.

Past and present directors of the ILL. From left to right: Brian Fender, Peter Day, Peter Schofield, Peter Armbruster, John Enderby, Ruprecht Haensel, Tasso Springer, Wolfgang Gläser, Bernard Jacrot, Jacques Joffrin, Alan Leadbetter, Reinhard Scherm, Dirk Dubbers, Christian Vettier and Colin Carlile

The two-day programme was very intensive, wide-ranging, and of high quality. The 7 plenary sessions covered a large span of subjects:

- the development of instrumentation at the ILL;
- the quantum many body problem in condensed matter physics;
- new challenges in structural biology;
- the role of neutrons in modern biology;
- fields of investigation with slow neutrons in nuclear and particle physics;
- the use of neutrons in chemistry at the molecular level;
- the key role of neutrons in soft condensed matter;

Beside the plenary talks, 40 oral presentations and more than 120 posters were organised in 6 parallel sessions: Life sciences, Supramolecular systems, Molecular systems, Electronic systems, Nuclei and Particles, Industrial relevance of neutrons, Instrumentation.

Time was found for two open-forum panel sessions where the audience was invited to express its views and comments on the organisation of the ILL and on future science at the Institute.

There was unanimous agreement on the success of the User Meeting and that the objectives of the symposium had been achieved. Our thanks to all those who helped to organise the event and contributed with enthusiasm to its success. The conference proceedings are available on the ILL web site (www.ill.fr, Events).

Serge Claisse – in charge of logistics at the ILL – between Colin Carlile (ILL Director, left) and Reinhard Scherm (PTB Braunschweig, right).

Perfect crystal neutron optics - TMR workshop

The 4th workshop of the TMR-European-Network on Perfect Crystal Neutron Optics (PECNO) was held at the ILL from 1 – 4 March 2001. PECNO is a network of 14 laboratories from 8 different countries co-ordinated by the Atominstitut der Österreichischen Universitäten, Vienna. The network was created early in 1997 and will end by the end of 2001. It receives 1.595 million euro in funding.

The aim of this network is to take the step from geometrical to quantum optics, with the neutron, as a probing particle, being treated as a quantum object rather than a classic particle. Using perfect crystals the wave function can be calculated throughout the system. The project seeks to optimise the use of existing neutron sources and prepare the ground for the full exploitation of more intense sources.

As the leading neutron research centre the ILL was a perfect choice of location for this workshop. Samuel Werner and Helmut Kaiser were special guests to the event. They opened the workshop with a report on the neutron interferometer programme in the United States. Berthold Georg Englert from the MPI Garching reviewed the wave-particle duality in neutron interferometry. The first morning was rounded off with a talk by Roland Gähler on spin-echo and coherence. The afternoon continued with reports from several participants on the performance of the new perfect-crystal ultra-small-angle cameras (USANS) currently installed on the ILL S18 instrument, on SINQ at Villingen, and at HMI Berlin, the NPI at Rez and the Atominstitut Vienna.

Another topic was the continuing development of the perfect-crystal neutron resonator sys-

The PECNO-TMR workshop participants assemble in front of the ILL.

tem, on which up to 4000 back-and-forth reflections and multiple beam storage have been achieved. This narrow-band neutron resonator could become an essential tool for advanced beam tailoring at new pulsed spallation sources.

Recent theoretical calculations were presented by the partners from Bari and Olomouc, which are likely to stimulate new experimental work. News was also given of the theoretical background and preparatory work for the first attempt at neutron phase tomography to be made in November 2001 on ILL's S18.

A visit of ILL's facilities and reactor hall was organised for those participants not yet familiar with the Institute. Further information on PECNO can be found on its homepage: http://www.ati.ac.at/~neutr-web/pecno/pecno.html.

Collective aid for nomadic small-angle scatterers

The "canSAS" meetings aim at promoting and sharing SAS data-analysis methods. The third workshop, sponsored by the ILL, ESRF and the DUBBLE-CRG, was held at the ILL on 17-19 May, with 30 participants from European and American facilities. Beam line responsibles and leading scientists reviewed data formatting problems with computer experts before moving on to consider packages for graphical data treatment and finally place the results obtained in the perspective of genuine scientific problems.

The disparity in data formats had triggered the first canSAS meeting and given rise to a text file format, sasCIF. Recent modifications added the meta-data required for time-of-flight neutron data, and at this meeting a document matching sasCIF names and NeXus names was welcomed and discussed in working groups. At the end of the presentations the participants acknowledged that both XML and HDF5 data formats offer widely acceptable standards for self-describing data formats for the future. It was agreed that illustrative examples would be presented to the community at the SAS2002 meeting in Venice.

Platform-independent packages for SAS analysis are based on a range of products. The GRASP procedure using MATLAB from ILL was welcomed as it can be distributed freely to users. Recent progress was presented on the integration of data acquisition and treatment, which is becoming more and more necessary given the complex measurements that can be attempted with the high fluxes available.

The scientific presentations revealed the variety of studies underway, from super-alloys to biological molecules in solution and rope. The participants discussed the possibilities of further sharing analysis programs and of teaching new users analytical methods.

The meeting concluded with a proposal to create a dedicated canSAS website as a repository of information and programs on the technique.

Colloquium in honour of Bruno Dorner

In May 2001 Bruno Dorner left the ILL, after nearly thirty years of activity in the Institute and a long and active career in neutron and X-ray scattering. Over 50 of his friends and colleagues gathered at the ILL's Chadwick Amphitheatre for an informal colloquium organised on 15 June in his honour. The meeting included invited presentations on Bruno's main field of research (phonons) and scientific or personal recollections by his friends and collaborators.

Bruno is best known for his contributions to the development of the neutron three-axis technique and, especially, for his pioneering work on resolution effects and instrumental efficiency (1972).

Bruno Dorner arriving for his leaving "pot".

Bruno was a pioneer in the field of neutron Brillouin scattering, for which he produced the first numerical estimates and test measurements (1967). He was also a leading figure in the early development of the X-ray inelastic backscattering technique at HASYLab (1981-1986), a technique which later matured to become one of the most productive branches of modern X-ray synchrotron instrumentation. Bruno has been active in many different scientific fields: phonons in ionic and molecular crystals, structural phase transitions, magnetic excitations in low-dimensional systems, sound velocity measurements in liquids. In collaboration with M.C. Bellissent-Funel, J. Teixeira and S.H. Chen, he was the first to produce experimental evidence in support of the concept of "fast sound" in heavy water (1985).

Despite his many duties Bruno was known for devoting his time and expertise to people. He has always been keen on communicating his knowledge and experience, especially to the younger generation through his participation in numerous neutron courses, neutron summer schools and lectures at Regensburg University, which awarded him the Habilitation degree in 1981. During his years at ILL Bruno was associated with all aspects of in-house scientific and instrumental activity. His contribution to ILL's early years was essential: in 1972, together with Michael Steiner he co-authored the first publication on experimental work performed at ILL.
Bruno will be missed by everyone at the ILL. We regret his departure and we send him all our best wishes for his future life.

Self-assembled fibrillar networks (in chemistry, physics and biology)

The Euroconference on *Self-Assembled Fibrillar Networks*, SAFIN 2001, was held in Autrans on 24-28 November 2001. These fibrillar networks result from the reversible connection of one-dimensional objects (such as fibrils, rods, helices, ribbons and tubules). These objects are found in synthetic and biological systems, and are themselves formed by spontaneous aggregation of low mass molecules, or by chemically bound monomers forming macromolecules. SAFINs have now reached a stage where the number of studies constitutes a field of its own within the science of soft matter.

The conference was a great success, gathering 100 scientists from 15 countries. SAFIN 2001 pursued the initiative of the *Symposium on Organogels* held in November 1999 in Gröningen (The Netherlands), with the will both to open the conference to a wide community and to initiate a regular continuation of such meetings in the future. One of its objectives was to gather the communities of chemists, physicists, biologists, experimentalists or theoreticians working in the field of SAFINs. In the last decade, an impressive literature has been accumulated and a more recent tendency towards interdisciplinary studies suggests that it is now time to look for more conceptual and universal descriptions of SAFINs. Because SAFINs are supra-molecular assemblies, the field covers very different length and time scales, and therefore a variety of experimental techniques.

Dick Weiss and Jürgen Fuhrhop exchanging their impressions on the quality of the programme.

Thanks to the European Commission and to our generous sponsors (among whom the ILL), 25 young scientists were fully supported and were allocated a travel grant to attend the conference. They certainly learned a lot from the international experts present at the conference about the intricacies of SAFINs.

The conference was organised by Miguel Aubouy (CEA-Grenoble), Bruno Demé (ILL), and Pierre Térech (CEA-Grenoble).

A symposium marks the retirement of José Dianoux

The ILL celebrated the scientific work of José Dianoux on 7 December by organising a colloquium in his honour. José Dianoux has been one of the main pillars of the Institute over the last 30 years. His energetic enthusiasm contributed substantially to establish the ILL as the world's leading neutron source.

The ILL director Colin Carlile briefly introduced José's scientific curriculum vitae.

José Dianoux obtained his thesis at the Nuclear Research Center of Saclay studying the magnetic properties of Uranium-Fluoride compounds. A post-doctoral position in the Chemistry Department of the University of Illinois familiarised José with molecular motions in plastic solids. He joined the ILL in 1971 and became rapidly interested in the development of the spectrometer IN5 best suited for the investigation of motion in disordered systems. In 1977 he was nominated responsible for the construction of the time-focussing time-of-flight spectrometer IN6. In 1993 he finally became head of the time-of-flight high-resolution group.

In his scientific lecture Marc Bée (ILL & Université Joseph Fourier) gave a highly instructive overview of neutron scattering studies concerning particle diffusion, a field to which José Dianoux made essential contributions. Hinting at the past and stressing the present status of the field Marc Bée finally offered a glimpse into the future. The complexity of the subjects under investigation increases permanently. Further progress will, therefore, rely heavily on the successful combination of computer simulations and experimental investigations.

The second part of the colloquium was devoted to José's scientific contributions in a historical context. Rupp Lechner (HMI, Berlin), one of the main protagonists in the field and close collaborator of José Dianoux, told the fascinating story of quasielastic neutron scattering and its theoretical interpretation from the early days up to now. Reinhard Scherm (PTB Braunschweig) introduced the audience to the mysterious world of quantum liquids, demonstrating that with sufficiently energetic people – of whom José certainly was part - and the right instrument neutrons allow us to investigate nearly everything, i.e. even the materials you would otherwise only use to detect them. The session was closed by Stéphane Rols, formerly José's thesis student and now at IPNS Argonne, who presented the complex structure and dynamics of nanotubes.

José thanking the assembly during the symposium organised in his honour.

The meeting ended with an enjoyable dinner at the Château de Sassenage, in a splendid setting in the Grenoble region. José retires to devote himself fully to his favourite hobbies: mountaineering and *"ski de randonnée"*! He will be missed by many of us. We all wish him a long and sunny retirement and we hope to see him often at the ILL .

Emotions revealed

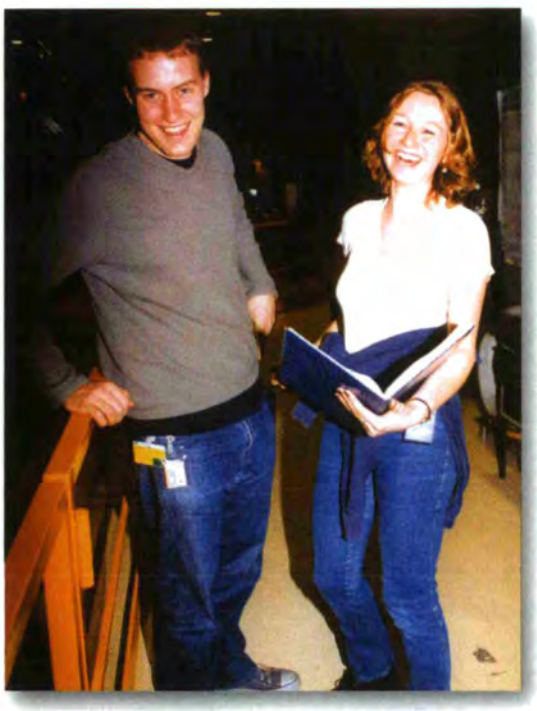

◀ Smiles on their faces following a successful experiment on D7 for Phil Bentley and Judith Preston (University of Leeds)!

Concentration on their faces whilst setting up another experiment on D17. From the left, Beate Kloesgen (FU Berlin), Giovanna Fragneto (D16 instrument responsible) and Thomas Gutberlet (HMI). ▼

▲ Fiona Jewiss (Paul-Drude Institute, Berlin) in a thoughtful mood whilst carrying out an experiment on D7 on MnAs.

Rudi Loidl, looking serious, and Matthias Baron, looking jolly in the enclosure of the S18 neutron interferometer, a CRG instrument from the University of Vienna. ▶

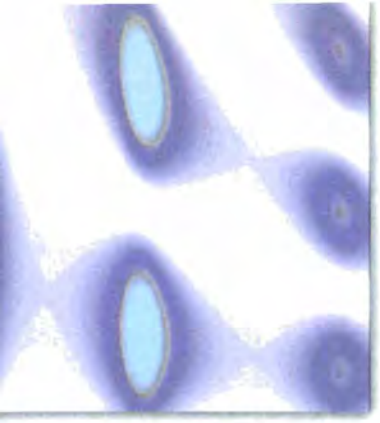

experimental and user programme 2001

Reactor operation

User operation

Instrument list

Beam-time allocation

Instrument performance

Industrial use of neutrons

The ILL's instrument suite (December 2001)

ILL INSTRUMENTS

D1A (50%)	powder diffractometer	operational
D2B	powder diffractometer	operational
D3*	single-crystal diffractometer	operational
D4 (50% with IN1)*	liquids diffractometer	operational
D7	diffuse-scattering spectrometer	operational
D9*	single-crystal diffractometer	operational
D10	single-crystal diffractometer	operational
D11	small-angle scattering diffractometer	operational
D16	small momentum-transfer diffractometer	operational
D17	reflectometer	operational
D19	single-crystal diffractometer	operational
D20	powder diffractometer	operational
D22	small-angle scattering diffractometer	operational
IN1 (50% with D4)*	three-axis spectrometer	operational
IN3	three-axis spectrometer	operational
IN4	time-of-flight spectrometer	operational
IN5	time-of-flight spectrometer	under reconstruction
IN6	time-of-flight spectrometer	operational
IN8	three-axis spectrometer	under reconstruction
IN10	backscattering spectrometer	operational
IN11	spin-echo spectrometer	operational
IN14	three-axis spectrometer	operational
IN16	backscattering spectrometer	operational
IN20	three-axis spectrometer	operational
PF1	neutron beam for fundamental physics	operational
PF2	ultracold neutron source for fundamental physics	operational
PN1	fission product mass-spectrometer	operational
PN3	gamma-ray spectrometer	operational
Strain Imager	residual stress diffractometer	*under construction*
VIVALDI	thermal neutron Laue diffractometer	*commissioning*

* hot neutron instruments

JOINTLY FUNDED INSTRUMENTS

DB21 (50%)	single-crystal diffractometer	operational (EMBL)
LADI (50%)	LAUE diffractometer	operational (EMBL)
IN15	spin-echo spectrometer	operational (FZ Jülich and HMI Berlin)

CRG INSTRUMENTS

D1B	powder diffractometer	CRG-A operational (CNRS)
IN13	backscattering spectrometer	CRG-A operational (INFM Italy)
ADAM	reflectometer	CRG-B operational (Bochum University)
BRISP	Brillouin spectrometer	CRG-B under construction (INFM Italy)
D15	single-crystal diffractometer	CRG-B operational (CEA Grenoble)
D23	single-crystal diffractometer	CRG-B operational (CEA Grenoble)
EVA	reflectometer	CRG-B operational (MPI Stuttgart)
IN12	three-axis spectrometer	CRG-B operational (FZ Jülich)
IN22	three-axis spectrometer	CRG-B operational (CEA Grenoble)
S18	interferometer	CRG-C operational (Atominstitut Wien)

TEST BEAMS

CT1, CT2	detector test facilities
S42	Laue-crystal alignment facility
T3	neutron optics test facility
T13A,C	monochromator test facilities
T17	cold neutron test facility

Instrument layout

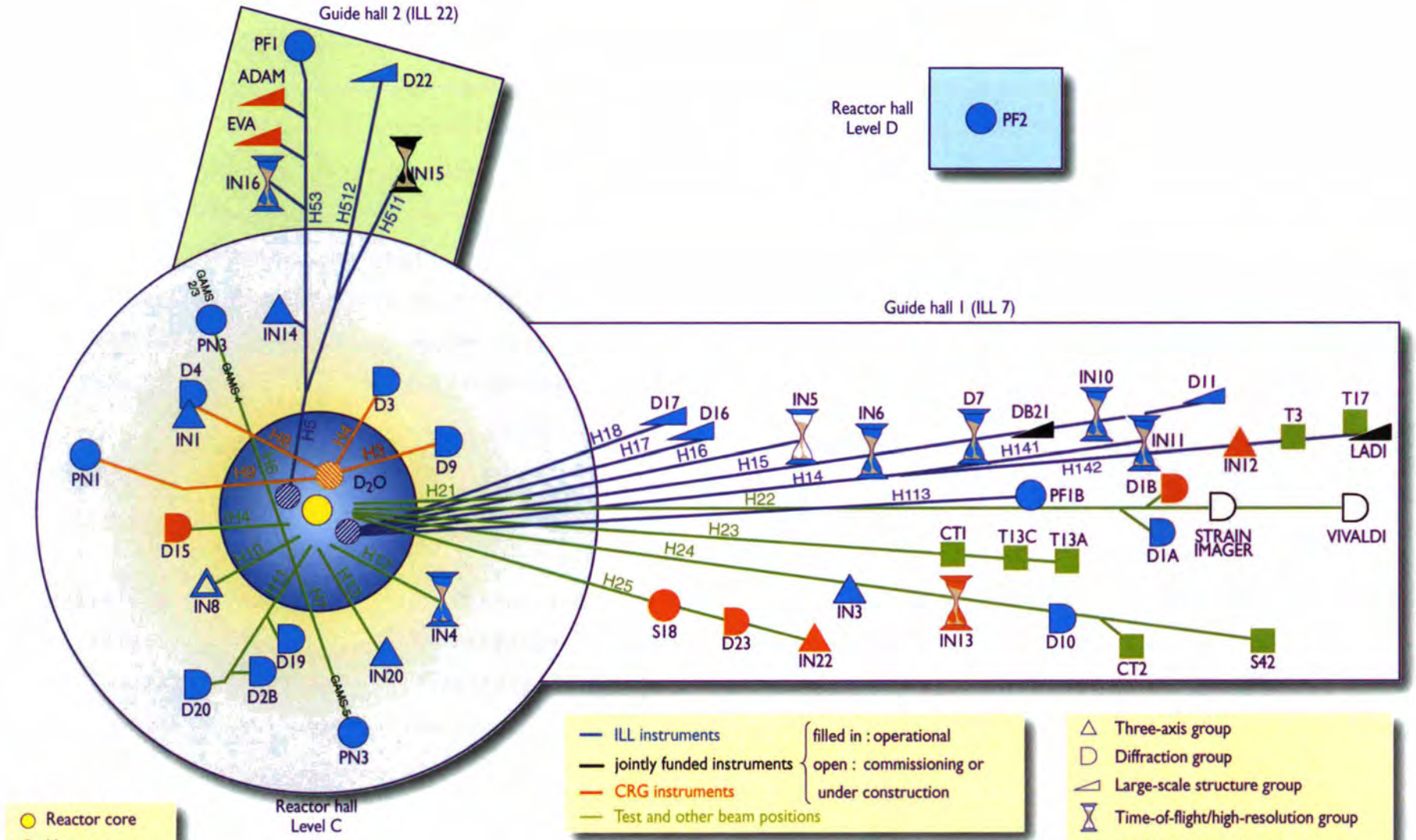

A. Filhol 2000

Reactor operation

The 200 operating days scheduled for scientific work in the year 2001 were completed successfully. On the whole, no particular problems were experienced with reactor operations over the period. The time lost during two short shutdowns was recovered.

The construction of the new reactor emergency control room (known as the PCS) and the closure of the old facility were completed at the beginning of the year.

New developments in the reactor block included the insertion into the reactor of the beam tube IH3 in preparation for the new BRISP instrument. The H13 thimble was replaced with a larger diameter thimble in order to improve IN20's performances. The H4 thimble, the reactor block's central chimney and the control rod absorber material were replaced as part of the reactor block maintenance programme. At the beginning of the year, the V4 irradiation tube and its cooling system were installed, making it possible to carry out irradiations and develop new fission chambers for the Mini Inca programme.

The detritiation facility was shut down on 8 November 2000 to allow for maintenance work. No tritium was produced or despatched this year.

The French nuclear safety authorities have decided to carry out a review of the safety of the reactor and its auxiliary installations. Preparations for this review have generated a considerable workload, in particular concerning the analysis of the reactor's behaviour under seismic conditions, a study which has required the development of a non-linear, elastoplastic method of analysis. The review will end with the holding of a meeting of a safety commission known as the "Groupe Permanent", which is scheduled for March 2002.

Fuel cycle activities continue to require constant attention. This year, six fuel elements were sent for reprocessing. The delivery of uranium from the Russia will allow us to continue fuel element manufacture for a number of years to come.

Cycle	Starting date	Finishing date	Days scheduled	Days of operation	Unscheduled shutdowns
126	14.03.01	02.05.01	50	50	
127	22.05.01	11.07.01	50	50	
128	09.08.01	30.09.01	50	50	2
129	16.10.01	05.12.01	50	50	
		Total	200	200	2

Table 1: Reactor operation in 2001.

User operation

The ILL User Support is there to assist all our users. If you are coming to the ILL to carry out experiments, the User Office is here to give you the organisational and administrative support you need for the successful operation of your experiments. Neutron beams and instrument facilities are free of charge for proposers of accepted experiments. Scientists affiliated to ILL member countries will also, in general, be assisted with necessary travel and daily subsistence for a limited period. The User Support Team makes all arrangements for accommodation and transport and will process claims for expenses after you have completed your experiment.

The hostesses, Vera Gontier (left) and Syriane Lalliat (right) welcoming our visitors with their beautiful smiles.

The ILL Visitors Club

All administrative tools for our scientific visitors are now grouped together and directly accessible on the web, thanks to the Visitors Club.

All information is presented in a user friendly environment.

After having logged in with your own personal identification, you will access directly all the available information which con-

The friendly User Support Team is here to assist all users. From the left: Diana Dijoux, Brigitte Aubert, Katja Mayer-Jenkins and Giovanna Cicognani.

cerns you. Users with particular responsibilities have privileged access to other tools according to their role.

You may already be familiar with our electronic proposal and experimental reports submission procedure. The ILL Visitors Club includes these two systems and makes available additional services on the web, such as acknowledgement of receipt, subcommittee results and user satisfaction form. In the future, invitation forms and all information about scheduling, hotel/guesthouse reservations, reimbursement and so on, will also be accessible via the Visitors Club.

If you have submitted a proposal to the ILL from 1998 onwards, you have been automatically registered in the Visitors Club and received an email with your personal username and password. If not and you wish to join the ILL Visitors Club, you can register on the ILL web site or directly at http://vitraill.ill.fr/cv/.

Extensive information about the ILL, its facilities and application for beam-time is available on our web-site: **http://www.ill.fr/**, User & Science, User Information.

Proposal submission

There are three different ways of submitting a proposal to the ILL:

- standard submission of a research proposal - twice a year (in the first & third quarters).
- fast access to the ILL beam time – twice a year (in the second & fourth quarters).
- Director's discretion time (DDT) – no time restriction.

Special access for proprietary research and industrial users is also possible at the ILL (see page 139).

In 2002, a common ILL/EMBL ***deuteration laboratory*** will be made available to external users. The aim of the laboratory is to provide a focus for European scientists wishing to make their own deuterated materials for neutron scattering or NMR experiments. Information about the availability of this facility for external users will be given in due term on the ILL website (http://www.ill.fr/pages/science/User/Uproposals.html). In the meantime please contact the Head of the Deuteration Facility, Dr Michael Härtlein (haertlein@ill.fr).

The ILL scientific life is organised into 10 colleges:

College 1	*Instrumentation*
College 2	*Theory*
College 3	*Nuclear and Fundamental Physics*
College 4	*Structural and Magnetic Excitations*
College 5A	*Crystallography*
College 5B	*Magnetism*
College 6	*Structure and Dynamics of Liquids and Glasses*
College 7	*Materials Science, Surfaces and Spectroscopy*
College 8	*Structure and Dynamics of Biological Systems*
College 9	*Structure and Dynamics of Soft-condensed Matter*

The ILL college secretaries (from the left): Ross Stewart (Coll.4), Hubert Humblot (Coll.1), Clemens Ritter (Coll.5B), Valery Nesvizhevsky (Coll.3), Miguel Gonzalez (Coll.6), Giovanna Fragneto (Coll.8), Isabelle Grillo (Coll.9), Gwenaelle Rousse (Coll.5A) and Charles Dewhurst (Coll.7).

Submission of a standard research proposal

Applications for beam time should be submitted electronically, via our Electronic Proposal Submission system (EPS), available on the Visitors Club web-site. Proposals can be submitted to the ILL twice a year, end of February and end of September. The web system is activated two months before each deadline.

Submitted proposals are divided amongst the different colleges, (see indent page 133) according to their main subject area.

Proposals are judged by a Peer Review Committee, the Subcommittees of the ILL Scientific Council. Subcommittee members are specialists in relevant areas of each College and they evaluate the proposals for scientific merit, assigning priorities and beam time to accepted proposals.

Before the meeting, the subcommittee receives a report on the technical feasibility and safety of a proposed experiment from the appropriate College at the ILL. Two proposal review rounds are held each year, approximately six weeks after the deadlines for submission of applications.

There are normally 4.5 reactor cycles a year each of which lasts 50 days. In 2001, however, the reactor operated for 4 cycles: the winter shutdown was longer because of the ILL renewal programme.

Coffee break during one of the two User Forums organised last year at the ILL to gather valuable feed-back from our users.

Accepted proposals submitted by February will receive beam time in the second half of the year and those submitted by September in the first half of the following year.

More detailed information on application for beam-time and dead-lines are given on our web-site at http://www.ill.fr/pages/science/User/UProposals.htm.

Submission of a proposal by the Fast Access route (FAST)

To be more responsive to user needs where appropriate and where possible, the ILL has introduced Faster Access Special beam Time (FAST) on specific instruments. This covers scientific areas where fast response time is a crucial point. FAST gives rapid beam time on selected instruments. The dead-lines are three months offset from standard research proposal submissions. Proposals must be submitted through the web, using EPS. Internal review and peer-review assessment by the Subcommittees are also conducted electronically. The delay time between the proposal submission and the running of experiments is of the order of two months.

Precise information on the applicability of FAST access is given on our web-site at http://www.ill.fr/ pages/ science/User/UProposals.htm.

Exchanging views on the Annual Report during the User Forum. From the left: Robert Wimpory (Imperial College, London), Giovanna Cicognani, Roberto Coppola (ENEA, Rome), Peter Timmins, Alan Hewat and Albert Wright.

Submission of a proposal to the Director's Discretion Time (DDT)

This option allows a researcher to obtain beam time quickly, without going through the peer-review procedure. DDT is normally used for hot topics, new ideas, feasibility tests, and to encourage new users. Applications for Director's Discretion Time can be submitted to the Head of the Science Division, Dr. Christian Vettier, at any time (vettier@ill.fr).

Feedback from our Users

We value feedback from our users as an indicator of how well our facility is ful-

filling their needs and to initiate actions when we are not. Therefore this year we have again organised two ***User Forums***, in June and in November. Users who are on-site that day are invited to an informal meeting with the ILL Directors, the User Support Office and Group Leaders of both the Science and the Projects and Techniques Divisions. The objective is to obtain important feedback on the quality of the instruments and services at the ILL.

We very much appreciate the enthusiasm and co-operation of our users in giving their views, on such topics as instrument upgrading and implementation, new sample environment and instrumentation, quality of the Restaurant and the Guest House, and so on. Every effort will be made to implement suggestions. Following your comments, we have already improved our EPS system and the restaurant service in the evening and at week ends.

The ongoing system of ***User Feedback Forms***, now dealt with electronically, is another measure of gathering the opinion of our users. Levels of satisfaction are in general high but we particularly appreciate the written comments on these forms.

Out of hours support

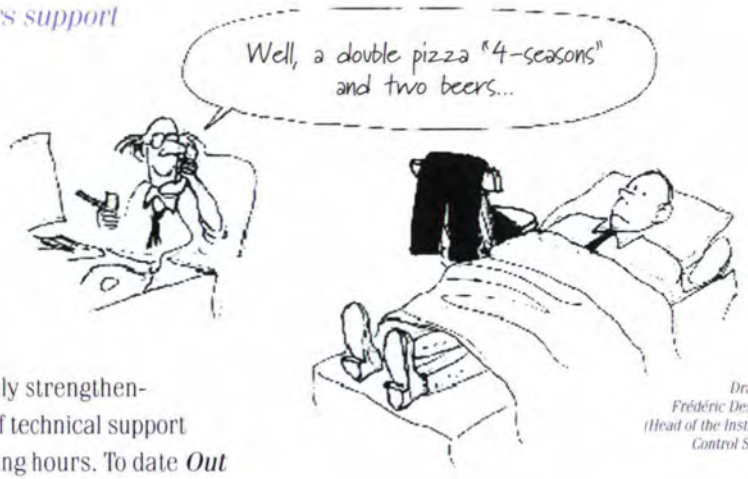

Drawings: Frédéric Descamps (Head of the Instrument Control Service)

We are actively strengthening the level of technical support outside working hours. To date ***Out of Hours Support (OHS)*** has been implemented within the Instrument Control Service, as a starting point. Comprehensive documentation – web-based – has been put in place. We plan to extend gradually this kind of support to all the other services at the ILL.

Alexander Frank (JINR, Dubna) and Christian Vettier

We have been testing user satisfaction since July 2000 via a questionnaire - the ***User Satisfaction Form***. Users who have just finished an experiment at the ILL are asked to complete the questionnaire and to give us their views on different topics. User comments and solutions are entered into a database and summarised for the ILL Directors, the User Support Office, Group Leaders and Instrument Responsibles.

You may already be acquainted with our User Satisfaction Form. Now, it is available on the web, on the Visitors Club. If you have been to the ILL for an experiment recently, and you have not done so yet, please fill in our satisfaction form.

Thank you in advance for taking the time to help us improve our services to you and future users!

User satisfaction with...

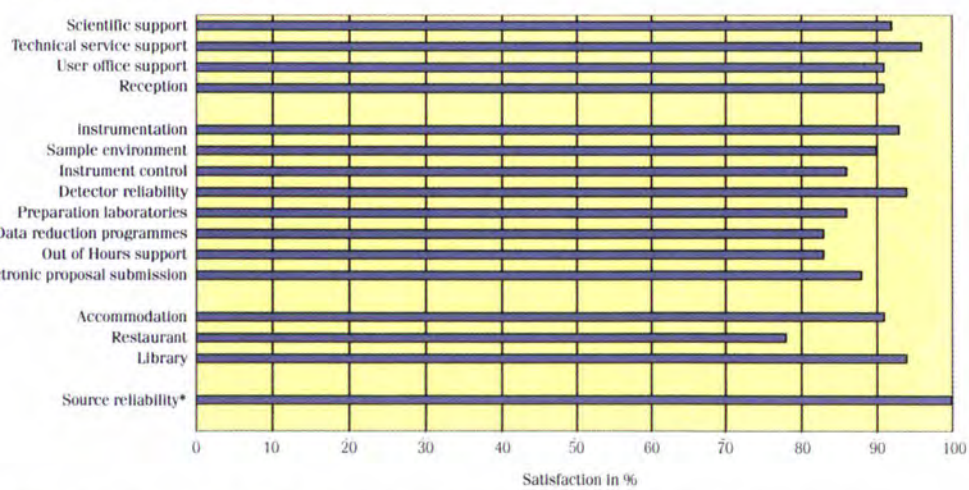

Figure 1: User satisfaction survey results (year 2001). (*) The source reliability has been calculated from table 1.

Lunch break at the ILL Scientific Council. From the left: Thomas Brückel (Forschungszentrum Jülich, Chairman of the Scientific Council), Ted Forgan (University of Birmingham), Bob Cywinski (University of Leeds) and Colin Carlile (ILL Director).

The results of the survey during 2001 (figure1) showed in most cases a very high satisfaction (higher than 90%) with the staff support and ILL equipment. The Out of Hours Support – recently established – met with the approval of most of those who needed it.

Instruments

The instrumental facilities at the ILL are shown in the schematic diagram on page 131. Besides the 25 ILL instruments there are 10 CRG-instruments, which are operated by external Collaborating Research Groups. There are currently three different categories of CRG instruments.

- CRG-A in which the external group leases an instrument owned by ILL. They have 50% of the beam time at their disposal and for the remaining 50% they support ILL's scientific user programme.

- The CRG-B category owns their instrument and retain 70% of the available beam time, supporting the ILL programme for the other 30%.

- Finally, CRG-C instruments are used full time for specific research programmes by the external group which has exclusive use of the beam.

DB21, LADI and IN15 have a special status, since they are joint ventures of the ILL with other laboratories: in the case of DB21 and LADI with EMBL and for IN15 with FZ Jülich and HMI Berlin.

The list of instruments as of December 2001 is summarised below (CRG instruments are marked with an asterisk *):

- powder diffractometers: D1A, D1B*, D2B, D20
- liquids diffractometer: D4
- polarised neutron diffractometers: D3, D23*
- single-crystal diffractometers: D9, D10, D15*
- large-scale structures diffractometers: D19, DB21, LADI
- small-angle scattering: D11, D22
- low momentum-transfer diffractometer: D16
- reflectometers: ADAM*, D17, EVA*
- diffuse scattering and polarisation analysis spectrometer: D7
- three-axis spectrometers: IN1, IN3, IN8, IN12*, IN14, IN20, IN22*
- time-of-flight spectrometers: IN4, IN5, IN6
- backscattering and spin-echo spectrometers: IN10, IN11, IN13*, IN15, IN16
- nuclear physics instruments: PN1, PN3
- fundamental physics instruments: PF1, PF2

D1A is shared between powder diffraction and strain scanner applications.

Details of the instruments can be found on the web under http://www.ill.fr (Users & Science / Instrument groups & Theory).

S18*, an interferometer, is a CRG-C instrument and is normally not available as a 'user' instrument, although some beam time is made available for prototype tests of USANS.

Beam-time allocation and utilisation for 2001

German users of the ILL: Petra Schiebel (Tübingen) and Jens-Boie Suck (Chemnitz)

During 2001 the reactor operated for 4 cycles representing 200 days of neutrons. Overall the Subcommittees of the Scientific Council (meetings in October 2000 and April 2001) scrutinised 948 proposals requesting 7960 days, out of which 585 proposals received beam time, allocating 3702 days of beam time on the different instruments. About 630 experiments were carried out. Table 3 (on page 138) shows the request and allocation of beam time per instrument.

Note that D4 and IN1 share a beam and that the CRG instruments offer a reduced number of days for ILL users. For PF2 several experiments share the beam taking neutrons alternatively, so the table contains the beam-days allocated but gives the total number of experiments running simultaneously.

In 2001, the member countries of the ILL were: France, Germany, UK, Spain, Switzerland, Austria, Italy, the Czech Republic and Russia.

In calculating the statistics of beam-time per country, shown in table 2, the attribution is based on the location of the laboratory of the proposers, not their individual nationality. For a proposal involving laboratories from more than one member country, the total number of days is divided equally amongst the collaborating countries. When a proposal involves a collaboration with a non-member country, the allocated time is attributed entirely to the collaborating member country (or coun-

Country	Requested days	Requested %	Allocated days	Allocated %
AUT	62.4	0.8	32.1	0.9
CH	285.2	3.6	146.1	4.0
CZ	82.9	1.0	32.8	0.8
D	1958.9	24.6	989.5	26.7
E	297.2	3.8	164.4	4.4
F	1973.6	24.8	994.5	26.8
GB	2155.4	26.9	919.5	25.1
I	349.9	4.4	178.2	4.7
RUS	795.1	10.0	245.1	6.5
Total	7960.5	100.0	3702.0	100.0

Table 2: Distribution of beam-time requested and allocated amongst the Associate and Scientific-member countries.

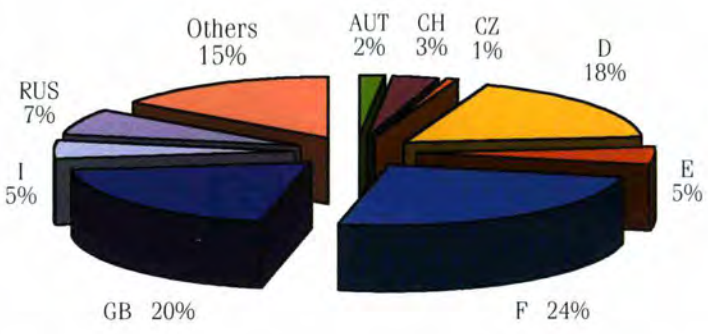

Figure 2: National affiliation of ILL users during 2001.

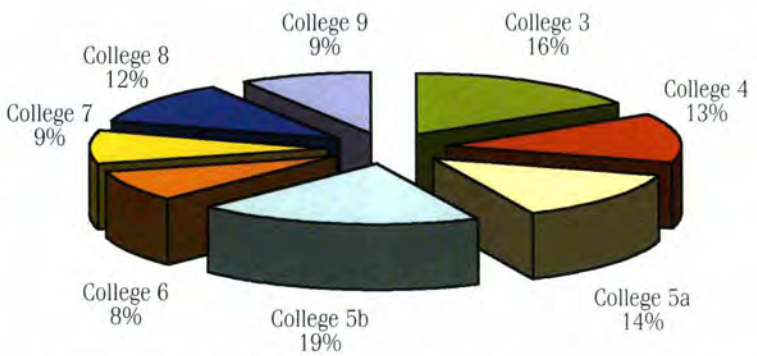

Figure 3: Beam-time allocation in 2001: distribution amongst the different Colleges.

Instrument	Days requested	Days allocated†	Number of experiments	Days used for users††	Days lost	Days used for commiss./test
ADAM	*89*	*41*	*7*	*54*	*0*	*0*
D10	435	138	17	175	6	15
D11	260	119	49	150	20	33
*D15**	*29*	*21*	*3*	*0*	*0*	*0*
D16	155	131	18	152	5	42
D17	157	129	29	161	9	30
D19	234	147	15	171	14	15
D1A	153	110	32	142	3	49
D1B	*124*	*75*	*20*	*92*	*8*	*3*
D20	177	105	42	155	11	37
D22	430	122	43	143	13	43
D23	*25*	*47*	*4*	*53*	*0*	*2*
D2B	239	114	49	156	15	29
D3*	331	75	7	69	6	26
D4	108	43	10	79	4	10
D7	286	130	14	149	10	42
D9	233	135	21	169	15	15
DB21	18	10	2	15	0	0
EVA	*109*	*76*	*6*	*77*	*2*	*0*
IN1	112	69	11	77	11	22
IN10	65	110	12	117	4	81
IN11	169	118	13	154	8	38
IN12	*48*	*33*	*3*	*48*	*1*	*6*
IN13	*140*	*69*	*7*	*57*	*0*	*17*
IN14	464	139	16	159	5	37
IN15	190	77	9	142	9	51
IN16	205	135	19	155	21	24
IN20	323	116	13	120	23	57
IN22	*142*	*47*	*7*	*54*	*1*	*2*
IN3	47	63	6	69	3	129
IN4	103	50	14	66	76	58 ***
IN5*	38	0	0	0	0	0
IN6	430	145	39	182	2	18
IN8*	85	10	1	0	0	0
LADI	256	155	12	157	5	39
PF1	495	144	8	190	4	6
PF2**	438	142	12	200	0	0
PN1	267	92	10	126	23	51
PN3	294	160	10	167	0	33
VIVALDI	57	60	10	60	0	0
Total	7960	3702	629	4462	337	1060

Table 3: Beam-time request / allocation by instrument and instrument performance. ILL use of the CRG instruments (italic and blue) corresponds to 30 or 50% of the total beam time used.
† 'days allocated' refers to only those days reviewed by the subcommittees (i.e., excluding CRG days for CRGs)
†† 'days used' refers to the total number of days delivered to users in ILL time (i.e., excluding CRG days for CRGs)
*IN5 was not officially scheduled in 2000, D15 was not running, IN8 has not started, D3 was reconstructed and therefore available only the second half of the year.
** PF2 consists of several long-term experiments so the number of days scheduled is given as an estimation.
*** includes backlog and commissioning/ test experiments with internal/external users.

tries). When ILL scientists are proposers or co-proposers, the allocated ILL time is attributed amongst the member countries according to their financial contributions to ILL. Local contacts are not counted as proposers except when they are members of the research team.

The ILL welcomed 1280 users in 2001. Approximately 85% came from the member countries including 320 from France, 231 from Germany and 252 from the UK (figure 2). Many of our visitors came to do experiments several times during the last year. There were thus almost 1854 visits in which about 630 experiments were carried out.

The distribution of beam time for these experiments amongst the different 'Colleges' is shown in figure 3.

Instrument performance

Table 3 gives a summary of instrument performance for 2001. For each cycle a record is kept of any time lost from the total available beam-time, and the reasons for the lost time are analysed for all the instruments. The table gives a global summary for the year.

Overall 4462 days were made available for ILL users on ILL and CRG instruments, which represents about 77% of the total days available. About 18% of the total beam time available on the ILL instruments is allowed for tests, calibrations, scheduling flexibility, minor breakdowns recuperation and director's discretion time. In 2001, 337 days were lost due to various malfunctions, which represents less than 6 % of the total available beam-time.
The breakdown by reason for beam time losses is shown in the figure 4.

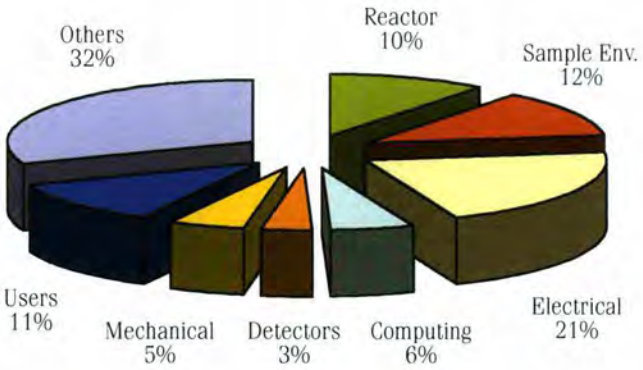

Figure 4: Reasons for beam time loss in 2001.

Detailed comments on the larger beam-time losses (20 days or more) are as follows:

- IN16 had various problems with electronic failures and control computing crashes.
- IN20 suffered time losses mainly because of the replacement of the electronics which could not be completed in time during a reactor shut-down.
- PN1 had to stop two weeks because of the target changing mechanism reparation; another week was lost due to a radiological protection default.
- on D11 three experiments failed because of a badly prepared sample.

Industrial use of neutrons

In 2001, a forum for neutron-wise industrial and applied scientists (Applied Neutron Network, ANNet) was established, following the founding meeting on 6 April at the occasion of the ILL Millennium Symposium. Its role is to stimulate communication among industrial companies, expert scientists and the world's leading neutron research facility, in order to find solutions to applied and industrial research problems. ANNet membership is open to all scientists and engineers who would like to work together on applied and industrial R&D projects using neutrons. ANNet welcomes members from public and university research laboratories as well as from applied and industrial commercial organisations. In the future the ILL will animate seminars and meetings of this forum to build relationships and develop a strategy for neutron applications for the benefit of all parties.

In September 2001, the ILL presented three "industrial" posters at the International Conference for Neutron Scattering ("ICNS 2001") in Munich. ANNet was officially launched at this conference with a well-received presentation of one of the posters and via the announcement on ILL's Industrial Web page (http://www.ill.fr, Industrial Use).

The year 2001 was again a good year for relations with high profile industrial companies. 6 commercial contracts with 5 customers (2 of them were new) were established, with a total of 11 days of beam time sold. Most of the experiments were performed in the field of small-angle neutron scattering (instruments D11 & D22), one experiment used the strain imaging technique at D1A and another experiment was a diffraction study at D2B.

The ILL's Industrial Liaison Group (Pierre Convert, Peter Lindner, Thilo Pirling and Albert Wright) continued to establish relations with potential customers to demonstrate the usefulness of neutron techniques for their applied and industrial research.

Industrial customers enjoying the performance of D11. From right to left: Robin Boothby, Tim Shaw and Mike Hutchings (AEAT) together with Peter Lindner.

Unsung heroes and heroines

The Infirmières de Travail Working Group from the Rhône-Alpes Region met at the ILL to plan the forthcoming International Convention. Catherine Chazette, ILL Infirmière, on the left. No prizes for spotting the odd man out. ▼

In all weathers and at all hours our guardians keep a watchful and friendly eye on all comings and goings on to site and into the experimental zones. ▼

▲ The pay at the ILL: duo in euro major! Janick Dekerpel-Peyrie and Carol Pratt.

▲ Dominique Feltin said au revoir to ILL after many years of sterling service in the ILL's detector group. He is here with Gabriel Cuello (D4 instrument scientist, which benefits from one of Dominique's detectors) and Bruno Dorner who also retired this year as Assistant to the Director.

facts and figures 2001

Facts and Figures for 2001

Name Institut Max von Laue - Paul Langevin (ILL)

Founded 1967

Associates

France	Commissariat à l'énergie atomique (CEA) Centre national de la recherche scientifique (CNRS)
Germany	Forschungszentrum Jülich (FZJ)
United Kingdom	Engineering and Physical Sciences Research Council (EPSRC)

Countries with Scientific membership

Spain	Ministerio de Ciencia y Tecnologìa (MCYT)
Switzerland	Schweizer Bundesamt für Bildung und Wissenschaft (SBBW)
Italy	Istituto Nazionale per la Fisica della Materia (INFM)
Russia	MINATOM

MENI (Middle European Neutron Initiative) Consortium, composed of
Austria: Österreichische Akademie der Wissenschaften
Czech Republic: Charles University of Prague

Staff 427 people including 54 experimentalists in the scientific sector
281 French, 56 British, 47 German, 43 others.

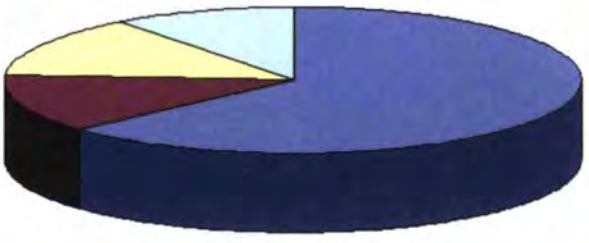

French	281	65.8%
British	56	13.1%
German	47	11.0%
Others	43	10.1%

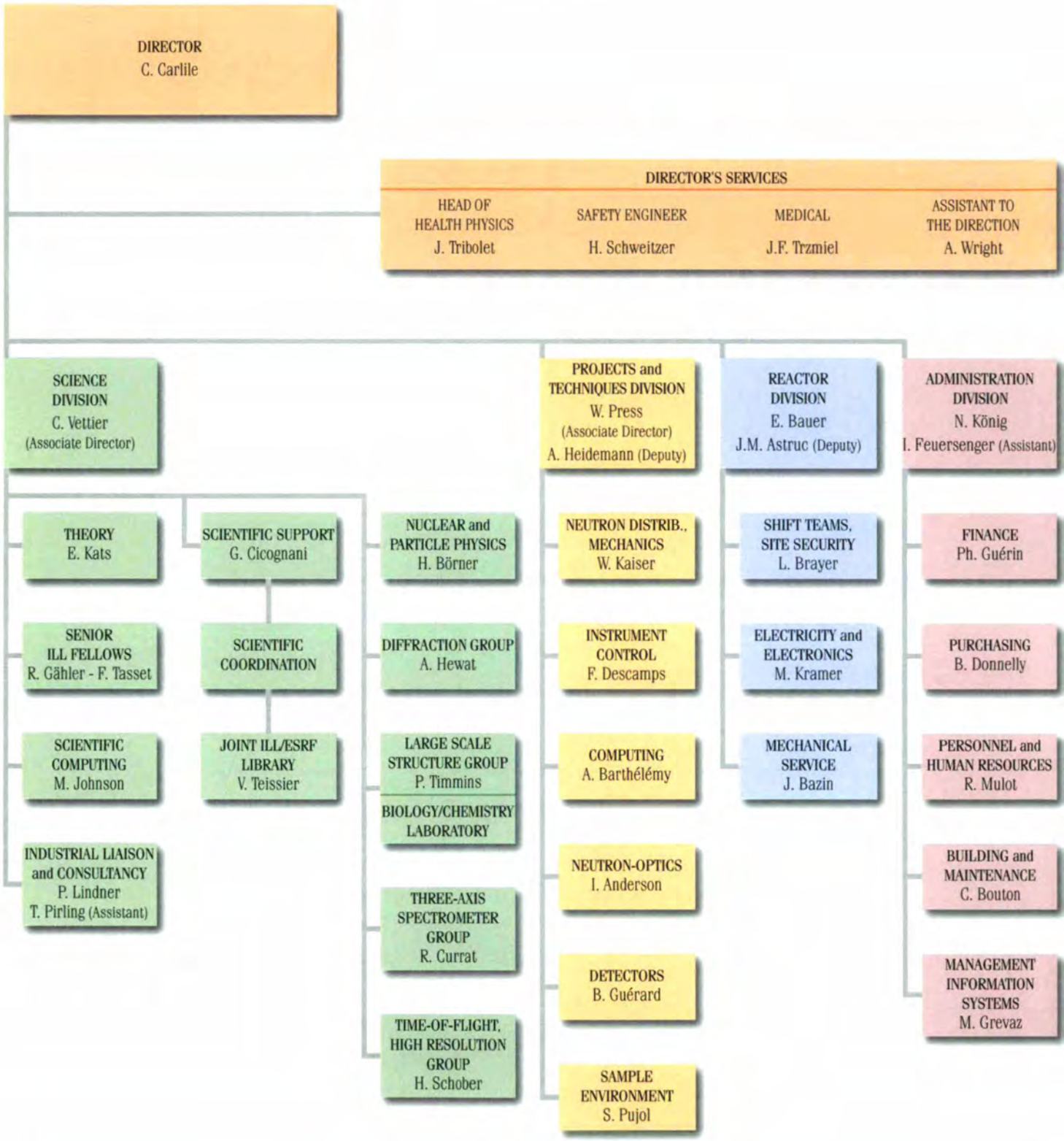

COLLEGE SECTOR

1. Instruments and Techniques
2. Theory
3. Nuclear and Particle Physics
4. Structural and Magnetic Excitations
5. Crystallography and Magnetic Structures
6. Structure and Dynamics of Liquids and Glasses
7. Materials Science, Surfaces and Spectroscopy
8. Structure and Dynamics of Biological Systems
9. Structure and Dynamics of Soft-Condensed Matter

Income (M€)

Income from Associates *(Divided: F 36.86%; D 36.14%; UK 27%)*	52.6	84.00%
Income from scientific members	8.2	14.20%
Own Income	1.2	1.80%
Total	**62.0**	**100%**

Expenditure (M€)

Staff costs	29.7	47.90%
Operating costs	10.8	17.42%
Investment costs	7.5	12.10%
Fuel cycle	14.0	22.58%
Total	**62.0**	**100%**

Distribution of ILL purchases (M€, excluding taxes)

France	9.24	72.70%
Germany	1.42	11.18%
United Kingdom	0.37	2.92%
Others	1.68	13.20%
Total	**12.71**	**100%**

Budget

62 M€ (excluding taxes)

Bodies

Steering Committee, meeting twice a year
Scientific Council with 8 Subcommittees, meeting twice a year

Reactor

58.3 MW, running 4 cycles in 2001 (with cycles of 50 days)

Experimental Programme

630 experiments (allocated by subcommittees) on
25 ILL-funded and 9 CRG instruments
1280 visitors coming from 33 countries
948 proposals submitted and 585 accepted

Experiment Selection by the Scientific Council via its 8 subcommittees

Nuclear and fundamental physics (college 3)
Structural and magnetic excitations (college 4)
Crystallographic structures (college 5a)
Magnetic structures (college 5b)
Structure and dynamics of liquids and glasses (college 6)
Materials science, surfaces and spectroscopy (college 7)
Structure and dynamics of biological systems (college 8)
Structure and dynamics of soft-condensed matter (college 9)

Scientific Life

based on 10 colleges
8 of which map on to the subcommittees plus two others:
instruments and techniques (college 1); theory (college 2)

◀ Alan Hewat, Head of ILL's diffraction group, showing his sample to Dorthe Lehmann of the ILL/ESRF joint medical service. Alan's samples are normally in powder form.

One of the many visits to ILL handled by Ingeborg te Groen and Bruno Dorner. This group of students, from the Physics Dept. of the University of Parma, was guided round in Italian by Claudia Mondelli and Ferdinando Formisano. ▼

▲ Ingrid Parrot and Trevor Forsyth looking at the hydrogen bonding network in cellulose on D19.

Colin Carlile wondering what Father Xmas has in store for the ILL in 2002 ▶ at the celebratory dinner for José Dianoux who retired from ILL this year.

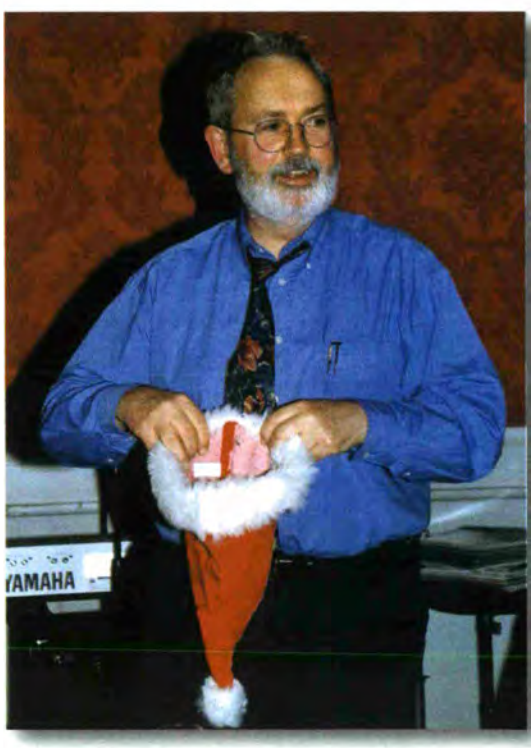

publications 001

In 2001, the ILL received notice of 344 publications by ILL staff and users of which 290 were published as journal articles, and 54 as conference proceedings in journals, books or reports. The distribution by subject is as follows: 19 in instruments and methods, 18 in theory, 13 in nuclear and particle physics, 54 in structural and magnetic excitations, 61 in crystallographic structures, 74 in magnetic structures, 24 in structure and dynamics of liquids and glasses, 41 in materials science, surfaces and spectroscopy, 18 in biology, 22 in structure and dynamics of soft-condensed matter.

Neutron Instruments and Methods:

BÖNI P., FURRER A., SCHEFER J. Principles of neutron scattering.
In "Proceedings of the Eighth Summer School on Neutron Scattering. Neutron Scattering in Novel Materials", FURRER A. (Ed.) (World Scientific, 2000) pp. 1-21

CALLOT V., CANET E., BROCHOT J., BERTHEZENE Y., VIALLON M., HUMBLOT H., BRIGUET A., TOURNIER H., CREMILLIEUX Y. Vascular and perfusion imaging using encapsulated laser-polarized helium.
Magnetic Resonance Materials in Physics, Biology and Medicine **12**, 16-22 (2001)

CLERGEAU J.F., CONVERT P., FELTIN D., FISCHER H.E., GUERARD B., HANSEN T., MANZIN G., OED A., PALLEAU P. Operation of sealed microstrip gas chambers at the ILL.
Nuclear Instruments and Methods in Physics Research A **471**, 60-68 (2001)

CLERGEAU J.F., CONVERT P., FELTIN D., FISCHER H.E., GUERARD B., HANSEN T., MANZIN G., OED A., PALLEAU P. Operation of sealed microstrip gas chambers at the ILL.
IEEE Transactions on Nuclear Science **48**, 1075-1080 (2001)

CUSSEN L.D., HØGHØJ P., ANDERSON I.S. Neutron collimator with rectangular beam profile.
Nuclear Instruments and Methods in Physics Research A **460**, 374-380 (2001)

CUSSEN L.D., VALE C.J., ANDERSON I.S., HØGHØJ P. Tests of a silicon wafer based neutron collimator.
Nuclear Instruments and Methods in Physics Research A **471**, 392-397 (2001)

DEMMEL F., BERNHARDT P., MAGERL A., STEICHELE E. Intensity optimisation of a high-resolution ToF diffractometer.
Nuclear Instruments and Methods in Physics Research A **459**, 265-272 (2001)

FRICK B., GONZALEZ M. Five years operation of the second generation backscattering spectrometer IN16 – a retrospective, recent developments and plans.
Physica B **301**, 8-19 (2001)

GAVRILOV S., PLAKHTY V., BURLET P., KULDA J., HUMBLOT H. Investigation of in-chain spin correlations in $YBa_2Cu_3O_{6+x}$ by neutron polarization analysis.
Physica B **297**, 75-77 (2001)

GUTBERLET T., HEINEMANN U., STEINER M. Protein crystallography with neutrons – status and perspectives.
Acta Crystallographica D **57**, 349-354 (2001)

LUDWIG W., CLOETENS P., HÄRTWIG J., BARUCHEL J., HAMELIN B., BASTIE P. Three-dimensional imaging of crystal defects by 'topo-tomography'.
Journal of Applied Crystallography **34**, 602-607 (2001)

MEZEI F., RUSSINA M. New opportunities in quasi elastic neutron scattering spectroscopy.
Physica B **301**, 94-98 (2001)

NICKEL B., RÜHM A., DONNER W., MAJOR J., DOSCH H., SCHREYER A., ZABEL H., HUMBLOT H. Spin-resolved off-specular neutron scattering maps from magnetic multilayers using a polarized ^{3}He gas spin filter.
Review of Scientific Instruments **72**, 163-172 (2001)

OED A. Micro pattern structures for gas detectors.
Nuclear Instruments and Methods in Physics Research A **471**, 109-114 (2001)

RAUCH H., WERNER S. Neutron interferometry: Lessons in experimental quantum mechanics (Book reviews).
Measurement Science and Technology **12**, 355 (2001)

ROBERTS T.W., HUMBLOT H., TASSET F., LELIEVRE-BERNA E., WILDES A.R., IVANOV A., PETOUKHOV A.K., REGNAULT L.P., HILLIER A.D., KULDA J., STEWART J.R., THOMAS M., MALBERT P., JULLIEN D., GIBERT Y., GAY R., BOURGEAT-LAMI E., CHUNG R. The current status of the ^{3}He neutron spin filter (NSF) project at the ILL.
Physica B **297**, 282-287 (2001)

SANCHEZ DEL RIO M., ALIANELLI L., PIKUZ T.A., FAENOV A.Y. A novel imaging X-ray microscope based on a spherical crystal.
Review of Scientific Instruments **72**, 3291-3303 (2001)

SCHOBER H. Neutron spectroscopy: An ideal tool for the material scientist.
In: "10. Journées de la Diffusion Neutronique. Rencontres Rossat-Mignot" PAULUS W., MEINNEL J. (Eds.) (2001)

Theory:

BELYAKOV V.A., KATS E.I. Surface anchoring and pitch variation in thin smectic *C** layers in an electric field.
Journal of Experimental and Theoretical Physics **93**, 380-392 (2001)

BICOUT D.J. Influence of environment fluctuations on incoherent neutron scattering functions.
Physical Review E **64**, 011910-1-011910-7 (2001)

BICOUT D.J. Turnover of activationless escape rate for collisional dynamics.
Physica A **292**, 299-306 (2001)

BICOUT D.J., BEREZHKOVSKII A.M., SZABO A. **Irreversible bimolecular reactions of Langevin particles.**
Journal of Chemical Physics **114**, 2293-2303 (2001)

BICOUT D.J., BURKHARDT T.W. **Absorption of a randomly accelerated particle: Gambler's ruin in a different game.**
Journal of Physics A **33**, 6835-6841 (2000)

BICOUT D.J., BURKHARDT T.W. **Simulation of a semiflexible polymer in a narrow cylindrical pore.**
Journal of Physics A **34**, 5745-5750 (2001)

BICOUT D.J., ZACCAI G. **Protein flexibility from the dynamical transition: A force constant analysis.**
Biophysical Journal **80**, 1115-1123 (2001)

BULLA R., COSTI T.A., VOLLHARDT D. **Finite-temperature numerical renormalization group study of the Mott transition.**
Physical Review B **64**, 045103-1-045103-9 (2001)

DOLGANOV V.K., KATS E.I., MALININ S.V. **Phase transition to anticlinic texture in free-standing smectic *C* films.**
Journal of Experimental and Theoretical Physics **93**, 533-541 (2001)

GOLO V.L., KATS E.I., PEYRARD M. **Concerted motion of protons in hydrogen bonds of DNA-type molecules.**
JETP Letters **73**, 202-206 (2001)

GOLO V.L., KATS E.I., VOLKOV Y.S., SALYANOV V.I., YEVDOKIMOV Y.M. **Novel cholesteric phase in dispersions of nucleic acids due to polymeric chelate bridges.**
Journal of Biological Physics **27**, 81-93 (2001)

GOLO V.L., KATS E.I., YEVDOKIMOV Y.M. **Network of hydrogen bonds as a medium for DNA interaction in solvents.**
Physics Letters A **285**, 101-107 (2001)

GOLO V.L., YEVDOKIMOV Y.M., KATS E.I., SALYANOV V.I. **Interaction of nucleic acid segments as a result of modification of the network of hydrogen bonds of the solvent.**
Journal of Experimental and Theoretical Physics **91**, 832-843 (2000)

HAUSCHILD T., JENTSCHEL M. **Comparison of maximum likelihood estimation and chi-square statistic applied to counting experiments.**
Nuclear Instruments and Methods in Physics Research A **457**, 384-401 (2001)

LEGGETT A.J., KROTSCHECK E., NEGELE J.W. **Philippe Nozières: Feenberg Medalist 2001. Microscopic and phemomenological foundations of the theory of quantum many-body systems.**
Journal of Low-Temperature Physics **124**, 411-417 (2001)

PICANO F., OSWALD P., KATS E.I. **Disjoining pressure and thinning transitions in smectic-*A* liquid crystal films.**
Physical Review E **63**, 021705-1-021705-9 (2001)

SAKAI T., CEPAS O., ZIMAN T. **An electron spin resonance selection rule for spin-gapped systems.**
Journal of the Physical Society of Japan **69**, 3521-3524 (2000)

SAKAI T., CEPAS O., ZIMAN T. **Selection rule of ESR for spin-gap systems.**
Physica B **294-295**, 26-29 (2001)

Nuclear and Particle Physics:

BÖRNER H.G., JENTSCHEL M. **High resolution gamma-ray spectroscopy.**
Yadernaya Fisica **64**, 1087-1090 (2001)

BÖRNER H.G., JENTSCHEL M., MUTTI P. **Applications of high resolution gamma spectroscopy in low energy nuclear structure research.**
In: "International Symposium on Nuclear Structure Physics. Celebrating the Career of Peter von Brentano" CASTEN R. et al (Eds.) (World Scientific, 2001) pp. 305-310

DANILYAN G.V., KRAKHOTIN V.A., PAVLOV V.S., FEDOROV A.V., KOROBKINA E.I., LELIEVRE-BERNA E. **Search for T-odd left-right asymmetry of prompt neutron emission in binary fission of the ^{233}U and ^{239}Pu nuclei by slow polarized neutrons.**
JETP Letters **72**, 593-594 (2000)

FIONI G., CRIBIER M., MARIE F., AUBERT M., AYRAULT S., BOLOGNESE T., CAVEDON J.M., CHARTIER F., DERUELLE O., DONEDDU F., FAUST H., GAUDRY A., GUNSING F., LECONTE P., LELIEVRE F., MARTINO J., OLIVER R., PLUQUET A., RÖTTGER S., SPIRO M., VEYSSIERE C. **Incineration of ^{241}Am induced by thermal neutrons.**
Nuclear Physics A **693**, 546-564 (2001)

FRANK A.I., BONDARENKO I.V., KOZLOV A.V., HØGHØJ P., EHLERS G. **Larmor clock and measuring of neutron interaction time with quantum objects.**
Physica B **297**, 307-310 (2001)

GENEVEY J., PINSTON J.A., FOIN C., REJMUND M., CASTEN R.F., FAUST H., OBERSTEDT S. **Conversion electron measurements of isomeric transitions in ^{130,132}Te and ^{134}Xe.**
Physical Review C **63**, 054315-1-054315-6 (2001)

GOEMINNE G., WAGEMANS C., WAGEMANS J., GELTENBORT P., LOISELET M., GAELENS M., DENECKE B., KOESTER U. **Investigation of the ^{37}Ar(n,p)^{37}Cl, ^{37}Ar(n,α)^{34}S and ^{39}Ar(n,α)^{36}S reactions**

at various stellar temperatures.
Nuclear Physics A **688**, 233c-236c (2001)

HASEGAWA Y., LOIDL R., BARON M., BADUREK G., RAUCH H. Off-diagonal geometric phase in a neutron interferometer experiment.
Physical Review Letters **87**, 070401-1-070401-4 (2001)

KESSLER E.G. Jr., DEWEY M.S., DES-LATTES R.D., HENINS A., BÖRNER H.G., JENTSCHEL M., LEHMANN H. The GAMS4 flat crystal facility.
Nuclear Instruments and Methods in Physics Research A **457**, 187-202 (2001)

MAZUMDER S., SEN D., ROY S.K., HAIN-BUCHNER M., BARON M., RAUCH H. Manifestation of the statistical nature of a medium in multiple small-angle scattering.
Journal of Physics Condensed Matter **13**, 5089-5102 (2001)

TASSET F. Neutron beams at the spin revolution.
Physica B **297**, 1-8 (2001)

TSEKHANOVICH I., DENSCHLAG H.O., DAVI M., BÜYÜKMUMCU Z., GÖNNEN-WEIN F., OBERSTEDT S., FAUST H.R. Mass and charge distributions in the very asymmetric mass region of the neutron induced fission of ^{238}Np.
Nuclear Physics A **688**, 633-658 (2001)

WAGEMANS J., WAGEMANS C., GOEMINNE G., GELTENBORT P. Detailed investigation of the ^{14}N(n,p)^{14}C, ^{17}O(n,α)^{14}C, ^{26}Al(n,p)^{26}Mg and ^{26}Al(n,α)^{23}Na reactions.
Nuclear Physics A **688**, 490c-492c (2001)

Structural and Magnetic Excitations:

ALBA M., POUGET S. Dynamic critical behavior of disordered 3D Heisenberg ferromagnets.
Journal of Magnetism and Magnetic Materials **226-230**, 542-544 (2001)

AOKI D., HUXLEY A., RESSOUCHE E., BRAITHWAITE D., FLOUQUET J., BRISON J.P., LHOTEL E., PAULSEN C. Coexistence of superconductivity and ferromagnetism in UrhGe (Letters to Nature).
Nature **413**, 613-616 (2001)

ARONSON M.C., OSBORN R., CHAU R., MAPLE M.B., RAINFORD B.D., MURANI A.P. Magnetic correlations and the quantum critical point of $UCu_{5-x}Pd_x$ (x = 1, 1.5).
Physical Review Letters **87**, 197205-1-197205-4 (2001)

BERGENTI I., DERIU A., LICCI F., TURILLI G., CICOGNANI G. Diffusive spin dynamics in lanthanomanganites with colossal magnetoresistance behaviour.
Physica B **301**, 105-109 (2001)

BRAMWELL S.T., HARRIS M.J., DEN HERTOG B.C., GINGRAS M.J.P., GARDNER J.S., MCMORROW D.F., WILDES A.R., CORNELIUS A.L., CHAMPION J.D.M., MELKO R.G., FENNELL T. Spin correlations in $Ho_2Ti_2O_7$: A dipolar spin ice system.
Physical Review Letters **87**, 047205-1-047205-4 (2001)

BRAND R.A., DIANOUX A.J., CALVAYRAC Y. The vibrational density of states revisited in the archetypical icosahedral quasicrystal $Al_{62}Cu_{25.5}Fe_{12.5}$.
Ferroelectrics **250**, 229-232 (2001)

BROWN P.J. Polarised neutrons and complex antiferromagnets: An overview.
Physica B **297**, 198-203 (2001)

BROWN P.J., NEUMANN K.U., ZIEBECK K.R.A. A polarized neutron investigation of the martensitic phase transition in V_3Si: Evidence for a band Jahn-Teller mechanism.
Journal of Physics Condensed Matter **13**, 1111-1117 (2001)

BROWN P.J., NEUMANN K.U., ZIEBECK K.R.A. The temperature dependence of the magnetization distribution in $Fe_{65}Ni_{35}$ invar: Incompatibility of the two-state model.
Journal of Physics Condensed Matter **13**, 1563-1569 (2001)

BURKEL E. Determination of phonon dispersion curves by means of inelastic X-ray scattering.
Journal of Physics Condensed Matter **13**, 7627-7644 (2001)

CAMPO J., PALACIO F., BECERRA C.C., WILDES A.R., REGNAULT L.P., LORENZO DIAZ J.E. Spin waves in the 3d S = $\frac{5}{2}$ Heisenberg antiferromagnetic systems $K_2Fe_{1-x}In_xCl_5 \cdot D_2O$ (x = 0.0 and 0.05).
Journal of Magnetism and Magnetic Materials **226-230**, 479-481 (2001)

CAVADINI N., HEIGOLD G., HENGGELER W., FURRER A., GÜDEL H.U., KRÄMER K., MUTKA H. Magnetic excitations in the quantum spin system $TlCuCl_3$.
Physical Review B **63**, 172414-1-172414-4 (2001)

CAVADINI N., HENGGELER W., FURRER A., KRÄMER K., GÜDEL H.U., MUTKA H., WILDES A., VORDERWISCH P. Triplet excitations in a family of S=1/2 unconventional antiferromagnets.
In: "Proceedings of the Eighth Summer School on Neutron Scattering. Neutron Scattering in Novel Materials" FURRER A. (Ed.) (World Scientific, 2000) pp. 237-251

CAVADINI N., RÜGG C., HENGGELER W., FURRER A., GÜDEL H.U., KRÄMER K., MUTKA H. Temperature renormalization of the magnetic excitations in S = 1/2 $KCuCl_3$.

European Physical Journal B **18**, 565-571 (2000)

CEPAS O., KAKURAI K., REGNAULT L.P., ZIMAN T., BOUCHER J.P., ASO N., NISHI M., KAGEYAMA H., UEDA Y. Dzyaloshinski-Moriya interaction in the 2D spin gap system $SrCu_2(BO_3)_2$.
Physical Review Letters **87**, 167205-1-167205-4 (2001)

EHLERS G., CASALTA H., LECHNER R.E., MALETTA H. Dynamics of frustrated magnetic moments in antiferromagnetically ordered TbNiAl probed by neutron time-of-flight and spin-echo spectroscopy.
Physical Review B **63**, 224407-1-224407-6 (2001)

ENDERLE M., RØNNOW H.M., MCMORROW D.F., REGNAULT L.P., DHALENNE G., REVCHOLEVSCHI A., VORDERWISCH P., SCHNEIDER H., SMEIBIDL P., MEIßNER M. Excitations of the field-induced quantum soliton lattice in $CuGeO_3$.
Physical Review Letters **87**, 177203-1-177203-4 (2001)

ENDERLE M., RØNNOW H.M., MCMORROW D.F., REGNAULT L.P., VORDERWISCH P., MEIßNER M., SMEIBIDL P., DHALENNE G., REVCOLEVSCHI A. Statics and dynamics of the magnetic soliton lattice in the high-field phase of $CuGeO_3$.
Journal of Magnetism and Magnetic Materials **226-230**, 465-467 (2001)

ESPESO J.I., MARCANO N., SEÑAS A., BLANCO J.A., REIFFERS M., GOMEZ SAL J.C. Neutron diffraction in the diluted $Nd_{1-x}R_xNi_5$ systems, with R = Ce and Pr.
Journal of Magnetism and Magnetic Materials **226-230**, 1150-1152 (2001)

FAVRE-NICOLIN V., BOS S., LORENZO J.E., HODEAU J.L., BERAR J.F., MONCEAU P., CURRAT R., LEVY F., BERGER H. Structural evidence for Ta-tetramerization displacements in the charge-density-wave compound $(TaSe_4)_2I$ from X-ray anomalous diffraction.
Physical Review Letters **87**, 015502-1-015502-4 (2001)

GARDNER J.S., EHLERS G., HEFFNER R.H., MEZEI F. Neutron spin echo studies of the glass-like pyrochlore $Y_2Mo_2O_7$.
Journal of Magnetism and Magnetic Materials **226-230**, 460-462 (2001)

GRENIER B., CEPAS O., REGNAULT L.P., LORENZO J.E., ZIMAN T., BOUCHER J.P., HIESS A., CHATTERJI T., JEGOUDEZ J., REVCOLEVSCHI A. Charge ordering and spin dynamics in NaV_2O_5.
Physical Review Letters **86**, 5966-5969 (2001)

HIESS A., BROWN P.J., ASO N., ROESSLI B., BERNHOEFT N., SATO N.K., LANDER G.H. Neutron scattering study of the static and dynamic magnetic properties of UNi_2Al_3.
Journal of Magnetism and Magnetic Materials **226-230**, 54-56 (2001)

HIRAKA H., ENDOH Y., FUJITA M., LEE Y.S., KULDA J., IVANOV A., BIRGENEAU R.J. Spin fluctuations in the underdoped high-T_c cuprate $La_{1.93}Sr_{0.07}CuO_4$.
Journal of the Physical Society of Japan **70**, 853-858 (2001)

HLINKA J., KULDA J., KAMBA S., PETZELT J. Resonant soft mode in Rochelle salt by inelastic neutron scattering.
Physical Review B **63**, 052102-1-052102-4 (2001)

IVANOV A.S., BOURGES P., PETITGRAND D., CASALTA H. High-energy spin dynamics in Pr_2CuO_4.
Journal of Magnetism and Magnetic Materials **226-230**, 485-486 (2001)

KATO T., BINEK C., PETRACIC O., KLEEMANN W., BERTRAND D., BURLET P., BOURDAROT F. Transverse magnetism of the diluted antiferromagnet $Fe_{1-x}Mg_xBr_2$ (x~0.15).
Journal of Magnetism and Magnetic Materials **226-230**, 618-620 (2001)

KENZELMANN M., ZHELUDEV A., RAYMOND S., RESSOUCHE E., MASUDA T., BÖNI P., KAKURAI K., TSUKADA I., UCHINOKURA K., COLDEA R. Spin waves and magnetic ordering in the quasi-one-dimensional $S = \frac{1}{2}$ antiferromagnet $BaCu_2Si_2O_7$.
Physical Review B **64**, 054422-1-054422-7 (2001)

KERNAVANOIS N., GRENIER B., HUXLEY A., RESSOUCHE E., SANCHEZ J.P., FLOUQUET J. Neutron scattering study of the ferromagnetic superconductor UGe_2.
Physical Review B **64**, 174509-1-174509-7 (2001)

KLOTZ S., BRADEN M., KULDA J., PAVONE P., STEININGER B. Transverse acoustic phonons of GaSb up to 7 GPa by inelastic neutron scattering.
Physica Status Solidi (b) **223**, 441-447 (2001)

KÖBLER U., MUELLER R.M., BROWN P.J., ARONS R.R., FISCHER K. Experimental identification of fourth-order exchange interactions in magnets with pure spin moments.
Journal of Physics Condensed Matter **13**, 6835-6852 (2001)

KRAMP S., ROTTER M., LOEWENHAUPT M., PYKA N.M., SCHMIDT W., VAN DE KAMP R. Spin waves in the ferrimagnetic phase of $NdCu_2$.
Journal of Magnetism and Magnetic Materials **226-230**, 470-472 (2001)

KULDA J., FARHI E., ZEYEN C.M.E. Ther-

mal variation of phonon frequency and line width in Ge studied by TAS spin-echo.
Physica B **297**, 37-39 (2001)

LAFOND A., HENGGELER W., MUTKA H., OULADDIAF B. Alteration of the stacked $2\pi/3$ magnetic structure in the triangular lattice anti-ferromagnet $LiCrS_2$.
Canadian Journal of Physics **79**, 1427-1432 (2001)

LANDER G.H., MANNIX D., WASTIN F., REBIZANT J., LIDSTRÖM E., VETTIER C., CACIUFFO R., BERNHOEFT N., NORMILE P., STIRLING W.G., HIESS A. X-ray magnetic scattering from transuranium systems.
AIP Conference Proceedings **532**, 35 (2000)

LETOUBLON A., YAKHOU F., LIVET F., BLEY F., BOISSIEU M. DE, MANCINI L., CAUDRON R., VETTIER C., GASTALDI J. Coherent X-ray diffraction and phason fluctuations in quasicrystals.
Europhysics Letters **54**, 753-759 (2001)

LISTER S.J.S., BOOTHROYD A.T., ANDERSEN N.H., LARSEN B.H., ZHOKHOV A.A., CHRISTENSEN A.N., WILDES A.R. Coupled magnetic excitations in single crystal $PrBa_2Cu_3O_{6.2}$.
Physical Review Letters **86**, 5994-5997 (2001)

MITTAL R., CHAPLOT S.L., SCHOBER H., MARY T.A. Origin of negative thermal expansion in cubic ZrW_2O_8 revealed by high pressure inelastic neutron scattering.
Physical Review Letters **86**, 4692-4695 (2001)

MUTKA H. Quasi-elastic scattering from unconventional antiferromagnetic compounds.
Physica B **301**, 20-27 (2001)

NEUBECK W., VETTIER C., BERGEVIN F. DE, YAKHOU F., MANNIX D., RANNO L., CHATTERJI T. Orbital moment determination of simple transition metal oxides using magnetic X-ray diffraction.
Journal of Physics and Chemistry of Solids **62**, 2173-2180 (2001)

PLAKHTY V.P., MALEYEV S.V., KULDA J., VISSER E.D., WOSNITZA J., MOSKVIN E.V., BRÜCKEL T., KREMER R.K. Spin chirality and polarised neutron scattering.
Physica B **297**, 60-66 (2001)

PLAKHTY V.P., SCHWEIKA W., BRÜCKEL T., KULDA J., GAVRILOV S.V., REGNAULT L.P., VISSER D. Chiral criticality in helimagnet Ho studied by polarized neutron scattering (Rapid communications).
Physical Review B **64**, 100402-1-100402-4 (2001)

PODURETS K.M., KLIMKO S.A., RUNOV V.V., SOMENKOV V.A., GLAZKOV V.P. Investigation of the magnetic phase transitions at high pressure by neutron depolarization.
Physica B **297**, 258-262 (2001)

RADAELLI P.G., IBBERSON R.M., ARGYRIOU D.N., CASALTA H., ANDERSEN K.H., CHEONG S.W., MITCHELL J.F. Mesoscopic and microscopic phase segregation in manganese perovskites.
Physical Review B **63**, 172419-1-172419-4 (2001)

RAYMOND S., REGNAULT L.P., FLOUQUET J., WILDES A., LEJAY P. Pressure dependence of the spin dynamics around a quantum critical point: An inelastic neutron scattering study of $Ce_{0.87}La_{0.13}Ru_2Si_2$.
Journal of Physics Condensed Matter **13**, 8303-8315 (2001)

RØNNOW H.M., MCMORROW D.F., HARRISON A., YOUNGSON I.D., COLDEA R., PERRING T.G., AEPPLI G., SYLJUÅSEN O. Correlations and fluctuations in the 2D Heisenberg antiferromagnet.
Journal of Magnetism and Magnetic Materials **236**, 4-5 (2001)

STRÄSSLE T., FURRER A., ALTORFER F., MATTENBERGER K., BÖHM M., MUTKA H. HoAs: A model compound for the cooling by the barocaloric effect.
Journal of Alloys and Compounds **323-324**, 392-395 (2001)

STUNAULT A., BERNHOEFT N., VETTIER C., DUMESNIL K., DUFOUR C. 4f and 5d magnetism in samarium.
Journal of Magnetism and Magnetic Materials **226-230**, 1116-1117 (2001)

TOLEDANO J.C., BERRY R.S., BROWN P.J., GLAZER A.M., METSELAAR R., PANDEY D., PEREZ-MATO J.M., ROTH R.S., ABRAHAMS S.C. Nomenclature of magnetic, incommensurate, composition-changed morphotropic, polytype, trasient-structural and quasicrystalline phases undergoing phase transitions. II. Report of an IUCr Working Group on phase transition nomenclature.
Acta Crystallographica A **57**, 614-626 (2001)

VETTIER C. Resonant X-ray scattering in transition metal and rare-earth materials.
Journal of Electron Spectroscopy and Related Phenomena **117-118**, 113-128 (2001)

VETTIER C. Magnetic scattering experiments.
Journal of Magnetism and Magnetic Materials **226-230**, 1053-1057 (2001)

WOLL H., RHEINSTÄDTER M.C., KRUCHTEN F., KIEFER K., ENDERLE M., KLÖPPER-PIEPER A., ALBERS J., KNORR K. Dipolar ordering and glassy freezing in methanol-β-hydroquinone-clathrate.

Physical Review B **63**, 224202-1-224202-12 (2001)

YAKHOU F., PLAKHTY V., SUZUKI H., GAVRILOV S., BURLET P., PAOLASINI L., VETTIER C., KUNII S. **k = 2π/*a* [1/2 1/2 1/2] zero-field ordering in the intermediate phase of CeB_6 observed by X-ray scattering: What orders?**
Physics Letters A **285**, 191-196 (2001)

Crystallography:

ALONSO J.A., MARTINEZ-LOPE M.J., CASAIS M.T., GARCIA-MUÑOZ J.L., FERNANDEZ-DIAZ M.T., ARANDA M.A.G. **High-temperature structural evolution of *R*NiO3 (*R*=Ho, Y, Er, Lu) perovskites: Charge disproportionation and electronic localization.**
Physical Review B **64**, 094102-1-094102-10 (2001)

AURELIO G., FERNANDEZ GUILLERMET A., CUELLO G.J., CAMPO J. **Structural properties and stability of metastable phases in the Zr-Nb system: Part I. Systematics of quenching-and-aging experiments.**
Metallurgical and Materials Transactions A **32**, 1903-1910 (2001)

BEDOYA C., MULLER C., BAUDOUR J.L., BOUREE F., SOUBEYROUX J.L., ROUBIN M. **Ferroelectric-paraelectric phase transition in $PbHf_{0.2}Ti_{0.8}O_3$ studied by neutron powder diffraction.**
Journal of Physics Condensed Matter **13**, 6453-6470 (2001)

BEGUE P., ENJALBERT R., CASTRO A. **The upper limit of the solid solution $Bi_{2-x}Sb_xMoO_6$: Structure refinement of $Bi_{1.1}Sb_{0.9}MoO_6$.**
Journal of Solid State Chemistry **159**, 72-79 (2001)

BERNERT A., CHATTERJI T., THALMEIER P., FULDE P. **Structure determination, valence, and superexchange in the dimerized low temperature phase of α'-NaV_2O_5.**
European Physical Journal B **21**, 535-546 (2001)

BOUOUDINA M., LENAIN C., AYMARD L., SOUBEYROUX J.L., FRUCHART D. **The effects of heat treatments on the microstructure and electrochemical properties of the $ZrCr_{0.7}Ni_{1.3}$ multiphase alloy.**
Journal of Alloys and Compounds **327**, 178-184 (2001)

BOUOUDINA M., SOUBEYROUX J.L., FRUCHART D. **Study of the hydrogenation/dehydrogenation processes of $ZrCr_{0.7}Ni_{1.3}$, a Laves phase-rich multicomponent system, by in-situ neutron diffraction under hydrogen gas pressure.**
Journal of Alloys and Compounds **327**, 185-194 (2001)

BRADEN M., MEVEN M., REICHARDT W., PINTSCHOVIUS L., FERNANDEZ-DIAZ M.T., HEGER G., NAKAMURA F., FUJITA T. **Analysis of the local structure by single-crystal neutron scattering in $La_{1.85}Sr_{0.15}CuO_4$.**
Physical Review B **63**, 140510-1-140510-4 (2001)

BREARD Y., MICHEL C., HERVIEU M., DUCOURET A., NGUYEN N., STUDER F., MAIGNAN A., RAVEAU B., SUARD E. **A layered oxycarbonate involving trivalent chromium : $Sr_4FeCrO_6CO_3$.**
Chemistry of Materials **13**, 2423-2429 (2001)

BRUNAUER G., BOYSEN H., FREY F., HANSEN T., KRIVEN W. **High temperature crystal structure of a 3:2 mullite from neutron diffraction data.**
Zeitschrift für Kristallographie **216**, 284-290 (2001)

CAMPBELL J.A., LAVAL J.P., FERNANDEZ-DIAZ M.T., FOSTER M. **The defect structure of CaF_2:U^{3+}.**
Journal of Alloys and Compounds **323-324**, 111-114 (2001)

COLE J.M., HOWARD J.A.K., MCINTYRE G.J. **Influence of hydrogen bonding on the second harmonic generation effect: Neutron diffraction study on 4-nitro-4'-methylbenzylidene aniline.**
Acta Crystallographica B **57**, 410-414 (2001)

CORBEL G., SUARD E., VOIRON J., LEBLANC M. **Hydrothermal synthesis and magnetic studies of transition metal nocerites $M_3(BO_3)F_3$ (*M*=Fe, Co, Ni).**
Journal of Magnetism and Magnetic Materials **234**, 423-430 (2001)

COWAN J.A., HOWARD J.A.K., LEECH M.A. **The 1:1 adduct of 2,5-dihydroxy-1,4-benzoquinone with 4,4'-bipyridine.**
Acta Crystallographica C **57**, 302-303 (2001)

COWAN J.A., HOWARD J.A.K., LEECH M.A. **Interpenetrating supramolecular lattices in 4,4'-bipyridine-2,3,5,6-tetrahydroxy-1,4-benzoquinone (3/2).**
Acta Crystallographica C **57**, 1196-1198 (2001)

COWAN J.A., HOWARD J.A.K., LEECH M.A., PUSCHMANN H., WILLIAMS I.D. **Hexahydroxybenzene-2,2'-bipyridine (1/2).**
Acta Crystallographica C **57**, 1194-1195 (2001)

COWAN J.A., HOWARD J.A.K., LEECH M.A., WILLIAMS I.D. **Bis(4-aminopyridinium) 2,5-dioxidobenzoquinone dihydrate.**
Acta Crystallographica E **57**, o563-o565 (2001)

CUELLO G.J., AURELIO G., FERNANDEZ GUILLERMET A., BENITES G.M., CAMPO

J. Bonding-induced atomic ordering in the athermal Ω phase: Neutron diffraction test and consequences upon models of the bond-length systematics in alloys.
Scripta Materialia **44**, 223-228 (2001)

CUELLO G.J., AURELIO G., FERNANDEZ GUILLERMET A., BENITES G.M., CAMPO J. Erratum: Bonding-induced atomic ordering in the athermal Ω phase: Neutron diffraction test and consequences upon models of the bond-length systematics in alloys.
Scripta Materialia **44**, 2821-2825 (2001)

DELMAS C., PRADO G., ROUGIER A., SUARD E., FOURNES L. Effect of iron on the electrochemical behaviour of lithium nickelate: From $LiNiO_2$ to 2D-$LiFeO_2$.
Solid State Ionics **135**, 71-79 (2000)

DUBOIS F., GOUTENOIRE F., LALIGANT Y., SUARD E., LACORRE P. *Ab-initio* determination of $La_2Mo_4O_{15}$ crystal structure from X-rays and neutron powder diffraction.
Journal of Solid State Chemistry **159**, 228-233 (2001)

EVDOKIMOV A., GILBOA A.J., KOETZLE T.F., KLOOSTER W.T., SCHULTZ A.J., MASON S.A., ALBINATI A., FROLOW F. Structures of furanosides: Geometrical analysis of low-temperature X-ray and neutron crystal structures of five crystalline methyl pentofuranosides.
Acta Crystallographica B **57**, 213-220 (2001)

FORRESTER J.S., PILTZ R.O., KISI E.H., MCINTYRE G.J. Temperature-induced phase transitions in the giant-piezoelectric-effect material PZN–4.5%PT (Letter to the editor).
Journal of Physics Condensed Matter **13**, L825-L833 (2001)

FRONTERA C., GARCIA-MUÑOZ J.L., LLOBET A., ARANDA M.A.G., RITTER C., RESPAUD M., VANACKEN J. Room temperature charge and orbital ordering and phase coexistence in $Bi_{0.5}Sr_{0.5}MnO_3$.
Journal of Physics Condensed Matter **13**, 1071-1078 (2001)

FRYZUK M.D., JOHNSON S.A., PATRICK B.O., ALBINATI A., MASON S.A., KOETZLE T.F. New mode of coordination for the dinitrogen ligand: Formation, bonding, and reactivity of a tantalum complex with a bridging N_2 unit that is both side-on and end-on.
Journal of the American Chemical Society **123**, 3960-3973 (2001)

GALEZ P., SOUBEYROUX J.L., HOPFINGER T., OPAGISTE C., LOMELLO-TAFIN M., BERTRAND C., JORDA J.L. Pathway for the formation of the Tl-2223 phase: An *in situ* neutron powder diffraction study.
Superconductor Science and Technology **14**, 583-598 (2001)

GARCIA-MUÑOZ J.L., ARANDA M.A.G., LLOBET A., FRONTERA C., MARTINEZ-LOPE M.J., RITTER C., RESPAUD M., BROTO J.M. Phase segregation and orbital ordering in $Bi_{1-x}Ca_xMnO_3$ ($x \geq 0.75$): A neutron and synchrotron X-ray diffraction study.
Journal of Alloys and Compounds **323-324**, 408-411 (2001)

GARCIA-MUÑOZ J.L., FRONTERA C., ARANDA M.A.G., LLOBET A., RITTER C. High-temperature orbital and charge ordering in $Bi_{1/2}Sr_{1/2}MnO_3$.
Physical Review B **63**, 064415-1-064415-4 (2001)

GOUTENOIRE F., ISNARD O., RETOUX R., LACORRE P. Crystal structure of $La_2Mo_2O_9$, a new fast oxide-ion conductor.
Chemical Materials **12**, 2575-2580 (2000)

GOUTENOIRE F., ISNARD O., SUARD E., BOHNKE O., LALIGANT Y., RETOUX R., LACORRE P. Structural and transport characteristics of the LAMOX family of fast oxide-ion conductors, based on lanthanum molybdenum oxide $La_2Mo_2O_9$.
Journal of Materials Chemistry **11**, 119-124 (2001)

HECTOR A.L., HUTCHINGS J.A., NEEDS R.L., THOMAS M.F., WELLER M.T. Structural and Mössbauer study of Sr_2FeO_3X (X = F, Cl, Br) and the magnetic structure of Sr_2FeO_3F.
Journal of Materials Chemistry **11**, 527-532 (2001)

HEWAT A.W. Neutron powder diffraction and new materials.
In: "Proceedings of the Eighth Summer School on Neutron Scattering. Neutron Scattering in Novel Materials" FURRER A. (Ed.) (World Scientific, 2000) pp. 52-69

ISNARD O. Diffusion, diffraction des neutrons en temps réel et études réalisées *in situ*.
In: "10. Journées de la Diffusion Neutronique. Rencontres Rossat-Mignot" PAULUS W., MEINNEL J. (Eds.) (2001)

KEARLEY G.J., JOHNSON M.R., PLAZANET M., SUARD E. Structure and vibrational dynamics of the strongly hydrogen-bonded model peptide: *N*-methyl acetamide.
Journal of Chemical Physics **115**, 2614-2620 (2001)

KILCOYNE S.H., MANUEL P., RITTER C. Synthesis and characterization of a novel Y-Fe phase via kinetic neutron diffraction.
Journal of Physics Condensed Matter **13**, 5241-5250 (2001)

KOHLMANN H., BERTHEVILLE B., HANSEN T., YVON K. High-pressure synthesis of novel europium magnesium hydrides.

Journal of Alloys and Compounds **322**, 59-68 (2001)

KOHLMANN H., FAUTH F., FISCHER P., SKRIPOV A.V., KOZHANOV V.N., YVON K. Low-temperature deuterium ordering in the cubic Laves phase derivative α-$ZrCr_2D_{0.66}$ (Letter).
Journal of Alloys and Compounds **327**, L4-L9 (2001)

LALIGANT Y., LE BAIL A., GOUTENOIRE F. *Ab-initio* structure determination of lanthanum cyclo-tetratungstate α-$La_2W_2O_9$ from X-ray and neutron powder diffraction.
Journal of Solid State Chemistry **159**, 223-227 (2001)

LANGAN P., ROBINSON R., BROWN P.J., ARGYRIOU D.N., HENDRICKSON D.N., CHRISTOU G. A low-temperature neutron diffraction study of Mn_{12}-acetate.
Acta Crystallographica C **57**, 909-910 (2001)

LEINEWEBER A., JACOBS H., EßMANN R., ALLENSPACH P., FAUTH F., FISCHER P. $Co(NH_3)_2Cl_2$ and $Co(ND_3)_2Cl_2$: Order-disorder behaviour of $N(H,D)_3$ and antiferromagnetic structure.
Zeitschrift für Anorganische und Allgemeine Chemie **627**, 2063-2069 (2001)

LEINEWEBER A., JACOBS H., FISCHER P., BÖTTGER G. Uniaxial orientational order – disorder transitions in diammine magnesium halides, $Mg(ND_3)_2Cl_2$ and $Mg(ND_3)_2Br_2$, investigated by neutron diffraction.
Journal of Solid State Chemistry **156**, 487-499 (2001)

LERCH M., BOYSEN H., HANSEN T. High-temperature neutron scattering investigation of pure and doped lanthanum gallate.
Journal of Physics and Chemistry of Solids **62**, 445-455 (2001)

LLOBET A., FRONTERA C., GARCIA-MUNOZ J.L., RITTER C., ARANDA M.A.G. Chemical heterogeneity in a single phase: $Bi_{0.15}Ca_{0.85}MnO_3$, a case example of macroscopic phase segregation.
Chemical Materials **12**, 3648-3657 (2000)

MASSET A.C., TOULEMONDE O., PELLOQUIN D., SUARD E., MAIGNAN A., STUDER F., HERVIEU M., MICHEL C. $(Bi_{0.4}Sr_{0.45}Co_{0.15})Sr_2CoO_{5-\delta}$: A new 1201-type oxygen dependent series of cobaltites.
International Journal of Inorganic Materials **2**, 687-699 (2000)

MONTAGNAT M., DUVAL P., BASTIE P., HAMELIN B., BRISSAUD O., ANGELIS M. DE, PETIT J.R., LIPENKOV V.Y. High crystalline quality of large single crystals of subglacial ice above Lake Vostok (Antartica) revealed by hard X-ray diffraction.
Comptes Rendus de l'Académie des Sciences **333**, 419-425 (2001)

MULLER C., VALMALETTE J.C., SOUBEYROUX J.L., BOUREE F., GAVARRI J.R. Structural disorder and ionic conductivity in $LiVO_3$: A neutron powder diffraction study from 340 to 890 K.
Journal of Solid State Chemistry **156**, 379-389 (2001)

PALMER R.A., POTTER B.S., LISGARTEN J.N., FENN R.H., MASON S.A., MILLS O.S., ROBINSON P.M., WATT C.I.F. X-ray and neutron structure of 1,8-(3,6,9-trioxaundecane-1,11-diyldioxy)-9,10-dihydro-10,10-dimethylanthracene-9-ol (P326); some pitfalls of automatic data collection.
Acta Crystallographica B **57**, 339-345 (2001)

PERRIN C., MENGUY N., SUARD E., MULLER C., CARANONI C., STEPANOV A. Neutron diffraction study of the relaxor-ferroelectric phase transition in disordered $Pb(Sc_{1/2}Nb_{1/2})O_3$.
Journal of Physics Condensed Matter **12**, 7523-7539 (2000)

POUILLERIE C., SUARD E., DELMAS C. Structural characterization of $Li_{1-z-x}Ni_{1+z}O_2$ by neutron diffraction.
Journal of Solid State Chemistry **158**, 187-197 (2001)

PRADO G., SUARD E., FOURNES L., DELMAS C. Cationic distribution in the $Li_{1-z}(Ni_{1-y}Fe_y)_{1+z}O_2$ electrode materials.
Journal of Materials Chemistry **10**, 2553-2560 (2000)

RIDEAU D., MONCEAU P., CURRAT R., REQUARDT H., NAD F., LORENZO J.E., BRAZOVSKII S., DETLEFS C., GRÜBEL G. High resolution X-ray scattering techniques for studying the sliding CDWS distortions, in $NbSe_3$.
Nuclear Instruments and Methods in Physics Research A **467-468**, 1010-1013 (2001)

RIDEAU D., MONCEAU P., CURRAT R., REQUARDT H., NAD F., LORENZO J.E., BRAZOVSKII S., DETLEFS C., GRÜBEL G. X-ray scattering evidence for macroscopic strong pinning centers in the sliding CDW state of $NbSe_3$.
Europhysics Letters **56**, 289-295 (2001)

SALVADO M.A., PERTIERRA P., GARCIA-GRANDA S., BARCINA L.M., LLAVONA R., RODRIGUEZ J. Hydrogen bond network of the layered phosphates γ-$Zr(H_2PO_4)(PO_4)\cdot 2H_2O$ and γ-$Hf(H_2PO_4)(PO_4)\cdot 2H_2O$ determined by neutron powder diffraction.
Zeitschrift für Kristallographie **216**, 326-330 (2001)

SCHERER W., SIRSCH P., GROSCHE M., SPIEGLER M., MASON S.A., GARDINER M.G. Agostic deformations based on electron delocalization in the alkyl-

lithium-complex [{2-($Me_3Si)_2CLiC_5H_4N}_2$]. Chemical Communications, 2072-2073 (2001)

SOUBEYROUX J.L., CLARET N., PELLETIER J.M. **Crystallization behaviour of $Zr_{65-x-y}Ti_xAl_yHf_5Cu_{20}Ni_{10}$ bulk metallic alloys by *in-situ* neutron diffraction.**
Materials Science Forum **360-362**, 37-42 (2001)

STEINER T., MASON S.A. **Erste Neutronendiffraktionsstudie einer Wasser-zu-Phenyl Wasserstoffbrücke.**
Zeitschrift für Kristallographie Supplement **18**, 93 (2001)

SUNDARESAN A., THOLENCE J.L., MAIGNAN A., RAVEAU B., SUARD E., BORDET P. **Kondo-like effect in the double exchange ferromagnet $La_{0.5-x}Ce_xSr_{0.5}MnO_3$.**
Journal of Magnetism and Magnetic Materials **226-230**, 777-779 (2001)

VAN DUIJN J., ATTFIELD J.P., WATANUKE R., SUZUKI K. **Layer stacking and twinning in HoB_2C.**
Journal of Physics and Chemistry of Solids **62**, 1423-1429 (2001)

VELASCO P., ALONSO J.A., MARTINEZ-LOPE M.J., CASAIS M.T., MARTINEZ J.L., FERNANDEZ-DIAZ M.T., DE PAOLI J.M. **Electron injection in Te-doped derivatives of $Tl_2Mn_2O_7$ pyrochlore.**
Physical Review B **64**, 184436-1-184436-6 (2001)

Magnetic Structures:

ALONSO J.A., MARTINEZ-LOPE M.J., CASAIS M.T., GARCIA-MUÑOZ J.L., FERNANDEZ-DIAZ M.T., ARANDA M.A.G. **Simultaneous structural and metal-insulator transition in $RNiO_3$ perovskites (R = Ho, Y, Er, Lu).**
Materials Science Forum **378-381**, 482-486 (2001)

AMARA M., MORIN P., BURLET P., LEJAY P. **Magnetic structures in the quadrupolar compound $TmAu_2$.**
Journal of Physics Condensed Matter **13**, 929-943 (2001)

BASLER R., TREGENNA-PIGGOTT P.L.W., ANDRES H., DOBE C., GÜDEL H.U., JANSSEN S., MCINTYRE G.J. **Magnetic excitations of $CsMn(SO_4)_2 \cdot 12D_2O$, measured by inelastic neutron scattering.**
Journal of the American Chemical Society **123**, 3377-3378 (2001)

BATTLE P.D., BELL A.M.T., BLUNDELL S.J., COLDEA A.I., CUSSEN E.J., HARDY G.C., MARSHALL I.M., ROSSEINSKY M.J., STEER C.A. **Chemically induced magnetism and magnetoresistance in $La_{0.8}Sr_{1.2}Mn_{0.6}Rh_{0.4}O_4$.**
Journal of the American Chemical Society **123**, 7610-7615 (2001)

BENSCH W., SANDER B., NÄTHER C., KREMER R.K., RITTER C. **Synthesis, crystal structure, magnetic properties and spin glass behaviour of the new ternary compound Cr_4TiSe_8.**
Solid State Science **3**, 559-568 (2001)

BENSCH W., SANDER B., NÄTHER C., RITTER C., KREMER R.K. **Darstellung, Struktur, magnetische Eigenschaften und Spinglas-Verhalten von Cr_4TiSe_8.**
Zeitschrift für Kristallographie Supplement **18**, 113 (2001)

BLASCO J., GARCIA J., SANCHEZ M.C., LARREA A., CAMPO J., SUBIAS G. **Magnetic properties and structure of $LaNi_{3/4}Mn_{1/4}O_3$ (Letter to the editor).**
Journal of Physics Condensed Matter **13**, L729-L736 (2001)

BOMBARDI A., KERNAVANOIS N., DALMAS DE REOTIER P., LANDER G.H., SANCHEZ J.P., YAOUANC A., BURLET P., LELIEVRE-BERNA E., ROGALEV A., VOGT O., MATTENBERGER K. **On the evolution of the ground state in the system $U_xLa_{1-x}S$: Polarized neutron diffraction and X-ray magnetic circular dichroism study.**
European Physical Journal B **21**, 547-552 (2001)

BRINKS H.W., RODRIGUEZ CARVAJAL J., FJELLVÅG H., KJEKSHUS A., HAUBACK B.C. **Crystal and magnetic structure of orthorhombic $HoMnO_3$.**
Physical Review B **63**, 094411-1-094411-12 (2001)

BROWN P.J., COSTA M.M.R., ZIEBECK K.R.A. **The spatial distribution of the paramagnetically aligned moments in the high-temperature insulating phase of V_2O_3.**
Journal of Physics Condensed Matter **13**, 10261-10268 (2001)

BRÜCKEL T., HUPFELD D., STREMPFER J., CALIEBE W., MATTENBERGER K., STUNAULT A., BERNHOEFT N., MCINTYRE G.J. **Antiferromagnetic order and phase transitions in GdS as studied with X-ray resonance-exchange scattering.**
European Physical Journal B **19**, 475-490 (2001)

BUDZIAK A., FIGIEL H., ZUKROWSKI J., GRATZ E., OULADDIAF B. **Magnetic ordering in $TbMn_2D_2$ (Letter to the editor).**
Journal of Physics Condensed Matter **13**, L871-L877 (2001)

CHACON C., ISNARD O. **The structural and magnetic properties of $Y_{n+1}Co_{3n+5}B_{2n}$ compounds investigated by neutron diffraction.**
Journal of Physics Condensed Matter **13**, 5841-5851 (2001)

CHACON C., ISNARD O. **Crystal and magnetic structure of $YCo_{4-x}Fe_xB$.**
Journal of Applied Physics **89**, 71-75 (2001)

CHACON C., ISNARD O., SUARD E. Neutron diffraction study on the deuterium site occupation and magnetic structure of the $Nd_2(Fe,Ga)_{14}BD_y$ compounds.
Journal of Alloys and Compounds **317-318**, 60-66 (2001)

CHAMPION J.D.M., WILLS A.S., FENNELL T., BRAMWELL S.T., GARDNER J.S., GREEN M.A. Order in the Heisenberg pyrochlore: The magnetic structure of $Gd_2Ti_2O_7$.
Physical Review B **64**, 140407-1-140407-4 (2001)

CHOUAIBI N., DAIDOUH A., PICO C., SANTRICH A., VEIGA M.L. Neutron diffraction, Mössbauer spectrum, and magnetic behavior of $Ag_2FeMn_2(PO_4)_3$ with alluaudite-like structure.
Journal of Solid State Chemistry **159**, 46-50 (2001)

COLLINS S.P., LAUNDY D., STUNAULT A. Anisotropic resonant diffraction from $HoFe_2$.
Journal of Physics Condensed Matter **13**, 1891-1905 (2001)

DEEN P.P., GOFF J.P., YAKHOU F., SARTHOUR R.S., WARD R.C.C., WELLS M.R., MCINTYRE G.J., MCMORROW D.F. The magnetism of Ce-Y alloys.
Journal of Magnetism and Magnetic Materials **226-230**, 1145-1147 (2001)

DUSEK M., CHAPUIS G., SCHOBINGER-PAPAMANTELLOS P., WILKINSON C., PETRICEK V. The modulated and composite model descriptions of $La_2Co_{1.7}$.
Ferroelectrics **250**, 115-119 (2001)

ESPESO J.I., GARCIA SOLDEVILLA J., BLANCO J.A., RODRIGUEZ FERNANDEZ J., GOMEZ SAL J.C., FERNANDEZ-DIAZ M.T. Neutron scattering on the strongly correlated electron $CeNi_{1-x}Cu_x$ system: From non-magnetic behaviour to long-range magnetic order.
European Physical Journal B **18**, 625-632 (2000)

FAUTH F., SUARD E., CAIGNAERT V., DOMENGES B., MIREBEAU I., KELLER L. Interplay of structural, magnetic and transport properties in the layered Co-based perovskite $LnBaCo_2O_5$ (Ln = Tb, Dy, Ho).
European Physical Journal B **21**, 163-174 (2001)

FERNANDEZ-DIAZ M.T., ALONSO J.A., MARTINEZ-LOPE M.J., CASAIS M.T., GARCIA-MUÑOZ J.L. Magnetic structure of the $HoNiO_3$ perovskite.
Physical Review B **64**, 144417-1-144417-5 (2001)

FRONTERA C., GARCIA-MUÑOZ J.L., ARANDA M.A.G., RITTER C., LLOBET A., RESPAUD M., VANACKEN J. Low-temperature charge and magnetic order of $Bi_{0.5}Sr_{0.5}MnO_3$.
Physical Review B **64**, 054401-1-054401-8 (2001)

FRUNZKE J., HANSEN T., HARRISON A., LORD J.S., OAKLEY G.S., VISSER D., WILLS A.S. Magnetic ordering in diluted kagome antiferromagnets.
Journal of Materials Chemistry **11**, 179-185 (2001)

FULTHORPE B.D., HASE T.P.A., TANNER B.K., MARROWS C.H., HICKEY B.J. Structural and magnetic changes on annealing permalloy/copper multilayers.
Journal of Magnetism and Magnetic Materials **226-230**, 1733-1734 (2001)

GIBSON B.J., PÖTTGEN R., SCHNELLE W., OULADDIAF B., KREMER R.K. Crystal and magnetic structure of antiferromagnetic HoAuGe.
Journal of Physics Condensed Matter **13**, 2593-2606 (2001)

GRENIER B., RESSOUCHE E., REGNAULT L.P., LORENZO J.E., LELIEVRE-BERNA E., DHALENNE G., REVCOLEVSCHI A. Magnetization distribution in Si-doped spin-Peierls compound $CuGeO_3$.
Physica B **297**, 221-225 (2001)

HIESS A., BOURDAROT F., COAD S., BROWN P.J., BURLET P., LANDER G.H., BROOKS M.S.S., KACZOROWSKI D., CZOPNIK A., TROC R. Spin and orbital moments in itinerant magnets.
Europhysics Letters **55**, 267-272 (2001)

HIESS A., BROWN P.J., LELIEVRE-BERNA E., ROESSLI B., BERNHOEFT N., LANDER G.H., ASO N., SATO N.K. Spherical neutron polarimetry of the magnetic structure in UNi_2Al_3.
Physical Review B **64**, 134413-1-134413-4 (2001)

HODGES J.A., BONVILLE P., GENAND-RIONDET N., TOMALA K., KERNAVANOIS N., RESSOUCHE E., SANCHEZ J.P., VULLIET P. ^{170}Yb Mössbauer and neutron diffraction measurements on spin-chain Yb_2BaNiO_5.
Journal of Physics Condensed Matter **12**, 9973-9983 (2000)

IBARRA M.R., DE TERESA J.M., ALGARABEL P.A., MARQUINA C., GARCIA-LANDA B., MORELLON L., RITTER C., MAHENDIRAN R., DEL MORAL A. Magnetostriction in mixed valent magnetic oxides.
In: "Modern Trends in Magnetostriction Study and Application" GIBBS M.R.J. (Ed.) (Kluwer Academic Publishers, 2000) pp. 171-204

JAVORSKY P., SECHOVSKY V., SCHWEIZER J., BOURDAROT F., LELIEVRE-BERNA E., ANDREEV A.V., SHIOKAWA Y. Magnetization densities in UCoAl studied by polarized neutron diffraction.
Physical Review B **63**, 064423-1-064423-8 (2001)

KAMENEV K.V., MCINTYRE G.J., ARNOLD Z., KAMARAD J., LEES M.R., BALAKRISHNAN G., CHUNG E.M.L., PAUL D.MCK. **Pressure-enhanced 3D antiferromagnetic correlations in $La_{1.4}Sr_{1.6}Mn_2O_7$.**
Physical Review Letters **87**, 167203-1-167203-4 (2001)

KEALEY P.G., CHARALAMBOUS D., FORGAN E.M., LEE S.L., JOHNSON S.T., SCHLEGER P., CUBITT R., PAUL D.MCK., AEGERTER C.M., TAJIMA S., RYKOV A. **Transverse-field components of the flux-line lattice in the anisotropic superconductor $YBa_2Cu_3O_{7-\delta}$.**
Physical Review B **64**, 174501-1-174501-4 (2001)

KLEIN T., JOUMARD I., BLANCHARD S., MARCUS J., CUBITT R., GIAMARCHI T., LE DOUSSAL P. **A Bragg glass phase in the vortex lattice of a type II superconductor.**
Nature **413**, 404-406 (2001)

KRÄMER K.W., GÜDEL H.U., FISCHER P., FAUTH F., FERNANDEZ-DIAZ M.T., HAUß T. **Triangular antiferromagnetic order in the honeycomb layer lattice of $ErCl_3$.**
European Physical Journal B **18**, 39-47 (2000)

KREISEL J., VINCENT H., TASSET F., PATE M., GANNE J.P. **An investigation of the magnetic anisotropy change in $BaFe_{12-2x}Ti_xCo_xO_{19}$ single crystals.**
Journal of Magnetism and Magnetic Materials **224**, 17-29 (2001)

KREYSSIG A., SCHNEIDEWIND A., LOEWENHAUPT M., RITTER C., FREUDENBERGER J., FUCHS G., MÜLLER K.H. **Magnetoelastic effects in rare earth nickel borocarbides.**
In: "Rare Earth Transition Metal Borocarbides (Nitrides): Superconducting, Magnetic and Normal State Properties" MÜLLER K.H., NAROZHNYI V. (Eds.) (Kluwer Academic Publishers, 2001) pp. 181-186

LONGFIELD M.J., STIRLING W.G., LIDSTRÖM E., MANNIX D., LANDER G.H., STUNAULT A., MCINTYRE G.J., MATTENBERGER K., VOGT O. **$U(As_{1-x}Se_x)$ solid solutions. I. Resonant X-ray and neutron scattering study of the magnetic phase diagram.**
Physical Review B **63**, 134401-1-134401-8 (2001)

MARGADONNA S., ASLANIS E., LI W.Z., PRASSIDES K., FITCH A.N., HANSEN T.C. **Crystal structure of superconducting $K_3Ba_3C_{60}$: A combined synchrotron X-ray and neutron diffraction study.**
Chemical Materials **12**, 2736-2740 (2000)

MIREBEAU I., GONCHARENKO I.N., ANDREANI D., SUARD E. **Influence of aluminum doping and hydrogen disorder on the magnetism of the frustrated Laves hydrides $Y(Mn_{1-x}Al_x)_2H_y$.**
Physical Review B **62**, 9493-9497 (2000)

MORALES M., BACMANN M., WOLFERS P., FRUCHART D., OULADDIAF B. **Impact of hydrogen and carbon insertion on the fundamental characteristics of $ErMn_{12-x}Fe_x$ compounds.**
Journal of Magnetism and Magnetic Materials **236**, 83-92 (2001)

MORALES M., BACMANN M., WOLFERS P., FRUCHART D., OULADDIAF B. **Magnetic properties and interactions in the $RMn_{12-x}Fe_x$ series (R = Y, Ho, Er, Nd; $x \leq 9$).**
Physical Review B **64**, 144426-1-144426-8 (2001)

MORELLON L., MAGEN C., ALGARABEL P.A., IBARRA M.R., RITTER C. **Magnetocaloric effect in $Tb_5(Si_xGe_{1-x})_4$.**
Applied Physics Letters **79**, 1318-1320 (2001)

MÜLLER-BUSCHBAUM P., WOLKENHAUER M., WUNNICKE O., STAMM M., CUBITT R., PETRY W. **Structure formation in two-dimensionally confined diblock copolymer films.**
Langmuir **17**, 5567-5575 (2001)

MUÑOZ A., ALONSO J.A., CASAIS M.T., MARTINEZ-LOPE M.J., MARTINEZ J.L., FERNANDEZ M.T. **Study of the incommensurate-commensurate magnetic transition in $HoMnO_3$ perovskite.**
Journal of Alloys and Compounds **323-324**, 486-489 (2001)

MUÑOZ A., ALONSO J.A., MARTINEZ-LOPE M.J., CASAIS M.T., MARTINEZ J.L., FERNANDEZ-DIAZ M.T. **Evolution of the magnetic structure of hexagonal $HoMnO_3$ from neutron powder diffraction data.**
Chemistry of Materials **13**, 1497-1505 (2001)

MUÑOZ A., CASAIS M.T., ALONSO J.A., MARTINEZ-LOPE M.J., MARTINEZ J.L., FERNANDEZ-DIAZ M.T. **Complex magnetism and magnetic structures of the metastable $HoMnO_3$ perovskite.**
Inorganic Chemistry **40**, 1020-1028 (2001)

PAIXÃO J.A., RAMOS SILVA M., WAERENBORGH J.C., GONCALVES A.P., LANDER G.H., BROWN P.J., GODINHO M., BURLET P. **Magnetic structures of $MFe_{4+\delta}Al_{8-\delta}$ (M = Lu,Y).**
Physical Review B **63**, 054410-1-054410-12 (2001)

PAUL D.MCK., BANCROFT N.J., TOMY C.V., DEWHURST C.D., CUBITT R., YETHIRAJ M., AEGERTER C.M., LEE S.L., LLOYD S.H., KEALEY P.G., FORGAN E.M. **High resolution neutron diffraction studies of the flux-line lattice in borocarbide superconductors.**
In: "Rare Earth Transition Metal Borocarbides (Nitrides): Superconducting, Ma-

gnetic and Normal State Properties" MÜLLER K.H., NAROZHNYI V. (Eds.) (Kluwer Academic Publishers, 2001) pp. 323-332

PROKES K., SECHOVSKY V., BOURDAROT F., BURLET P., KULDA J., MENOVSKY A. **Magnetic structure of a UNiAl single crystal under pressure.**
Journal of Magnetism and Magnetic Materials **226-230**, 1186-1187 (2001)

RITTER C., BLASCO J., MORELLON L., DE TERESA J.M., GARCIA J., IBARRA M.R. **The influence of doping on the magnetic and structural properties of the double perovskite Sr_2FeMoO_6.**
Journal of Magnetism and Magnetic Materials **226-230**, 1070-1072 (2001)

ROESSLI B., SCHEFER J., PETRAKOVSKII G.A., OULADDIAF B., BOEHM M., STAUB U., VOROTINOV A., BEZMATERNIKH L. **Formation of a magnetic soliton lattice in copper metaborate.**
Physical Review Letters **86**, 1885-1888 (2001)

ROTTER M., DOERR M., LOEWENHAUPT M., WITTE U., SVOBODA P., VEJPRAVOVA J., SASSIK H., RITTER C., ECKERT D., HANDSTEIN A., HINZ D. **Anomalous magnetic exchange interactions in $SmCu_2$.**
Physical Review B **64**, 134405-1-134405-6 (2001)

SADYKOV R.A., ZARITSKII V.N., MESOT J., FAUTH F. **Neutron and X-ray diffraction study of superstructure and localized magnetic moments in $Cu_{0.5}Fe_{0.5}Cr_2S_4$ and $Cu_{0.5}In_{0.5}Cr_2S_4$ compounds.**
Crystallography Reports **46**, 21-25 (2001)

SAOUDI M., DEPORTES J., OULADDIAF B. **Magnetic ground state of $Ti_{1-x}Sc_xFe_2$ system.**
Journal of Magnetism and Magnetic Materials **231**, 265-272 (2001)

SCHMITT D., OULADDIAF B., ROUTSI C.D., YAKINTHOS J.K. **Antiferromagnetic ordering in $DyPdGe_2$.**
Journal of Magnetism and Magnetic Materials **234**, 62-64 (2001)

SCHNEIDEWIND A., LOEWENHAUPT M., HIESS A., KRAMP S., REIF T., NEUBECK W., VETTIER C. **Non-resonant magnetic X-ray scattering on $NdCu_2$.**
Journal of Magnetism and Magnetic Materials **233**, 113-118 (2001)

SCHOBINGER-PAPAMANTELLOS P., BUSCHOW K.H.J., DUONG N.P., RITTER C. **Magnetic phase diagram of ErCuSi studied by neutron diffraction and magnetic measurements.**
Journal of Magnetism and Magnetic Materials **223**, 203-214 (2001)

SCHWEIZER J., BENCINI A., CARBONERA C., EPSTEIN A.J., GOLHEN S., LELIEVRE-BERNA E., MILLER J.S., OUAHAB L., PONTILLON Y., RESSOUCHE E., ZHELUDEV A. **Magnetization and spin density in $[FeCp^*_2]^{+\bullet}$. A look-back at the magnetic interactions in the chains $[FeCp^*_2]^{+\bullet}$ $[TCNE]^{-\bullet}$.**
Polyhedron **20**, 1771-1778 (2001)

SCHWEIZER J., GOLHEN S., LELIEVRE-BERNA E., OUAHAB L., PONTILLON Y., RESSOUCHE E. **Magnetic interactions and spin densities in molecular compounds: An example.**
Physica B **297**, 213-220 (2001)

STÜßER N., DING Y., HOFMANN M., REEHUIS M., OULADDIAF B., EHLERS G., GÜNTHER D., MEIßNER M., STEINER M. **Evidence for interpenetrating magnetic structures across an IC-C phase transition in $Mn_{0.88}Fe_{0.12}WO_4$.**
Journal of Physics Condensed Matter **13**, 2753-2766 (2001)

SÜLLOW S., MCINTYRE G.J., HAEN P., RAINFORD B.D., FUKUHARA T. **The magnetic pressure phase diagram of $CeRu_2(Ge,Si)_2$ studied by neutron diffraction.**
Journal of Magnetism and Magnetic Materials **226-230**, 179-181 (2001)

TOBOLA J., BACMANN M., FRUCHART D., WOLFERS P., KAPRZYK S., KOUMINA A.A. **Structure and magnetism in the polymorphous MnFeAs.**
Journal of Alloys and Compounds **317-318**, 274-279 (2001)

VAN DIJK N.H., RODIERE P., YAKHOU F., FERNANDEZ-DIAZ M.T., FÅK B., HUXLEY A., FLOUQUET J. **Magnetic order of UPt_3 under uniaxial pressure.**
Physical Review B **63**, 104426-1-104426-7 (2001)

VERNIERE A., KLOSEK V., WELTER R., VENTURINI G., ISNARD O., MALAMAN B. **Neutron diffraction study of the CeFeSi-type RTiGe compounds (R = Pr, Nd, Tb-Er).**
Journal of Magnetism and Magnetic Materials **234**, 261-273 (2001)

WALLACHER D., ACKERMANN R., HUBER P., ENDERLE M., KNORR K. **Diffraction study of solid oxygen embedded in porous glasses.**
Physical Review B **64**, 184203-1-184203-9 (2001)

WILDES A.R., COWLAM N., AL-HENITI S., KISS L.F., KEMENY T. **Non-collinear ferromagnetism in Fe-Zr metallic glasses.**
Journal of Magnetism and Magnetic Materials **226-230**, 1470-1472 (2001)

WILLS A.S. **Long-range ordering and representational analysis of the jarosites.**
Physical Review B **63**, 064430-1-064430-13 (2001)

WOLF J., KIEFER K., RHEINSTÄDTER M.C., KNORR K., ENDERLE M. **Tuning**

anisotropy by impurities: Magnetocaloric experiments on $CsNi_{0.9}Fe_{0.1}Cl_3$.
European Physical Journal B **22**, 461-471 (2001)

WOLFERS P., BACMANN M., FRUCHART D. Single crystal neutron diffraction investigations of the crystal and magnetic structures of $R_2Fe_{14}B$ (R=Y, Nd, Ho, Er).
Journal of Alloys and Compounds **317-318**, 39-43 (2001)

ZIMMER O. Spin contrast variation for macromolecular research.
In: "Proceedings of the Eighth Summer School on Neutron Scattering. Neutron Scattering in Novel Materials" FURRER A. (Ed.) (World Scientific, 2000) pp. 159-169

Structure and Dynamics of Liquids and Glasses:

ADAMS M.A. - Superfluid 4helium - A very novel material.
In "Proceedings of the Eighth Summer School on Neutron Scattering. Neutron Scattering in Novel Materials", FURRER A. (Ed.) (World Scientific, 2000) pp. 289-301

ALMARZA N.G., ENCISO E., GARCIA M.F., GONZALEZ M.A., BERMEJO F.J. Reentrant miscibility in fluids with spherical interactions.
Physical Review E **64**, 012501-1-012501-4 (2001)

ANDONOV P., FISCHER H.E., PALLEAU P., KIMURA S. Structural study of liquid lithium niobate by neutron diffraction. Role of the Li atom in the clustering near solidification.
Zeitschrift für Naturforschung A **56**, 395-406 (2001)

ANTONOV V.E., BARKALOV O.I., CALVO-DAHLBORG M., DAHLBORG U., FEDOTOV V.F., HARKUNOV A.I., HANSEN T., PONYATOVSKY E.G., WINZENICK M. Phase transformations of the amorphous Zn-Sb alloy under high pressures.
High Pressure Research **17**, 261-272 (2000)

APAJA V., GODFRIN H., KROTSCHECK E., LAUTER H.J. An interpretation of dispersionless modes in neutron diffraction experiments on helium films.
Journal of Low Temperature Physics **124**, 599-607 (2001)

BOVE L.E., SACCHETTI F., PETRILLO C., DORNER B., FORMISANO F., BAROCCHI F. Neutron investigation of the ion dynamics in liquid mercury: Evidence for collective excitations.
Physical Review Letters **87**, 215504-1-215504-4 (2001)

BUCHANAN P., BARNES A.C., WHITTLE K.R., HAMILTON M.A., FITCH A.N., FISCHER H.E. A determination of the structure of liquid Ga_2Te_3 using combined X-ray diffraction and neutron diffraction with isotopic substitution.
Molecular Physics **99**, 767-772 (2001)

CABRILLO C., BERMEJO F.J., JIMENEZ-RUIZ M., FERNANDEZ-DIAZ M.T., GONZALEZ M.A., MARTIN Y MARERO D. Partial ordering of supercooled liquid ethanol into a rotator-phase crystal as an entropy-driven transition.
Physical Review B **64**, 064206-1-064206-6 (2001)

CARLSSON P., ZORN R., ANDERSSON D., FARAGO B., HOWELLS W.S., BÖRJESSON L. The segmental dynamics of a polymer electrolyte investigated by coherent quasielastic neutron scattering.
Journal of Chemical Physics **114**, 9645-9656 (2001)

COURTENS E., FORET M., HEHLEN B., VACHER R. The vibrational modes of glasses.
Solid State Communications **117**, 187-200 (2001)

COUSSON A. Apport des neutrons à l'analyse structurale des composés partiellement désordonnés.
In: "10. Journées de la Diffusion Neutronique. Rencontres Rossat-Mignot" PAULUS W., MEINNEL J. (Eds.) (2001)

FARHI E., FÅK B., ZEYEN C.M.E., KULDA J. Roton lifetime measurement in superfluid ^{4}He using the spin-echo option on the IN20 triple-axis spectrometer.
Physica B **297**, 32-36 (2001)

FRICK B., COMBET J., PFISTER C. Neutron backscattering and its application in soft matter investigations.
Journal of the Physical Society of Japan Supplement A **70**, 311-316 (2001)

GOLDAMMER M., LOSERT C., WUTTKE J., PETRY W., TERKI F., SCHOBER H., LUNKENHEIMER P. Calcium rubidium nitrate: Mode-coupling β scaling without factorization.
Physical Review E **64**, 021303-1-021303-8 (2001)

HAMILTON M.A., BARNES A.C., HOWELLS W.S., FISCHER H.E. Ag^+ dynamics in the superionic and liquid phases of Ag_2Se and Ag_2Te by coherent quasi-elastic neutron scattering.
Journal of Physics Condensed Matter **13**, 2425-2436 (2001)

KÖBLER U., FISCHER K. The impact of fourth-order exchange interactions on the critical temperatures of $Eu_xSr_{1-x}S$ and $Eu_xSr_{1-x}Te$.
Journal of Physics Condensed Matter **13**, 123-139 (2001)

MEYER A., SCHOBER H., NEUHAUS J. Microscopic dynamics in liquid GeO_2.
Physical Review B **63**, 212202-1-212202-3 (2001)

MORENO A.J., ALEGRIA A., COLMENERO J., FRICK B. Methyl group dynamics in poly(methyl methacrylate): From quantum tunneling to classical hopping.
Macromolecules **34**, 4886-4896 (2001)

NICOLAUS K., NEUHAUS J., PETRY W., BOSSY J. Phonon dispersion of bcc cerium.
European Physical Journal B **21**, 357-361 (2001)

PLANTEVIN O., FÅK B., GLYDE H.R., MULDERS N., BOSSY J., CODDENS G., SCHOBER H. Excitations of superfluid ^{4}He in porous media: Aerogel and Vycor.
Physical Review B **63**, 224508-1-224508-11 (2001)

WASSE J.C., PETRI I., SALMON P.S. Structure of glassy AsTe: The effect of adding a small quantity of Cu or Ag.
Journal of Physics Condensed Matter **13**, 6165-6176 (2001)

WILLS A.S., OAKLEY G.S., VISSER D., FRUNZKE J., HARRISON A., ANDERSEN K.H. Short-range order in the topological spin glass $(D_3O)Fe_3(SO_4)_2(OD)_6$ using xyz polarized neutron diffraction.
Physical Review B **64**, 094436-1-094436-8 (2001)

Material Science, Surfaces and Spectroscopy:

ALVAREZ L., RIGHI A., ROLS S., ANGLARET E., SAUVAJOL J.L., MUÑOZ E., MASER W.K., BENITO A.M., MARTINEZ M.T., DE LA FUENTE G.F. Diameter dependence of Raman intensities for single-wall carbon nanotubes.
Physical Review B **63**, 153401-1-153401-4 (2001)

ANDRES H., BASLER R., GÜDEL H.U., AROMI G., CHRISTOU G., BÜTTNER H., RUFFLE B. Inelastic neutron scattering and magnetic susceptibilities of the single-molecule magnets $[Mn_4O_3X(OAc)_3(dbm)_3]$ (X = Br, Cl, OAc, and F): Variation of the anisotropy along the series.
Journal of the American Chemical Society **122**, 12469-12477 (2000)

ANDRES H., CLEMENTE-JUAN J.M., BASLER R., AEBERSOLD M., GÜDEL H.U., BORRAS-ALMENAR J.J., GAITA A., CORONADO E., BÜTTNER H., JANSSEN S. Magnetic polyoxometalates: Anisotropic antiferro- and ferromagnetic exchange interactions in the pentameric cobalt(II) cluster $[Co_3W(D_2O)_2(CoW_9O_{34})_2]^{12-}$. A magnetic and inelastic neutron scattering study.
Inorganic Chemistry **40**, 1943-1950 (2001)

ANDRES H.P., DECURTINS S., GÜDEL H.U. Neutron scattering of molecular magnets.
In: "Frontiers of Neutron Scattering" FURRER A. (Ed.) (World Scientific, 2000) pp. 149-167

AUFFERMANN G., SIMON A., GULDEN T., KEARLEY G.J., IVANOV A. Location and vibrations of hydrogen in $La_2C_3H_{1.5}$.
Zeitschrift für Anorganische und Allgemeine Chemie **627**, 307-311 (2001)

BENES N.E., JOBIC H., VERWEIJ H. Quasi-elastic neutron scattering study of the mobility of methane in microporous silica.
Microporous and Mesoporous Materials **43**, 147-152 (2001)

BERNARD L., AWITOR K.O., COUPAT B., FOURNIER J.P., BASTIE P., HAMELIN B. Growth of mercuric iodide single crystals by physical vapor transport: Development of a new "monothermal" furnace non-destructive bulk characterization by a laboratory hard X-ray method.
Journal of Crystal Growth **225**, 79-91 (2001)

BETA I.A., JOBIC H., GEIDEL E., BÖHLIG H., HUNGER B. Inelastic neutron scattering and infrared spectroscopic study of furan adsorption on alkali-metal cation-exchanged faujasites.
Spectrochimica Acta A **57**, 1393-1403 (2001)

CHATTERJI T., REGNAULT L.P., THALMEIER P., VAN DE KAMP R., SCHMIDT W., HIESS A., VORDERWISCH P., SURYANARAYANAN R., DHALENNE G., REVCOLEVSCHI A. Spin dynamics of quasi-2D ferromagnet $La_{1.2}Sr_{1.8}Mn_2O_7$ (Invited talk).
Journal of Alloys and Compounds **326**, 15-26 (2001)

CHEUNG J., MESSOLORAS S., RYCROFT S., STEWART R.J., BINNS M.J. Oxygen precipitation in Czochralski grown silicon heat treated at 550°C.
Semiconductor Science and Technology **15**, 782-788 (2000)

COPPOLA R., MAGNANI M., MAY R.P., MÖSLANG A., VALLI M. Study of He-bubble growth in α-particle implanted F82H-mod martensitic steel.
Journal of Nuclear Materials **283-287**, 183-187 (2000)

DESMEDT A., GUILLAUME F., COMBET J., DIANOUX A.J. A high resolution quasielastic neutron scattering study of the guest molecules dynamics in the cyclohexane/thiourea inclusion compound.
Physica B **301**, 59-64 (2001)

FRONTERA C., GARCIA-MUNOZ J.L., LLOBET A., RESPAUD M., BROTO J.M., LORD J.S., PLANES A. Phase coexistence, magnetic inhomogeneity, and disorder in the charge-ordered state of $Pr_{2/3}Ca_{1/3}MnO_3$.
Physical Review B **62**, 3381-3388 (2000)

GUTT C., PRESS W., HÜLLER A., TSE J.S., CASALTA H. The isotope effect and orientational potentials of methane molecules in gas hydrates.
Journal of Chemical Physics **114**, 4160-4170 (2001)

HALM T., NOMSSI NZALI J., HOYER W., MAY R.P., BIONDUCCI M. Short-range and medium-range order in molten Ga-Tl alloys.
Journal of Non-Crystalline Solids **293-295**, 182-186 (2001)

HEDOUX A., DEROLLEZ P., GUINET Y., DIANOUX A.J., DESCAMPS M. Low-frequency vibrational excitations in the amorphous and crystalline states of triphenyl phosphite: A neutron and Raman scattering investigation.
Physical Review B **63**, 144202-1-144202-8 (2001)

JANOT C., BOISSIEU M. DE, AGLIOZZO S., LORETO L., FARINATO R., SATO T.J., TSAI A.P., GRILLO I. Small angle neutron scattering with single grain quasicrystals.
Physica B **300**, 52-60 (2001)

JOBIC H., BEE M., METHIVIER A., COMBET J. Influence of the cation composition on the dynamics of xylenes in X-type zeolites.
Microporous and Mesoporous Materials **42**, 135-155 (2001)

JOBIC H., SMIRNOV K.S., BOUGEARD D. Inelastic neutron scattering spectra of zeolite frameworks - experiment and modeling.
Chemical Physics Letters **344**, 147-153 (2001)

JOHNSON M., KEARLEY G. L'effet tunnel et les protéines.
Pour la Science **281**, 64-69 (2001)

JOHNSON M.R., KEARLEY G.J. Quantitative atom-atom potentials from rotational tunneling: Their extraction and their use.
Annual Review of Physical Chemistry **51**, 297-321 (2000)

JOHNSON M.R., KEARLEY G.J., ECKERT J. Preface to special issue of Chemical Physics: Condensed matter structure and dynamics: A combined neutron scattering and numerical modelling approach.
Chemical Physics **261**, vii-ix (2000)

KAISERMAYR M., COMBET J., IPSER H., SCHICKETANZ H., SEPIOL B., VOGL G. Determination of the elementary jump of Co in CoGa by quasielastic neutron scattering.
Physical Review B **63**, 054303-1-054303-8 (2001)

KOMPATSCHER M., DEMÉ B., HECHT J., HEINRICH H., KOHLBRECHER J., SCHNEIDER J.M., SCHÖNFELD B., KOSTORZ G. Early stages of decomposition in Ni-rich Ni-Ti.
Materials Research Society. Symposium Proceedings **580**, 63-68 (2000)

KOMPATSCHER M., SCHÖNFELD B., HEINRICH H., KOSTORZ G. Small-angle neutron scattering investigation of the early stages of decomposition in Ni-rich Ni-Ti.
Journal of Applied Crystallography **33**, 488-491 (2000)

KRAVTSOV E., LAUTER-PASYUK V., LAUTER H.J., TOPERVERG B., NIKONOV O., PETRENKO A., MILYAEV M., ROMASHEV L., USTINOV V. Interface formation and magnetic ordering in Fe/Cr hybrid nanostructures.
Physica B **297**, 118-121 (2001)

LAUTER-PASYUK V., LAUTER H.J., TOPERVERG B., NIKONOV O., KRAVTSOV E., ROMASHEV L., USTINOV V. Magnetic neutron off-specular scattering for the direct determination of the coupling angle in exchange-coupled multilayers.
Journal of Magnetism and Magnetic Materials **226-230**, 1694-1696 (2001)

MOLVINGER K., COURT J., JOBIC H. Evidence for the anchoring of 2-amino-3-methyl-1-butanol at the surface of NiB_2 agglomerate by inelastic neutron spectroscopy.
Journal of Molecular Catalysis A: Chemical **174**, 245-248 (2001)

MORENO A.J., ALEGRIA A., COLMENERO J., PRAGER M., GRIMM H., FRICK B. Methyl group dynamics in glassy toluene: A neutron scattering study.
Journal of Chemical Physics **115**, 8958-8966 (2001)

NEUMANN M.A., JOHNSON M.R., RADAELLI P.G. The low temperature phase transition in octane and its possible generalisation to other *n*-alkanes.
Chemical Physics **266**, 53-68 (2001)

OHL M., MAYR F., REEHUIS M., SCHMIDT W., LOIDL A. Lattice vibrations in the mixed crystals $(NH_4I)_{0.3}(KI)_{0.7}$, $(ND_4I)_{0.3}(KI)_{0.7}$ and $(NH_4Br)_{0.3}(KBr)_{0.7}$.
Journal of Physics Condensed Matter **13**, 10221-10229 (2001)

ROTTER M., SIERKS C., LOEWENHAUPT M., FREUDENBERGER J., SCHOBER H. Crystal field effects in borocarbides studied by inelastic neutron scattering.
In: "Rare Earth Transition Metal Borocarbides (Nitrides): Superconducting, Magnetic and Normal State Properties" MÜLLER K.H., NAROZHNYI V. (Eds.) (Kluwer Academic Publishers, 2001) pp. 137-154

SELLMANN R., FRITZSCHE H., MALETTA H., LEINER V., SIEBRECHT R. Spin-reorientation transition and magnetic phase

diagrams of thin epitaxial Au(111)/Co films with W and Au overlayers.
Physical Review B **64**, 054418-1-054418-10 (2001)

STRIDE J.A., JAYASOORIYA U.A., MBOGO N., WHITE R.P., NICOLAI B., KEARLEY G.J. Hydrogen-bonding in the self-organising system 3,5-dimethylpyrazole.
New Journal of Chemistry **25**, 1069-1072 (2001)

SWENSON J., SMALLEY M.V., HATHARASINGHE H.L.M., FRAGNETO G. Interlayer structure of a clay-polymer–salt–water system.
Langmuir **17**, 3813-3818 (2001)

SYROMYATNIKOV V.G., TOPERVERG B.P., KENTZINGER E., DERIGLAZOV V.V., KAMPMANN R., PLESHANOV N.K., PUSENKOV V.M., SCHEBETOV A.F., SIEBRECHT R., UL'YANOV V.A. Off-specular polarized neutron scattering from periodic Co/Ti and aperiodic Fe/Al magnetic multilayers.
Physica B **297**, 175-179 (2001)

TOPERVERG B., NIKONOV O., LAUTERPASYUK V., LAUTER H.J. Towards 3D polarization analysis in neutron reflectometry.
Physica B **297**, 169-174 (2001)

VOROBIEV A., GORDEEV G., DONNER W., DOSCH H., NICKEL B., TOPERVERG B.P. Reflectivity and off-specular neutron scattering from the free ferrofluid surface and silicon – ferrofluid interface.
Physica B **297**, 194-197 (2001)

WEBSTER P.J. Analyse des constraintes résiduelles et texture dans les matériaux : applications industrielles.
In: "10. Journées de la Diffusion Neutronique. Rencontres Rossat-Mignot" PAULUS W., MEINNEL J. (Eds.) (2001)

WILMER D., FELDMANN H., COMBET J., LECHNER R.E. Ion conducting rotor phases – new insights from quasielastic neutron scattering.
Physica B **301**, 99-104 (2001)

WITHERS P.J, WEBSTER P.J. Neutron and synchrotron X-ray strain scanning.
Strain **37**, 19-33 (2001)

Structure and Dynamics of Biological Systems:

ARZT S., BAUDIN F., BARGE A., TIMMINS P.A., BURMEISTER W.P., RUIGROK R.W.H. Combined results from solution studies on intact influenza virus M1 protein and from a new crystal form of its N-terminal domain show that M1 is an elongated monomer.
Virology **279**, 439-446 (2001)

ASLAM M., PERKINS S.J. Folded-back solution structure of monomeric factor H of human complement by synchrotron X-ray and neutron scattering, analytical ultracentrifugation and constrained molecular modelling.
Journal of Molecular Biology **309**, 1117-1138 (2001)

BELLET-AMALRIC E., BLAUDEZ D., DESBAT B., GRANER F., GAUTHIER F., RENAULT A. Interaction of the third helix of Antennapedia homeodomain and a phospholipid monolayer, studied by ellipsometry and PM-IRRAS at the air–water interface.
Biochimica et Biophysica Acta **1467**, 131-143 (2000)

DOSTER W., DIEHL M., LEYSER H., PETRY W., SCHOBER H. Terahertz spectroscopy of proteins: Viscoelastic damping of boson peak oscillations.
In: "Spectroscopy of Biological Molecules: New Directions" GREVE J. et al. (Eds.) (Kluwer Academic Publishers, 2000) pp. 655-658

DOSTER W., DIEHL M., PETRY W., FERRAND M. Elastic resolution spectroscopy: A method to study molecular motions in small biological samples.
Physica B **301**, 65-68 (2001)

EGEA P.F., ROCHEL N., BIRCK C., VACHETTE P., TIMMINS P.A., MORAS D. Effects of ligand binding on the association properties and conformation in solution of retinoic acid receptors RXR and RAR.
Journal of Molecular Biology **307**, 557-576 (2001)

FRAGNETO G., CHARITAT T., GRANER F., MECKE K., PERINO-GALLICE L., BELLET-AMALRIC E. A fluid floating bilayer.
Europhysics Letters **53**, 100-106 (2001)

FRAGNETO-CUSANI G. Neutron reflectivity at the solid/liquid interface: Examples of applications in biophysics.
Journal of Physics Condensed Matter **13**, 4973-4989 (2001)

GRIZOT S., GRANDVAUX N., FIESCHI F., FAURE J., MASSENET C., ANDRIEU J.P., FUCHS A., VIGNAIS P.V., TIMMINS P.A., DAGHER M.C., PEBAY-PEYROULA E. Small angle neutron scattering and gel filtration analyses of neutrophil NADPH oxidase cytosolic factors highlight the role of the C-terminal end of $p47^{phox}$ in the association with $p40^{phox}$.
Biochemistry **40**, 3127-3133 (2001)

GUTSCHE I., HOLZINGER J., RAUH N., BAUMEISTER W., MAY R.P. ATP-induced structural change of the thermosome is temperature-dependent.
Journal of Structural Biology **135**, 139-146 (2001)

KOZIELSKI F., SVERGUN D., ZACCAI G., WADE R.H., KOCH M.H.J. The overall conformation of conventional kinesins studied by small angle X-ray and neutron scattering.

Journal of Biological Chemistry **276**, 1267-1275 (2001)

MADERN D., EBEL C., MEVARECH M., RICHARD S.B., PFISTER C., ZACCAI G. Insights into the molecular relationships between malate and lactate dehydrogenases: Structural and biochemical properties of monomeric and dimeric intermediates of a mutant of tetrameric L-[LDH-like] malate dehydrogenase from the halophilic archaeon *Haloarcula marismortui*.
Biochemistry **39**, 1001-1010 (2000)

MEEK K.M., QUANTOCK J. The use of X-ray scattering techniques to determine corneal ultrastructure.
Progress in Retinal and Eye Research **20**, 95-137 (2001)

PEBAY-PEYROULA E., ROSENBUSCH J.P. High-resolution structures and dynamics of membrane protein–lipid complexes: A critique.
Current Opinion in Structural Biology **11**, 427-432 (2001)

TARBOURIECH N., CURRAN J., EBEL C., RUIGROK R.W.H., BURMEISTER W.P. On the domain structure and the polymerization state of the Sendai virus P protein.
Virology **266**, 99-109 (2000)

WEICHENRIEDER O., STEHLIN C., KAPP U., BIRSE D.E., TIMMINS P.A., STRUB K., CUSACK S. Hierarchical assembly of the *Alu* domain of the mammalian signal recognition particle.
RNA **7**, 731-740 (2001)

WILLUMEIT R., DIEDRICH G., FORTHMANN S., BECKMANN J., MAY R.P., STUHRMANN H.B., NIERHAUS K.H. Mapping proteins of the 50S subunit from *Escherichia coli* ribosomes.
Biochimica et Biophysica Acta **1520**, 7-20 (2001)

Structure and Dynamics of Soft-Condensed Matter:

ARBE A., MONKENBUSCH M., STELLBRINK J., RICHTER D., FARAGO B., ALMDAL K., FAUST R. Origin of internal viscosity effects in flexible polymers: A comparative neutron spin-echo and light scattering study on poly (dimethylsiloxane) and polyisobutylene.
Macromolecules **34**, 1281-1290 (2001)

ARRIGHI V., PAPPAS C., TRIOLO A., POUGET S. Temperature dependence of local chain dynamics in atactic polypropylene: A neutron spin-echo study.
Physica B **301**, 157-162 (2001)

ASEYEV V.O., KLENIN S.I., TENHU H., GRILLO I., GEISSLER E. Neutron scattering studies of the structure of a polyelectrolyte globule in a water–acetone mixture.
Macromolecules **34**, 3706-3709 (2001)

BEE M., DJURADO D., COMBET J., TELLING M., RANNOU P., PRON A., TRAVERS J.P. Dynamics of camphor sulfonic acid in polyaniline (PANI-CSA): A quasielastic neutron scattering study.
Physica B **301**, 49-53 (2001)

BERGHAUSEN J., ZIPFEL J., LINDNER P., RICHTERING W. Influence of water-soluble polymers on the shear-induced structure formation in lyotropic lamellar phases.
Journal of Physical Chemistry B **105**, 11081-11088 (2001)

BERRET J.F., GAMEZ-CORRALES R., SERERO Y., MOLINO F., LINDNER P. Shear-induced micellar growth in dilute surfactant solutions.
Europhysics Letters **54**, 605-611 (2001)

COLE J.M., MCINTYRE G.J., LEHMANN M.S., MYLES D.A.A., WILKINSON C., HOWARD J.A.K. Rapid neutron-diffraction data collection for hydrogen-bonding studies: Application of the Laue diffractometer (LADI) to the case study zinc (tris)thiourea sulfate.
Acta Crystallographica A **57**, 429-434 (2001)

DINGENOUTS N., SEELENMEYER S., DEIKE I., ROSENFELDT S., BALLAUFF M., LINDNER P., NARAYANAN T. Analysis of thermosensitive core–shell colloids by small-angle neutron scattering including contrast variation.
Physical Chemistry Chemical Physics **3**, 1169-1174 (2001)

DUBOIS M., DEMÉ B., GULIK-KRZYWICKI T., DEDIEU J.C., VAUTRIN C., DESERT S., PEREZ E., ZEMB T. Self-assembly of regular hollow icosahedra in salt-free catanionic solutions.
Nature **411**, 672-675 (2001)

FARAGO B., GRADZIELSKI M. The effect of charge density of microemulsion droplets on the bending elasticity of their amphiphilic film.
Journal of Chemical Physics **114**, 10105-10122 (2001)

FÖRSTER S., BERTON B., HENTZE H.P., KRÄMER E., ANTONIETTI M., LINDNER P. Lyotropic phase morphologies of amphiphilic block copolymers.
Macromolecules **34**, 4610-4623 (2001)

LE T.D., OLSSON U., MORTENSEN K., ZIPFEL J., RICHTERING W. Nonionic amphiphilic bilayer structures under shear.
Langmuir **17**, 999-1008 (2001)

MÜLLER-BUSCHBAUM P., GUTMANN J.S., STAMM M., CUBITT R. Surface structure analysis of thin dewetted polymer blend films.

Macromolecules Symposium **149**, 283-288 (2000)

NETTESHEIM F., ZIPFEL J., LINDNER P., RICHTERING W. Influence of sodium dodecyl sulfate on structure and rheology of aqueous solutions of the nonionic surfactant tetraethyleneglycolmonododecyl ether ($C_{12}E_4$).
Colloids and Surfaces A **183-185**, 563-574 (2001)

PLESTIL J., POSPISIL H., KRIZ J., KADLEC P., TUZAR Z., CUBITT R. Characterization of nanoparticles based on block copolymer micelles.
Langmuir **17**, 6699-6704 (2001)

ROUX J.N., BROSETA D., DEMÉ B. SANS study of asphaltene aggregation: Concentration and solvent quality effects.
Langmuir **17**, 5085-5092 (2001)

SEELENMEYER S., DEIKE I., ROSENFELDT S., NORHAUSEN C., DINGENOUTS N., BALLAUFF M., NARAYANAN T., LINDNER P. Small-angle X-ray and neutron scattering studies of the volume phase transition in thermosensitive core–shell colloids.
Journal of Chemical Physics **114**, 10471-10478 (2001)

VERSMOLD H., MUSA S., DUX C., LINDNER P., URBAN V. Shear-induced structure in concentrated dispersions: Small angle synchrotron X-ray and neutron scattering.
Langmuir **17**, 6812-6815 (2001)

WELLS S.L., TAYLOR D., ADAM M., DESIMONE J.M., FARAGO B. Study of the association of a diblock copolymer and absorption of an insoluble homopolymer in CO_2.
Macromolecules **34**, 6161-6163 (2001)

WESTERMANN S., PYCKHOUT-HINTZEN W., RICHTER D., STRAUBE E., EGELHAAF S., MAY R. On the length scale dependence of microscopic strain by SANS.
Macromolecules **34**, 2186-2194 (2001)

ZIPFEL J., NETTESHEIM F., LINDNER P., LE T.D., OLSSON U., RICHTERING W. Cylindrical intermediates in a shear-induced lamellar-to-vesicle transition.
Europhysics Letters **53**, 335-341 (2001)

Thesis:

BURDIN S. Le réseau Kondo à basse température : du liquide de Fermi au liquide de spin.
Thèse présentée à l'Université Joseph Fourier Grenoble I, Grenoble, France (2001)

FREUDENBERGER J. Paarbrechung in Seltenerd-Übergangsmetall-Borkarbiden.
Inaugural-Dissertation zur Erlangung des Doktorgrades der Naturwissenschaften Doctor rerum naturalium, vorgelegt der Fakultät Mathematik und Naturwissenschaften der Technischen Universität Dresden, Germany

HOFMANN D. Messung der paritätsverletzenden Neutronenspin-Rotation in ^{139}La unter Einsatz von ^{3}He-Neutronenspin-Filtern.
Dissertation zur Erlangung des Grades "Doktor der Naturwissenschaften" am Fachbereich Physik der Johannes Gutenberg-Universität in Mainz, Germany (2000)

KREYßIG A. Einfluß der magnetischen Ordnung auf Supraleitung und Kristallstruktur in Seltenerd-Nickel-Borkarbid-Verbindungen.
Dissertation zur Erlangung des akademischen Grades Doctor rerum naturalium der Fakultät Mathematik und Naturwissenschaften der Technischen Universität Dresden, Germany (2001)

ROLS S. Structure et dynamique des nanotubes de carbone. Une étude par diffusion élastique et inélastique des neutrons.
Thèse présentée à l'Université de Montpellier II Sciences et Techniques du Languedoc, Montpellier, France (2000)

ZIPFEL J. Shear induced structures in lamellar surfactant mesophases with different membrane properties.
Inauguraldissertation zur Erlangung der Doktorwürde der Fakultät für Chemie und Pharmazie der Albert-Ludwigs-Universität, Freiburg im Breisgau, Germany (2000)

ILL 2001 CD-ROM (Mac/PC)

Including the Annual Report 2001 and the Interactive Yellow Book

The enclosed CD-ROM contains both the ILL 2001 Annual Report and the Interactive Yellow Book describing the ILL instrument suite.

The Annual Report is presented as a Portable Document Format (PDF) file. You will need a PDF file reader (Adobe® Acrobat® Reader®) to view it.

The Interactive Yellow Book gives an overview of the neutron source and spectrometers at the ILL in the form of photos, animations, videos, charts of technical data. The list of contact persons and instrument responsibles is also provided. To access the specific data for a given instrument, click on the instrument symbol in the map or on its name in the list. To return to the map, press the button "Menu" or the space bar on your keyboard.

NEUTRONS
FOR SCIENCE

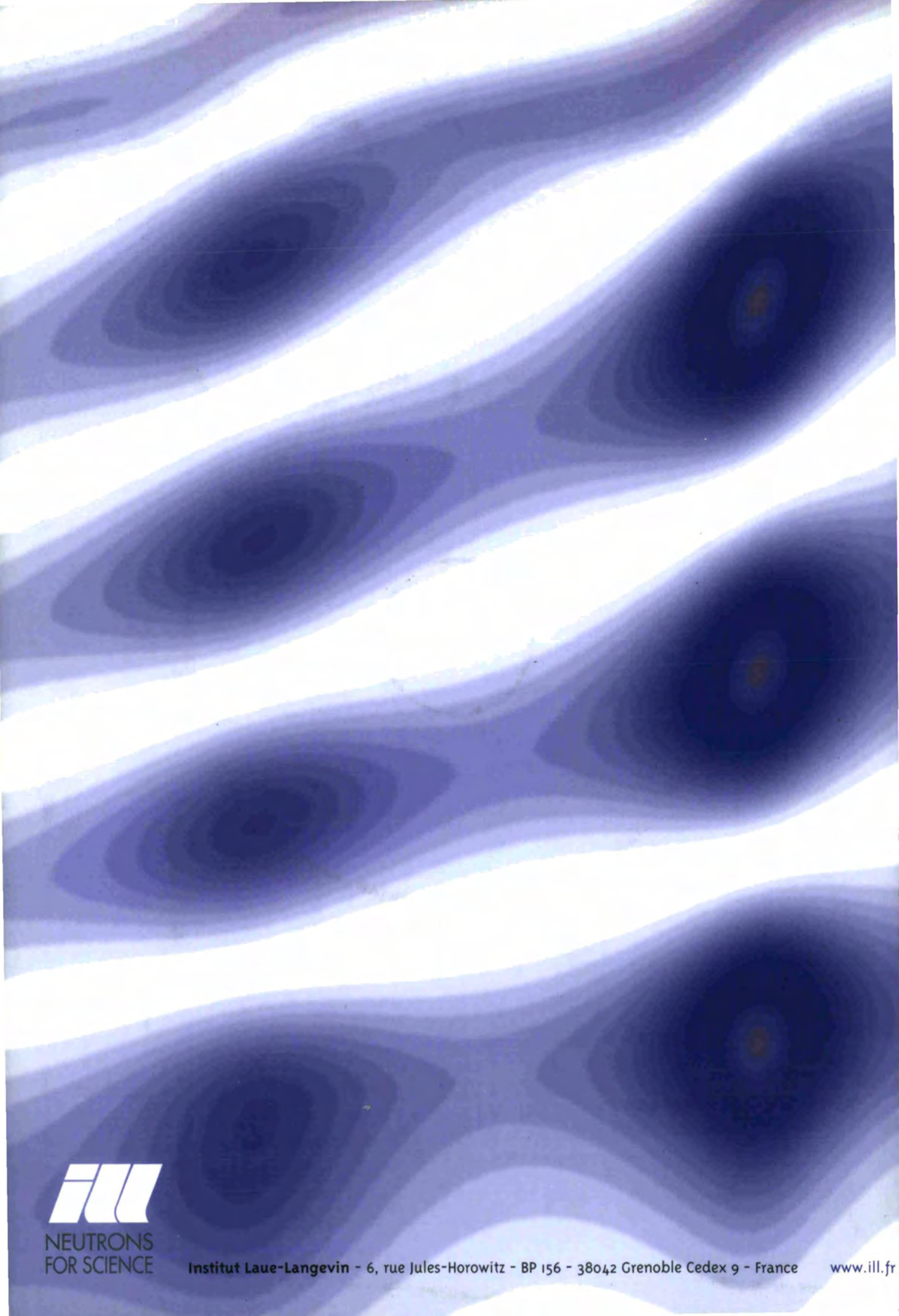

NEUTRONS
FOR SCIENCE

Institut Laue-Langevin - 6, rue Jules-Horowitz - BP 156 - 38042 Grenoble Cedex 9 - France www.ill.fr